University of Southampton

Faculty of Engineering and Physical Sciences

School of Chemistry

Coordination Chemistry of Group 14 with Pnictine Ligands and the Development of Precursors for the Electrodeposition of Antimony Chalcogenides

by

Rhys Paul King

Thesis for the degree of Doctor of Philosophy

December 2021

University of Southampton

Abstract

Faculty of Engineering

Chemistry

Doctor of Philosophy

Coordination Chemistry of Group 14 with Pnictine Ligands and the Development of Precursors for the Electrodeposition of Antimony Chalcogenides

by

Rhys Paul King

The work in this thesis describes the development of several new series of group 14 pnictine complexes, focusing on the generation of new neutral and cationic complexes, in conjunction with the development of new precursors for the electrodeposition of antimony chalcogenide semiconductors. Chapter 1 details the relevant background literature for the material discussed in the later chapters, with the introduction to each subsequent chapter detailing the most relevant background literature for the work described therein. Chapter 2 describes the synthesis of a series of tin(IV) halide pnictine complexes (halide = Cl, Br), as well as the halide abstraction chemistry of these complexes with TMSOTf ($Me_3SiO_3SCF_3$), AlX_3 and $Na[BAr^F]$ (BAr^F = B{3,5-$(CF_3)_2C_6H_3$}$_4$). The effect of the halide abstractor on reaction outcome is explored. In Chapter 3 the chemistry of GeF_4 with a range of mono-, bi- and multidentate phosphine ligands is explored. The reactions of the monodentate and bidentate complexes with TMSOTf are described and the effect of sequential fluoride extraction on spectroscopic and crystallographic properties investigated. The complex $[GeF_3(PMe_3)_2(OTf)]$ was found to be unstable in solution and formed the Ge(II) complex $[Ge(PMe_3)_3][OTf]_2$ through reductive defluorination. This provided inspiration to investigate homoleptic pnictine-stabilised dicationic Ge(II) complexes, as detailed in Chapter 4. The differences and similarities in the coordination chemistry of mono- and multi-dentate phosphine and arsine ligands towards Ge(II) was explored mainly through single crystal XRD and NMR spectroscopic studies. Chapter 5 details the fluoride abstraction chemistry of $[SnF_4(PMe_3)_2]$ and $[SnF_4(P^iPr_3)_2]$ with TMSOTf, and the complexes were characterised mainly through multinuclear NMR spectroscopy (^1H, $^{19}F\{^1H\}$, $^{31}P\{^1H\}$ and ^{119}Sn). Some of the triflate complexes were shown to undergo redox chemistry in solution, including through reductive defluorination to form Sn(II) species. In Chapter 6 the chemistry of Si(IV) halides with phosphine ligands was explored and the first SiI_4 complexes with phosphine ligands are described. The halide abstraction chemistry of the lighter halide phosphine complexes is investigated providing a series of novel cationic and neutral Si(IV) complexes. The last experimental chapter describes the synthesis of new salts of $[SbS_4]^{3-}$ with tetraalkylammonium counter cations. The electrochemistry of the anion $[SbS_4]^{3-}$ is then investigated in aqueous and non-aqueous solutions. In aqueous solution it has been shown that the electrodeposition of Sb_2S_3 thin films onto glassy carbon electrodes from the single source $[SbS_4]^{3-}$ anion is possible.

Table of Contents

Table of Tables

Table of Tables

Table of Figures

Table of Figures

Table of Figures

Table of Figures

Table of Schemes

List of Accompanying Materials

All the cif files of single crystal X-ray structures described in this thesis are included in the ESI, as well as spectroscopic and computational data. This can be found at DOI: https://doi.org/10.5258/SOTON/D2082

Research Thesis: Declaration of Authorship

Print name: Rhys Paul King

Title of thesis: Coordination chemistry of group 14 with pnictine ligands and the development of precursors for the electrodeposition of antimony chalcogenides

I declare that this thesis and the work presented in it are my own and has been generated by me as the result of my own original research.

I confirm that:

1. This work was done wholly or mainly while in candidature for a research degree at this University;
2. Where any part of this thesis has previously been submitted for a degree or any other qualification at this University or any other institution, this has been clearly stated;
3. Where I have consulted the published work of others, this is always clearly attributed;
4. Where I have quoted from the work of others, the source is always given. With the exception of such quotations, this thesis is entirely my own work;
5. I have acknowledged all main sources of help;
6. Where the thesis is based on work done by myself jointly with others, I have made clear exactly what was done by others and what I have contributed myself;
7. Parts of this work have been published as:-

   "***Neutral and cationic phosphine and arsine complexes of tin(IV) halides: synthesis, properties, structures and anion influence***" V. K. Greenacre, R. P. King, W. Levason and G. Reid, *Dalton Trans.*, 2019, **48**, 17097–17105.

   "***Pyramidal dicationic Ge(II) complexes with homoleptic neutral pnictine coordination: A combined experimental and density functional theory study***" R. P. King, V. K. Greenacre, W. Levason, J. M. Dyke and G. Reid, *Inorg. Chem.*, 2021, **60**, 12100–12108.

   "***Tin(IV) fluoride complexes with neutral phosphine coordination and comparisons with hard N- and O-donor ligands***" R. P. King, M. S. Woodward, J. Grigg, G. McRobbie, W. Levason and G. Reid, *Dalton Trans.*, 2021, **50**, 14400–14410.

   "***Neutral and cationic germanium(IV) fluoride complexes with phosphine coordination – synthesis, spectroscopy and structures***" R. P. King, W. Levason and G. Reid, *Dalton Trans.,* 2021, **50**, 17751-17765.

Signature: ..... Date: 24/12/2021

Acknowledgements

I would first and foremost like to thank my supervisors Professor Gillian Reid and Professor William Levason for their constant support and guidance throughout my PhD. I would like to thank Dr Victoria Greenacre and Professor John Dyke for their assistance with DFT calculations. I would also like to thank Dr Alexander Wallace, Dr Shibin Thomas and Alexander Black for performing electrochemical experiments for me as well as the characterisation of thin film deposits. I also thank Dr Mark Light for assistance and advice for the more difficult to solve crystal structures, as well as Dr Neil Wells for his help with all aspects of NMR spectroscopy. I would like to thank the EPSRC for providing the funding for the project, and also to the wider ADEPT team who provided me with the opportunity to be part of such an interesting interdisciplinary project.

I would like to thank Lackshana, Hannah and Charlotte for being fantastic project students. I would also like to extend my thanks to the Reid group past and present, who have made my time here an enjoyable experience and provided countless hours of distraction. Finally, I would like to thank my friends and family for their continued support throughout my PhD

Definitions and Abbreviations

δ	chemical shift (ppm)
ppm	parts per million
eV	electron volt
Coordination shift ($\delta_{complex}$-$\delta_{free\ ligand}$)	
NOE	Nuclear Overhauser Effect
n.o.	not observed
Å	10^{-10} m (angstrom)
Me	methyl
NHC	N-heterocyclic carbene
Mes	mesityl
$[BAr^F]^-$	tetrakis[3,5-bis(trifluoromethyl)phenyl]borate
HSAB	Hard-Soft Acid-Base theory
η	chemical hardness
η_s	absolute hardness
I_a	ionisation potential
A_s	electron affinity
Et	ethyl
^{i}Pr	isopropyl
^{n}Pr	n-propyl
hex	n-hexyl
Bn	benzyl
LUMO	lowest unoccupied molecular orbital
HOMO	highest occupied molecular orbital
Cy	cyclohexyl
Ph	phenyl
R	alkyl or aryl group

Definitions and Abbreviations

R^F	fluorinated alkyl group
L	general ligand
M	metal
E	pnictogen
3c-4e	three centre four electron bond
σ	sigma symmetry orbital
π	pi symmetry oribital
θ	angle
X	halide
o-	ortho
^{n}Bu	n-butyl
J	joule
Tol	toluene ($C_6H_5CH_3$)
[BAr^{Cl}_4]	tetrakis(3,5-Cl_2-C_6H_3)borate
WCA	weakly coordinating anion
Cp	cyclopentadienyl
Cp*	pentamethylcyclopentadienyl
DMAP	4-dimethylaminopyridine
18-crown-6	1,4,7,10,13,16-Hexaoxacyclooctadecane
15-crown-5	1,4,7,10,13-Pentaoxacyclopentadecane
12-crown-4	1,4,7,10-Tetraoxacyclododecane
Me3tacn	1,4,7-trimethyl-1,4,7-triazacyclononane
[24]aneS8	1,4,7,10,13,16,19,22-octathiacyclotetrcosane
2,2,2-crypt	4,7,13,16,21,24-hexaoxa-1,10-diazabicyclo[8.8.8]hexacosane
tBu	tert-butyl
Dipp	2,6-diisopropylphenyl
IR	infrared
THF	tetrahydrofuran
Dioxane	1,4-dioxacyclohexane

Definitions and Abbreviations

TMSOTf	trimethylsilyl trifluoromethanesulfonate (Me3SiO3CF3)
OTf	triflate (CF3SO3-)
Ch	chalcogen
l-triphos	bis(diphenylphosphinoethyl)phenylphosphine
tbbipy	tbbipy = 4,4’-di-tertbutyl-2,2’-bipyridine
DMSO	dimethylsulfoxide
HMPA	hexamethylphosphoramide
PET	positron emission tomography
MeCN	acetonitrile
NMR	nuclear magnetic resonance
efg	electric field gradient
J	coupling constant
s	singlet
d	doublet
t	triplet
q	quartet
quint	quintet
m	multiplet
DFT	density functional theory
NBO	natural bond orbital
rcov	covalent radius
rvdw	van der Waals radius
d(M-X)	bond distance between M and X
{1H}	proton decoupled
%	percentage
Hz	Hertz
v	frequency
py	pyridine
Bipy	2,2’-bipyridine

Definitions and Abbreviations

Terpy	2,6-bis(2-pyridyl)pyridine
Phen	1,10-phenanthroline
Me4cyclam	1,4,8,11-tetramethyl-1,4,8,11-tetraazacyclotetradecane
Me4cyclen	1,4,7,10-tetramethyl-1,4,7,10-tetraazacyclododecane
Me3[9]aneN3	1,4,7-trimethyl-1,4,7-triazacyclononane
[9]aneS3	1,4,7-trithiacyclononane
BIMEt	tris(1-ethyl-benzoimidazol-2-ylmethyl)amine
pmdta	N1-[2-dimethylamino)ethyl]-N1,N3,N3-trimethylethane-1,2-diamine
pyNO	pyridine-1-oxide
˚C	degrees Celsius
K	Kelvin
fac	facial
mer	meridional
TEMPO	2,2,6,6-tetramethylpiperidin-1-yl)oxyl
AACVD	aerosol assisted chemical vapour deposition
LPCVD	low pressure chemical vapour deposition
FTO	fluorine doped tin oxide
GST	germanium antimony telluride
CV	Cyclic voltammetry
GC	Glassy Carbon
V	Volt
WE	working electrode
RE	reference electrode
CE	counter electrode
EDX	energy dispersive X-ray spectroscopy
SEM	scanning electron microscopy
XRD	X-ray diffraction
SCE	saturated calomel electrode

Chapter 1 Introduction

The work described in thesis is concerned with the development of the chemistry of group 14 complexes with pnictine ligands, with the primary aim of generating cationic complexes and exploring their properties and structures. It also describes the development of single source precursors for the electrodeposition of Sb_2S_3 and Sb_2Se_3 thin films. This introductory chapter sets out to provide a general background for the chemistry described in the thesis. The introductions to each individual chapter will provide the more detailed backgrounds directly relevant for the work therein.

1.1 Modern main group chemistry

Main group (group 13-18) chemistry has undergone a renaissance in the last 50 years. One of the most important findings was the discovery of multiply bonded species between heavier main group elements. Prior to this it was thought that elements past row two could not form multiple bonds.[1] One of the earliest developments in this field was the isolation of compound with a Sn=Sn double bond. The distannylene $[Sn\{CH(SiMe_3)_2\}_2]_2$ was reported in 1976 (shown in **Figure 1.1**). It has a bent geometry, which is in contrast to alkene double bonds which are planar.[2] This was followed by the first disilylene, $[Si\{2,4,6\text{-}(Me)_3C_6H_2\}]_2$ which was reported in 1981 (with the structure reported in 1983),[3] the digermylene, $[Ge\{CH(SiMe_3)_2\}_2]_2$ followed in 1984,[4] with the first crystallographically authenticated diplumbylene, $[Pb\{Si(SiMe_3)_3\}\{2,4,6\text{-}(CF_3)_3C_6H_2\}]_2$ discovered in 1998.[5] Multiply-bonded main group species are of fundamental interest due to their ability to act as transition metal mimics and have been shown to be able to activate dihydrogen.[6]

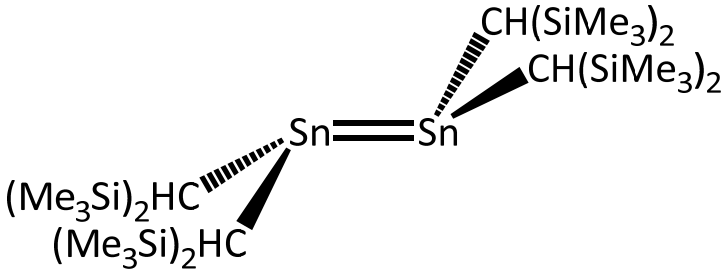

Figure 1.1 – The structure of the distannylene $[Sn\{CH(SiMe_3)_2\}_2]_2$.[2]

One way of stabilising reactive main group species is through the use of bulky ligands. Bulky amide ligands are a popular choice, and have been used to stabilise a variety of unusual complexes. An important recent example was the isolation of pseudo-one coordinate complexes of M(II) (M = Ge – Pb), using the bulky carbazolyl ligand (L = 1,8-bis(3,5-di-tert-butylphenyl)-3,6-di-tert-butyl-carbazole), the structure of the cation for M = Ge is shown in **Figure 1.2** below. Other related bulky amide ligands and their applications to main group chemistry are covered in a recent review.[7]

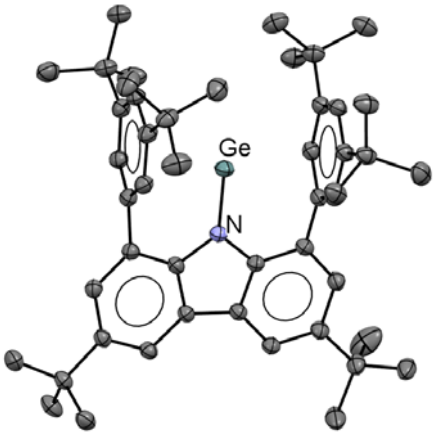

Figure 1.2 – A pseudo-one coordinate germanium dication in $[Ge(L)][Al(OC_4F_9)_4]$. Redrawn from Ref. 8.

Another way to stabilise reactive main group species is by using strong donor ligands. A leap forward in this area was the discovery of N-heterocyclic carbenes (NHCs). The first stable NHC was 1,3-di(1-adamantyl)imidazlin-2-ylidene discovered by Arduengo and co-workers, (see **Figure 1.3** below).[9] NHCs are good sigma-donors and therefore are very useful ligands to stabilise main group species, especially those in low oxidation states or highly charged species, with one of the earliest examples being the carbene adduct, $[(IMes)GeI_2]$ (IMes = 1,3-di(mesityl)imidazlin-2-ylidene), where germanium in is the +2 oxidation state.[10] It has even been possible to isolate zero-valent species, including the complex [LSi=SiL] (L = $:C(N(2,6\text{-}^{i}Pr_2C_6H_3)CH)_2$), which is an example of a Lewis base stabilised silicon-silicon double bond.[11] Carbenes can also be used to stabilise highly charged cations, for example in the dication $[Ge(NHC)_3]^{2+}$ (NHC = 1,3-diisopropyl-4-5-dimethylimidazol-2-ylidene) as reported by Baines *et al.*[12]

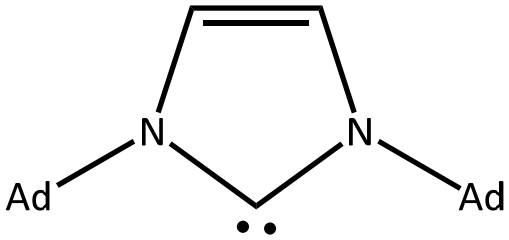

Figure 1.3 – Arduengo's NHC (Ad = $(C)(CH)_3(CH_2)_6$) .[9]

NHCs and phosphines can be compared as they are both neutral two-electron σ-donors, although NHC ligands are far more widely used for the stabilisation of reactive main group species. In transition metal chemistry NHCs are often preferred over phosphines due to the fact they are weaker π-acceptors and hence lead to more electron rich metal centres. However, back-donation from main group elements to the ligand is usually not possible. Therefore, there should be no fundamental reason why phosphine should not in principle be able to stabilise reactive main group centres. A recent computational study suggests that M=M (M = Si – Pb) complexes stabilised by phosphines should be stable if an appropriate route is found for their synthesis.[13] Recently some examples of main group cations of group 13 stabilised by phosphine ligands have even been reported.[14,15] These facts demonstrate that there may be a wide range of reactive main group species that can be stabilised by phosphines.

Highly reactive main group cations often require the use of weakly coordinating anions (WCAs) such as halometallates ($[AlCl_4]^-$, $[SbF_6]^-$) and triflate ($[OTf]^-$). These and other WCAs are discussed in a recent review.[16] Perhaps one of the most significant developments in this area was the synthesis of $Na[BAr^F]$ (the anion is shown in **Figure 1.4** below) by the group of Kobayashi. This large, diffuse anion can be used to stabilise cations with a variety of p-block elements from groups 13 to 15.[17–19]

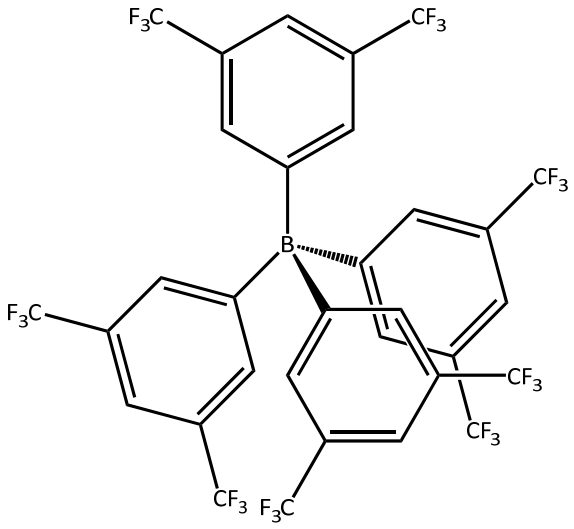

Figure 1.4 – The structure of the $[BAr^F]^-$ anion.

1.2 Hard/Soft Acid/Base theory

The hard/soft acid/base theory categorises chemical species into four broad groups; it is based on the Lewis definition of acids and bases,[20] where acids are electron-pair acceptors and bases are electron-pair donors. Here 'hard' refers to species that are small, highly charged and weakly polarisable; hard acids tend to be in high oxidation states. For example, the alkali metals and $AlCl_3$ are hard acids, while species such as F^- and OH^- are hard bases. 'Soft' species are highly polarisable, tend to be in lower oxidation states and are large. For example, PR_3 and I^- are soft Lewis bases and Ag^+ and CH_3Hg^+ are soft Lewis acids. Within this system, hard-hard and soft-soft interactions lead to more stable complexes.[21] However, this is only a qualitative theory, and there are many examples where this theory fails, for example, the formation of complex $[Na([24]aneS_8)][BAr^F]$ ([24]$aneS_8$ = 1,4,7,10,13,16,19,22-octathiacyclotetrcosane) (shown in **Figure 1.5**), Na^+ is a hard Lewis acid and thioethers are soft Lewis bases, which suggest that the formation of the complex would be unfavourable. It is clear that the complexes with mismatched hard/soft pairs can form under specific conditions. In the case above, a weakly coordinating solvent (CH_2Cl_2) was used, as well as the bulky, non-coordinating $[BAr^F]^-$ anion, which allowed for the isolation of such an unusual complex.[22]

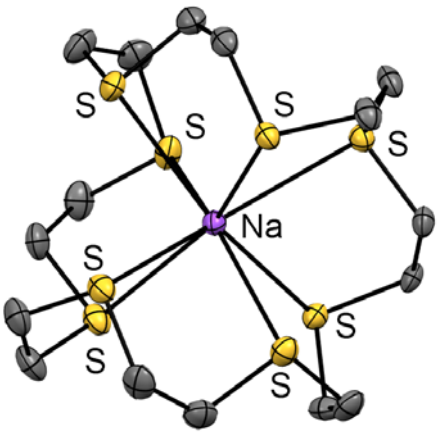

Figure 1.5 – Structure of the unusual cation, $[Na[24]aneS_8]^+$ Redrawn from Ref. 22.

Hard-Soft Acid-Base (HSAB) theory was first a qualitative theory. To turn it into a more quantitative theory, the concept of chemical hardness (η) was introduced. Pearson and Parr defined Absolute Hardness (η_s) which is exactly equal to half the second derivative of energy with respect to change in the number of electrons (**equation 1.1**); using the finite difference formula, it can be estimated to be half the ionisation potential (I_s) minus the electron affinity (A_s) (**equation 1.2**). Species with high values of absolute hardness are classified as 'hard' and those with a low values are classified as 'soft'.[23]

$$\eta_s = \frac{1}{2}\left(\frac{\partial^2 E}{\partial N^2}\right)_z \qquad \textbf{equation 1.1}$$

$$\eta_s \approx \frac{1}{2}(I_s - A_s) \qquad \textbf{equation 1.2}$$

One of the themes of this thesis is the reaction of group 14 halides (Si-Sn) with pnictine ligands and the halide abstraction chemistry of the resultant complexes. In these cases, the group 14 halides would be considered hard acids with hardness increasing from iodine to fluorine. Pnictine ligands in this scheme would be soft bases, becoming softer down the group. Also, as the charge on the metal centre increases, so does the hardness of that centre.

1.3 Bonding in p-block pnictine complexes

For the phosphine complexes of transition metals, a σ-bonding and π-acceptor model can be used, with the phosphine lone pair donating into an empty metal d-orbital and a filled d orbital back-donating into an empty P-R σ* orbital.[24] However, in the p-block, the filled (n-1)d-orbitals are too low in energy to interact with the antibonding orbitals on the ligand. Therefore, the bonding in most phosphine complexes of p-block elements is dominated by σ-donation from the phosphine ligand to a suitable empty orbital on the metal centre.[25] Within the pnictine ligands, ER_3 (E = N-Bi), ns-np orbital separation increases as the group is descended, meaning that there is less s-p mixing, which increases the s-character of the lone pair, and as a consequence the lone pair is less directional; the orbitals also become more diffuse.[25] These two effects together mean that the σ-donor power of ER_3 decreases as the series is descended, and hence arsines are generally weaker σ-donor ligands than phosphines. Electron donating substituents can increase the σ-donor power of pnictine ligands; an example of this is that alkyl phosphines are much better donors than their aryl phosphine counterparts.[26]

Most of the complexes discussed in this thesis are formally hypervalent, which means they break the octet rule, i.e. more than 8 valence electrons around the central atom.[27] For a linear X-M-X unit, the bonding can be explained by a 3c-4e bonding model where a p-orbital parallel to the X-M-X unit from both ligands interacts with a p-orbital on the metal centre, forming a set of three molecular orbitals in which one is bonding, another is non-bonding, and the last is antibonding, the four electrons from the ligands occupy the bonding and non-bonding orbitals (see **Figure 1.6**). The non-bonding orbitals formally reside on the ligands themselves, so the octet rule at the metal centre is restored.[28] If the substituents on the Lewis acid are different then the σ-bonding orbital will be polarised towards the more electronegative element.[29]

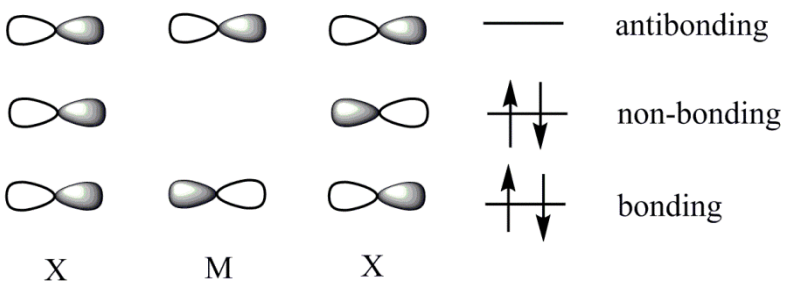

Figure 1.6 – A 3c-4e model of a linear X-M-X unit.[25]

While the d-block elements have an extensive chemistry with pnictine ligands, in recent years pnictine complexes of p-block elements have received more attention, though still to a lesser extent than the d-block. The recent developments in p-block pnictine chemistry have been summarised in a recent review.[30] The E-C bond gets weaker as group 15 is descended, because orbital overlap decreases, hence the bond can more easily break. This in turn means complexes with stibine and bismuthine ligands are rarer than those with phosphine or arsine ligands. Though there are main group complexes featuring stibine and bismuthine ligands, in the case of stibine a set of group 13 halide complexes of the form $[MX_3(SbR_3)]$ (M = B-In; X = Cl-I; R = Et, ^{i}Pr) have been synthesised,[31] and in the case of bismuthine, only complexes with trialkyl-aluminium or -gallium acceptors are known.[32] Due to these facts, the studies in this thesis are mostly restricted to phosphine and arsine complexes, though in some cases attempts to make stibine complexes have been made.

Pnictine ligands can also act as π-acceptors through the E-C σ* antibonding orbitals, these interactions can be described by the Orpen-Connelly model (see **Figure 1.7**), previously it was thought that the phosphorus 3d orbitals were involved in this interaction, but that has been discredited.[33] In most main group complexes pnictine ligands can only act as sigma-donors, though in some cases for main group species with lone pairs back donation can occur (see Chapter 4).

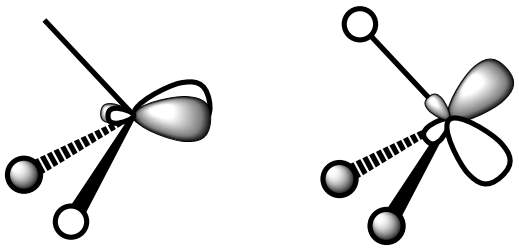

Figure 1.7 – π-acceptor LUMOs on the phosphorus ligand utilise for back-bonding in the Orpen-Connolly model.

Phosphines are the most well studied of this ligand class and are important co-ligands for many homogeneous transition metal catalysed processes, for example the first generation Grubbs olefin metathesis catalyst, ([$PhHCRuCl_2(PCy_3)_2$]),[34] Wilkinson's catalyst, ([$Rh(PPh_3)_3Cl$]) for alkene hydrogenation,[35] among others.[36]

The electronic and steric parameters of pnictine ligands can be tuned by altering the R groups. If all the R groups are different then the phosphine can be stereochemically active at phosphorus.[37] One advantage of phosphines over amines is the higher inversion barrier which prevents racemisation.[38] Tolman's cone angle (θ) is one of the most popular metrical parameters for quantifying the steric requirements of phosphine ligands. The Tolman cone angle is defined as the apex angle of a cylindrical cone centred 2.28 Å from the phosphorus atom and which touches the van der Waals radii of the outermost atoms (see **Figure 1.8**).[26] The restriction on the bond distance means that this cone angle has some limitations in term of being quantitative. The larger the cone angle, the larger the steric requirement of the ligand in question (e.g. for PMe_3 θ = 118˚ but for the bulkier P^iPr_3 ligand θ = 160˚). Tolman's cone angle is defined based on phosphine complexes of nickel and is found to underestimate the steric demand of phosphine ligands.

Recently a lot of computational effort has gone into alleviating these problems, one example being determination of the exact cone angles (θ˚) which do not depend on the ligand being 2.28 Å away from the coordination centre and also do not have requirements for the nature of the metal centre. The exact cone angle is defined as the apex of a cone that originates at the metal centre and contains all the atoms of the ligand, where each atom is defined as a sphere with a radius that is the same size as the van der Waals radius .[39] Another computational approach uses calculated Tolman cones angles of complexes with three different geometries. Cone angles are defined for three coordination environments, which are: linear (θ_L), tetrahedral (θ_T) and octahedral (θ_O). Each cone angle

is determined by the lowest energy geometry of a prototypical complex for each geometry, which are: [AuCl(L)] for linear, [$Ni(CO)_3$(L)] for tetrahedral and [$IrCl_3(CO)_2$(L)] for octahedral, where L is the phosphine ligand. The computed cone angles are in general larger than those calculated from crystal structures. For small ligands there is little change between the three cone angles and usually as the congestion at the metal centre increases the cone angle decreases. For larger ligands there can be a strong dependence on coordination environment, in these cases the large change in cone angle is related to a change in the ligands most stable configuration.[40] As group 15 is descended, the cone angle decreases slightly.[41] There are also definitions for both asymmetrically substituted ligands and polydentate ligands.[26]

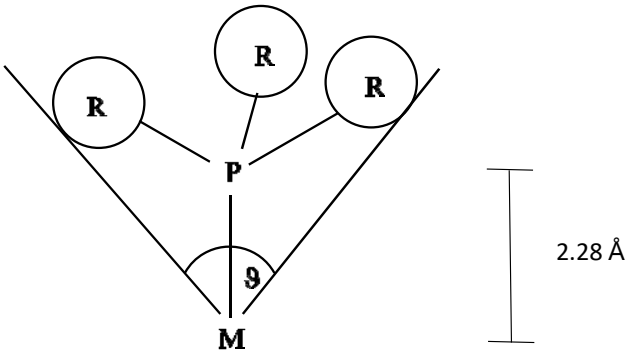

Figure 1.8 – Definition of Tolman's cone angle.[26]

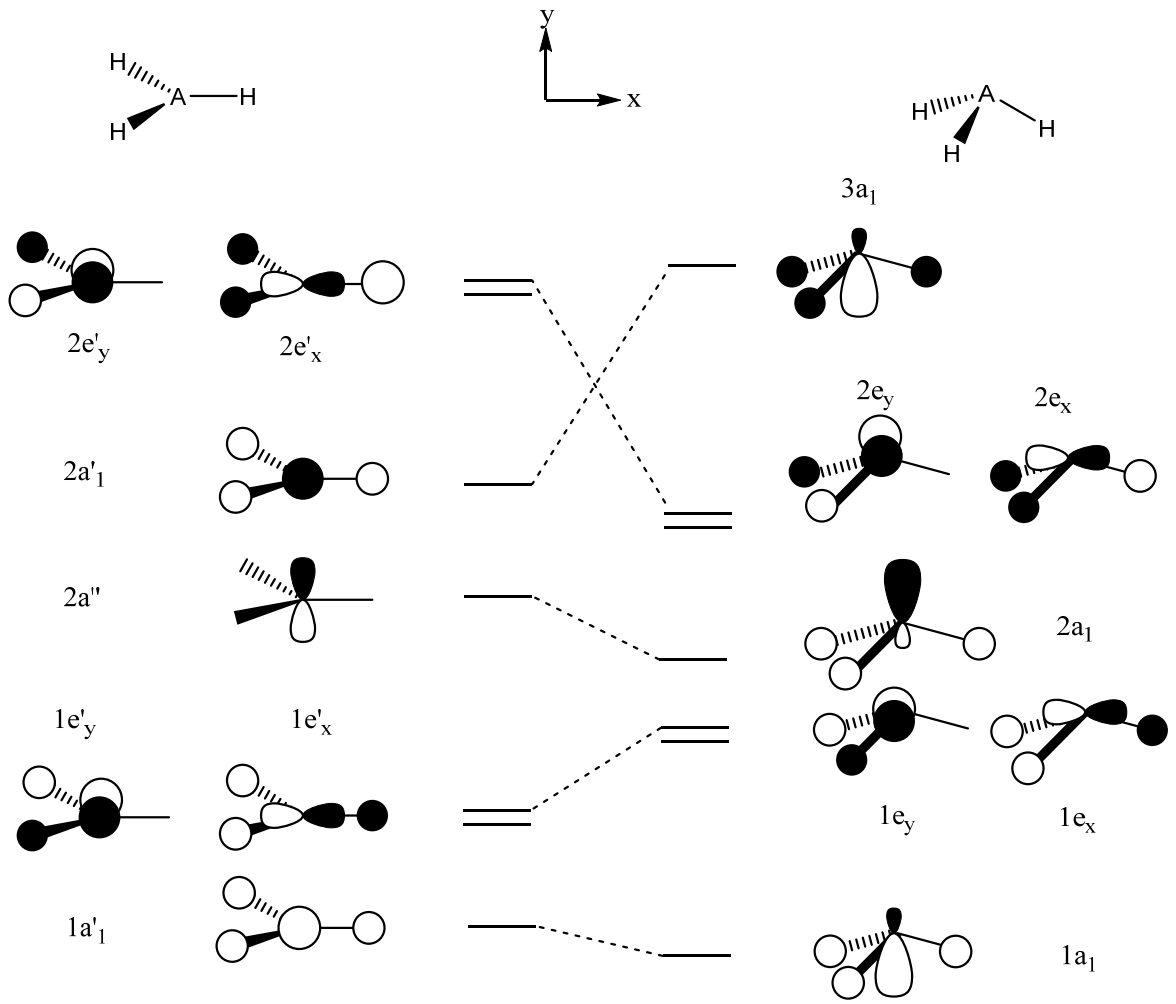

Figure 1.9 – Walsh diagram of the deformation of a PX_3 unit from D_{3h} to C_{3v}.[42]

The Walsh diagram in **Figure 1.9** above shows the effect of planarisation on the relative orbital energies for a PX_3 unit, and this qualitative model can be used to rationalise the alteration of the geometry of a phosphine ligand on coordination. σ-donation from the phosphine lone pair to a metal centre leads to a depopulation of the $2a_1$ orbital, which leads to a higher degree of planarity in the ligand (i.e increases the C-P-C bond angle); allowing for better s-p mixing in the ligand, which leads to a shortening of the P-C distance. π-back-donation fills the 2e type orbitals favouring a pyramidal geometry at the ligand, and in the case of the early transition metals means that the coordinated ligand has a shallower C-P-C angle (illustrated in **Figure 1.10**). However, most main group complexes, especially those in the highest oxidation state, have no orbitals that can participate in back-donation, so the sigma donation effect predominates and hence the C-P-C angles increase. This means for similar complexes, the better a Lewis acceptor a metal centre is, the more planar the ligand will be.[42]

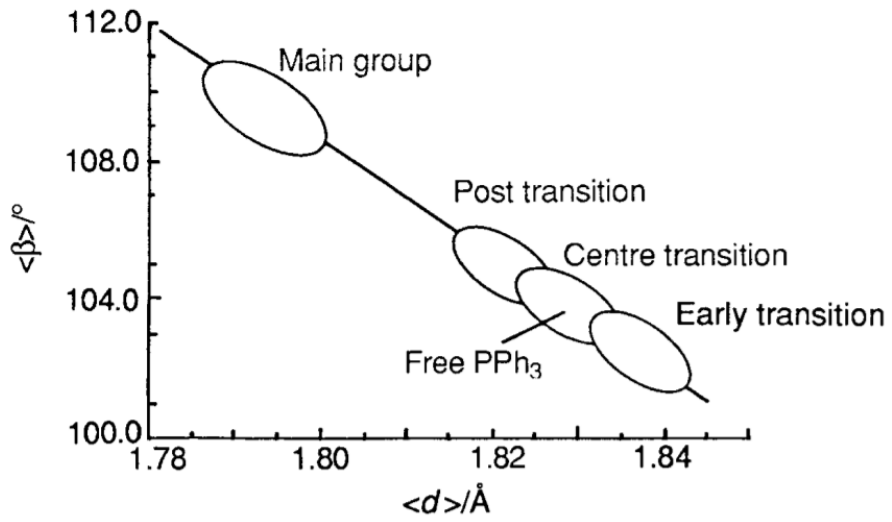

Figure 1.10 – A schematic illustration of the mean C-P-C bond angle <β> against the mean C-P distance <*d*> in $MPPh_3$ compounds reproduced from Ref. 42.

Amongst the pnictogens, only phosphorus has a spin-1/2 nucleus that is naturally abundant, ^{31}P. This means that NMR spectroscopy is an extremely useful probe in the chemistry of phosphine ligands. Coordination of a phosphine to a Lewis acid causes the chemical shift of the phosphorus to change, usually in the high-frequency direction, although this is not always the case.[43] For polydentate phosphines, the size of the chelate ring is also an important contributing factor to the observed chemical shift, with a chelate ring size of five causing a much greater positive shift than otherwise expected.[44]

The most widely used synthetic method for the generation of phosphines is the reaction of halogenophosphines with organometallic reagents, most commonly Grignard reagents.[45] For example, the reaction of PCl_3 with three equivalents of PhMgBr leads to the formation of PPh_3. Alkylphosphines can also be prepared from the reaction of phosphides with alkylhalides.[46] Reduction of phosphine oxides is another popular route to synthesise phosphines, the most common methods using trichlorosilane (Cl_3SiH) as a reducing agent, but other reducing agents have also been used ($LiAlH_4$, AlH_3, BH_3, etc).[47]

Many of the methods used for synthesising monodentate phosphines can be extended to multidentate phosphines. For example, the tripodal phosphine, $CH_3C(CH_2PPh_2)_3$, can be synthesised by the reaction of sodium diphenylphosphide with $CH_3C(CH_2Cl)_3$ (**Scheme 1.1**). Similarly, many bidentate phosphines are obtained by the reaction of $NaPPh_2$ with the appropriate dihaloalkanes.[48] Phosphides synthesised through deprotonation can also

be used to generate diphosphines, for example, the synthesis of DuPhos shown in **Scheme 1.2** below.

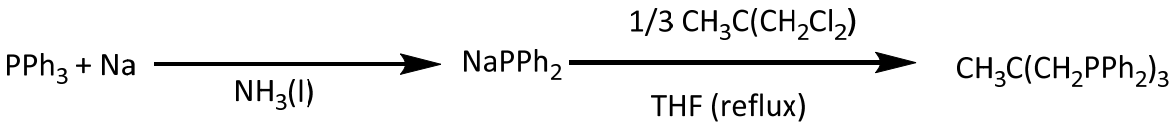

Scheme 1.1 – Synthesis of the tripodal phosphine $CH_3C(CH_2PPh_2)_3$.[48]

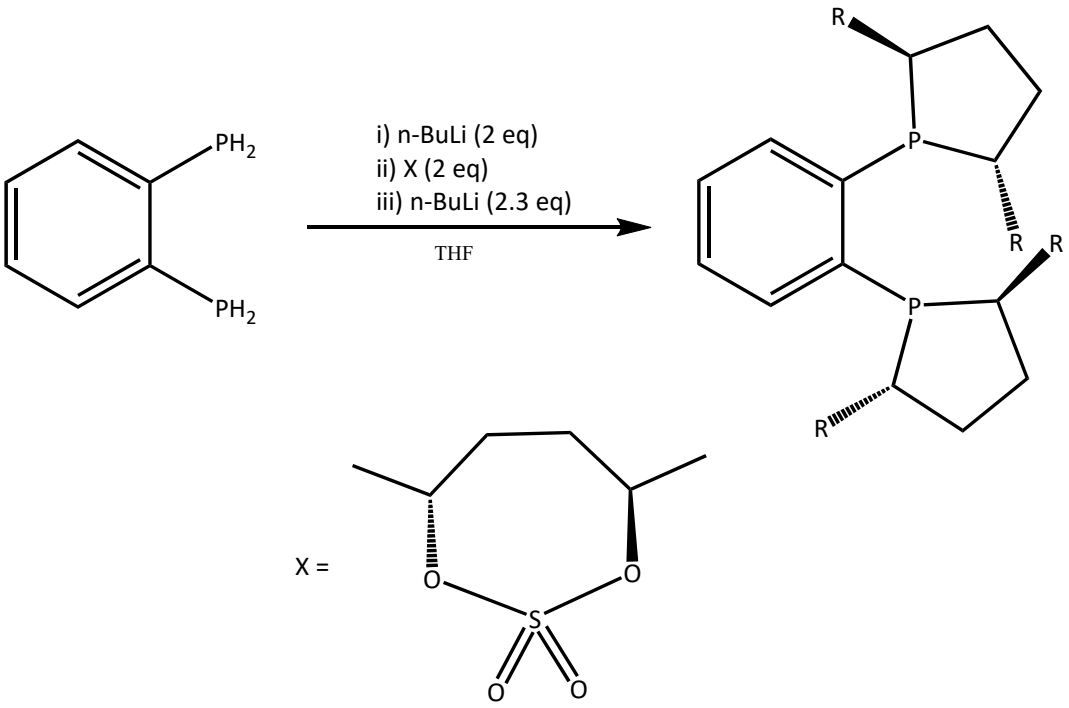

Scheme 1.2 – Synthesis of the chiral ligand DuPhos.

Multidentate phosphine and arsine ligands are important because they can confer extra stability to their resultant complexes through the chelate effect. This means that coordination environments not accessible for monodentate ligands may be accessible for multidentate ligands.

Most of the phosphines used in this thesis can be purchased commercially, but *o*-$C_6H_4(PMe_2)_2$ is not commercially available, so it had to be made in house (either by me or Dr Wenjian Zhang) from a commercially available *o*-$C_6H_4\{P(O)(OMe)_2\}$ precursor. First, the precursor is reduced to 1,2-bis(phosphino)benzene, and through sequential deprotonation and methylation steps, the ligand can be synthesised as illustrated in the reaction scheme below (**Scheme 1.3**) .[49]

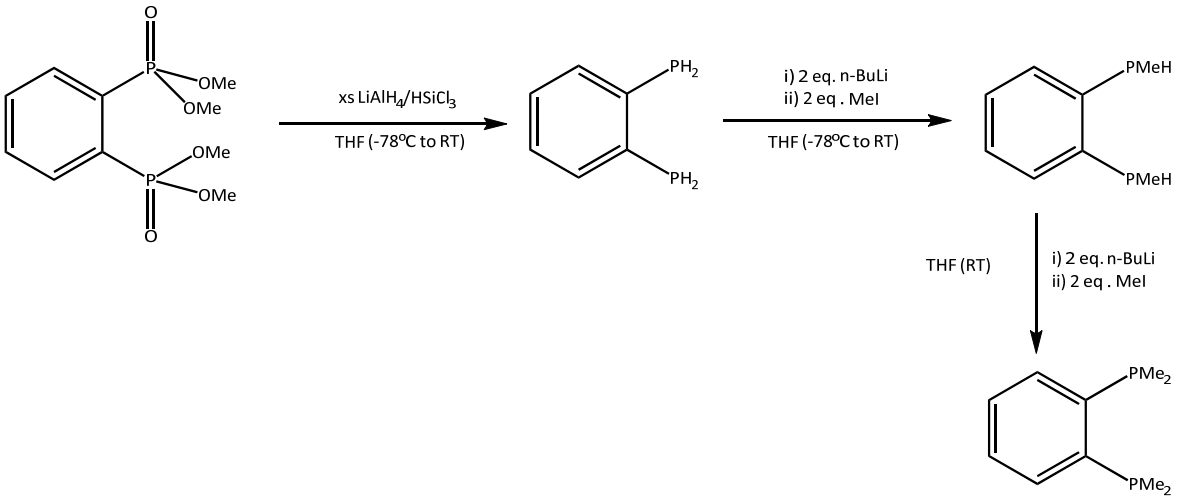

Scheme 1.3 – The synthesis of the ligand *o*-$C_6H_4(PMe_2)_2$.

Similarly, the arsine ligands *o*-$C_6H_4(AsMe_2)_2$ (synthesised by Dr Danielle Smith) and $CH_3C(CH_2AsMe_2)_3$ (made previously in the group) were prepared in-house. Both of them are formed by reaction of a suitable organohalides with an arsenide anion generated *in situ* from the reaction of $IAsMe_2$ with sodium in THF (see **Scheme 1.4**).[50] These methyl substituted pnictine ligands were synthesised because they are stronger donors than their commercial phenyl analogues.

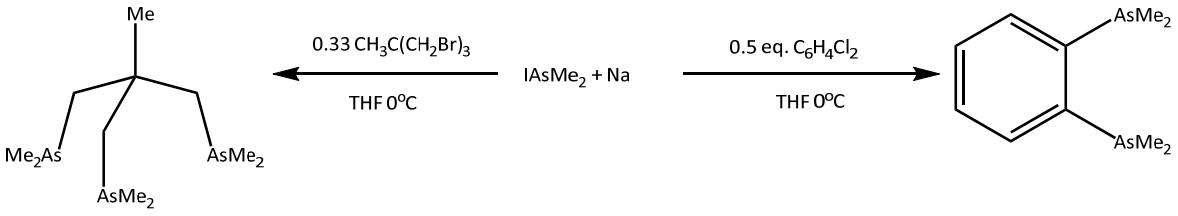

Scheme 1.4 – Synthesis of polydentate arsines.

1.4 Group 14 coordination chemistry

The group 14 elements (C-Pb) have an ns^2np^2 ground state configuration, which means that +4 and +2 are the most common oxidation state for these elements, although examples of these elements in formal +1 and +3 oxidation states are known.[51–53] Due to the inert pair effect, as the group is descended the +2 oxidation state becomes favoured. This explains why silicon chemistry is dominated by Si(IV) complexes and lead chemistry is dominated by Pb(II). The elements in this group are very diverse in their properties and chemistry. Carbon is classed as a non-metal, silicon and germanium as semi-metals, and tin and lead as metals; they are much less electropositive than s-block metals and tend to form covalent complexes. The increase s-p separation down the group means that the +2 oxidation state becomes more stable with respect to the +4 oxidation state; this can be demonstrated by the instability of Pb(IV) compounds, PbF_4 behaving as a strong fluorinating agent.[54] Whereas tin(II) chloride and derivatives are widely used as reducing agents in organic chemistry.[55] Though for silicon, germanium and tin, there are known complexes in both oxidation states.[56–58]

The strongest M-X bond in group 14 (where M = C-Pb and X = F-I) is the Si-F bond with a bond energy of 697 kJ/mol. In general, the bond energies decrease as you go down the halogens and as you go down the series from silicon to lead, with only carbon not following this trend (see **Table 1.1** below). As group 14 is descended, there is a monotonic increase in the covalent radius of the element, whereas the van der Waals radii all fall within a small range for Si-Pb (see Table 1.2).

Table 1.1 – Bond energies of M-X group 14 halide bonds (based on MX_4).[59] (kJ/mol)

	F	Cl	Br	I
C	547	297	242	192
Si	697	462	369	284
Ge	464	352	285	213
Sn	456	305	277	218
Pb	389	297	242	192

Table 1.2 – Covalent and van der Waals radii of group 14 elements.

	Covalent Radius[60]/Å	Van der Waals Radius[61]/Å
C	0.73	1.70
Si	1.11	2.10
Ge	1.20	2.11
Sn	1.39	2.17
Pb	1.49	2.02

The group 14 tetrahalides (Si-Sn) can act as Lewis acids forming stable complexes with both neutral and anionic donor atom ligands. This Lewis acidic behaviour means that they have been exploited as catalysts for a variety of organic transformations.[62] The most common ligand types include nitrogen and oxygen donor atoms, though complexes with softer donor atoms (S, P, As) are known.[63–66] Reactions of the group 14 tetrahalides with neutral ligands can lead to neutral octahedral complexes of the form $[MX_4(L)_2]$ (with L = monodentate ligand) or $[MX_4(L)]$ (L = bidentate ligand). There are two predominant geometries, *trans*-octahedral and *cis*-octahedral. For complexes with bidentate ligands only the *cis* conformation is observed. In monodentate ligand systems both isomers can co-exist, for example in the complex $[SnF_4(OPMe_3)_2]$ solution state data indicate both isomers are present (see Chapter 5).[67] Displacement or abstraction of one halide from a metal centre can lead to formation of complexes that have three neutral donor ligands

coordinated. This can lead to two different six-coordinate geometries, facial (*fac*) and meridional (*mer*) coordination (see **Figure 1.1**). The reaction of Me_3tacn with $SnCl_4$ leads to the formation of *fac*-$[SnCl_3(Me_3tacn)]_2[SnCl_6]$.[68] The reaction of $SiCl_4$ with pmdta (N^1-[2-dimethylamino)ethyl]-N^1,N^3,N^3-trimethylethane-1,2-diamine) and $Na[BAr^F]$ leads to the formation of the complex *mer*-$[SiCl_3(pmdta)][BAr^F]$.[69]

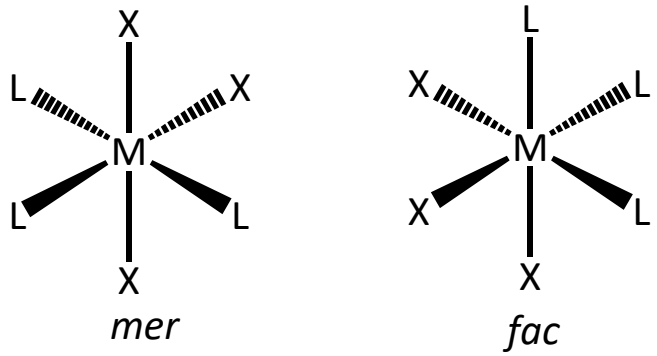

Figure 1.11 – Diagram showing *fac* and *mer* geometries of an octahedral complex.

In systems where the monodentate ligand is bulky or a weak σ-donor, five-coordinate complexes are sometimes seen, for example the reaction of $GeCl_4$ or $SnCl_4$ with the NHC $HCNDipp)_2C$ (Dipp = 2,6-$^iPr_2C_6H_3$) leads to the formation of trigonal bipyramidal complexes of the form $[MCl_4(NHC)]$.[70] The weak σ-donor $AsPh_3$ reacts with $SnBr_4$ to form the complex $[SnBr_4(AsPh_3)]\cdot AsPh_3$ in contrast, $AsPh_3$ reacts with $SnCl_4$ to form *trans*-$[SnCl_4(AsPh_3)_2]$.[71] Five-coordinate complexes are also common when a bidentate mono-anionic ligand is used, one example being the reaction of $LiOCH_2CH_2Me_2$ with $SiCl_4$, which leads to the formation of $[SiCl_3(OCH_2CH_2NMe_2)]$.[72] Halide abstraction can also be used to generate trigonal bipyramidal complexes, for example $[SnCl_3(PMe_3)_2][AlCl_4]$ (see Chapter 2).[73] Only a few complexes with square-based pyramidal geometries are known for the group 14 halides.[74] Four-coordinate M(IV) halide (M = Si – Pb) complexes stabilised by neutral ligands are much rarer, but some are known such as the phosphine complexes $[SnCl_2(PMe_3)_2][AlCl_4]_2$ and $[(PMe_3)_2IPbIPbI(PMe_3)_2][I]$.[73,75]

For the M(II) halides there is the question of lone pair participation, whether it is stereochemically active or not. For low-coordinate complexes the lone pair tends to be stereochemically active. For three-coordinate complexes the most common geometry is pyramidal, with examples known with nitrogen,[76] oxygen,[77] phosphorus (see Chapter 4),[78]

sulfur[79] and carbene[80] donor ligands. For four-coordinate M(II) halide complexes with neutral ligands the disphenoidal structure is the most common, e.g. $[PbBr_2(DMSO)_2]$,[81] $[SnCl_2\{Me_2P(CH_2)_2PPMe_2\}]$.[78] In all the cases described above the lone pair is stereochemically active. However, when the coordination number is greater than six the lone pair is usually stereochemically inactive, for example, in the eight-coordinate complex, $[Ge(12\text{-crown-}4)_2][GeBr_3]_2$[82] and the 10-coordinate complex $[Sn(15\text{-crown-}5)_2][OTf]_2$.[83]

1.5 Cationic main group compounds

1.5.1 Routes to cationic main group compounds

This section describes the synthetic routes to form cationic main group complexes (here defined as the p-block). Cationic main group species are of fundamental interest due to their unusual structures and reactivity. The development in the applications of cationic main group species is another impetus to investigate this area further. Cationic main group species can be used to perform a variety of different reactions, for example $[SiCp^*][BAr^F]$ can be used to catalyse hydrosilylation of alkenes by alkylsilanes,[84] $[Sb(C_6F_5)_4][B(C_6F_5)_4]$ can be used to activate C-F bonds,[85] while the fluorostibocenium salt, $[Cp^*SbF][B(C_6H_5)_4]$, was found to perform a fluorodechlorination of both CH_2Cl_2 and $PPhCCl_3$.[86] As well as being catalysts, low-valent main group compounds can also act ligands, for example both $SnCl_2$ and $GeCl_2$ can act as ligands to transition metal centres.[87] Recently it has been shown that even dicationic complexes can act as ligands to transition metal centres.[88] These factors demonstrate that investigations into the synthesis and reactivity of cationic main group complexes are important to discover new chemistry and maybe replace toxic transition metal catalysts with more benign main group catalysts.

There are many routes to access cationic main group complexes, which have been summarised in a recent review.[16] Oxidation reactions can also lead to the formation of cationic main group complexes, and this can be exemplified by the oxidation of Ga metal with $Ag[Al\{OC(CF_3)\}_4]$ in toluene to form $[Ga(tol)_2][Al\{OC(CF_3)\}_4]$, the reaction of this salt with three equivalents of PPh_3 in *o*-$C_6H_4F_2$ leads to the formation of the complex $[Ga(PPh_3)_3][Al\{OC(CF_3)\}_4]$ through a ligand exchange process, featuring an unusual homoleptic group 13 cation.[14] The heterolysis of element-halogen bonds by Lewis acids

can also be used to generate main group cations. Silyl, silylium or carbenium reagents are commonly used for this type of chemistry. For example, $[Et_3Si][HCB_{11}Cl_{11}]$ can react with Mes_2BF to form the complex $[Mes_2B][HCB_{11}Cl_{11}]$, in which the boronium cation is stabilised by two sterically bulky aryl ligands.[89] Cationic complexes of various p-block elements have been made through this method, including Sb,[86] Al,[90] P,[91] Si,[69] and Ge.[69] Neutral group 13 Lewis acids can be used to generate main group cations, for example, the generation of Sn(IV) phosphine cations and dications (see chapter 2), or the reaction of equimolar amounts of $AlCl_3$ and $MeSe(CH_2)_2SeMe$, which leads to the formation of $[AlCl_2\{MeSe(CH_2)SeMe\}_2][AlCl_4]$ as shown in **Figure 1.12** below.[92]

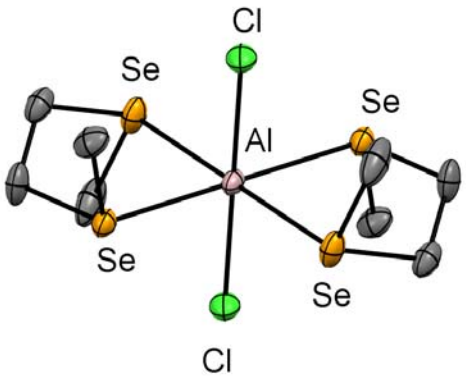

Figure 1.12 – Structure of the cation in $[AlCl_2\{MeS(CH_2)SMe\}_2][AlCl_4]$ redrawn from Ref. 92.

Salt elimination reactions are another widely used class of reactions to generate main group cations. The reaction of $[BCl_3(NHC)]$ (NHC = 1,3-ditertbutylimidazol-2-ylidene) with $Na[BAr^{Cl}_4]$ ($[BAr^{Cl}_4$ = $B(3,5\text{-}Cl_2\text{-}C_6H_3)_4$) leads to the formation of $[BCl_2(NHC)][BAr^{Cl}_4]$ with precipitation of NaCl.[93] This method can be extended to other systems.[69,94,95] Alkyl or hydride metathesis reactions can also lead to the generation of cationic main group complexes; here, Lewis acids are used to abstract an alkyl group or a hydride from a metal centre. Carbenium cations, such as $[CPh_3]^+$ can be used to abstract hydrides, for example, the reaction of $[SiArMe_2H]$ with $[CPh_3][B(C_6F_5)_4]$ leads to the formation of $[SiArMe_2][B(C_6F_5)]$[96]. Electron deficient boranes can act as alkyl group abstractors. For example, the reaction of $AlMe_3$ with $B(C_6F_5)_3$ in Et_2O leads to the formation of the ionic complex $[Me_2Al(OEt_2)_2][MeB(C_6F_5)_3]$.[97]

Insertion of a main group species into a cation has also been used to generate cationic compounds, the reaction of $[NO][Al\{OC(CF_3)_3\}_4]$ with P_4 leads to the insertion of the NO^+ moiety into one of the P-P bonds of the P_4 species leading to the formation of the cation $[P_4NO]^+$.[98] Protonation can also lead to the isolation of cationic complexes. Here Brookhart-like ethereal acids of the form $[H(OEt_2)_2][WCA]$ are commonly used, one example being the protonation of $AlCp_3$ with $[H(OEt_2)_2][Al(OR^F)_4]$ ($R^F = C(CF_3)_3$) in diethyl ether leading to the complex $[AlCp_2{\cdot}2Et_2O][Al(OR^F)_4]$ and CpH.[99] Ion-like weakly associated complexes can also undergo an ionisation process to generate cations, the reaction of $^iPr_3Si(HCB_{11}Cl_{11})$ (in which the carborane is weakly associated with the silicon through a hydrogen bridge) with *o*-$C_6H_4Cl_2$ leads to the formation of $[^iPr_3Si{\cdot}o\text{-}C_6H_4Cl_2][HCB_{11}Cl_{11}]$ where there is a weak association between one of the chlorines in *o*-$C_6H_4Cl_2$ and the silicon centre.[100]

1.5.2 Group 14 cations

The first known example of a group 14 cation was the trityl cation ($[Ph_3C]^+$), which was synthesised in 1887 by Henderson.[101] Fifteen years later, Bayer and Villiger proposed that a solution of triphenylmethane in concentrated sulfuric acid was yellow due to the presence of a carbocation.[102] Even though it was discovered in the 1800's it took until the mid-1900s until it was structurally authenticated. Mesqita determined the structure of the perchlorate salt of the trityl cation, which is approximately trigonal planar at the central carbon.[103] Now many examples of the cation with other anions are known in the literature.[104,105] Similar cations are known for the heavier homologues, with silylium cations being the most explored due to their potent Lewis acidity; bulky counter anions are needed to isolate them as true cations. The first free silylium cation structurally authenticated was in the salt $[Mes_3Si][HCB_{11}Me_5Br_6]$.[106] Similar salts are known for tin[107] and germanium[108]. Most silicon cations are organosilicon compounds, with examples with purely inorganic silicon centres being rarer (this is covered in the introduction to chapter 6).

There are few cationic complexes of the heavier group 14 elements for which the group 14 element is in the +4 oxidation state. Although there are examples known with hard donor ligands, an interesting example being the series of DMAP (4-dimethylaminopyridine) complexes $[Me_2M(DMAP)_2(OTf)_2]$ (M = Si, Ge, Sn). In the Si

complex, the anions are not coordinated to Si, in the Ge complex there are weak contacts between the anions and the germanium, and in the Sn complex the anions are coordinated to the tin centre. The complexes demonstrate a systematic change in behaviour as the group is decended[109] Another example important for this work is the series of tin complexes $[SnCl_{4-n}(PMe_3)_2][AlCl_4]_n$ (n = 0, 1, 2). Here $AlCl_3$ is used as a halide abstraction agent to generate mono- and dications. This is explored more in chapter 2.

More cations and dications are known for Ge and Sn when the metal is in the +2 oxidation state; there are many examples where hard oxygen or nitrogen donor ligands are used. One of the first examples is the complex $[Sn(15\text{-crown-}5)_2][SnCl_3]_2$, which is synthesised by the reaction of $SnCl_2$ with half an equivalent of the crown ether in hot methanol, with the complex crystallising out upon cooling.[110] Complexes of germanium(II)[111] and lead(II)[111] are also known with crown ether ligands with the resultant geometry strongly dependant on the size of the crown ether and metal in question. Examples are also known with mixed oxa-thia macrocycles.[112] There is only one example of a crown ether stabilised cation of silicon, and that is in the complex $[Cp^*Si(12\text{-crown-}4)][B(C_6F_5)_4]$.[113]

1.5.3 Cationic main group complexes stabilised by pnictine ligands

The chemistry of the main group elements with pnictine ligands has been summarised in a recent review.[25] The main group element halides usually form neutral complexes, however, there are examples of cationic complexes and even di-, tri- and tetra-cationic examples known, although they are much rarer. This section will focus on cationic inorganic complexes (i.e. those that do not contain an M-C bond where M is Lewis acid) with pnictine ligand coordination. The reaction of $[BX_3(SMe_2)_2]$ (X = F, Cl) or BX_3 (X = Br, I) with *o*-$C_6H_4(PMe_2)_2$ leads to the formation of cationic complexes of the form $[BX_2\{o\text{-}C_6H_4(PMe_2)_2\}][BX_4]$ (X = F, Cl, Br) or $[BI_2\{o\text{-}C_6H_4(PMe_2)_2\}][I_3]$, the crystal structures of X = Cl-I (e.g. **Figure 1.13**) confirm the ionic nature of these complexes and the tetrahedral geometry around the boron. Analogous cationic complexes can also form with *o*-$C_6H_4(AsMe_2)_2$, demonstrating that changing the donor atom has little effect on the complexes, although the arsine complexes are less stable. The reaction of excess BF_3 with *o*-$C_6H_4(AsMe_2)_2$ leads to the formation of $[BF_2\{o\text{-}C_6H_4(AsMe_2)_2\}][B_2F_7]$, the counter anion results from the reaction of $[BF_4]^-$ with another BF_3 molecule. BF_3 gas is used in this case because the ligand is not basic enough to displace SMe_2 from the $[BF_3(SMe_2)]$. The other

complexes are synthesised directly by the reaction of the ligand with the parent boron trihalide.[114]

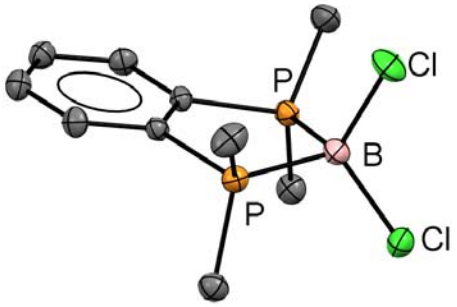

Figure 1.13 – Structure of the cation $[BCl_2\{o\text{-}C_6H_4(PMe_2)_2\}]^+$ in $[BCl_2\{o\text{-}C_6H_4(PMe_2)_2\}][BCl_4]$ redrawn from Ref. 114.

The heavier group 13 halides also form cationic complexes with bidentate pnictine ligands. The reaction of $GaCl_3$ with the preorganised $o\text{-}C_6H_4(PMe_2)_2$ ligand forms $[GaCl_2\{o\text{-}C_6H_4(PMe_2)_2\}_2][GaCl_4]$, which contains a six-coordinate cation, using bulkier ligands can result in the formation of a four-coordinate cations. For example, the reaction of $o\text{-}C_6H_4(PPh_2)_2$ with $GaCl_3$ leads to the formation of $[GaCl_2\{o\text{-}C_6H_4(PPh_2)_2\}][GaCl_4]$, which contains a four-coordinate cation.[115] The reaction of the PNP pincer ligand (shown in **Figure 1.14**) with $GaCl_3$ and $GaBr_3$ leads to the displacement of one of the halides to form five-coordinate cationic complexes of the form $[GaX_2(PNP)][GaX_4]$ (X = Cl, Br).[116] There are no known cations of Tl(III) stabilised by phosphine ligands.

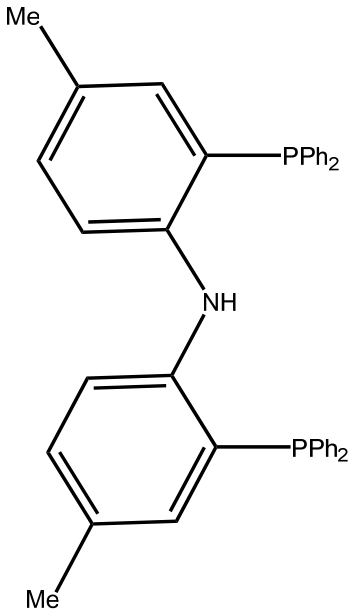

Figure 1.14 – Structure of the PNP ligand.[116]

The reaction of the triarsine ligand $CH_3C(CH_2AsMe_2)_3$ with GaX_3 leads to a variety of products depending on the ratio of GaX_3 used. The reaction of $CH_3C(CH_2AsMe_2)_3$ with three equivalents of GaX_3 (X = Cl or I) leads to the formation of the neutral complex $[\{CH_3C(CH_2AsMe_2)_3\}(GaX_3)_3]$, whereas the reaction of one or two equivalents of $GaCl_3$ with $CH_3C(CH_2AsMe_2)_3$ leads to isolation of crystals of the cationic complexes $[\kappa^2\text{-}\{CH_3C(CH_2AsMe_2)_3\}GaCl_2][GaCl_4]$ and $[\kappa^2,\kappa^1\text{-}\{CH_3C(CH_2AsMe_2)_3\}(GaCl_2)(GaCl_3)][GaCl_4]$. The formation of cations in this system was unexpected due to other non-preorganised arsine ligands only forming neutral complexes under similar conditions.[117]

There is less known about the sub-valent chemistry of group 13 elements due to their inherent instability, with disproportion to the M(0) and M(III) oxidation states being commonly observed for the lighter elements, whereas for thallium, the +1 oxidation state is by far the most common. There are, however, examples of M(I) complexes stabilised by phosphines, including the pyramidal cations $[M(PPh_3)_3]^+$ (M = Ga or In), as well as the carbene-analogous, $[M(P^tBu_3)_2]^+$.[14,15] There are many examples of Tl(I) complexes stabilised by tripodal phosphine ligands, although in these cases, the ligands are anionic and have the form RBP_3 with an anionic borate bridgehead.[118–120]

There are fewer examples of cationic group 14 complexes stabilised by pnictine ligands. For silicon there is only one example, $[SiCl_3(PMe_3)_2][ClO_4]$, reported in the 1960s; however, it was only characterised by partial elemental analysis (Cl content) and IR

spectroscopy, although the spectroscopic data were not reported.[121] For germanium, there are a few cationic phosphine complexes known, although all of these are with Ge(II). This is due to redox chemistry preventing the isolation of Ge(IV) halides complexes with pnictines for halides other than fluoride. The reaction of $[GeCl_2(dioxane)]$ or GeX_2 (X = Br, I) with *o*-$C_6H_4(PMe_2)_2$ in CH_2Cl_2 leads to the formation of the neutral complexes $[GeX_2\{o\text{-}C_6H_4(PMe_2)_2\}]$, however with the related ligand *o*-$C_6H_4(AsMe_2)_2$ the complex $[GeCl\{o\text{-}C_6H_4(AsMe_2)_2\}][GeCl_3]$ forms, featuring a three-coordinate cation. For X = Br, I, the neutral $[GeX_2\{o\text{-}C_6H_4(AsMe_2)_2\}]$ complexes form instead, demonstrating that a subtle change in ligand properties can lead to unpredictable reactivity.[122] Solvent is also important; the reaction of $Ph_2P(CH_2)_3PPh_2$ with two equivalents of $[GeCl_2(dioxane)]$ in THF leads to the formation of $[GeCl\{Ph_2P(CH_2)_3PPh_2\}][GeCl_3]$.[123] There are also a number of cationic complexes featuring mixed PNNP donor ligands (**Figure 1.15**), the reaction of these ligands with two equivalents of $[GeCl_2(dioxane)]$ and two equivalents of TMSOTf leads to the formation of the dicationic complexes $[PNNP(GeCl)_2][OTf]_2$, with each pair of PN donor atoms bonding to one $GeCl^+$ unit.[124] There are no reported examples of Ge(IV) halide cations stabilised by phosphine ligands.

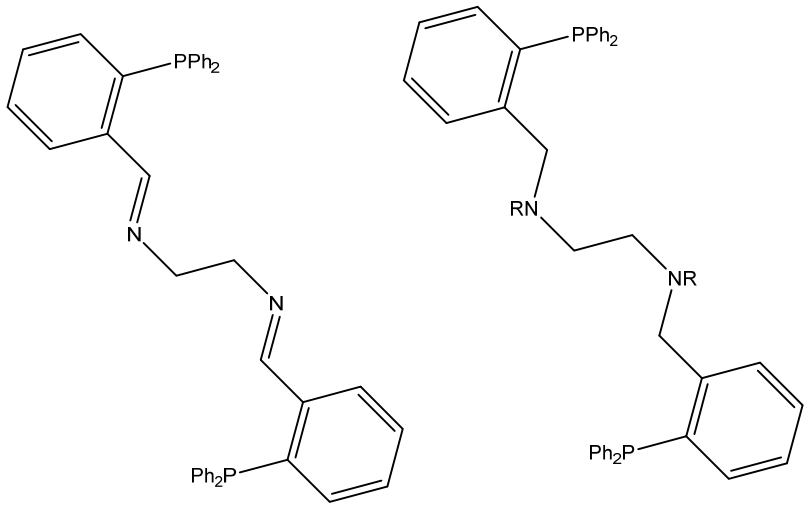

Figure 1.15 – The structure of the PNNP ligands (R = H, Me).

Phosphine stabilised cationic complexes are known for Sn(IV). In 2013 Macdonald *et al.* described the formation of the cationic and dicationic complexes, $[SnCl_3(PMe_3)_2][AlCl_4]$ and $[SnCl_2(PMe_3)_2][AlCl_4]_2$, the first featuring a trigonal bipyramidal cation in the solid state and the second featuring pseudo-tetrahedral dication with two long cation-anion contacts in the solid state.[73] A few pnictine stabilised Sn(II) cations are also known. Like for Ge(II), the reaction of bidentate phosphine ligands with $[SnCl_2(dioxane)]$ leads to the formation of neutral complexes $[SnCl_2(diphosphine)]$ (diphosphine = *o*-$C_6H_4(PMe_2)_2$, *o*-$C_6H_4(PPh_2)_2$, $Me_2P(CH_2)_2PMe_2$) or $[(SnCl_2)\{Ph_2P(CH_2)_2PPh_2\}]$, but like Ge(II), the reaction of $[SnCl_2(dioxane)]$ with *o*-$C_6H_4(AsMe_2)_2$ leads to the formation of the ionic complex, $[SnCl\{o\text{-}C_6H_4(AsMe_2)_2\}][SnCl_3]$, shown in **Figure 1.16** below.[125]

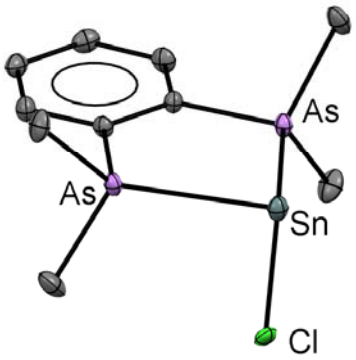

Figure 1.16 – Crystal structure of $[SnCl\{o\text{-}C_6H_4(AsMe_2)_2\}]^+$ redrawn from Ref. 125

For lead, only one cationic pnictine complex has been reported, $[(PMe_3)_2IPbIPbI(PMe_3)_2][I]$, it features a dimeric iodide bridged core [IPb-I-PbI] with two *trans* coordinated phosphines on each lead centre (see **Figure 1.17**).[75]

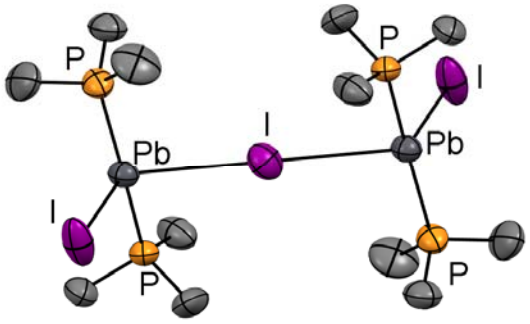

Figure 1.17 – Crystal structure of the $[(PMe_3)_2IPbIPbI(PMe_3)_2]^+$ monocation, redrawn from Ref. 75.

There are many phosphine complexes of antimony(III) chlorides known, with a series of PMe_3 complexes reported by Burford *et al.* featuring neutral, anionic, cationic, and dicationic complexes. The cationic and dicationic complexes were isolated as their triflate salts (**Figure 1.18**).[126,127]

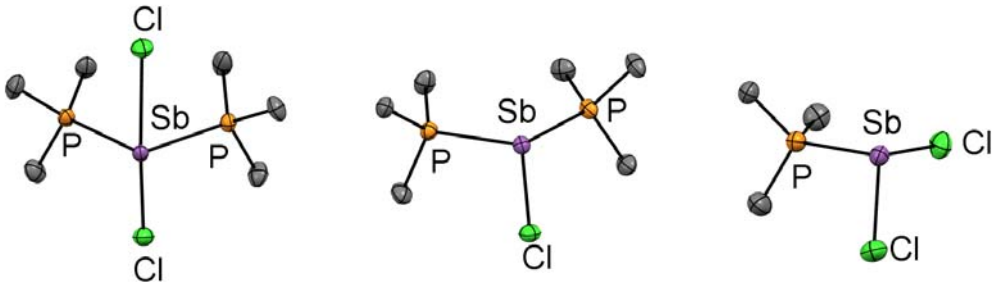

Figure 1.18 – A series of cationic or dicationic Sb(III) halide PMe_3 complexes redrawn from Ref 126 and 127.

There are also examples known with antimony fluoride, the reaction of $[SbF_2(OTf)]$ with one equivalent of TMSOTf and two equivalents of PR_3 leads to the isolation of the complexes $[SbF(PR_3)_2][OTf]_2$ (R = Me, Et). The reaction of SbF_3 with two equivalents of TMSOTf and slightly more than 2 equivalents of PMe_3 leads to the formation of $[(PMe_3Sb)_4][OTf]_4$, featuring a tetracationic Sb_4 square with four coordinated PMe_3 ligands.[128] From a 1:3:3 mixture of SbF_3:TMSOTf:PMe_3 the complex $[Sb(PMe_3)_3][OTf]_3$ can be co-crystallised with $[Me_3PPMe_3][OTf]_2$, the former featuring a $[Sb(PMe_3)_3]^{3+}$ trication.

However, this complex could not be isolated in bulk and decomposes to the tetracation described before. The reaction of $[SbF_2(OTf)]$ with one equivalent of TMSOTf and $Me_2P(CH_2)_2PMe_2$ leads to the formation of $[SbF(OTf)\{Me_2P(CH_2)_2PMe_2\}][OTf]$ (shown in **Figure 1.19**), which is an unusual example of a main group cation containing a metal-fluorine bond.[128]

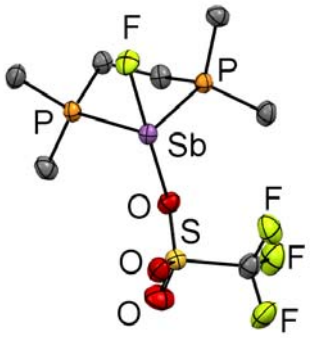

Figure 1.19 – Structure of the cation $[SbF(OTf)\{Me_2P(CH_2)_2PMe_2\}]^+$ redrawn from Ref. 128.

The reaction of the $E(OTf)_3$ (generated from the reaction of $PnCl_3$ with Ag(OTf)) salt (E = As – Bi) with l-triphos ($PhP(Ph_2PCH_2CH_2)_2$) leads to a variety of reaction products; for E = Bi, Sb, simple adducts are observed with the ligand acting in a tridentate manner the crystal structure of $[Sb(l\text{-triphos})(OTf)_3]$ reveals that the triflates are bound in a *fac* arrangement. For E = P, only two chlorides could be removed even with excess Ag(OTf) forming $PCl(OTf)_2$. The reaction of $PCl(OTf)_2$ with l-triphos leads to the formation of the salt $[P\{\kappa^2\text{-}Ph_2P(CH_2)_2PPh(CH_2)_2PPh_2Cl\}][OTf]_2$, here the phosphorus from $PCl(OTf)_2$ is reduced to P(I) and one of the terminal phosphorus atom is oxidised to P(V). The non-oxidised arm and centre phosphorus from the l-triphos ligand coordinate to the P(I) centre. If the halide-free [tbbipy{$P(OTf)_3$}] (tbbipy = 4,4'-di-tertbutyl-2,2'-bipyridine) is used as a source of '$P(OTf)_3$' then the salt $[P\{\kappa^2\text{-}Ph_2P(CH_2)_2PPh(CH_2)_2PPh_2\}][OTf]_2$ can be isolated instead. E = As leads to a mixture of undefined products.[129]

Some cationic E(I) salts are also known; the reaction of AsI_3 with $Ph_2P(CH_2)_2PPh_2$ leads to the formation of the salt $[As\{Ph_2P(CH_2)_2PPh_2\}][As_2I_7\{Ph_2P(CH_2)_2PPh_2\}]$ featuring an As(I) monocation and an As(III) monoanion, with the release of I_2.[130] A phosphorus(I) analogue, $[P\{Ph_2P(CH_2)_2PPh_2\}][I]$, is also known, formed by the reaction of PI_3 with $Ph_2P(CH_2)_2PPh_2$.[131]

There are only a few cationic group 16 complexes stabilised by pnictine ligands known. Complexes of the form $[Ch\{Ph_2P(CH_2)_2PPh_2\}][OTf]_2$ (Ch = Se or Te), which feature two-coordinate Ch(II) dications, can be synthesised by reacting diimide chalcogen triflate precursors (shown in **Figure 1.20a**) with one equivalent of $Ph_2P(CH_2)_2PPh_2$ in CH_2Cl_2. Analogous arsine complexes can be prepared from a similar route, with one example shown in **Figure 1.20b** below.[132]

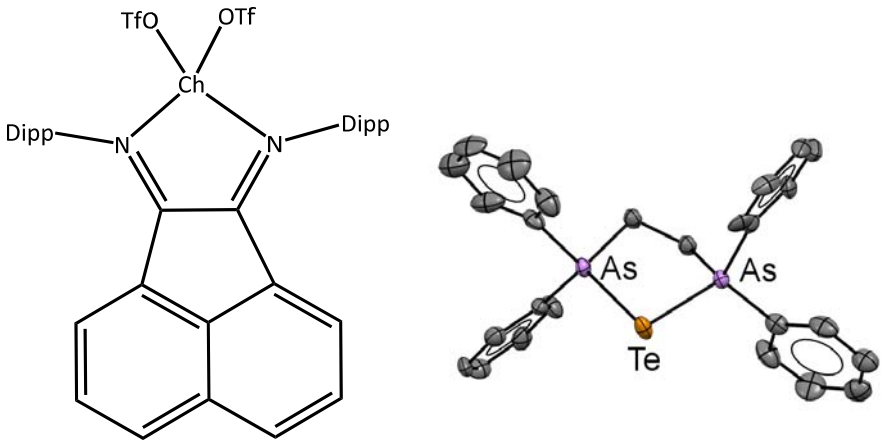

(a) (b)

Figure 1.20 – (a) The structure of the diimide chalcogen triflate precursors (Ch = Se, Te) (b) Crystal structure of the dication $[Te\{Ph_2As(CH_2)_2AsPh_2\}]^{2+}$ redrawn from Ref. 132.

This work demonstrates the existence of a wide range of cationic p-block complexes stabilised by pnictine ligands. However, there are no known complexes of this type stabilised by either stibine or bismuthine ligands and relatively few stabilised by arsine ligands. Apart from antimony and phosphorus (*vide infra*), there are no examples containing fluoride as a co-ligand.

1.6 Main group fluoride chemistry

In the past 15 years there has been a growing interest in the coordination chemistry of main group fluorides driven by two reasons. Firstly, the realisation that the coordination chemistry of fluoride complexes is fundamentally different from that of the other halides, and secondly, the potential to use such compounds as ^{18}F PET (positron emission tomography) tracers.[133]

The coordination chemistry of GeF_4 and SnF_4 towards neutral ligands is reviewed in Chapters 3 and 5, respectively, including rare examples of cationic fluoride complexes. Main group fluorides can be classified into a number of groups depending on their properties. Some are not Lewis acidic, so do not form complexes (e.g. NF_3 or CF_4). Certain fluorides are strongly oxidising and will react with ligands rather than form stable adducts (for example PbF_4). Some main group fluorides exist as monomers and can directly react with ligands (with or without solvent), for example GeF_4 or SiF_4, although complexes of GeF_4 are often synthesised from the reaction of an adduct of GeF_4 with the ligand of choice (here $[GeF_4(MeCN)_2]$ is commonly used). Weakly polymeric fluorides like SbF_5 can react with neutral ligands in solution, whereas others like SnF_4 are strongly polymeric, requiring use of a suitable molecular synthon instead, typically, $[SnF_4(MeCN)_2]$. For elements that form inert polymers with fluoride, substitution of a heavier halide for fluoride can be used for example reacting $[ScCl_3(BnMe_2tacn)]$ with $[NMe_4]F$ to form $[ScF_3(BnMe_2tacn)]$.[134] For indium and gallium the anhydrous trifluorides are inert polymers, but their corresponding hydrates can be used to generate complexes with neutral ligands through hydrothermal synthesis, although the harsh reaction conditions means that ligand scope is limited. For some elements, the chemistry is entirely intractable and no complexes with neutral ligands are known (e.g. BiF_3 and PbF_2).[135]

Cationic main group fluoride complexes (those that do not contain M-C bonds) are even rarer than those of the other halides. In group 15, although there are many examples known for antimony,[128,136–139] examples for the other group 15 acceptors are sparse, although there are examples known arsenic and for phosphorus where the complex $[PF_4\{o\text{-}C_6H_4(PMe_2)_2\}][PF_6]$ is known.[140,141] For group 14, there are examples for silicon ($[SiF_3(Me_3tacn)]$),[142] germanium (discussed in chapter 3) and tin (discussed in chapter 5), although there are no examples with pnictine ligands. For group 13, boron has the most

known examples,[143–146] with a few known for aluminium,[147–149] and one example for gallium, which is the fluoride bridged dication $[\{Ga(terpy)F\}_2\text{-}(\mu\text{-}F)_2][PF_6]_2\cdot 4H_2O$.[150] For most of the examples above, neutral nitrogen donor ligands are used to stabilise the metal centre, and only two cases use phosphine ligands, $[SbF(OTf)\{Me_2P(CH_2)_2PMe_2\}][OTf]$ (shown in **Figure 1.19**) and the phosphine system described above. $[SbF(OTf)\{Me_2P(CH_2)_2PMe_2\}][OTf]$ is synthesised by the reaction of $[SbF_2(OTf)]$ with one equivalent of TMSOTf and $Me_2P(CH_2)_2PMe_2$.[128]

Both phosphines and high valent main group centres can be redox active, and increasing the charge on the metal centre may lead to unusual reactivity, this is therefore an interesting area to study.

1.7 Semiconductors

Semiconductors are technologically very important materials which can be used for a wide variety of electronic applications ranging from thermoelectric materials,[151] phase change memory,[152] and transistors.[153] For semiconductors the valence band is near in energy to the conduction band and the separation between these is termed the band gap (E_g). In intrinsic semiconductors the conduction band is partially filled by thermally excited electrons allowing the material to become conductive. Intrinsic semiconductors become more conductive as the temperature is increased, when the temperature approaches absolute zero they behave like insulators.

Deliberate introduction of small amounts of dopants into an intrinsic semiconductor increases the charge carrier concentration in the material. When the dopant causes an excess of electrons, this is termed n-type doping, for example silicon can be doped with phosphorus atoms to form an n- type semiconductor. When the dopant causes an excess of holes, the semiconductor is said to be p-type.

1.7.1 Antimony(III) chalcogenides

Antimony(III) sulfide, Sb_3S_3, is a direct band gap semiconductor with a band gap of 1.7 eV[154] and can be either n-type or p-type depending on how it is prepared. The structure is formed of infinite ribbon-like chains with the formula $[Sb_4S_6]_n$. These ribbons consist two trigonal pyramids and two square pyramids. The ribbons are connected through longer Sb-S contacts (see **Figure 1.21**).[155,156] The overall one-dimensional structure can give rise to anisotropic optical and electronic properties. Antimony(III) selenide is isostructural with a band gap of 1.2 eV.[157]

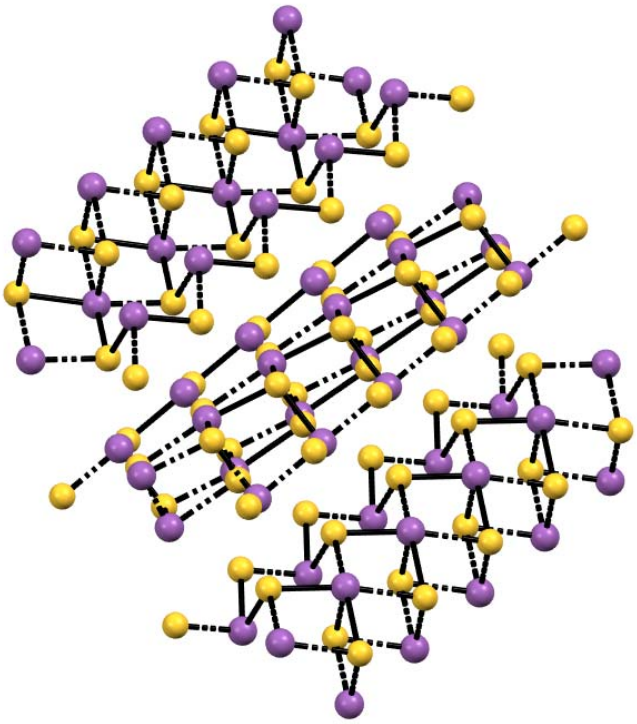

Figure 1.21 – The ribbon-like structures in the crystal structure of Sb_2S_3 (purple = antimony, yellow = sulfur).[156]

Chapter 7 summarises the prior work using various deposition methods for the preparation of antimony chalcogenide thin films and details the development of $[SbS_4]^{3-}$ salts as single source precursors for the electrodeposition of Sb_2S_3 thin films conducted as part of this project.

1.8 Analytical techniques

A variety of analytical techniques have been used to characterise the compounds that have been synthesised in these studies. X-ray crystallography and infrared spectroscopy have been the main techniques used to explore properties in the solid state. Multinuclear NMR spectroscopy is the main technique for characterising the complexes in the solution state and, in some cases, Raman spectroscopy. Elemental analysis (C, H, N) has been used to determine the purity of new compounds, as contaminants can be spectroscopically silent.

1.8.1 Infrared spectroscopy and Raman spectroscopy

All polyatomic molecules vibrate, the vibrational structure of a molecule can be probed by vibrational spectroscopy; infrared spectroscopy is one such technique. Group theory can be used to determine the normal vibrational modes of a molecule. If a vibrational mode has the same symmetry as the coordinate axes, then the mode is IR active as there is a change in the electric dipole moment during the vibration. To be Raman active, there needs to be a change in the anisotropic polarisability of the molecule during the vibration, and this means that Raman spectroscopy is a complementary technique to infrared spectroscopy. In the special case that a molecule is centrosymmetric (i.e. has a centre of inversion), IR and Raman bands cannot be coincident (the rule of mutual exclusion). **Table 1.3** below shows the normal vibrational modes of some common structure types seen in this thesis, showing which modes are IR active.

The position of bands in vibrational spectroscopy depends on two main factors, the masses of the atoms involved and the bond strength between the atoms. If the bond is modelled as a spring, then Hooke's law can provide a relation between the bond strength (κ), reduced mass (μ) and the wavenumber ($\tilde{\nu}$) (**Equation 1.3**). For example, for a series of halide compounds, as you descend the series, the relation predicts that the wavenumber of the band will decrease, this is a useful technique for comparing similar complexes.

$$\tilde{\nu} = \frac{1}{2\pi c}\sqrt{\frac{\kappa}{\mu}}$$

Equation 1.3

Table 1.3 – Normal stretching modes of common complex geometries found in this study[a]

	Point group	ν(M-X)	ν(M-L)
cis-MX_4L_2	C_{2v}	$2A_1 + B_1 + B_2$	$A_1 + B_1$
trans-MX_4L_2	D_{4h}	$A_{1g} + B_{1g} + E_u$	$A_{1g} + A_{2u}$
MX_3L_2	D_{3h}	$A_1' + E'$	$A_1' + A_2''$
MX_3L_2T	C_{2v}	$2A_1 + B_1$	$A_1 + B_2$
Tetrahedral-MX_4	T_d	$A_1 + T_2$	-
Tetrahedral-MX_2L_2	C_{2v}	$A_1 + B_1$	$A_1 + B_1$

[a] Infrared-active modes are italicised

1.8.2 Multinuclear NMR spectroscopy

The main technique for investigating solution state behaviour of the complexes prepared in this thesis is NMR spectroscopy, and a variety of nuclei have been used (see **Table 1.4**), with chemical shifts and coupling constants reported where appropriate. By studying related systems, the magnitudes of these parameters can give valuable information about bonding and trends in these complexes. Most of the NMR spectroscopy in this thesis deals with nuclei that are spin-1/2, which are usually easy to observe. However, in the cases of ^{29}Si and ^{119}Sn, the large negative magnetogyric ratios mean that if the spectra are run ^{1}H-decoupled, then a negative NOE (Nuclear Overhauser Effect) is observed, which diminishes the signal observed, even to the extent of completely nulling the signal. For this reason, these NMR experiments were run without decoupling.[158]

As parts of the work in this thesis, the quadrupolar nuclei ^{27}Al and ^{121}Sb were also used. In these systems, the main relaxation pathway is via quadrupolar relaxation, which is often very fast. Relaxation here is determined by the electric field gradient (efg). In the example of ^{121}Sb NMR spectroscopy, because of the large quadrupole moment, only highly symmetrical species can be observed (e.g. $[SbS_4]^{3-}$ or $[SbCl_6]^{-}$) because they have an efg near zero, which eliminates this relaxation mechanism.[159] A species with symmetry much lower than this, for example, SbR_3, will have lines so broad that they are typically unobservable. ^{73}Ge is a low abundance NMR active nucleus with I = 9/2, therefore in low

symmetry environments the lines are too broad to observe and hence this technique was not used in this thesis.

Dynamic behaviour of complexes in the solution state can also cause line broadening and prevent couplings from being seen. In these cases variable temperature NMR spectroscopy can be used to study dynamic processes that occur on the NMR time-scale.

Table 1.4 – NMR parameters of nuclei used in this thesis[160]

Nucleus	Spin	Natural Abundance (%)	Receptivity Relative to ^{13}C	Quadrupole Moment (10^{-28} m^2)	Magnetogyric ratio (10^6 rad/Ts)
^{1}H	1/2	99.9	5.67×10^3	–	267.5
^{13}C	1/2	1.1	1.00	–	67.28
^{19}F	1/2	100	4.73×10^3	–	251.8
^{27}Al	5/2	100	1.17×10^3	0.14	69.76
^{29}Si	1/2	4.7	2.1	-	-53.19
^{31}P	1/2	100	3.77×10^2	–	168.3
^{119}Sn	1/2	8.6	25.7	–	-100.1
^{121}Sb	5/2	57.25		-0.28	64.35

J-coupling (or spin-spin coupling) is mediated through the Fermi contact mechanism, which requires interactions between the spin of the nucleus to the spin of the electrons in a chemical bond.[161] This requires there to be a non-zero probability of finding an electron at the position of the nucleus, which only holds for s-orbitals, meaning that this interaction can only be mediated through the s-orbital electrons. Thus, the magnitude of the *J*-coupling depends on the s-character of bonds between the atoms.[162] The magnitude of a *J*-coupling also depends on the magnetogyric ratio of the nuclei in question. Coupled nuclei will share a *J*-coupling constant, so these can be used to establish connectivity between atoms in a molecule.

Nearby heavy atoms also affect the chemical shift of atoms; this is termed the 'heavy atom effect'.[163] This effect can help explain why the chemical shifts of group 14 tetraiodides have a much more negative chemical shifts than for the lighter tetrahalide analogues (see **Table 1.5** below).

Table 1.5 – Chemical shift of the tetrahalides of group 14 [160]

	$\delta(^{29}Si)$/ppm[a]	$\delta(^{73}Ge)$/ppm[b]	$\delta(^{119}Sn)$/ppm[c]
MF_4	-109	-	-
MCl_4	-20	31	-150
MBr_4	-94	-311	-623
MI_4	-346	-1081	-1701

[a] Relative to $SiMe_4$ [b] Relative to $GeMe_4$ [c] Relative to $SnMe_4$

1.8.3 X-ray crystallography

Single crystal X-ray diffraction is a very powerful technique for determining the structures of compounds in the solid state. Developments in the equipment used for X-ray diffraction means that data acquisition is relativity quick in the modern age and as a consequence, it has become a central technique for the study of molecular species in the solid state. This technique requires the growth of single crystals, which must be of a suitable size and quality. Many different methods have been developed to allow the formation of single crystals. However, in this thesis, either slow evaporation or layering techniques were used. Crystals are periodic structures; the smallest unit that can be used to generate the crystals through the use of symmetry operations (listed in **Table 1.6**) of the space group is called the asymmetric unit.[164] The space groups can be classified into groups depending on the geometry of the unit cell (see **Table 1.7**), the symmetry of the crystal system determines whether there will be systematic absences. The crystal structure of a compound gives information on chemical identity and geometric parameters.

Table 1.6 – Symmetry operations and their definitions[164]

Translation	All points of the object undergo an equal displacement in a direction
Rotations	A rotation of 360/n about an axis
Rototranslation (screw axis)	The product of a rotation around an axis and a translation along the axial direction
Inversion	Inversion through a particular point
Reflection	Reflection by a mirror plane
Rotoinversion	The product of a rotation around an axis and an inversion with respect to a point on that axis
Glide plane	The product of a reflection and a translation parallel to the reflection plane
Rotoreflection	The product of a rotation and a reflection with respect to a plane perpendicular to the rotation axis

Table 1.7 – Summary of the possible crystal systems and their Laue groups.[164]

Crystal system	Unit cell parameters	Symmetry
Cubic	$a = b = c; \alpha = \beta = \gamma = 90$	$2/m\bar{3}\,, m\bar{3}m$
Hexagonal	$a = b \neq c; \alpha = \beta = 90\,\gamma = 120$	$6/m, 6/mmm$
Trigonal (Rhombohedral) (Hexagonal)	$a = b = c; \alpha = \beta = \gamma \neq 90$ $a = b \neq c; \alpha = \beta = 90\,\gamma = 120$	$\bar{3}, \bar{3}m$ $\bar{3}, \bar{3}m$
Tetragonal	$a = b \neq c; \alpha = \beta = \gamma = 90$	$4/m, 4/mmm$
Orthorhombic	$a \neq b \neq c; \alpha = \beta = \gamma = 90$	mmm
Monoclinic	$a \neq b \neq c; \alpha = \gamma = 90, \beta \neq 90$	$2/m$
Triclinic	$a \neq b \neq c; \alpha \neq \beta \neq \gamma \neq 90$	$\bar{1}$

1.8.4 Cyclic voltammetry and electrodeposition

As part of this work, the design of single source precursors for the electrodeposition of antimony chalcogenide materials was investigated. The electrochemical behaviour of the precursors was studied by cyclic voltammetry (CV) using the experimental set up shown in **Figure 1.22**. The set-up is comprised of three electrodes. For this work glassy carbon electrodes were used as the working electrode (both button and plate types). The reference electrode was the SCE (saturated calomel electrode) (E = +0.241 V *vs* the standard hydrogen electrode), and a platinum rod was used as the counter electrode. The three electrodes are submerged into the electrolyte solution which contains the precursor and the supporting electrolyte.

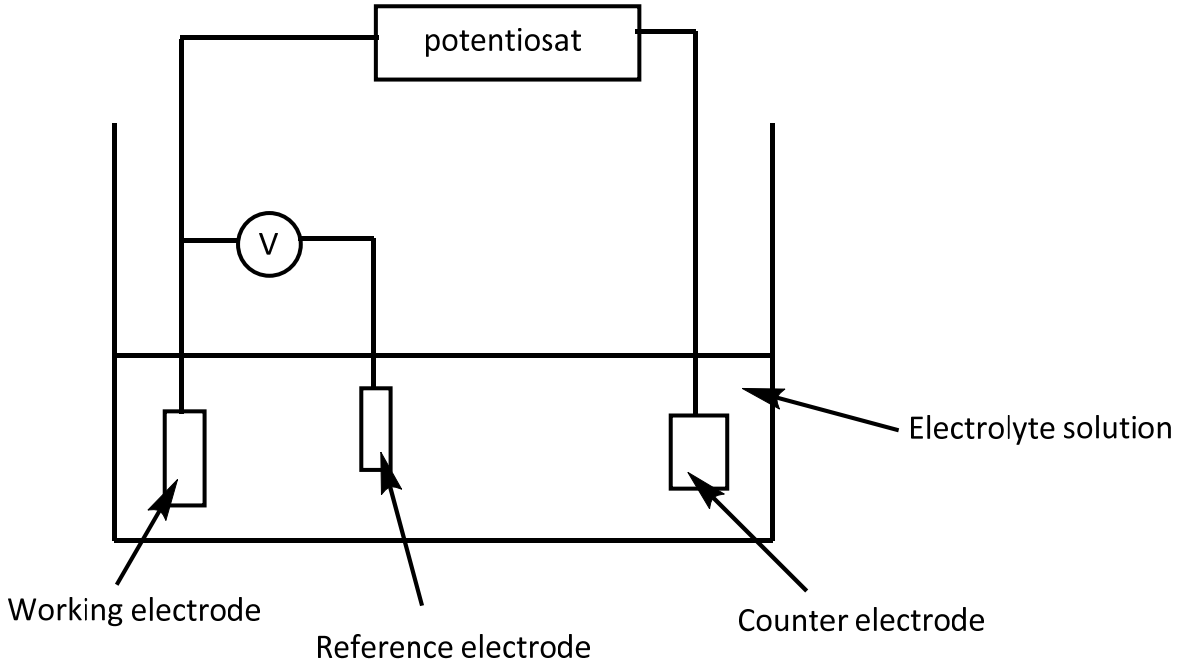

Figure 1.22 – Schematic of the standard three-electrode electrochemical cell showing the working electrode (WE), reference electrode (RE) and counter electrode (CE) immersed in the electrochemical solution.

In a typical cyclic voltammetry (CV) experiment the potential is swept either positively or negatively from one potential (E_1) to another (E_2). The rate at which the potential is swept is called the scan rate. When the second potential is reached, the direction in which the potential is swept is reversed, either back to E_1 or to a third potential (E_3) (see **Figure**

1.23). In a given electrolyte system there is a limit to how far the potential can be swept before the solvent or the electrolyte break down, this is termed the potential window.

Electrodeposition is the process of depositing a material electrochemically. The substrate chosen for electrodeposition must be electrically conducting. One advantage of electrodeposition is that there are many parameters that are controllable, including: substrate, potential, electrolyte, solvent, and precursor. Also, since electrodeposition is not a line-of-sight technique, it is possible to deposit into complex substrate architectures.[152] Potentiostatic electrodeposition is a common way of depositing materials onto an electrode's surface. Here the potential is kept constant as a current is passed, the current passed can be monitored as a function of time, this can be plotted as a chronoamperogram, which usually has a characteristic shape and can give information about the total charged passed and therefore can be used to predict film thicknesses. Films can also be deposited galvanostatically, where the current is kept constant.[165] The cyclic voltammetry process itself can also be used to electrodeposit materials onto electrodes.[166]

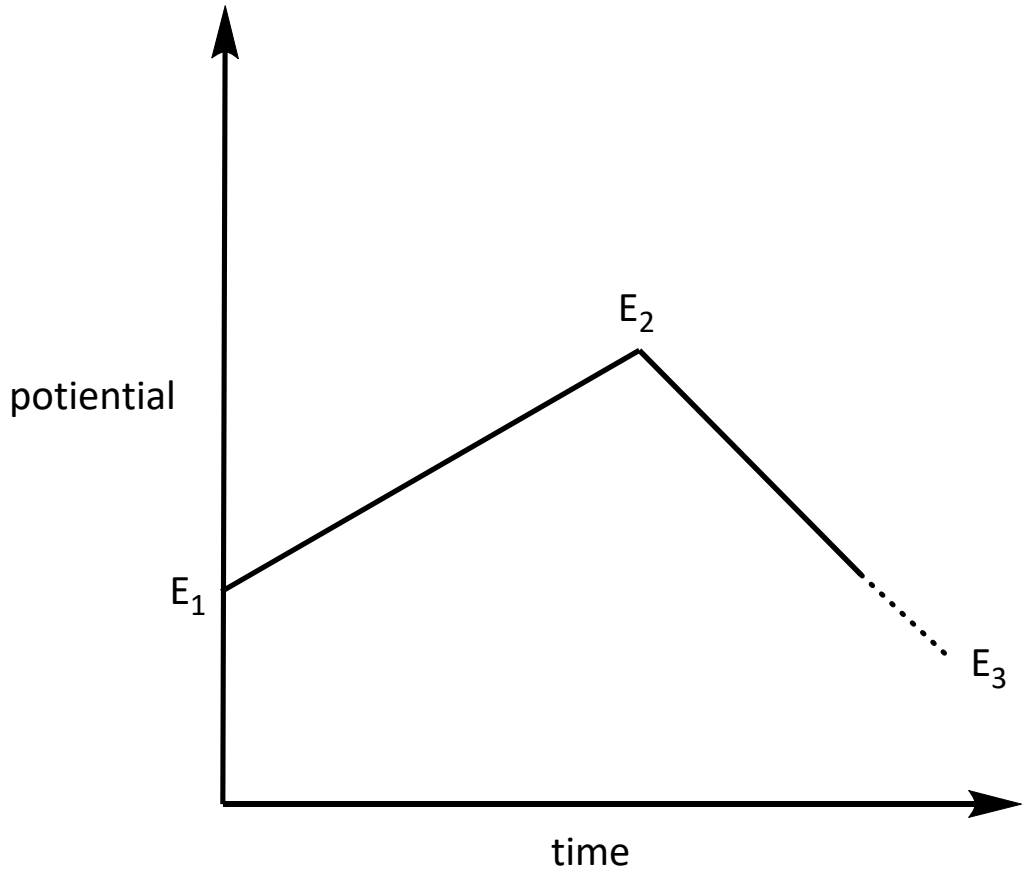

Figure 1.23 – A graph showing the change in potential as a function of time during a cyclic voltammetry experiment

1.9 Density functional theory

Density functional theory (DFT) is a computational modelling method that can be used to investigate the electronic structure of molecules. It can be used to predict the ground-state structure of a molecule and various properties like normal vibrational frequencies and hence IR and Raman spectra, electron density and orbital energies. Here the properties of the molecule are derived from the spatial electron density using functionals which only depend on the three spatial coordinates, rather than dealing with each of the electrons separately, where for N electrons, there would be 3N spatial coordinates.[167]

For DFT, a basis set has to be chosen; here, the molecular orbitals are calculated as the sum of a basis functions multiplied by some coefficient determined by the calculation. In practice, Gaussian basis functions are usually chosen over Slater type functions because they are easier to compute, even though Slater type functions have a more physically correct shape. The exact type of basis set functions used is called the basis set, of which

there are many types. Different types of functions can be added into the basis set to improve the accuracy of the calculation, including polarisation functions and diffuse functions. There is a payoff between accuracy and computational intensity, which means a certain basis set may be sufficient for some systems but not others, hence benchmarking against experimental data is very important.

NBO (natural bond orbital) theory can be used to calculate a set of localised orbitals that describe the electron density on atoms and the bonds between them; NBO's describe the optimal calculated Lewis structure of the molecule (one that has the maximum amount of charge in Lewis type orbitals.[168]

In the present study DFT calculations were performed for several of the systems, specifically those described in Chapters 2, 4, and 6.

1.10 Aims

The primary aim of the work in this thesis was to expand the known coordination chemistry of Group 14 elements (Si-Sn), especially towards pnictine ligands. A specific target was to attempt to generate cationic complexes, which are much rarer than neutral complexes in the p-block and even rarer among neutral pnictine complex of p-block elements. To this end, a halide abstraction methodology was used to try to generate cationic pnictine complexes of Si(IV), Ge(IV), Sn(IV) and Ge(II).

The secondary aim of this thesis was to develop a single-source precursor suitable for use in the electrodeposition of Sb_2S_3 either from an aqueous or non-aqueous solvent to compliment the suite of electrochemical precursors developed previously within the EPSRC ADEPT programme grant and mostly based on halometallate salts to deposit p-block materials. The lack of any suitable sulfur-based haloanions necessitated using an alternative precursor type in order to access p-block sulfide materials, in this case, tetrathio-metallates. Recent work has shown that salts of the tetrathiomoybdate dianion have proven utility for the electrodeposition of MoS_2 thin films,[169,170] providing an important precedent for this work.

1.11 References

1 P. P. Power, Organometallics, 2020, 39, 4127–4138.

2 D. E. Goldberg, D. H. Harris, M. F. Lappert and K. M. Thomas, J. Chem. Soc., Chem. Commun., 1976, 261.

3 M. J. Fink, M. J. Michalczyk, K. J. Haller, R. West and J. Michl, J. Chem. Soc., Chem. Commun., 1983, 1010.

4 P. B. Hitchcock, M. F. Lappert, S. J. Miles and A. J. Thorne, J. Chem. Soc., Chem. Commun., 1984, 480–482.

5 K. W. Klinkhammer, T. F. Fässler and H. Grützmacher, Angew. Chem. Int. Ed., 1998, 37, 124–126.

6 G. H. Spikes, J. C. Fettinger and P. P. Power, J. Am. Chem. Soc., 2005, 127, 12232–12233.

7 D. L. Kays, Chem. Soc. Rev., 2016, 45, 1004–1018.

8 A. Hinz, Chem. Eur. J., 2019, 25, 2367–3271.

9 A. J. Arduengo, R. L. Harlow and M. Kline, J. Am. Chem. Soc., 1991, 113, 361–363.

10 A. J. Arduengo, H. V. R. Dias, J. C. Calabrese and F. Davidson, Inorg. Chem., 1993, 32, 1541–1542.

11 Y. Wang, Y. Xie, P. Wei, R. B. King, H. F. Schaefer, P. von R. Schleyer and G. H. Robinson, Science, 2008, 321, 1069–1071.

12 P. A. Rupar, V. N. Staroverov, P. J. Ragogna and K. M. Baines, J. Am. Chem. Soc., 2007, 129, 15138–15139.

13 D. J. D. Wilson, S. A. Couchman and J. L. Dutton, Inorg. Chem., 2012, 51, 7657–7668.

14 J. M. Slattery, A. Higelin, T. Bayer and I. Krossing, Angew. Chem. Int. Ed., 2010, 49, 3228–3231.

15 A. Higelin, U. Sachs, S. Keller and I. Krossing, Chem. Eur. J., 2012, 18, 10029–10034.

16 T. A. Engesser, M. R. Lichtenthaler, M. Schleep and I. Krossing, Chem. Soc. Rev., 2016, 45, 789–899.

17 S. Bestgen, M. Mehta, T. C. Johnstone, P. W. Roesky and J. M. Goicoechea, Chem. Eur. J., 2020, 26, 9024–9031.

18 N. R. Bunn, S. Aldridge, D. L. Kays, N. D. Coombs, A. Rossin, D. J. Willock, J. K. Day, C. Jones and L. Ooi, Organometallics, 2005, 24, 5891–5900.

19 T. Li, H. Wei, Y. Fang, L. Wang, S. Chen, Z. Zhang, Y. Zhao, G. Tan and X. Wang, Angew. Chem. Int. Ed., 2017, 56, 632–636.

20 G. N. Lewis, Valence and the structure of atoms and molecules, Chemical Catalog Company, Incorporated, New York, 1923.

21 R. G. Pearson, Coord. Chem. Rev., 1990, 100, 403–425.

22 M. J. D. Champion, J. M. Dyke, W. Levason, M. E. Light, D. Pugh, H. Bhakhoa, L. Rhyman, P. Ramasami and G. Reid, Inorg. Chem., 2015, 54, 2497–2499.

23 R. G. Parr and R. G. Pearson, J. Am. Chem. Soc., 1983, 105, 7512–7516.

24 P. B. Dias, M. E. M. de Piedade and J. A. M. Simões, Coord. Chem. Rev., 1994, 135–136, 737–807.

25 J. Burt, W. Levason and G. Reid, Coord. Chem. Rev., 2014, 260, 65–115.

26 C. A. Tolman, Chem. Rev., 1977, 77, 313–348.

27 R. H. Crabtree, Chem. Soc. Rev., 2017, 46, 1720–1729.

28 R. E. Rundle, J. Am. Chem. Soc., 1963, 85, 112–113.

29 G. A. Landrum, N. Goldberg and R. Hoffmann, J. Chem. Soc., Dalton Trans., 1997, 3605–3613.

30 J. Burt, W. Levason and G. Reid, Coord. Chem. Rev., 2014, 260, 65–115.

31 V. K. Greenacre, W. Levason and G. Reid, Organometallics, 2018, 37, 2123–2135.

32 A. Kuczkowski, S. Fahrenholz, S. Schulz and M. Nieger, Organometallics, 2004, 23, 3615–3621.

33 A. G. Orpen and N. G. Connelly, Organometallics, 1990, 9, 1206–1210.

34 P. Schwab, R. H. Grubbs and J. W. Ziller, J. Am. Chem. Soc., 1996, 118, 100–110.

35 J. F. Young, J. A. Osborn, F. H. Jardine and G. Wilkinson, J. Chem. Soc., Chem. Commun., 1965, 131–132.

36 L. H. Pignolet, Ed., Homogeneous Catalysis with Metal Phosphine Complexes, Springer US, Boston, MA, 1983.

37 D. Gatineau, L. Giordano and G. Buono, J. Am. Chem. Soc., 2011, 133, 10728–10731.

38 C. Kölmel, C. Ochsenfeld and R. Ahlrichs, Theor. Chim. Acta, 1992, 82, 271–284.

39 J. A. Bilbrey, A. H. Kazez, J. Locklin and W. D. Allen, J. Comput. Chem., 2013, 34, 1189–1197.

40 J. Jover and J. Cirera, Dalton Trans., 2019, 48, 15036–15048.

41 W. Levason and G. Reid, Coord. Chem. Rev., 2006, 250, 2565–2594.

42 B. J. Dunne, R. B. Morris and A. G. Orpen, J. Chem. Soc., Dalton Trans., 1991, 653–661.

43 M. F. Davis, W. Levason, G. Reid and M. Webster, Dalton Trans., 2008, 2261–2269.

44 P. E. Garrou, Inorg. Chem., 1975, 14, 1435–1439.

45 I. Wauters, W. Debrouwer and C. V Stevens, Beilstein J. Org. Chem., 2014, 10, 1064–1096.

46 D. E. C. Corbridge, Phosphorus: An Outline of its Chemistry, Biochemistry, and Technology (5th ed.)., Elsevier, Amsterdam, 5th edn., 1995.

47 E. Podyacheva, E. Kuchuk and D. Chusov, Tetrahedron Lett., 2019, 60, 575–582.

48 W. Hewertson and H. R. Watson, J. Chem. Soc., 1962, 1490.

49 E. P. Kyba, S. T. Liu and R. L. Harris, Organometallics, 1983, 2, 1877–1879.

50 R. D. Feltham, A. Kasenally and R. S. Nyholm, J. Organomet. Chem., 1967, 7, 285–288.

51 W. D. Woodul, E. Carter, R. Müller, A. F. Richards, A. Stasch, M. Kaupp, D. M. Murphy, M. Driess and C. Jones, J. Am. Chem. Soc., 2011, 133, 10074–10077.

52 H. Fang, Z. Ling, K. Lang, P. J. Brothers, B. de Bruin and X. Fu, Chem. Sci., 2014, 5, 916–921.

53 P. P. Power, C. Stanciu, I. Nowik and R. H. Herber, Inorg. Chem., 2005, 44, 9461–9463.

54 E. R. Bissell and D. B. Fields, J. Org. Chem., 1964, 29, 1591–1593.

55 T. Mukaiyama, K. Tomimori and T. Oriyama, Chem. Lett., 1985, 14, 813–816.

56 V. S. V. S. N. Swamy, S. Pal, S. Khan and S. S. Sen, Dalton Trans., 2015, 44, 12903–12923.

57 H. Fang, Z. Wang and X. Fu, Coord. Chem. Rev., 2017, 344, 214–237.

58 J. N. Jones, J. A. Moore, A. H. Cowley and C. L. B. Macdonald, Dalton Trans., 2005, 3846–3851.

59 Y.-R. Luo, Comprehensive Handbook of Chemical Bond Energies, CRC Press, 2007.

60 B. Cordero, V. Gómez, A. E. Platero-Prats, M. Revés, J. Echeverría, E. Cremades, F. Barragán and S. Alvarez, Dalton Trans., 2008, 2832–2838.

61 M. Mantina, A. C. Chamberlin, R. Valero, C. J. Cramer and D. G. Truhlar, J. Phys. Chem. A, 2009, 113, 5806–5812.

62 K. R. Enslow and A. T. Bell, Catal. Sci. Technol., 2015, 5, 2839–2847.

63 K. George, A. L. Hector, W. Levason, G. Reid, G. Sanderson, M. Webster and W. Zhang, Dalton Trans., 2011, 40, 1584–1593.

64 R. Hulme, G. J. Leigh and I. R. Beattie, J. Chem. Soc., 1960, 366–371.

65 W. Levason, D. Pugh and G. Reid, Inorg. Chem., 2013, 52, 5185–5193.

66 M. F. Davis, W. Levason, G. Reid, M. Webster and W. Zhang, Dalton Trans., 2008, 533–538.

67 M. F. Davis, W. Levason, G. Reid and M. Webster, Polyhedron, 2006, 25, 930–936.

68 G. R. Willey, T. J. Woodman, U. Somasundaram, D. R. Aris and W. Errington, J. Chem. Soc., Dalton Trans., 1998, 2573–2576.

69 M. Everett, A. Jolleys, W. Levason, M. E. Light, D. Pugh and G. Reid, Dalton Trans., 2015, 44, 20898–20905.

70 S. M. Ibrahim Al-Rafia, P. A. Lummis, A. K. Swarnakar, K. C. Deutsch, M. J. Ferguson, R. McDonald and E. Rivard, Aust. J. Chem., 2013, 66, 1235–1245.

71 M. F. Mahon, N. L. Moldovan, K. C. Molloy, A. Muresan, I. Silaghi-Dumitrescu and L. Silaghi-Dumitrescu, Dalton Trans., 2004, 4017–4021.

72 M. Hagemann, A. Mix, R. J. F. Berger, T. Pape and N. W. Mitzel, Inorg. Chem., 2008, 47, 10554–10564.

73 E. MacDonald, L. Doyle, S. S. Chitnis, U. Werner-Zwanziger, N. Burford and A. Decken, Chem. Commun., 2012, 48, 7922–7924.

74 Y. Ding, X. Liu, X. Ma, Y. Liu, M. Zhong, W. Li, Z. Yang and Y. Yang, J. Organomet. Chem., 2018, 868, 55–60.

75 M. D. W. Chunhua Tony Hu, Yuzhou Liu, CSD Commun., 2020, 1977387.

76 Y. Li, Y. Wu, D. Mei and T. Doert, Z. Anorg. Allgem. Chem., 2020, 646, 288–295.

77 M. Ozaki, Y. Katsuki, J. Liu, T. Handa, R. Nishikubo, S. Yakumaru, Y. Hashikawa, Y. Murata, T. Saito, Y. Shimakawa, Y. Kanemitsu, A. Saeki and A. Wakamiya, ACS Omega, 2017, 2, 7016–7021.

78 C. Gurnani, A. L. Hector, E. Jager, W. Levason, D. Pugh and G. Reid, Dalton Trans., 2013, 42, 8364.

79 P. G. Harrison, B. J. Haylett and T. J. King, Inorg. Chim. Acta, 1983, 75, 259–264.

80 C. Jones, A. Sidiropoulos, N. Holzmann, G. Frenking and A. Stasch, Chem. Commun., 2012, 48, 9855–9857.

81 A. D. Baranyi, M. Onyszchuk, Y. Le Page and G. Donnay, Can. J. Chem., 1977, 55, 849–855.

82 F. Cheng, A. L. Hector, W. Levason, G. Reid, M. Webster and W. Zhang, Angew. Chem. Int. Ed., 2009, 48, 5152–5154.

83 R. Bandyopadhyay, B. F. T. Cooper, A. J. Rossini, R. W. Schurko and C. L. B. Macdonald, J. Organomet. Chem., 2010, 695, 1012–1018.

84 E. Fritz-Langhals, Reactions, 2021, 2, 442–456.

85 B. Pan and F. P. Gabbaï, J. Am. Chem. Soc., 2014, 136, 9564–9567.

86 O. Coughlin, T. Krämer and S. L. Benjamin, Dalton Trans., 2020, 49, 1726–1730.

87 S. Bajo, M. G. Alférez, M. M. Alcaide, J. López-Serrano and J. Campos, Chem. Eur. J., 2020, 26, 16833–16845.

88 R. K. Raut and M. Majumdar, Chem. Commun., 2017, 53, 1467–1469.

89 Y. Shoji, N. Tanaka, K. Mikami, M. Uchiyama and T. Fukushima, Nat. Chem., 2014, 6, 498–503.

90 A. V. Korolev, E. Ihara, I. A. Guzei, V. G. Young, and R. F. Jordan, J. Am. Chem. Soc., 2001, 123, 8291–8309.

91 M. Olaru, A. Schröder, L. Albers, D. Duvinage, S. Mebs and J. Beckmann, Chem. Eur. J., 2019, 25, 9861–9865.

92 K. George, M. Jura, W. Levason, M. E. Light and G. Reid, Dalton Trans., 2014, 43, 3637.

93 S. Muthaiah, D. C. H. Do, R. Ganguly and D. Vidović, Organometallics, 2013, 32, 6718–6724.

94 M. Di Vaira, F. Mani and P. Stoppioni, J. Chem. Soc., Dalton Trans., 1998, 3209–3214.

95 Z. Liu, R. Ganguly and D. Vidović, Dalton Trans., 2017, 46, 753–759.

96 S. Duttwyler, Q.-Q. Do, A. Linden, K. K. Baldridge and J. S. Siegel, Angew. Chem. Int. Ed., 2008, 47, 1719–1722.

97 J. Klosin, G. R. Roof, E. Y.-X. Chen and K. A. Abboud, Organometallics, 2000, 19, 4684–4686.

98 T. Köchner, S. Riedel, A. J. Lehner, H. Scherer, I. Raabe, T. A. Engesser, F. W. Scholz, U. Gellrich, P. Eiden, R. A. Paz Schmidt, D. A. Plattner and I. Krossing, Angew. Chem. Int. Ed., 2010, 49, 8139–8143.

99 M. Huber, A. Kurek, I. Krossing, R. Mülhaupt and H. Schnöckel, Z. Anorg. Allgem. Chem., 2009, 635, 1787–1793.

100 S. P. Hoffmann, T. Kato, F. S. Tham and C. A. Reed, Chem. Commun., 2006, 767–769.

101 G. G. Henderson, J. Chem. Soc., Trans., 1887, 51, 224–228.

102 A. Baeyer and V. Villiger, Berichte der Dtsch. Chem. Gesellschaft, 1902, 35, 1189–1201.

103 A. H. Gomes de Mesquita, C. H. MacGillavry and K. Eriks, Acta Crystallogr., 1965, 18, 437–443.

104 A. Schäfer, M. Reißmann, S. Jung, A. Schäfer, W. Saak, E. Brendler and T. Müller, Organometallics, 2013, 32, 4713–4722.

105 O. Hiemisch, D. Henschel, P. G. Jones and A. Blaschette, Z. Anorg. Allg. Chem., 1996, 622, 829–836.

106 K. Kim, C. A. Reed, D. W. Elliott, J. Mueller, L, F. Tham, Lin, L. and J. B. Lambert, Science, 2002, 297, 825–827.

107 J. B. Lambert, L. Lin, S. Keinan and T. Müller, J. Am. Chem. Soc., 2003, 125, 6022–6023.

108 A. Sekiguchi, T. Fukawa, V. Y. Lee, M. Nakamoto and M. Ichinohe, Angew. Chem. Int. Ed., 2003, 42, 1143–1145.

109 A. P. M. Robertson, J. N. Friedmann, H. A. Jenkins and N. Burford, Chem. Commun., 2014, 50, 7979–7981.

110 E. Hough, D. G. Nicholson and A. K. Vasudevan, J. Chem. Soc., Dalton Trans., 1989, 2155–2159.

111 A. Swidan and C. L. B. Macdonald, Chem. Soc. Rev., 2016, 45, 3883–3915.

112 C. Beattie, P. Farina, W. Levason and G. Reid, Dalton Trans., 2013, 42, 15183–15190.

113 K. Leszczyńska, A. Mix, R. J. F. Berger, B. Rummel, B. Neumann, H.-G. Stammler and P. Jutzi, Angew. Chem. Int. Ed., 2011, 50, 6843–6846.

114 J. Burt, J. W. Emsley, W. Levason, G. Reid and I. S. Tinkler, Inorg. Chem., 2016, 55, 8852–8864.

115 F. Cheng, A. L. Hector, W. Levason, G. Reid, M. Webster and W. Zhang, Inorg. Chem., 2007, 46, 7215–7223.

116 K. Yurkerwich and G. Parkin, Inorg. Chim. Acta, 2010, 364, 157–161.

117 F. Cheng, A. L. Hector, W. Levason, G. Reid, M. Webster and W. Zhang, Dalton Trans., 2007, 2207–2210.

118 P. J. Fischer, S. Senthil, J. T. Stephan, M. L. Swift, M. D. Storlie, E. T. Chan, M. V. Vollmer and V. G. Young, Dalton Trans., 2018, 47, 6166–6176.

119 T. A. Betley and J. C. Peters, Inorg. Chem., 2003, 42, 5074–5084.

120 I. Arenas, M. A. Á. Fuentes, E. Álvarez, Y. Díaz, A. Caballero, S. Castillón, P. J. Pérez, E. Alvarez, Y. Diaz, A. Caballero, S. Castillion and P. J. Perez, Inorg. Chem., 2014, 53, 3991–3999.

121 I. R. Beattie and G. A. Ozin, J. Chem. Soc. A, 1969, 2267–2269.

122 F. Cheng, A. L. Hector, W. Levason, G. Reid, M. Webster and W. Zhang, Inorg. Chem., 2010, 49, 752–760.

123 V. A. Béland, Z. Wang, C. L. B. Macdonald, T. Sham and P. J. Ragogna, Chem. Eur. J., 2019, 25, 14790–14800.

124 P. Sahoo, R. K. Raut, D. Maurya, V. Kumar, P. Rani, R. G. Gonnade and M. Majumdar, Dalton Trans., 2019, 48, 7344–7351.

125 C. Gurnani, A. L. Hector, E. Jager, W. Levason, D. Pugh and G. Reid, Dalton Trans., 2013, 42, 8364–8374.

126 S. S. Chitnis, B. Peters, E. Conrad, N. Burford, R. McDonald and M. J. Ferguson, Chem. Commun., 2011, 47, 12331–12333.

127 S. S. Chitnis, N. Burford, R. McDonald and M. J. Ferguson, Inorg. Chem., 2014, 53, 5359–5372.

128 S. S. Chitnis, A. P. M. Robertson, N. Burford, J. J. Weigand and R. Fischer, Chem. Sci., 2015, 6, 2559–2574.

129 S. S. Chitnis, K. A. Vos, N. Burford, R. McDonald and M. J. Ferguson, Chem. Commun., 2016, 52, 685–688.

130 B. D. Ellis and C. L. B. Macdonald, Inorg. Chem., 2004, 43, 5981–5986.

131 B. D. Ellis, M. Carlesimo and C. L. B. Macdonald, Chem. Commun., 2003, 1946–1947.

132 J. W. Dube, M. M. Hänninen, J. L. Dutton, H. M. Tuononen and P. J. Ragogna, Inorg. Chem., 2012, 51, 8897–8903.

133 K. Chansaenpak, B. Vabre and F. P. Gabbaï, Chem. Soc. Rev., 2016, 45, 954–971.

134 E. Curnock, W. Levason, M. E. Light, S. K. Luthra, G. McRobbie, F. M. Monzittu, G. Reid and R. N. Williams, Dalton Trans., 2018, 47, 6059–6068.

135 W. Levason, F. M. Monzittu and G. Reid, Coord. Chem. Rev., 2019, 391, 90–130.

136 R. Suter, H. Sinclair, N. Burford, R. McDonald, M. J. Ferguson and E. Schrader, Dalton Trans., 2017, 46, 7681–7685.

137 A. Swidan, R. Suter, C. L. B. Macdonald and N. Burford, Chem. Sci., 2018, 9, 5837–5841.

138 A. L. Balch, V. J. Catalano, M. A. Chatfield, J. K. Nagle, M. M. Olmstead and P. E. Reedy, J. Am. Chem. Soc., 1991, 113, 1252–1258.

139 S. S. Chitnis, N. Burford and M. J. Ferguson, Angew. Chem. Int. Ed., 2013, 52, 2042–2045.

140 M. Yasumoto, W. Satoh, R. Nadano, Y. Yamamoto and K. Akiba, Chem. Lett., 1999, 28, 791–792.

141 J. M. Dyke, J. W. Emsley, V. K. Greenacre, W. Levason, F. M. Monzittu, G. Reid and G. De Luca, Inorg. Chem., 2020, 59, 4517–4526.

142 F. Cheng, A. L. Hector, W. Levason, G. Reid, M. Webster and W. Zhang, Chem. Commun., 2009, 1334–1336.

143 L. Weber, I. Domke, J. Kahlert and H.-G. Stammler, Eur. J. Inorg. Chem., 2006, 2006, 3419–3424.

144 K. J. Shaffer, T. M. McLean, M. R. Waterland, M. Wenzel and P. G. Plieger, Inorg. Chim. Acta, 2012, 380, 278–283.

145 S. K. Sarkar and P. Thilagar, Chem. Commun., 2013, 49, 8558–8560.

146 H. Euler, A. Kirfel, S. J. Freudenthal and C. E. Müller, Zeitschrift für Krist. - New Cryst. Struct., 2002, 217, 543–545.

147 A. Dimitrov, D. Heidemann, K. I. Khallow and E. Kemnitz, Inorg. Chem., 2012, 51, 11612–11622.

148 A. Dimitrov, D. Heidemann and E. Kemnitz, Inorg. Chem., 2006, 45, 10807–10814.

149 M. Gonsior, I. Krossing and N. Mitzel, Z. Anorg. Allgem. Chem., 2002, 628, 1821–1830.

150 R. Bhalla, W. Levason, S. K. Luthra, G. McRobbie, F. M. Monzittu, J. Palmer, G. Reid, G. Sanderson and W. Zhang, Dalton Trans., 2015, 44, 9569–9580.

151 M. Scheele, N. Oeschler, K. Meier, A. Kornowski, C. Klinke and H. Weller, Adv. Funct. Mater., 2009, 19, 3476–3483.

152 Y. J. Noori, L. Meng, A. H. Jaafar, W. Zhang, G. P. Kissling, Y. Han, N. Abdelazim, M. Alibouri, K. LeBlanc, N. Zhelev, R. Huang, R. Beanland, D. C. Smith, G. Reid, K. de Groot and P. N. Bartlett, ACS Appl. Electron. Mater., 2021, 3, 3610–3618.

153 B. J. Baliga, J. Appl. Phys., 1982, 53, 1759–1764.

154 M. Sultan, Y. Khan, S. T. Hussain and M. Shafiq, Mater. Lett., 2013, 104, 44–47.

155 A. Kyono, M. Kimata, M. Matsuhisa, Y. Miyashita and K. Okamoto, Phys. Chem. Miner., 2002, 29, 254–260.

156 W. R. Wadt and P. J. Hay, J. Chem. Phys., 1985, 82, 284–298.

157 Z. Li, X. Liang, G. Li, H. Liu, H. Zhang, J. Guo, J. Chen, K. Shen, X. San, W. Yu, R. E. I. Schropp and Y. Mai, Nat. Commun., 2019, 1–9.

158 J. D. Kennedy and W. McFarlane, in Multinuclear NMR, Springer US, Boston, MA, 1987, pp. 305–333.

159 R. G. Kidd and R. W. Matthews, J. Inorg. Nucl. Chem., 1975, 37, 661–663.

160 J. Mason, Multinuclear NMR, Springer US, Boston, MA, 1987.

161 E. L. Hahn and D. E. Maxwell, Phys. Rev., 1952, 88, 1070–1084.

162 S. J. Wilkens, W. M. Westler, J. L. Markley and F. Weinhold, J. Am. Chem. Soc., 2001, 123, 12026–12036.

163 M. Kaupp, O. L. Malkina, V. G. Malkin and P. Pyykkö, Chem. Eur. J., 1998, 4, 118–126.

164 C. Giacovazzo, H. L. Monaco, G. Artioli, D. Viterbo, M. Milanesio, G. Gilli, P. Gilli, G. Zanotti, G. Ferraris and M. Catti, Fundamentals of Crystallography, Oxford University Press, 2011.

165 A. Gupta and C. Srivastava, Surf. Coatings Technol., 2021, 425, 127709.

166 H. Heydari, M. B. Gholivand and A. Abdolmaleki, Mater. Sci. Eng. C, 2016, 66, 16–24.

167 N. Argaman and G. Makov, Am. J. Phys., 2000, 68, 69–79.

168 F. Weinhold, J. Comput. Chem., 2012, 33, 2363–2379.

169 S. Thomas, D. E. Smith, V. K. Greenacre, Y. J. Noori, A. L. Hector, C. H. de Groot, G. Reid and P. N. Bartlett, J. Electrochem. Soc., 2020, 167, 106511.

170 R. Levinas, N. Tsyntsaru and H. Cesiulis, Catalysts, 2020, 10, 1182.

Chapter 2 Synthesis of neutral, cationic and anionic complexes of tin(IV) halides

2.1 Introduction

2.1.1 Tin(IV) halide pnictine complexes

Both phosphine and arsine ligands can form complexes with main group Lewis acids, and these are covered extensively in a recent review[1] and the main trends detailed in Chapter 1. Such complexes also include adducts of the tin tetrahalides. For phosphines, the complexes are most commonly synthesised by the reaction of the corresponding tin tetrahalide (halide = Cl, Br or I) or, for X = F, a soluble molecular adduct, such as $[SnF_4(MeCN)_2]$, with an appropriate ratio of ligand in a non-coordinating solvent, for instance CH_2Cl_2. This method can be used to synthesise a variety of neutral tetrahalide complexes, including *trans*-$[SnF_4(PCy_3)_2]$,[2] *trans*-$[SnCl_4(PEt_3)_2]$,[3] and $[SnCl_4\{Et_2P(CH_2)_2PEt_2\}]$.[2] However, some complexes cannot be accessed through this route, in which case an alternative route utilising the reaction of $I_2P^nPr_3$ with unactivated tin powder in Et_2O has been used to yield the complex *trans*-$[SnI_4(P^nPr_3)_2]$ - a rare example of a tin(IV) complex containing both phosphine and iodide ligands.[4]

For arsines, a range of complexes have been isolated, including $[SnCl_4(AsPh_3)_2]$ and $[SnBr_4(AsPh_3)]\cdot AsPh_3$, which can both be synthesised by the reaction of the appropriate tin tetrahalide with two equivalents of the ligand in CH_2Cl_2 for the former and hexane for the latter.[5] Interestingly, in this case, the structures (shown in **Figure 2.1**) are completely different. For the chloride derivative, both arsine ligands are bound to tin forming a *trans*-octahedral complex; this is analogous to the monodentate phosphine complexes above. However, in the case of the bromide complex, only one of the arsines is bound to the tin centre, and the complex has a pseudo-trigonal bipyramidal geometry with the arsine in an axial position. The non-coordinated arsine is 3.568 Å away from the closest bromide; this is probably due to crystal packing effects rather than a significant bonding interaction as the distance is well above Σr_{cov}(As-Br) = 2.39 Å,[6] but it is within Σr_{vdW}(As-Br) = 3.68 Å.[7] A variety of multidentate arsine complexes are also known, including $[SnI_4\{o\text{-}C_6H_4(AsMe_2)_2\}]$ and $[SnBr_4(\kappa^2\text{-}CH_3C(CH_2AsMe_2)_3)]$; in both cases, the ligand binds in a *cis*-bidentate fashion,

for the ligand $CH_3C(CH_2AsMe_2)_3$ there is a possibility for the pendant arm to coordinate, but in this case, the third arm is un-coordinated. [2,8]

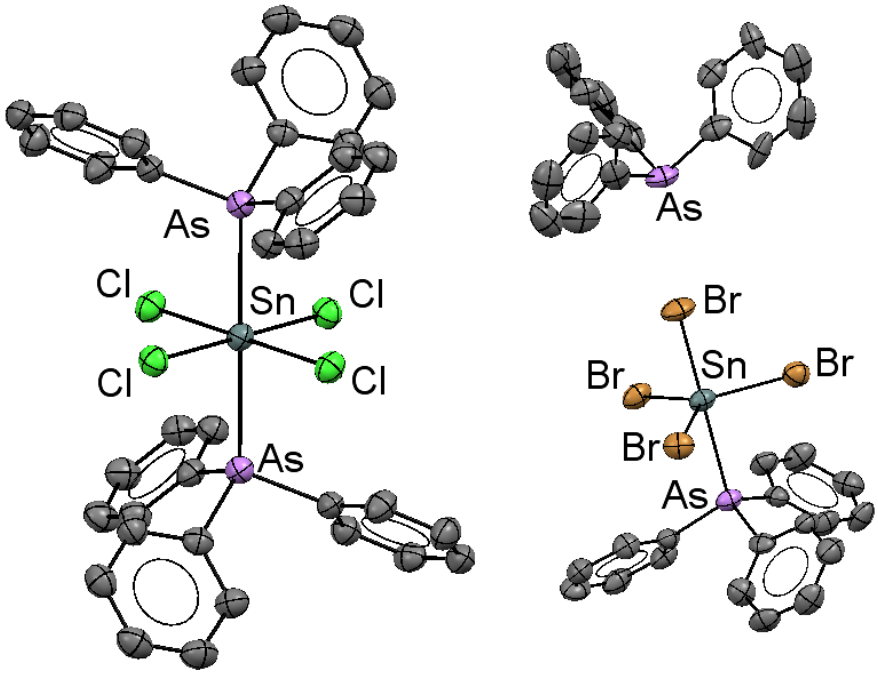

(a) (b)

Figure 2.1 – Crystal structures of (a) $[SnCl_4(AsPh_3)_2]$ and (b) $[SnBr_4(AsPh_3)]\cdot AsPh_3$ redrawn from Ref. 5.

The chemistry of ionic tin(IV) halide pnictine complexes is much more sparse compared to that of neutral complexes. Macdonald *et al* reported the synthesis of a set of complexes of the form $[SnCl_{4-n}(PMe_3)_2][AlCl_4]_n$ (n = 0, 1, 2). These were generated by the reaction of the neutral complex with n equivalents of $AlCl_3$ (chloride abstractor) in CH_2Cl_2.[9] The structures of the complexes are shown in **Figure 2.2** below. The neutral complex has a pseudo-octahedral structure, the monocationic complex has a trigonal bipyramidal structure with axial phosphines, and the dicationic complex has a distorted octahedral structure with close contacts to both $[AlCl_4]^-$ anions. In the solid state, there is a contraction of both the d(Sn-P) and d(Sn-Cl) distances as the charge on the complex increases. In the solution state, both ^{119}Sn and $^{31}P\{^1H\}$ NMR spectroscopy show stepwise high-frequency shifts with an increase in charge.[9] There are no reports to our knowledge of cationic tin(IV) bromide complexes stabilised by pnictine ligands or any cationic tin(IV)

halide complexes stabilised by pnictine ligands where the pnictogen is heavier than phosphorus.

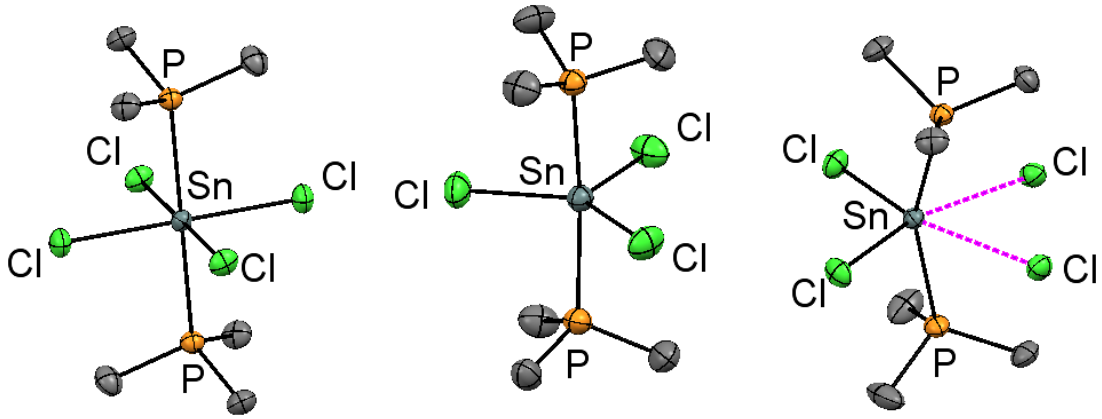

(a) (b) (c)

Figure 2.2 – Crystal structures of (a) $[SnCl_4(PMe_3)_2]$, the cation (b) $[SnCl_3(PMe_3)_2]^+$ and the dication (c) $[SnCl_2(PMe_2)_2]^{2+}$ showing the close contacts to the counter anions by the dashed lines; only the coordinated Cl of the $AlCl_4^-$ anions are shown) redrawn from Ref. 9.[9]

More extensive work has been done on anionic tin(IV) halide complexes. This mainly focused on *in situ* NMR spectroscopic work. It was found that for the series, $[SnCl_{5-n}Br_n(P^nBu_3)]^-$ (n = 0-5), both the ^{119}Sn and $^{31}P\{^1H\}$ NMR resonances shift to low frequency in a stepwise manner as more bromides are incorporated.[10] There is also one report of a zwitterionic complex with a diphosphine ligand bound to a $[SnCl_5]^-$ anion, shown in **Figure 2.3** below. One phosphorus atom from the ligand is bound to the anion, and the other has been protonated.[11] To our knowledge, there are no known complexes of this type with pnictine ligands heavier than phosphorus.

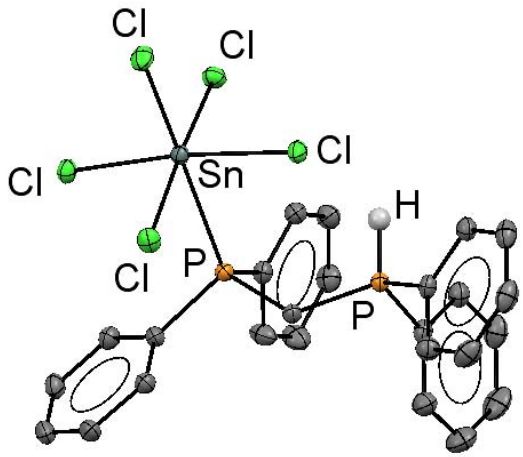

Figure 2.3 – Crystal structure of the zwitterion [$SnCl_5${$PPh_2CH_2P(H)Ph_2$}] redrawn from Ref. 11.

2.2 Aims

The aim of this chapter is to further develop the coordination chemistry of $SnCl_4$ and $SnBr_4$ with pnictine ligands, with a focus on the generation of cationic complexes through halide abstraction. With a goal to investigate how the choice of ligand and abstraction agent affects the reaction outcome.

2.3 Results and discussion

2.3.1 Neutral tin(IV) halide complexes with phosphine and arsine ligands

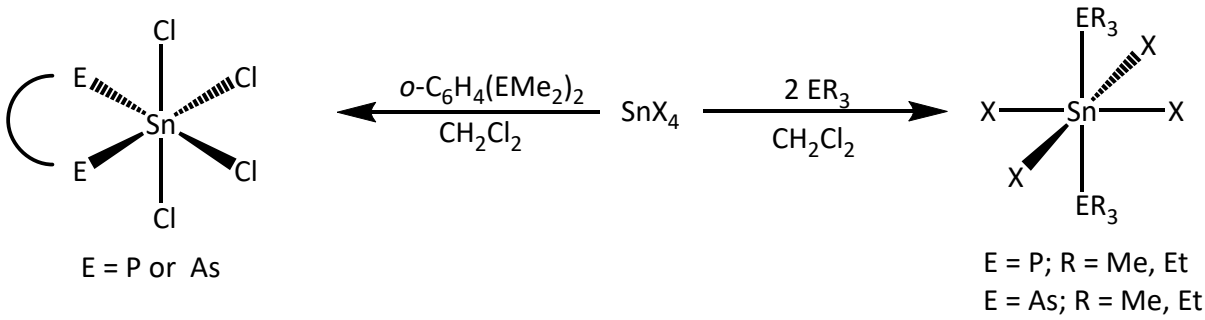

Scheme 2.1 – Synthesis of neutral pnictine complexes of tin tetrahalides.

The reaction of tin(IV) chloride with ER_3 (E = P, R = Me, Et; E = As, R = Et) in a 1:2 ratio in CH_2Cl_2 leads to the formation of the complexes *trans*-$[SnCl_4(ER_3)_2]$ as white air and moisture sensitive solids (see **Scheme 2.1** above). The reaction of $SnBr_4$ with two equivalents of $AsEt_3$ in CH_2Cl_2 leads to the isolation of *trans*-$[SnBr_4(AsEt_3)_2]$ as a yellow solid; this can be contrasted with $AlBr_3$, which undergoes halide exchange with the solvent under similar conditions.[12] Small crystals of $[SnCl_4(PEt_3)_2]$ deposited from the reaction filtrate, which were amenable to single-crystal X-ray analysis; the structure is shown below in **Figure 2.4**. The structure of this complex had been reported previously, but only from data collected at room temperature, resulting in a relatively high R factor of 9.9% (c.f. 3.1% for the present structure). The phosphines are *trans* to each other, typical for *bis*-monodentate phosphine complexes of main group halides. The space group of both structures match, but the literature data overestimates d(Sn-Cl) and underestimates d(Sn-P) slightly, though this could be due to the different collection temperatures.[3]

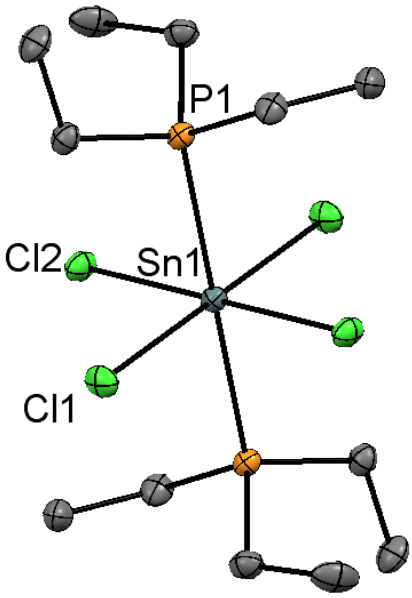

Figure 2.4 – The crystal structure of $[SnCl_4(PEt_3)_2]$ showing the atom labelling scheme. The ellipsoids are drawn at the 50% probability level, and H atoms are omitted for clarity. Selected bond lengths (Å) and angles (°) are: Sn1–P1 = 2.5996(4), Sn1–Cl1 = 2.4533(5), Sn1–Cl2= 2.4588(4), Cl1–Sn1–Cl2 = 90.202(17), 89.798(17). Symmetry operation: (-X,-Y,-Z).

From CH_2Cl_2 solutions of $[SnX_4(AsEt_3)_2]$ (X = Cl, Br), suitable crystals were also grown, and their X-ray structures were determined. $[SnCl_4(AsEt_3)_2]$ is isomorphous with the phosphine analogue, belonging to the $P2_1/n$ space group. However, the bromide analogue belongs to the higher symmetry Pbca space group. Both structures are shown below in **Figure 2.5**.

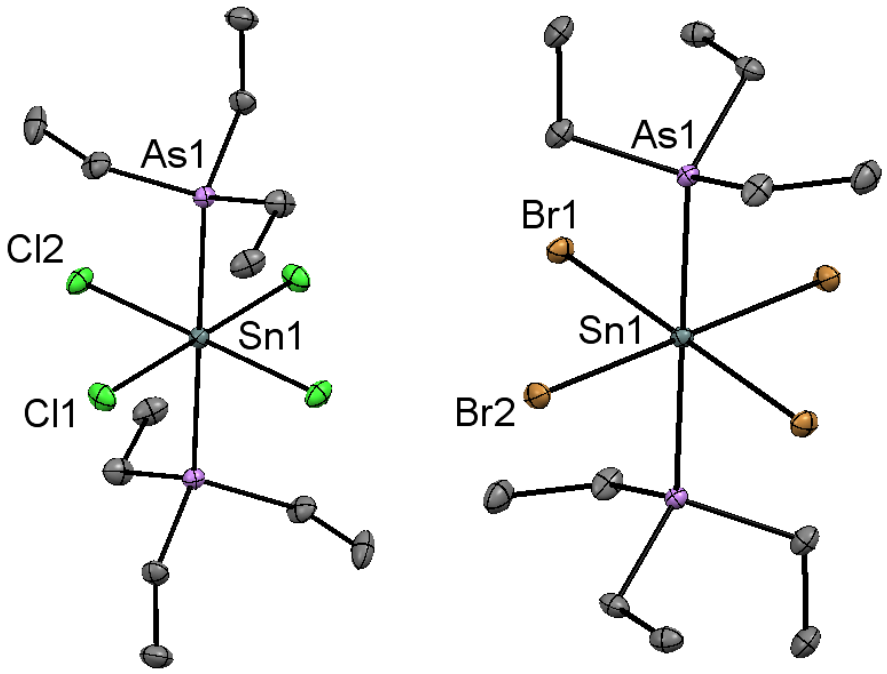

(a) (b)

Figure 2.5 – (a) structure of $[SnCl_4(AsEt_3)_2]$ showing the atom labelling scheme. The ellipsoids drawn at the 50% probability level and H atoms omitted for clarity. Selected bond lengths (Å) and angles (°) are: Sn1–Cl1 = 2.4498(4), Sn1–Cl2 = 2.4544(4), Sn1–As1 = 2.65964(16), Cl1–Sn1–Cl2 = 90.367(15). Symmetry operation: (-X,-Y,-Z) ; (b) structure of $[SnBr_4(AsEt_3)_2]$ showing the atom labelling scheme. The ellipsoids drawn at the 50% probability level and H atoms omitted for clarity. Selected bond lengths (Å) and angles (°) are: Sn1–Br1 = 2.6286(3), Sn1–Br2 = 2.6173(3), Sn1–As1 = 2.6773(3), Br1– Sn1–Br2 = 89.298(11). Symmetry operation: (-X, -Y, -Z).

Table 2.1 – Comparison of key structural parameters in the monodentate pnictine complexes.

	$[SnCl_4(PEt_3)_2]$	$[SnCl_4(AsEt_3)_2]$	$[SnBr_4(AsEt_3)_2]$
Sn-E (Å)	2.5996(4)	2.65962(16)	2.6773(3)
Sn-Hal (Å)	2.4588(4) 2.4533(5)	2.4544(4) 2.4498(4)	2.6286(3) 2.6173(3)
Hal-Sn-Hal *cis* (˚)	89.798(17) 90.202(17)	89.633(15) 90.367(15)	89.298(11) 90.702(11)

Interestingly, both tin halides form *bis*-arsine complexes with $AsEt_3$. This can be contrasted with the complexes formed with $AsPh_3$ (which is poorer σ-donor than $AsEt_3$), where the bromide only forms a (five-coordinate) mono-arsine complex. Various structural parameters are included in **Table 2.1**. Comparing the tin chloride complexes, the phosphine complex has a smaller d(Sn-E) distance than the arsine analogue, by 0.06 Å, and this could be due to a number of factors, including the greater σ-donor strength of phosphine compared to arsine, as well as the larger covalent radius of As *vs* P. However, the difference is smaller than the difference in r_{cov}(0.12 Å). In the bromide complex, d(Sn-E) is longer than the chloride analogue by 0.018 Å, presumably mainly due to the poorer Lewis acidity of $SnBr_4$ *vs* $SnCl_4$.[13] Previous reports of the arsine complexes did not include ^{119}Sn NMR data, so this experiment was performed on these complexes. For $[SnCl_4(AsEt_3)_2]$ in CD_2Cl_2, the ^{119}Sn resonance comes at δ = -657, which can be compared to δ = -1173 for the bromide analogue, consistent with the heavy atom effect on the tin-119 NMR shifts. The phosphine analogue, however, has a more positive shift of δ = -572. The complexes, $[SnCl_4(o\text{-}C_6H_4(EMe_2)_2)]$ (E = P, As), have been synthesised and characterised previously.[2] The reaction of $SnCl_4$ with $SbEt_3$ in CH_2Cl_2 leads to the precipitation of $SnCl_2$ and the formation of $SbEt_3Cl_2$, identified by ^{1}H NMR spectroscopy, but with no evidence of complex formation. This is consistent with reported literature where the reaction of the weaker donor $SbPh_3$ with $SnCl_4$ lead to the formation of the analogous $SbPh_3Cl_2$, with the concomitant precipitation of $SnCl_2$.[14]

2.3.2 Reactions of pnictine tin(IV) halide complexes with aluminium halides

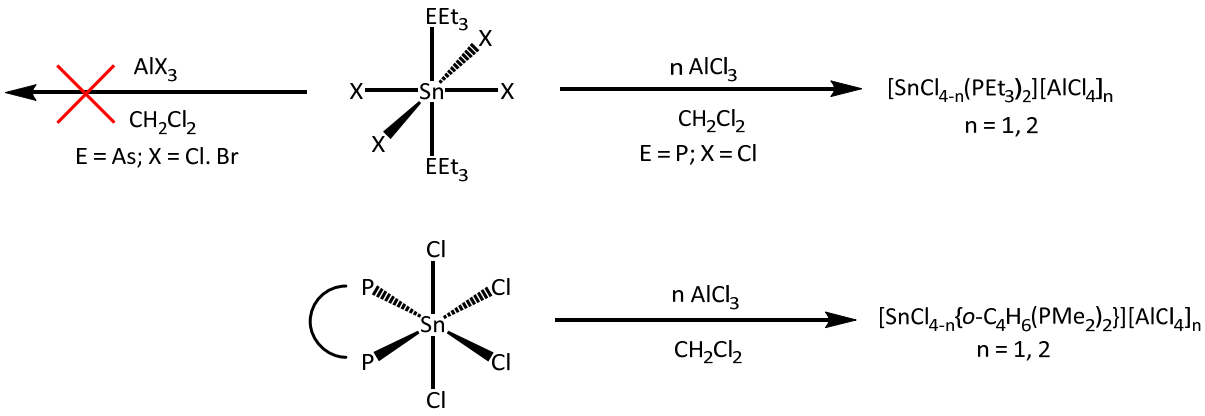

Scheme 2.2 – Reactivity of neutral tin halide pnictine complexes with aluminium halides.

Salts of the form $[SnCl_{4-n}(PMe_3)_2][AlCl_4]_n$ (n = 0, 1, 2) were first reported by Macdonald *et al.* in 2012 *via* a halide abstraction methodology using $AlCl_3$.[9] It was sought to determine if this methodology could be extended to other related complexes to establish whether the reaction might provide a general route to Sn(IV) cations (see **Scheme 2.2**). Firstly, $[SnCl_4(PEt_3)_2]$ was reacted with one equivalent of $AlCl_3$ in CH_2Cl_2, which resulted in the formation of $[SnCl_3(PEt_3)_2][AlCl_4]$. The ^1H NMR spectrum reveals that the methylene resonance shifts by $\Delta\delta$ = +0.06 from the neutral complex, consistent with an increase in positive charge going from neutral to monocationic. There is also a large change in the $^{31}P\{^1H\}$ NMR chemical shift compared to the neutral complex, shifting from δ = +20.9 to +35.5 ppm, a change of +14.6 ppm (which is larger than for the PMe_3 analogue, where the shift is only +9.2 ppm).[9] There is also a high-frequency shift in the ^{119}Sn NMR spectrum with the resonance shifting from δ = -572 to δ = -350 upon halide abstraction, indicating an increase of positive charge at the tin centre. As the peak remains a triplet, this suggests that the phosphines are still in equivalent environments. There is also a decrease in the $^1J_{^{119}Sn\text{-}^{31}P}$ coupling constant (from 2391 to 2307 Hz), which indicates a change in the geometric and electronic environment of the complex.

Table 2.2 – Selected NMR spectroscopic data for the monodentate phosphine systems.[a]

Compound	$\delta(^{31}P\{^{1}H\})$/ppm	$\delta(^{119}Sn)$ /ppm	$^{1}J(^{119}Sn\text{-}^{31}P)$/Hz	Ref
$[SnCl_4(PMe_3)_2]$	+1.6	–554	2635	[9]
$[SnCl_3(PMe_3)_2][AlCl_4]$	+10.8	–456	2725	[9]
$[SnCl_2(PMe_3)_2][AlCl_4]_2$	+16.9	–333	2591	[9]
$[SnCl_4(PEt_3)_2]$	+20.9	–572	2391	This work
$[SnCl_3(PEt_3)_2][AlCl_4]$	+35.5	–350	2307	This Work
$[SnCl_2(PEt_3)_2][AlCl_4]_2$	+40.8	–300	2274	This work

[a] NMR data from CD_2Cl_2 solution at 298 K

The addition of two equivalents of $AlCl_3$ to $[SnCl_4(PEt_3)_2]$ in CH_2Cl_2 leads to the abstraction of two chlorides. In the ^{1}H NMR spectrum the methylene resonance shifts to $\delta = 2.38$, which is a further shift of +0.06 ppm from the monocationic complex (i.e. a total of +0.12 ppm from the neutral species). The $^{31}P\{^{1}H\}$ NMR resonance shifts by a further +5.3 ppm from the monocationic complex; the resonance is sharp, and the expected 117- and 119-tin satellites are evident (see **Figure 2.6**).

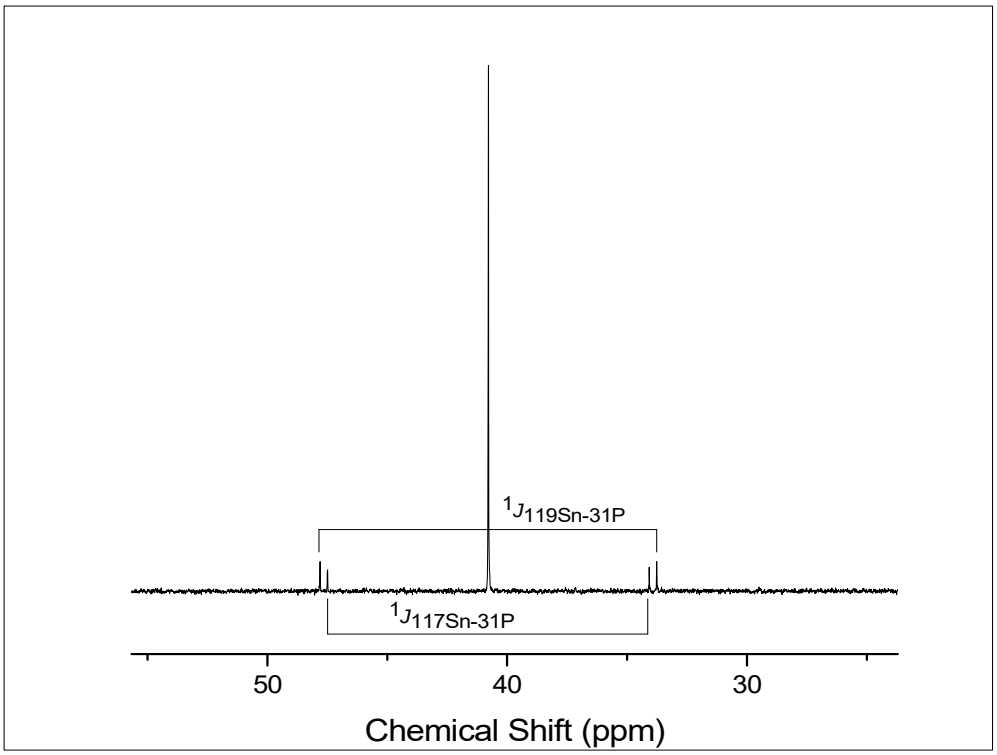

Figure 2.6 – $^{31}P\{^{1}H\}$ NMR spectrum of $[SnCl_2(PEt_3)_2][AlCl_4]_2$ showing the tin satellite couplings.

The ^{119}Sn NMR resonance shifts a further +49 ppm from the monocationic complex; this could be due to the change in charge and coordination number. There is also a small decrease in the $^{1}J_{119Sn\text{-}31P}$ coupling constant (from 2307 Hz in the monocation to 2274 Hz in the dication). Key multinuclear NMR data for these complexes are included in **Table 2.2** above. Elemental analysis also confirms the formulation of the bulk solids produced from both of these reactions.

A CH_2Cl_2 solution of $[SnCl_2(PEt_3)_2][AlCl_4]_2$ left to stand in an NMR tube for two weeks led to the deposition of some crystals, one of which proved to be the rearrangement product, $[SnCl_2(PEt_3)_3][AlCl_4]_2$, the dication component is shown in **Figure 2.7** below.

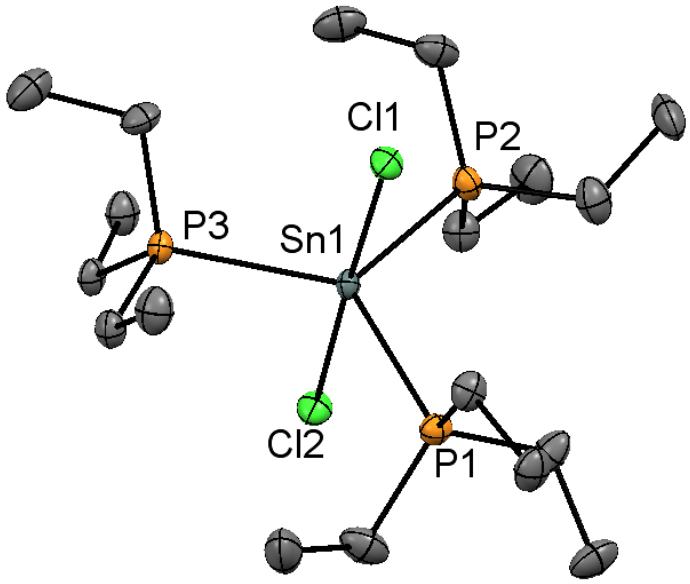

Figure 2.7 – Crystal structure of the dication in $[SnCl_2(PEt_3)_3][AlCl_4]_2$ showing the atom labelling scheme. Note there are two similar, but crystallographically independent $[SnCl_2(PEt_3)_3][AlCl_4]_2$ units in the asymmetric unit. Ellipsoids are drawn at the 50% level and H atoms are omitted for clarity. Selected bond lengths (Å) and angles (°) are: Sn1–Cl1 = 2.4531(13), Sn1–Cl2 = 2.4589(13), Sn1– P1 = 2.5679(14), Sn1–P2 = 2.5610(13), Sn1–P3 = 2.5525(13), Cl2–Sn1– P3 = 91.10(4), Cl2–Sn1–P2 = 92.07(5), Cl2–Sn1–P1 = 86.01(4), Cl1–Sn1– Cl2 = 178.28(4), Cl1–Sn1–P3 = 90.52(4), Cl1–Sn1–P2 = 87.51(4), Cl1– Sn1–P1 = 92.63(4), P3–Sn1–P2 = 123.83(4), P3–Sn1–P1 = 122.85(4), P2–Sn1–P1 = 113.31(5).

The dication features an approximately linear [Cl-Sn-Cl]$^{2+}$ unit with three phosphines trigonally disposed around the tin centre, leading to a trigonal bipyramidal geometry. This is a unique bonding motif for tin phosphine complexes. There are no close contacts between the tin centre and the anions; the closest approach between the anion and tin centre is 5.316 Å. This is in contrast with MacDonald's dication $[SnCl_2(PMe_3)_2][AlCl_4]_2$, where there are two long Sn-Cl contacts (2.9233(6) and 2.9907(6) Å) between the dication and counter anions.[9] Complexes of main group elements with more than two monodentate phosphine ligands bound are relatively rare, and in group 14, only one other complex is known, which is the tin(II) complex $[Sn(PPh_3)_4][SO_3]$.[15] The d(Sn-P) is shorter in the $[SnCl_2(PEt_3)_3]^{2+}$ dication compared to the neutral ($[SnCl_4(PEt_3)_2]$) species (2.5525(13)-2.5698(13) *vs* 2.6013(5) Å), consistent with the increase in Lewis acidity due to the positive charge.

In an attempt to prepare a bulk sample of the *tris*-phosphine complex, an *in situ* reaction of $[SnCl_2(PEt_3)_2][AlCl_4]_2$ with one equivalent of PEt_3 in CD_2Cl_2 was performed, leading to a mixture of products, including $[AlCl_4]^-$, $[AlCl_3(PEt_3)]$ (identified by a characteristic sextet in the $^{31}P\{^1H\}$ NMR spectrum)[12] and a new, unidentified tin *bis*-phosphine complex that displays a triplet resonance at δ = -449 ($^1J_{31P\text{-}119Sn}$ = 2394 Hz) in the ^{119}Sn NMR spectrum, which is substantially different to the Sn(IV) mono- and di-cations, but clearly not a *tris*-phosphine complex, therefore this chemistry was not pursued further.

Having shown that the scope of this halide abstraction methodology extends to other monodentate phosphines, the next target was to determine the outcome using bidentate phosphines. Addition of one equivalent of $AlCl_3$ to a suspension of $[SnCl_4\{o\text{-}C_6H_4(PMe_2)_2\}]$ in CH_2Cl_2 lead to immediate dissolution of the solid to form a light yellow solution containing $[SnCl_3\{o\text{-}C_6H_4(PMe_2)_2\}][AlCl_4]$. In the ^1H NMR spectrum, the methyl resonance shifts from δ = 1.95 for the neutral complex to δ = 2.06 in the monocation. This is accompanied by a modest change in the $^{31}P\{^1H\}$ NMR shift, from δ = -28.1 to δ = -24.7. However, the ^{119}Sn spectrum shows a more substantial change, going from -616 ppm to -469 ppm. This shift of +147 ppm is indicative of cation formation. The triplet structure of the resonance is maintained, which suggests that the phosphines are in the same environment in the solution state. Based on this, the likely geometry of the cation is a square-based pyramid with a P_2Cl_2 base, consistent with other five-coordinate complexes with bidentate phosphines (e.g. $[NiCl_3\{o\text{-}C_6H_4(PPh_2)_2\}]$).[16] The $^1J_{119Sn\text{-}31P}$ coupling constant

changes when the chloride is abstracted, increasing by +27 Hz (from 945 to 972 Hz). One thing to note here is the effect of the geometry of the complex on the $^{1}J_{119Sn\text{-}31P}$ coupling constant; in general, *cis*-coordinated phosphines have a much smaller coupling constant than *trans*-coordinated phosphines.

The addition of two equivalents of $AlCl_3$ leads to the formation of $[SnCl_2\{o\text{-}C_6H_4(PMe_2)_2\}][AlCl_4]_2$. The methyl resonance in the ^{1}H NMR spectrum shifts by +0.23 ppm (from δ = 1.95 to 2.18) compared with the neutral complex. While there is a slight positive shift in the phosphorus and tin NMR chemical shifts, there is, however, a marked decrease in the $^{1}J_{119Sn\text{-}31P}$ from 972 Hz to 850 Hz, indicating a significant change in the electronic environment and geometry of the complex. Key multinuclear NMR data are included in **Table 2.3** below.

Table 2.3 – Selected NMR spectroscopic data for the *o*-$C_6H_4(PMe_2)_2$ systems[a]

Compound	$\delta(^{31}P\{^{1}H\})$	$\delta(^{119}Sn)$	$^{1}J(^{119}Sn\text{-}^{31}P)$/Hz
$[SnCl_4\{o\text{-}C_6H_4(PMe_2)_2\}]$	–28.1	–616	945
$[SnCl_3\{o\text{-}C_6H_4(PMe_2)_2\}][AlCl_4]$	–24.7	-469	972
$[SnCl_2\{o\text{-}C_6H_4(PMe_2)_2\}][AlCl_4]_2$	–23.7	–429	875

[a] NMR data from CD_2Cl_2 solution at 298 K

A sample of $[SnCl_2\{o\text{-}C_6H_4(PMe_2)_2\}][AlCl_4]_2$ left to stand in CD_2Cl_2 for a week deposited crystals, one of which was determined to be $[o\text{-}C_6H_4(PMe_2)_2][AlCl_4]_2$, the structure of which is shown in **Figure 2.8** below, featuring an *o*-$C_6H_4(PMe_2)_2$ based dication. The two phosphorus atoms from the ligand have coupled together to form a four-membered C_2P_2 ring, leading to a P-P distance of 2.2102(14) Å, which is much shorter (by ~ 1 Å) than the average non-bonded P-P distance of *o*-$C_6H_4(PMe_2)_2$ complexes. This distance is within the normal range for a P-P single bond. This 1,2-diphosphonium salt is highly unusual; most examples of 1,2-diphosphonium salts are acyclic. The most similar examples are a group of compounds synthesised by Kilian *et al.*, where a naphthalene backbone (an example shown in **Figure 2.9**) is used to stabilise a five-membered ring containing a $P^{+}\text{-}P^{+}$ unit (here the P-P distance is 2.225 Å).[17]

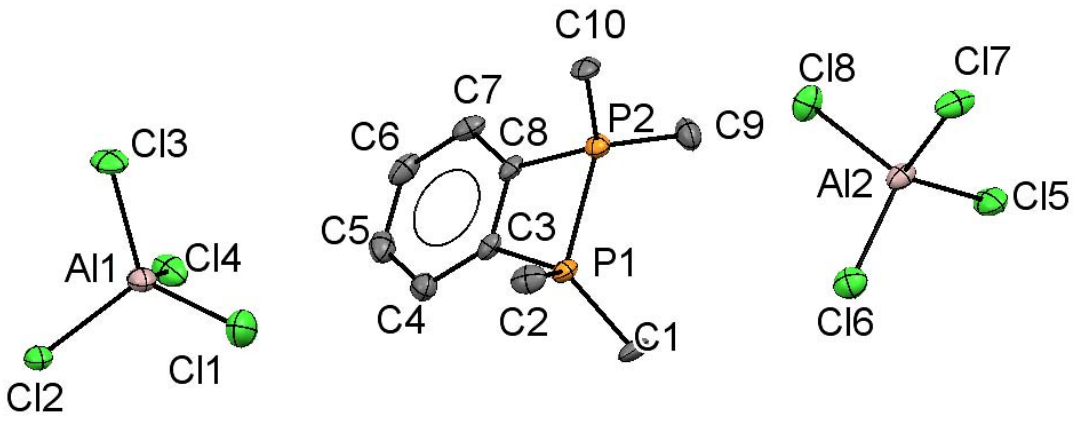

Figure 2.8 – Crystal structure of [*o*-$C_6H_4(PMe_2)_2$][$AlCl_4$]$_2$ showing the atom labelling scheme. Ellipsoids are drawn at the 50% level and H atoms are omitted for clarity. Selected bond lengths (Å) and angles (°) are: P1–P2 = 2.2102(14), P1–P2–C8 = 77.25(13), P2–P1–C3 = 76.57(13), P2–C8–C3 = 102.6(2), P1–C3–C8 = 103.5(3).

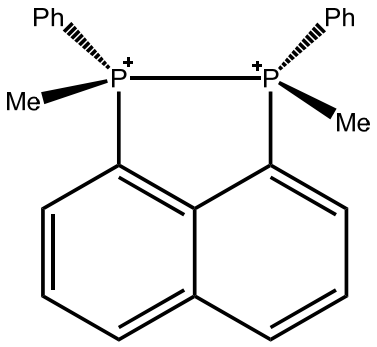

Figure 2.9 – Structure of a naphthalene backbone stabilised P^+-P^+ dication.

DFT calculations using the B3LYP-D3 functional with the 6-311G(d) basis set were performed on the [*o*-$C_6H_4(PMe_2)_2$]$^{2+}$ dication to elucidate the bonding situation in this ion. The computed geometry and the X-ray data match closely, as shown in **Table 2.3** below. NBO analysis shows that there is a single σ-bond between the P-P atoms and that they both contribute equally to this bond, implying it is formally a P^{IV}-P^{IV} bonding situation rather than a donor-acceptor P^{III}-P^{V} bonding situation. Going from the neutral ligand to the dication there is an increase in the natural charge on each of the P atoms from +0.783 to +1.26, with the rest of the charge being distributed among the other atoms. This means that there is a significant positive charge on both the phosphorus atoms; hence the P-P bond must be strong enough to overcome this repulsive interaction. There is a

large contraction by 0.949 Å of the computed P-P distance going from the neutral *o*-$C_6H_4(PMe_3)_2$ to the dication, consistent with formation of a P-P bond.

Table 2.3 – Comparison of the computed geometry and the experimental crystallographic geometry of $[o\text{-}C_6H_4(PMe_2)_2]^{2+}$.

	DFT (B3LYP-D3) (av)	X-ray
P-P distance (Å)	2.254	2.2102(14)
P-Me (Å)	1.807	1.770(4)-1.800(4)
P-C(aromatic) (Å)	1.806	1.786(4)-1.788(3)
C(aromatic)-P-P (˚)	76.62	76.57(13)-77.25(13)
C(aromatic)-C(aromatic)-P (˚)	103.4	102.6(2)-103.5(3)

One possible mechanism for the formation of the salt $[o\text{-}C_6H_4(PMe_2)_2][AlCl_4]_2$ is the reductive elimination of $SnCl_2$ from the complex $[SnCl_2\{o\text{-}C_6H_4(PMe_2)_2\}][AlCl_4]_2$, with the simultaneous oxidative coupling of the phosphines. Through this process the oxidation state of the tin centre changes from Sn(IV) to Sn(II), and the oxidation state of each of the phosphorus centres changes from P(III) to P(IV).

Reactions of $[SnCl_4(AsEt_3)_2]$ and $[SnBr_4(AsEt_3)_2]$ with $AlCl_3$ and $AlBr_3$, respectively, led to mixture of unidentified compounds with significant amounts of ligand halogenation; in one case, crystals of $[ClAsEt_3][SnCl_5(AsEt_3)]$ deposited from a Et_2O filtrate. The structure is shown in **Figure 2.10** below.

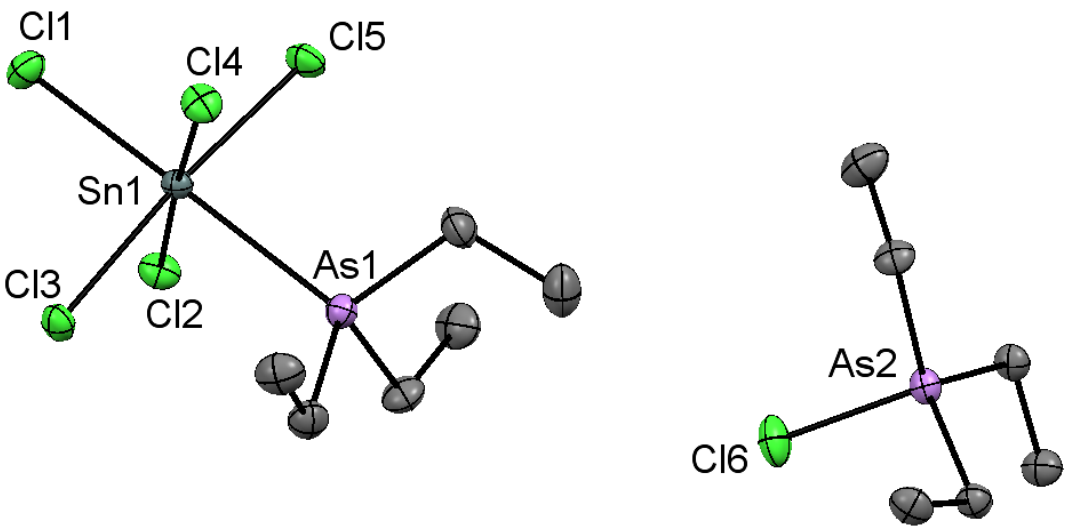

Figure 2.10 – Crystal structure of $[SnCl_5(AsEt_3)][ClAsEt_3]$ showing the atom labelling scheme. Ellipsoids are drawn at the 50% level and H atoms are omitted for clarity. Selected bond lengths (Å) and angles (°) are: Sn1– As1 = 2.6696(5), Sn1–Cl3 = 2.4453(8), Sn1–Cl4 = 2.4304(9), Sn1–Cl2 = 2.4365(8), Sn1–Cl1 = 2.3930(9), Sn1–Cl5 = 2.4254(8), Cl3–Sn1–As1 = 87.09(2), Cl4–Sn1–As1 = 85.21(2), Cl4–Sn1–Cl3 = 91.59(3), Cl2–Sn1–As1 = 92.00(2, Cl2–Sn1–Cl3 = 88.20(3), Cl1–Sn1–Cl3 = 90.72(3, Cl1–Sn1–Cl4 = 90.90(3), Cl1–Sn1–Cl2 = 91.88(3), Cl1–Sn1–Cl5 = 93.86(3), Cl5–Sn1–As1 = 88.54(2), Cl5–Sn1–Cl4 = 91.32(3), Cl5–Sn1–Cl2 = 88.66(3).

This is the first structurally characterised complex with a $[ClAsEt_3]^+$ cation, the analogous phosphorus cations are relatively common and can be generated, for example, by the reaction of the corresponding phosphine with $GeCl_4$.[18] There are also reported crystal structures for two antimony analogues, $[ClSbPh_3][SbCl_6]$[19] and $[ClSb(Mes)_3][SbCl_6]$[20]. This is consistent with the fact that the +5 oxidation state is more stable for P and Sb than for As. The structure also includes the new anion, $[SnCl_5(AsEt_3)]^-$. Anions of this type are rare with pnictine ligands. There is $^{31}P\{^1H\}$ NMR evidence that phosphine complexes of this type exist,[10] but there are no previous examples showing that this chemistry could be extended to arsine ligands; in fact, there was even some evidence against it.[21] The d(Sn-As) distance in the anion $[SnCl_5(AsEt_3)]^-$ (2.6696(5) Å) is significantly longer than in tetrahalide complex $[SnCl_4(AsEt_3)_2]$ (2.65962(16) Å), this is due to the weaker Lewis acidity of the $[SnCl_5]^-$ *vs.* $SnCl_4$.

2.3.3 Reactions of tin halide pnictine complexes with TMSOTf and Na[BAr^F]

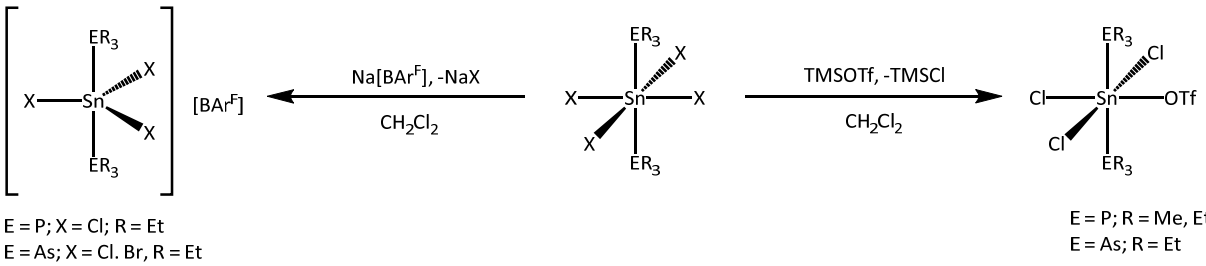

Scheme 2.3 – Reactions of tin tetrahalide pnictine complexes with TMSOTf and Na[BAr^F].

In the previous section, aluminium halides were shown to be effective halide abstractors to form mono- and dicationic complexes from some tin tetrahalide phosphine complexes, but were found to have unwanted reactivity with arsine complexes. An alternative halide abstractor, trimethylsilyl trifluoromethanesulfonate (TMSOTf), was therefore selected. One advantage this reagent has over aluminium halides is that one of the resulting products from halide abstraction using TMSOTf is that the by-product, Me_3SiCl, is volatile and therefore readily leaves the reaction mixture, preventing any further reaction.

Reacting $[SnCl_4(PR_3)_2]$ (R = Me, Et) or $[SnCl_4(AsEt_3)_2]$ with one equivalent of TMSOTf in CH_2Cl_2 leads to the formation of the corresponding monotriflate complexes (see **Scheme 2.3**). For the complexes where R = Et, there is a corresponding shift of Δδ = +0.07 for the methylene resonance in the ^{1}H NMR spectrum. For R = Me, this shift, Δδ, is +0.04 ppm. In all cases, this is smaller than the chemical shift differences seen with the cationic complexes described above in section 1.3.2. There is also a smaller shift in the ^{119}Sn NMR resonances; for example, $[SnCl_3(PMe_3)_2(OTf)]$ comes δ = -517, compared to δ = -554 reported by Macdonald for $[SnCl_4(PMe_3)_2]$.[9] There is also a large increase in $^1J_{119Sn\text{-}31P}$ going from the tetrachloride complex to the trichloride species (2635 Hz to 2963 Hz for R = Me). For $[SnCl_3(PEt_3)_2(OTf)]$ the $^{31}P\{^1H\}$ and ^{119}Sn NMR spectra are broad at room temperature, but sharpen when cooled to 183 K. This suggests there is a dynamic process occurring at room temperature, possibly reversible OTf-coordination and/or reversible PEt_3 dissociation. At 183 K, the ^{119}Sn NMR spectrum appears as the expected triplet ($^1J_{119Sn\text{-}31P}$ = 2737 Hz), as shown in **Figure 2.11** below. The analogous bromide complexes do not react with TMSOTf, and the triflate complexes do not react with the further equivalents of TMSOTf.

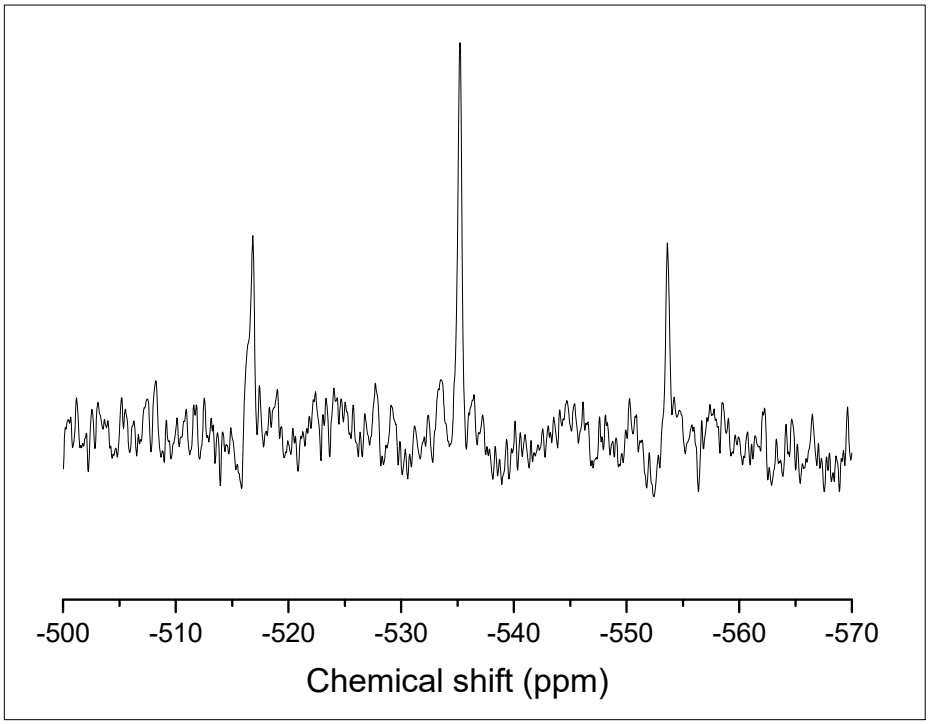

Figure 2.11 – The ^{119}Sn NMR spectrum of $[SnCl_3(PEt_3)_2(OTf)]$ at 183 K in CD_2Cl_2.

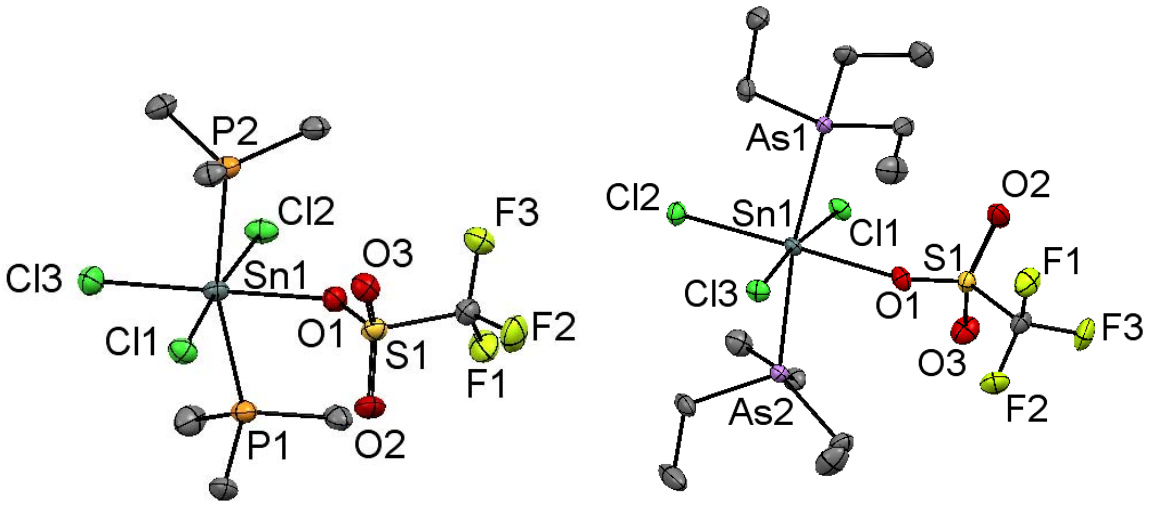

(a) (b)

Figure 2.12 – (a) Crystal structure of $[SnCl_3(PMe_3)_2(OTf)]$ showing the atom labelling scheme. Ellipsoids are drawn at the 50% level and H atoms are omitted for clarity. Selected bond lengths (Å) and angles (°) are: Sn1–Cl1 = 2.4457(9), Sn1–Cl2 = 2.4558(9), Sn1–Cl3 = 2.4085(10), Sn1–P1 = 2.5496(9), Sn1–P2 = 2.5506(9), Sn1–O1 = 2.266(3), P1–Sn1–P2 = 164.16 (3), Cl1–Sn1–Cl2 = 174.66(3), Cl3–Sn1–Cl1 = 92.67(3), Cl3–Sn1–Cl2 = 92.68(4), O1–Sn1–Cl1 = 89.25(7), O1–Sn1–Cl2 = 85.41(7), O1–Sn1–P1 = 82.17(7), O1–Sn1–P2 = 82.51(7); (b) Crystal structure of $[SnCl_3(AsEt_3)_2(OTf)]$ showing the atom labelling scheme. Ellipsoids are drawn at the 50% level and

H atoms are omitted for clarity. selected bond lengths (Å) and angles (°) are: Sn1–Cl1 = 2.4480(7), Sn1– Cl2 = 2.4168(8), Sn1–Cl3 = 2.4533(7), Sn1–As1 = 2.6451(4), Sn1–As2 = 2.6530(4), Sn1–O1 = 2.259(2), As1–Sn1–As2 = 172.239(12), Cl1–Sn1–Cl2 = 92.83(3), Cl3–Sn1–Cl1 = 173.76(3), Cl3–Sn1–Cl2 = 93.17(3), O1–Sn1– As2 = 86.28(6), O1–Sn1–As1 = 85.96(6), O1–Sn1–Cl1 = 88.46(6), O1– Sn1–Cl3 = 85.52(6).

Crystals amenable to X-ray diffraction studies were grown from the slow evaporation of CH_2Cl_2 solutions of the complexes. $[SnCl_3(PMe_3)_2(OTf)]$ and $[SnCl_3(AsEt_3)_2(OTf)]$ both feature *pseudo*-octahedral coordination environments at tin with the pnictine ligands *trans* to each other (see **Figure 2.12**). There are close contacts to triflate in both complexes, both longer than Σr_{cov}(Sn-O) = 2.05 Å,[6] but well within the sum of the van der Waals radii, Σr_{vdW}(Sn-O) = 3.69 Å.[7] This is at the lower end of the range of Sn-O distances in tin triflate complexes (2.026-3.073 Å, mean = 2.409 Å; standard deviation = 0.193 Å), suggesting that the triflates are quite strongly bound in these complexes in the solid state. In both complexes, the pnictine ligand is bent towards the triflate, more so for the phosphine than the arsine complex, and the d(Sn-Cl) distances are shorter in the triflate complexes compared to the tetrachloride ones, the d(Sn-Cl) for the chloride *trans* to the triflate are more contracted to those *cis*.

To test whether a cationic tin(IV) chloride with a stibine co-ligand could form, a mixture of $SnCl_4$:TMSOTf:2$SbEt_3$ was reacted in CH_2Cl_2 and resulted in the immediate precipitation of a white solid. The solid isolated from the filtrate from this reaction proved to be $[SbEt_3Cl(OTf)]$. The methylene proton resonance shifts from δ = 2.67 in $SbEt_3Cl_2$ to δ = 2.80 in $[SbEt_3Cl(OTf)]$. Slow evaporation of a CH_2Cl_2 solution of this compound deposited highly air and moisture sensitive crystals, which had to be mounted under a stream of cold nitrogen gas to avoid decomposition. From these, a rather poor quality data set for this compound was obtained and showed it to be trigonal bipyramidal with Cl and OTf in the axial positions, as shown in **Figure 2.13**. A related complex $[SbPh_3Cl(OTf)]$ is known in the literature; in this case, the complex was synthesised by the reaction of $[Ph_3SbCl_2]$ with AgOTf.[22] This suggests that in the triethylstibine case, the antimony centre is oxidised from Sb(III) to Sb(V) by $SnCl_4$, which itself is reduced to Sn(II), precipitating $SnCl_2$ as a white solid, followed by the abstraction of a chloride by TMSOTf.

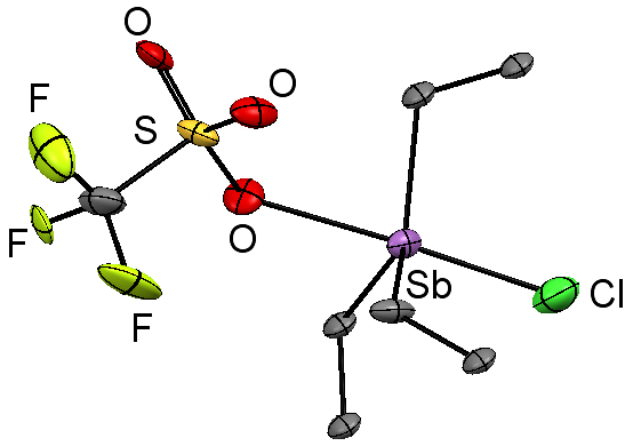

Figure 2.13 – Crystal structure of [$Et_3SbClOTf$] confirming the geometry of the complex. Bond lengths and angles are not quoted due to poor quality data; the structure, however, confirms the identity of the complex.

Na[BAr^F] was chosen as an alternative halide abstractor as it was less likely to coordinate than triflate and it also sequesters the halide by the precipitation of an insoluble solid (NaCl or NaBr) in organic media. [$SnCl_4(PEt_3)_2$] was found to react with Na[BAr^F] in CH_2Cl_2, forming a light yellowish solution with a small amount of precipitate, the filtrate of which formed a white solid upon the removal of the solvent. The $^{31}P\{^1H\}$ NMR spectrum of this product indicates formation of [$SnCl_3(PEt_3)_2$][BAr^F] as it has a similar shift to [$SnCl_3(PEt_3)_2$][$AlCl_4$] (37.1 *vs* 35.5 ppm). The similar $^1J_{^{119}Sn\text{-}^{31}P}$ coupling constants (with $[AlCl_4]^-$ counter anion $^1J_{^{119}Sn\text{-}^{31}P}$ = 2317 Hz, with $[BAr^F]^-$ counter anion $^1J_{^{119}Sn\text{-}^{31}P}$ = 2311 Hz) also suggest that the salt, [$SnCl_3(PEt_3)_2$][BAr^F], is formed. [$SnCl_4\{o\text{-}C_6H_4(PMe_2)_2\}$] also reacts with Na[$BAr^F$] to form [$SnCl_3\{o\text{-}C_6H_4(PMe_2)_2\}$][$BAr^F$] with data consistent with monocation formation. The addition of further equivalents of Na[BAr^F] does not lead to the abstraction of further halide, contrasting with the aluminium halide complexes.

The reaction of [$SnCl_4(AsEt_3)_2$] with Na[BAr^F] in CH_2Cl_2 leads to the formation of [$SnCl_3(AsEt_3)_2$][BAr^F] (multinuclear data for this and related complexes are shown in **Table 2.5** below). This is supported by the ^1H NMR spectrum where the methylene resonance shifts from δ = 1.37 to 1.44 (compared to δ = 1.39 in [$SnCl_3(AsEt_3)_2(OTf)$]). Perhaps the strongest evidence is the ^{119}Sn NMR resonance observed as a singlet at δ = -389 (shown in **Figure 2.14** below), which is a similar shift to the phosphine monocations and is much more positive than the neutral triflate and tetrachloride complexes. This abstraction

agent allows tin(IV) cations stabilised by monodentate arsine ligands to be generated cleanly, whereas the two other halide abstractors did not form these species.

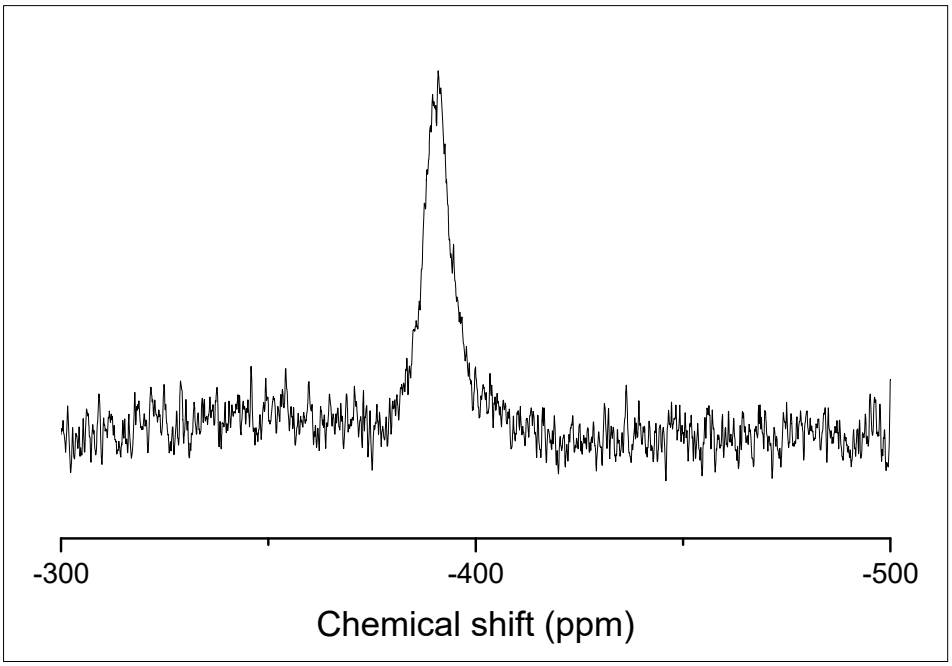

Figure 2.14 – ^{119}Sn NMR spectrum of $[SnCl_3(AsEt_3)_2][BAr^F]$ in CH_2Cl_2 at 183K.

Table 2.5 – Selected NMR spectroscopic data for the [OTf] and $[BAr^F]$ systems.[a]

Compound	$\delta(^{31}P\{^1H\})$ / ppm	$\delta(^{119}Sn)$ / ppm	$^1J(^{119}Sn\text{-}^{31}P)$ / Hz
$[SnCl_4(PMe_3)_2]$	+1.6	–554	2635
$[SnCl_3(PMe_3)_2(OTf)]$	+8.7	–516	2963
$[SnCl_4(PEt_3)_2]$	+20.9	–572	2391
$[SnCl_3(PEt_3)_2(OTf)]$	+33.4[b]	–535[b]	2737[b]
$[SnCl_3(PEt_3)_2][BAr^F]$	+37.1	–379	2311
$[SnCl_4(AsEt_3)_2]$	-	–657	-
$[SnCl_3(AsEt_3)_2(OTf)]$	-	–620	-
$[SnCl_3(AsEt_3)_2][BAr^F]$	-	-388[b]	-

[a] NMR data from CD_2Cl_2 solution at 298 K unless otherwise stated, [b]recorded at 183 K.

Following the success of forming an arsine-stabilised tin(IV) chloride cation, the corresponding bromide complex was investigated. It was found that upon reaction of $[SnBr_4(AsEt_3)_2]$ with $Na[BAr^F]$, the $[SnBr_3(AsEt_3)_2]^+$ cation did indeed form. This can be evidenced from the positive shift of the methylene proton resonance in the ^{1}H spectrum from δ = 2.36 to 2.48 ppm and by elemental analysis, which is consistent with the formation of the $[BAr^F]^-$ salt. No resonance was seen in the ^{119}Sn NMR spectrum in the range 183-298 K, although this could be due to fast exchange in solution.

2.4 Conclusions

The work in this chapter shows that the methodology to abstract chloride from tin tetrachloride phosphine complexes could be expanded from the originally reported synthesis of $[SnCl_{4-n}(PMe_3)_2][AlCl_4]_n$ (n = 0,1,2) to include other monodentate phosphines and bidentate phosphines. It was shown the reaction of $[SnCl_4(PEt_3)_2]$ with $AlCl_3$ leads to both monocationic and dicationic complexes. Also, during this study, the incipient crystallisation of $[SnCl_2(PEt_3)_3][AlCl_4]_2$, which is trigonal bipyramidal at tin, expanded the known bonding situations for these types of complexes. It was shown that this methodology could also be expanded to $[SnCl_4\{o\text{-}C_6H_4(PMe_2)_2\}]$, where the complexes $[SnCl_{4-n}\{o\text{-}C_6H_4(PMe_2)_2\}][AlCl_4]_n$ (n = 0, 1 ,2) where successfully synthesised. Here the complex with n = 2 was shown to be unstable, and a crystal structure suggests it decomposed into $[o\text{-}C_6H_4(PMe_2)_2][AlCl_4]_2$, which features a unique P-P bond in a strained C-C-P-P quadrilateral. However, this methodology could not be expanded to arsine complexes, where reactions lead to complicated mixtures of products that included chlorinated ligand.

It was also shown that TMSOTf could be used to abstract one chloride from the monodentate pnictine complexes forming *pseudo*-octahedral complexes with the triflate coordinated. Under the experimental conditions explored, there was no evidence of further halide abstraction being possible for the triflate complexes, the bromide complexes or the bidentate phosphine complexes. However, it was shown that $Na[BAr^F]$ could be used to abstract one halide from any of the neutral complexes to generate monocationic complexes, although addition of more $Na[BAr^F]$ did not lead to any further reaction.

2.5 X-Ray Crystallographic Data

Table 2.6 – X-ray crystallographic data[a]

Compound	$[SnCl_4(AsEt_3)_2]$	$[SnBr_4(AsEt_3)_2]$	$[SnCl_3(AsEt_3)_2(OTf)]$
Formula	$C_{12}H_{30}As_2Cl_4Sn$	$C_{12}H_{30}As_2Br_4Sn$	$C_{13}H_{30}As_2Cl_3F_3O_3SSn$
M	292.34	762.53	698.31
Crystal system	monoclinic	orthorhombic	orthorhombic
Space group (no.)	$P2_1/n$ (14)	Pbca (61)	$Pca2_1$ (29)
a /Å	7.1388(2)	13.8250(2)	13.21000(10)
b /Å	12.1065(2)	11.0254(2)	13.77830(10)
c /Å	11.9952(3)	14.4329(2)	13.2995(2)
α /°	90	90	90
β /°	91.301(2)	90	90
γ /°	90	90	90
U /Å^3	1036.43(4)	2199.95(6)	2420.66(4)
Z	4	4	4
μ(Mo-K_α) /mm^{-1}	4.905	11.401	4.220
F(000)	572	1432	1368
Total number reflns	27819	55967	66478
R_{int}	0.036	0.059	0.026
Unique reflns	3286	3615	7702
No. of params, restraints	91, 0	91, 0	242, 1
GOF	1.019	0.938	1.059
R_1, wR_2 [I > 2σ(I)][b]	0.020, 0.036	0.036, 0.110	0.020, 0.042
R_1, wR_2 (all data)	0.030, 0.038	0.044, 0.116	0.022, 0.042

Compound	$[SnCl_3(PMe_3)_2(OTf)]$	$[SnCl_5(AsEt_3)][ClAsEt_3]$	$[SnCl_2(PEt_3)_3][AlCl_4]_2$
Formula	$C_7H_{18}Cl_3F_3O_3P_2SSn$	$C_{12}H_{30}As_2Cl_6Sn$	$C_{18}H_{45}Al_2Cl_{10}P_3Sn$
M	526.25	655.59	881.60
Crystal system	monoclinic	monoclinic	Monoclinic
Space group (no.)	$P2_1/n$ (14)	$P2_1/n$ (14)	$P2_1/n$ (14)
a /Å	12.0116(4)	11.6759(3)	14.9000(3)
b /Å	12.9896(5)	10.3481(2)	25.4564(3)
c /Å	12.1849(3)	19.4678(5)	20.3339(4)
α /°	90	90	90
β /°	101.720(3)	92.168(3)	99.560(2)
γ /°	90	90	90
U /Å^3	1861.52(11)	2350.48(10)	7605.5(2)
Z	4	4	8
μ(Mo-K_α) /mm^{-1}	2.114	4.556	1.558
F(000)	1032	1280	3552
Total number reflns	38860	14864	83974
R_{int}	0.095	0.031	0.062
Unique reflns	5809	5392	14932
No. of params, restraints	187, 0	196, 0	631, 0
GOF	0.966	0.922	1.043
R_1, wR_2 $[I > 2\sigma(I)]$[b]	0.051, 0.131	0.034, 0.119	0.057, 0.136
R_1, wR_2 (all data)	0.076, 0.152	0.041, 0.125	0.089, 0.154

Compound	[*o*-$C_6H_4(PMe_2)_2$][$AlCl_4$]$_2$	[$SnCl_4(PEt_3)_2$]
Formula	$C_{10}H_{16}Al_2Cl_8P_2$	$C_{12}H_{30}Cl_4P_2Sn$
M	535.77	496.79
Crystal system	orthorhombic	monoclinic
Space group (no.)	$P2_12_12_1$ (19)	$P2_1/n$ (14)
a /Å	9.77600(10)	7.07190(10)
b /Å	14.3670(2)	11.9235(2)
c /Å	16.1794(2)	11.9193(2)
α /°	90	90
β /°	90	91.537(2)
γ /°	90	90
U /Å^3	2272.43(5)	1004.70(3)
Z	4	2
μ(Mo-K_α) /mm^{-1}	1.120	1.951
F(000)	1078	500
Total number reflns	110182	30805
R_{int}	0.065	0.086
Unique reflns	6363	3472
No. of params, restraints	203, 0	91, 0
GOF	1.010	1.118
R_1, wR_2 [I > 2σ(I)][b]	0.053, 0.123	0.032, 0.074
R_1, wR_2 (all data)	0.057, 0.125	0.036, 0.076

[a] Common items: T = 100 K; wavelength (Mo-K_α) = 0.71073 Å; θ(max) = 27.5°; [b] $R1 = \Sigma||F_o|-|F_c||/\Sigma|F_o|$; $wR_2=[\Sigma w(F_o^2-F_c^2)_2/\Sigma wF_o^4]^{1/2}$

CCDC NUMBERs: [$SnCl_4(AsEt_3)_2$] (1916557), [$SnBr_4(AsEt_3)_2$] (1916558), [$SnCl_3(PMe_3)_2(OTf)$] (1916559), [$SnCl_3(AsEt_3)_2(OTf)$] (1916560), [$SnCl_2(PEt_3)_3$][$AlCl_4$]$_2$ (1916561), [Et_3AsCl][$SnCl_5(AsEt_3)$] (1916562)

2.6 Experimental

For origin and purification of reagents and solvents, instrument specifications and NMR solvent references see appendix A. $[SnCl_4(PMe_3)_2]$[9] and $[SnCl_4\{o\text{-}C_6H_4(PMe_2)_2\}]$[2] were synthesised following literature preparations.

$[SnCl_4(AsEt_3)_2]$: A solution of $AsEt_3$ (0.058 g, 0.36 mmol) in CH_2Cl_2 (5 mL) was added to a solution of $SnCl_4$ (0.047 g, 0.18 mmol) in CH_2Cl_2 (5 mL). The colourless solution was left to stir for 1 h before the product was isolated by evaporation of the solvent under vacuum to afford a white solid. Crystals suitable for single crystal X-ray diffraction were grown by slow evaporation of a concentrated CH_2Cl_2 solution of the compound. Yield 0.093 g (88%). Required for $C_{12}H_{30}As_2Cl_4Sn$ (584.7): C, 24.6; H, 5.2. Found: C, 24.5; H, 5.0 %. IR (Nujol/cm^{-1}): ν = 288s (Sn-Cl). ^1H NMR ($CDCl_3$, 298 K): δ = 1.42 (t, [18H], $^3J_{HH}$ = 7.6 Hz, CH_3), 2.34 (q, [12H], $^3J_{HH}$ = 7.6 Hz, CH_2). $^{13}C\{^1H\}$ NMR ($CDCl_3$, 298 K): δ = 8.62 (CH_2), 15.04 (CH_3). ^{119}Sn NMR (CD_2Cl_2, 298 K): n.o. (not observed); (193 K): δ = –657.4.

$[SnBr_4(AsEt_3)_2]$: A solution of $AsEt_3$ (0.144 g, 0.89 mmol) in CH_2Cl_2 (5 mL) was added to a solution of $SnBr_4$ (0.195 g, 0.45 mmol) in CH_2Cl_2 (5 mL). The pale yellow solution was left to stir for 1 h before the product was isolated by removal of the solvent to afford a yellow solid. Crystals suitable for single crystal X-ray diffraction were grown by slow evaporation of a concentrated CH_2Cl_2 solution of the compound. Yield 0.175 g (50%). Required for $C_{12}H_{30}As_2Br_4Sn$ (762.5): C, 18.9; H, 4.0. Found: C, 19.0; H, 4.0 %. IR (Nujol/cm^{-1}): ν = 210s (Sn-Br). ^1H NMR (CD_2Cl_2, 298 K): δ = 1.43 (t, [18H], $^3J_{HH}$ = 7.6 Hz, CH_3), 2.35 (q, [12H], $^3J_{HH}$ = 7.6 Hz, CH_2). $^{13}C\{^1H\}$ NMR (CD_2Cl_2, 298 K): δ = 8.5 (CH_2), 14.8 (CH_3). ^{119}Sn NMR (CD_2Cl_2, 298 K): δ = –1173.4; (193 K): δ = –1125.3.

$[SnCl_3(AsEt_3)_2(OTf)]$: $[SnCl_4(AsEt_3)_2]$ (0.150 g, 0.26 mmol) was dissolved in CH_2Cl_2 (10 mL) to form a clear solution. To this TMSOTf (0.057 g, 0.26 mmol) was added in CH_2Cl_2 (5 mL) and the clear solution was stirred for 2 h. The solvent was removed and the white powder was dried *in vacuo*. Crystals suitable for single crystal X-ray diffraction were grown from slow evaporation of a solution of the compound in CH_2Cl_2. Yield 0.138 g (77%). Required for $C_{13}H_{30}As_2Cl_3F_3O_3SSn$ (698.1): C, 22.4, H, 4.3. Found C, 21.9; H, 4.2%. IR (Nujol/cm^{-1}): ν = 294s, 378w (Sn-Cl), 1156m (-OSO_2), 1200m, 1231m (CF_3). ^1H NMR (CD_2Cl_2, 298 K): δ = 1.39 (t, [18H], $^3J_{HH}$ = 7.8 Hz, CH_3), 2.38 (q, [12H], $^3J_{HH}$ = 7.8 Hz, CH_2). $^{13}C\{^1H\}$ NMR (CD_2Cl_2, 298 K): δ = 9.0 (CH_2), 16.0 (CH_3). $^{19}F\{^1H\}$ NMR (CD_2Cl_2, 298 K): δ = –78.7 (s, CF_3). ^{119}Sn NMR (CD_2Cl_2, 298 K): n.o.; (183 K): δ = –620 (s).

[$SnCl_3(PMe_3)_2(OTf)$]: [$SnCl_4(PMe_3)_2$] (0.300 g, 0.72 mmol) was suspended in CH_2Cl_2 (5 mL). To this TMSOTf (0.016 g, 0.72 mmol) was added in CH_2Cl_2 (5 mL). The solution was stirred for 16 h and the solvent and volatiles were removed and the resulting white powder dried *in vacuo.* The powder was then washed with diethyl ether (3 x 10 mL) and dried *in vacuo*. Crystals suitable for single crystal X-ray diffraction were grown by the slow evaporation of a saturated solution of the compound in CH_2Cl_2. Yield 0.215 g (57%). Required for $C_7H_{18}Cl_3F_3O_3P_2SSn$ (526.1): C, 16.0, H 3.5. Found C, 15.7; H, 3.4%. IR (Nujol/cm^{-1}): ν = 296m, 306m, 377w (Sn-Cl), 1173m (-OSO_2), 1200m, 1235m (CF_3). ^{1}H NMR (CD_2Cl_2, 298 K): δ =1.83 (m, CH_3). $^{13}C\{^1H\}$ NMR (CD_2Cl_2, 298 K): δ = 10.09 (t, $^1J + {}^3J_{31P\text{-}13C}$ = 19.4 Hz, CH_3). $^{31}P\{^1H\}$ NMR (CD_2Cl_2, 298 K): δ = 8.74 (s, $^1J_{31P\text{-}117Sn}$= 2814, $^1J_{31P\text{-}119Sn}$ = 2963 Hz). $^{19}F\{^1H\}$ NMR (CD_2Cl_2, 298 K): δ –78.6 (s, CF_3). ^{119}Sn (CD_2Cl_2, 298 K): δ = –516 (t, $^1J_{31P\text{-}119Sn}$ = 2963 Hz).

[$SnCl_3(PEt_3)_2(OTf)$]: [$SnCl_4(PEt_3)_2$] (0.08 g, 0.16 mmol) is dissolved in CH_2Cl_2 (10 mL). To this TMSOTf (0.036 g, 0.16 mmol) was added in CH_2Cl_2 (5 mL), resulting in a clear colourless solution which was stirred for 2 h. Solvent and volatiles were removed *in vacuo* and the resultant white powder was washed with diethyl ether (3 x 10 mL) and then dried *in vacuo.* Yield 0.065 g (66%). Required for $C_{13}H_{30}Cl_3F_3O_3P_2SSn$ (610.2): C, 25.6; H, 5.0. Found, C, 25.4; H, 5.1%. IR (Nujol/cm^{-1}): ν = 289m, 301w, 374w (Sn-Cl), 1187m (-OSO_2), 1235m (CF_3). ^{1}H NMR (CD_2Cl_2, 298 K): δ = 1.30 (m, [18H], CH_3), 2.33 (m, [12H], CH_2). $^{13}C\{^1H\}$ NMR (CD_2Cl_2, 298 K): δ = 7.59 (t, $^1J + {}^3J_{31P\text{-}13C}$ = 2.93 Hz, CH_2), 13.95 (t, $^1J + {}^3J_{31P\text{-}13C}$ = 11 Hz, CH_3). $^{19}F\{^1H\}$ NMR (CD_2Cl_2, 298 K): δ = –78.6 (s, CF_3). $^{31}P\{^1H\}$ (CD_2Cl_2, 298 K): δ = 28.45; (183 K): δ = 33.58 (s, $^1J_{31P\text{-}117Sn}$ = 2617 Hz, $^1J_{31P\text{-}119Sn}$ = 2734 Hz). ^{119}Sn NMR (CD_2Cl_2, 298 K): δ = –535; (CD_2Cl_2, 183 K): δ = –535 (t, $^1J_{31P\text{-}119Sn}$ = 2737 Hz).

[$SbEt_3Cl(OTf)$]: $SnCl_4$ (0.100 g, 0.38 mmol) was dissolved in 5 mL of CH_2Cl_2. To this, $SbEt_3$ (0.160 g, 0.77 mmol) was added in 5mL of CH_2Cl_2, resulting in the precipitation of a large amount of white solid. TMSOTf (0.085 g, 0.38 mmol) was added in CH_2Cl_2 (5 mL), and the reaction stirred for 16 h. The liquid was filtered away from the unidentified solid and concentrated to dryness *in vacuo*, leading to a white solid. Crystals suitable for single crystal X-ray diffraction were grown by slow evaporation of a concentrated CH_2Cl_2 solution of the compound. Yield 0.064 g (30%). Required for $C_7H_{15}ClF_3O_3SSb$ (393.3): C, 21.4; H, 3.8 Found C, 21.7; H, 4.2%. IR (Nujol/cm^{-1}): ν = 329m (Sb-Cl), 1167w (-OSO_2), 1198w, 1235w (CF_3). ^{1}H NMR (CD_2Cl_2, 298 K): δ = 1.62 (t, [9H], $^3J_{HH}$ = 7.7 Hz, CH_3), 2.80 (q, [6H], $^3J_{HH}$ = 7.7 Hz, CH_2). $^{13}C\{^1H\}$ (CD_2Cl_2, 298 K): δ = 9.68 (CH_2), 28.55 (CH_3).

[$SnCl_3${*o*-$C_6H_4(PMe_2)_2$}][$AlCl_4$]: [$SnCl_4${*o*-$C_6H_4(PMe_2)_2$}] 0.150 g, 0.33 mmol) was suspended in CH_2Cl_2 (5 mL), and $AlCl_3$ (0.044 g, 0.33 mmol) was added. This resulted in a pale yellow clear solution which was stirred for a further 2 h. The solution was then concentrated to dryness *in vacuo* producing a white powder, which was then washed with n-hexane (3 x 10 mL) and the solid separated and dried *in vacuo* to leave a white powder. Yield: 0.120 g (61%). Required for $C_{10}H_{16}AlCl_7P_2Sn$ (591.9): C, 20.3; H, 2.7, Found C, 20.4; H, 2.8%. IR (Nujol/cm^{-1}): ν = 322m, 342m (Sn-Cl), 451m, 497br ($[AlCl_4]^-$). ^{1}H NMR (CD_2Cl_2, 298 K): δ = 2.06 (t, ^2J +$^5J_{P\text{-}H}$ = 4.5 Hz, [12H], CH_3), 7.86-7.92 (m, [4H], Ar-*H*). $^{13}C\{^1H\}$ NMR (CD_2Cl_2, 298 K): δ = 11.52 (t, ^1J +$^3J_{31P\text{-}13C}$ = 16.4 Hz, CH_3), 130.7-131.3, 134.2, 135.3 (Ar). ^{27}Al NMR (CD_2Cl_2, 298 K): δ = 102.8 (s, $[AlCl_4]^-$). $^{31}P\{^1H\}$ NMR (CD_2Cl_2, 298 K): δ = –24.7 (s, $^1J_{31p\text{-}117Sn}$ = 930 Hz, $^1J_{31P\text{-}119Sn}$ = 972 Hz). ^{119}Sn (CD_2Cl_2, 298 K): δ = –469 (t, $^1J_{31\text{-}119Sn}$ = 972 Hz)

[$SnCl_2${*o*-$C_6H_4(PMe_2)_2$}][$AlCl_4$]$_2$: [$SnCl_4${*o*-$C_6H_4(PMe_2)_2$}] (0.100 g, 0.22 mmol) was suspended in CH_2Cl_2 (5 mL), and to this $AlCl_3$ (0.058 g, 0.44 mmol) was added. This resulted in a pale yellow clear solution, which was stirred for a further 2 h. The solution was then concentrated to dryness *in vacuo* producing a white sticky solid, which was then washed with n-hexane (3 x 10 mL), the solid separated and dried *in vacuo* to leave a white sticky solid. Yield: 0.81 g (51%). Required for $C_{10}H_{16}Al_2Cl_{10}P_2Sn$ (725.4): C, 16.7; H, 2.2. Found C, 17.5; H, 2.7%. IR (Nujol/cm^{-1}): ν = 294m, 310m (Sn-Cl), 452sh, 487s ($[AlCl_4]^-$). ^{1}H NMR (CD_2Cl_2, 298 K): δ = 2.18 (t, ^2J +$^5J_{PH}$ = 4.5 Hz, [12H], CH_3), 7.94-8.30 (m, [4H], Ar-H). $^{13}C\{^1H\}$ NMR (CD_2Cl_2, 298 K): δ = 12.28 (t,^1J +$^3J_{31P\text{-}13C}$ = 16.1 Hz, CH_3), 129.8-130.1, 134.4, 135.9 (Ar-H). $^{31}P\{^1H\}$ NMR (CD_2Cl_2, 298 K): δ = –23.7 ($^1J_{31P\text{-}117Sn}$ = 815 Hz, $^1J_{31P\text{-}119Sn}$ = 853 Hz). ^{27}Al NMR (CD_2Cl_2, 298 K): δ = 102.9 (s, $[AlCl_4]^-$). ^{119}Sn NMR (CD_2Cl_2, 298 K): δ = –429 (t, $^1J_{31P\text{-}119Sn}$ = 850 Hz).

[$SnCl_3(PEt_3)_2$][$AlCl_4$]: [$SnCl_4(PEt_3)_2$] (0.200 g, 0.40 mmol) was suspended in CH_2Cl_2 (5 mL) and $AlCl_3$ (0.054 g, 0.40 mmol) was added. The suspension was stirred for 2 h leaving a clear and colourless solution, the solution was concentrated to dryness leaving a fine white powder which was washed with Et_2O (3 x 10 mL) and dried in *in vacuo* to yield a white powder. Yield: 0.160 g (63%). Required for $C_{10}H_{16}AlCl_7P_2Sn$ (630.04): C, 22.9; H, 4.8. Found C, 23.1; H, 5.3%. IR (Nujol/cm^{-1}): ν = 280m, 289m (Sn-Cl), 484s, 503sh ($[AlCl_4]^-$). ^{1}H NMR (CD_2Cl_2, 298 K): δ = 1.36 (m, [18H], CH_3), 2.32 (m, [12H], CH_2). $^{13}C\{^1H\}$ NMR (CD_2Cl_2, 298 K): δ = 7.34 (t, ^2J +$^4J_{31P\text{-}13C}$ = 2.93 Hz, -CH_3), 14.12 (t, ^1J +$^3J_{31P\text{-}13C}$ = 22.45 Hz). $^{31}P\{^1H\}$ NMR (CD_2Cl_2, 298 K): δ = 35.22 ($^1J_{31P\text{-}117Sn}$ = 2208 Hz, $^1J_{31P\text{-}119Sn}$ = 2317 Hz); (CD_2Cl_2, 183 K): δ = 26.96 ($^1J_{31P\text{-}117Sn}$ = 2426 Hz, $^1J_{31P\text{-}119Sn}$ = 2520 Hz). ^{27}Al NMR (CD_2Cl_2, 298 K): δ = 103.2 (s, $[AlCl_4]^-$). ^{119}Sn NMR (CD_2Cl_2, 298 K): δ = –350.2 (br t, $^1J_{31P\text{-}119Sn}$ = 2307 Hz).

$[SnCl_2(PEt_3)_2][AlCl_4]_2$: $[SnCl_4(PEt_3)_2]$ (0.200 g, 0.40 mmol) was suspended in CH_2Cl_2 (5 ml), to this $AlCl_3$ (0.107 g, 0.80 mmol) was added, the suspension was stirred for 2 h leaving a clear and colourless solution, the solution was concentrated to dryness and washed with Et_2O (3 x 10 ml) then dried *in vacuo* leaving a sticky white solid which was dried *in vacuo*. Yield 0.201 g (66%). Anal. Required for $C_{12}H_{30}Al_2Cl_{10}P_2Sn$ (763.39) C, 18.9; H, 4.0. Found C, 19.0; H, 3.8, IR (Nujol/cm^{-1}): ν = 289m (Sn-Cl), 484s, ($[AlCl_4]^-$). ^1H NMR (CD_2Cl_2, 298 K): δ = 1.39 (m, [18H], CH_3), 2.38 (m, [12H], CH_2), $^{13}C\{^1H\}$NMR (CD_2Cl_2, 298 K): δ = 7.50 (t, $^2J + {}^4J_{31P\text{-}13C}$ = 2.93 Hz, -CH_3), 14.51 (t, $^1J + {}^3J_{31P\text{-}13C}$ = 13.2 Hz), ^{27}Al NMR (CD_2Cl_2, 298 K): δ = 103.0, $^{31}P\{^1H\}$ NMR (CD_2Cl_2, 298 K): δ = 40.78 ($^1J_{31P\text{-}117Sn}$ = 2172 Hz, $^1J_{31P\text{-}119Sn}$ = 2274 Hz). ^{119}Sn NMR (CD_2Cl_2, 298 K): δ = −301.4 (br, t, $^1J_{31P\text{-}119Sn}$ = 2291 Hz).

Reaction of $[SnCl_2(PEt_3)_2][AlCl_4]_2$ + PEt_3: $[SnCl_2(PEt_3)_2][AlCl_4]_2$ (0.100 g, 0.13 mmol) was dissolved in CH_2Cl_2 (3 mL), to this PEt_3 (0.015 g, 0.22 mmol) was added in CH_2Cl_2 (2 mL). To this 10 drops of CD_2Cl_2 is added. A portion of the solution was used for *in situ* NMR studies. ^{27}Al NMR (CD_2Cl_2, 298 K): δ = 103.1 (s, $[AlCl_4]^-$), 110.8 (d, $^1J_{31P\text{-}27Al}$ = 267 Hz, $[AlCl_3(PEt_3)]$). $^{31}P\{^1H\}$ NMR (CD_2Cl_2, 298 K): δ = −14.8 (sextet, $^1J_{27Al\text{-}31P}$ = 264 Hz, $[AlCl_3(PEt_3)]$), 32.2 ($^1J_{31P\text{-}117Sn}$ = 2312 Hz, $^1J_{31P\text{-}119Sn}$ = 2394 Hz, new Sn-PEt_3 containing cation – see text). ^{119}Sn NMR (CD_2Cl_2, 298 K): δ = −449 (t, $^1J_{31P\text{-}119Sn}$ = 2394 Hz).

$[SnCl_3(PEt_3)_2][BAr^F]$: A Schlenk was charged with $[SnCl_4(PEt_3)_2]$ (0.100 g, 0.20 mmol) and $Na[BAr^F]$ (0.178 g, 0.20 mmol). To this CH_2Cl_2 (5 mL) was added the resulting cloudy solution was stirred for 2 h, the solution was then filtered and concentrated to dryness *in vacuo* yielding a white solid. Yield: 0.201 g (75%). Required for $C_{44}H_{42}BCl_3F_{24}P_2Sn$ (1324.3): C, 39.9, H, 3.2 Found C, 39.8, H, 3.3%. IR (Nujol/cm^{-1}): ν = 286m (Sn-Cl). ^1H NMR (CD_2Cl_2, 298 K): δ = 1.35 (m, [18H], CH_3), 2.29 (m, [12H], CH_2), 7.57 (s, [4H], $[BAr^F]$), 7.72 (m, [8H], $[BAr^F]$); $^{19}F\{^1H\}$ NMR (CD_2Cl_2, 298 K): δ = –63.0 (s, -CF_3) $^{31}P\{^1H\}$ NMR (CD_2Cl_2, 298 K): δ = 37.1 ($^1J_{31P\text{-}117Sn}$ = 2208 Hz, $^1J_{31P\text{-}119Sn}$ = 2311 Hz); ^{119}Sn NMR (CD_2Cl_2, 298 K): δ = –379 (t, $^1J_{31P\text{-}119Sn}$ = 2311 Hz).

$[SnCl_3(AsEt_3)_2][BAr^F]$: A Schlenk was charged with $[SnCl_4(AsEt_3)_2]$ (0.100 g, 0.17 mmol) and $Na[BAr^F]$ (0.152 g, 0.17 mmol). To this CH_2Cl_2 (5 mL) was added the resulting cloudy solution was stirred for 2 h and then filtered and concentrated to dryness *in vacuo* yielding a white solid. Yield: 0.162 g (67%). Required for $C_{44}H_{42}BCl_3F_{24}As_2Sn$ (1412.2): C, 37.4, H, 3.0 Found C, 37.3, H, 2.8%. IR (Nujol/cm^{-1}): ν = 285m (Sn-Cl). ^1H NMR (CD_2Cl_2, 298 K): δ = 1.44 (t, $^3J_{HH}$ = 7.7 Hz, [18H], CH_3), 2.42 (q, $^3J_{HH}$ = 7.7 Hz, [12H], CH_2), 7.57 (s, [4H], $[BAr^F]$), 7.72 (m, [8H], $[BAr^F]$); $^{19}F\{^1H\}$ NMR (CD_2Cl_2, 298 K): δ = –63.0 (s, -CF_3); ^{119}Sn NMR (CD_2Cl_2, 183 K): δ = –388 (br s).

[$SnCl_3${*o*-$C_6H_4(PMe_2)_2$}][BAr^F]: A Schlenk was charged with [$SnCl_4${*o*-$C_6H_4(PMe_2)_2$}] (0.100 g, 0.17 mmol) and Na[BAr^F] (0.152 g, 0.17 mmol) and to this CH_2Cl_2 (5 mL) was added. The resulting cloudy solution was stirred for 2 h and then filtered and concentrated to dryness *in vacuo* yielding a white solid. Yield: 0.162 g (67%). Required for $C_{42}H_{28}BCl_3F_{24}P_2Sn$ (1286.2): C, 39.2, H, 2.2 Found C, 39.3, H, 2.0%. IR (Nujol/cm^{-1}): ν = 281m (Sn-Cl). ^{1}H NMR (CD_2Cl_2, 298 K): δ = 2.01 (t, $^2J + ^5J_{PH}$ = 4.7 Hz, [12H], CH_3), 7.57 (s, [4H], [BAr^F]), 7.72 (m, [8H], [BAr^F]), 7.82 (m, [4H], [BAr^F]); ^{19}F{^{1}H} NMR (CD_2Cl_2, 298 K): δ = –63.0 (s, -CF_3); ^{31}P{^{1}H} NMR (CD_2Cl_2, 298 K): δ = -24.50 ($^1J_{31P\text{-}119Sn}$ = 1007 Hz); ^{119}Sn NMR (CD_2Cl_2, 183/298 K): δ = n.o.

[$SnBr_3(AsEt_3)_2$][BAr^F]: A Schlenk was charged with [$SnBr_4(AsEt_3)_2$] (0.077 g, 0.10 mmol) and Na[BAr^F] (0.090 g, 0.10 mmol) to this CH_2Cl_2 (5 mL) was added; the resulting cloudy solution was stirred for 2 h and then filtered and concentrated to dryness *in vacuo* yielding a light yellow gum, which was then dissolved in Et_2O (5 mL), then the solution was concentrated to dryness *in vacuo* yielding a light yellow solid. Yield: 0.091 g (58%). Required for $C_{44}H_{42}As_2BBr_3F_{24}Sn$ (1448.2): C, 34.2, H, 2.7 Found C, 34.3, H, 2.9%. IR (Nujol/cm^{-1}): ν = 210m (Sn-Br). ^{1}H NMR (CD_2Cl_2, 298 K): δ = 1.39 (t, $^3J_{HH}$ = 7.6 Hz, [18H], CH_3), 2.42 (br, [12H], CH_2), 7.58 (s, [4H], [BAr^F]), 7.73 (m, [8H], [BAr^F]); ^{13}C{^{1}H} NMR (CD_2Cl_2, 298 K): δ = 9.1 (s, -CH_3), 15.9 (s, -CH_2), 118.1(s), 123.8(s), 126.5(s), 129.3(m), 135.4(s), 162.3(q, $^1J_{11B\text{-}13C}$ = 49.9 Hz); ^{19}F{^{1}H} NMR (CD_2Cl_2, 295 K): δ = –62.8 (s, -CF_3). ^{119}Sn NMR (CD_2Cl_2, 183/298 K): δ = n.o.

2.7 References

1 J. Burt, W. Levason and G. Reid, Coord. Chem. Rev., 2014, 260, 65–115.

2 M. F. Davis, M. Clarke, W. Levason, G. Reid and M. Webster, Eur. J. Inorg. Chem., 2006, 14, 2773–2782.

3 G. G. Mather, G. M. McLaughlin and A. Pidcock, J. Chem. Soc., Dalton Trans., 1973, 1823–1827.

4 N. Bricklebank, S. M. Godfrey, C. A. McAuliffe and R. G. Pritchard, J. Chem. Soc., Chem. Commun., 1994, 695.

5 M. F. Mahon, N. L. Moldovan, K. C. Molloy, A. Muresan, I. Silaghi-Dumitrescu and L. Silaghi-Dumitrescu, Dalton Trans., 2004, 4017–4021.

6 B. Cordero, V. Gómez, A. E. Platero-Prats, M. Revés, J. Echeverría, E. Cremades, F. Barragán and S. Alvarez, Dalton Trans., 2008, 2832–2838.

7 M. Mantina, A. C. Chamberlin, R. Valero, C. J. Cramer and D. G. Truhlar, J. Phys. Chem. A, 2009, 113, 5806–5812.

8 A. R. J. Genge, W. Levason and G. Reid, Inorg. Chim. Acta, 1999, 288, 142–149.

9 E. MacDonald, L. Doyle, S. S. Chitnis, U. Werner-Zwanziger, N. Burford and A. Decken, Chem. Commun., 2012, 48, 7922–7924.

10 R. Colton, D. Dakternieks and C.-A. Harvey, Inorg. Chim. Acta, 1982, 61, 1–7.

11 A. S. Batsanov, R. M. K. Deng, K. B. Dillon, A. E. Goeta, J. A. K. Howard, J. Meldrum, P. K. Monks, H. Puschmann and H. J. Shepherd, Heteroat. Chem., 2009, 20, 136–143.

12 J. Burt, W. Levason, M. E. Light and G. Reid, Dalton Trans., 2014, 43, 14600–14611.

13 E. I. Davydova, A. Y. Timoshkin, T. N. Sevastianova, A. V. Suvorov and G. Frenking, J. Mol. Struct. , 2006, 767, 103–111

14 D. Cunningham, M. J. Frazer and J. D. Donaldson, J. Chem. Soc. A, 1971, 2049–2054.

15 S. Parsons, P. Resouly, P. Bailey, I. Oswald and R. Johnstone, CSD Commun., 2006, 612916.

16 S. J. Hwang, B. L. Anderson, D. C. Powers, A. G. Maher, R. G. Hadt and D. G. Nocera, Organometallics, 2015, 34, 4766–4774.

17 D. M. U. K. Somisara, M. Bühl, T. Lebl, N. V. Richardson, A. M. Z. Slawin, J. D. Woollins and P. Kilian, Chem. Eur. J., 2011, 17, 2666–2677.

18 M. F. Davis, W. Levason, G. Reid and M. Webster, Dalton Trans., 2008, 2261.

19 M. Hall and D. B. Sowerby, J. Chem. Soc., Dalton Trans., 1983, 1095–1099.

20 M. Yang and F. P. Gabbaï, Inorg. Chem., 2017, 56, 8644–8650.

21 D. Cunningham, J. Finnegan, J. D. Donaldson and M. J. Frazer, J. Chem. Soc., Dalton Trans., 1977, 162–164.

22 S. S. Chitnis, H. A. Sparkes, V. T. Annibale, N. E. Pridmore, A. M. Oliver and I. Manners, Angew. Chem. Int. Ed., 2017, 56, 9536–9540.

Chapter 3 Synthesis of neutral and cationic germanium(IV) fluoride phosphine complexes

3.1 Introduction

3.1.1 Neutral complexes of germanium(IV) fluoride and related complexes

Germanium(IV) fluoride can form complexes with a variety of both hard and soft ligands. Complexes can be synthesised either by the reaction of GeF_4 (gas) directly with the neutral ligands or by the reaction of an appropriate adduct with the ligand; in this case, the adduct used is commonly $[GeF_4(MeCN)_2]$. $[GeF_4(MeCN)_2]$ can be conveniently synthesised by bubbling GeF_4 gas through acetonitrile, which causes the complex to precipitate out. Nitriles like $NCCH_2X$ (X = F and Cl) can also react with germanium fluoride to form isolatable complexes of the form $[GeF_4(NCCH_2X)_2]$. In this case, the nitrile ligands are *cis* to each other, as shown in **Figure 3.1** below.[1]

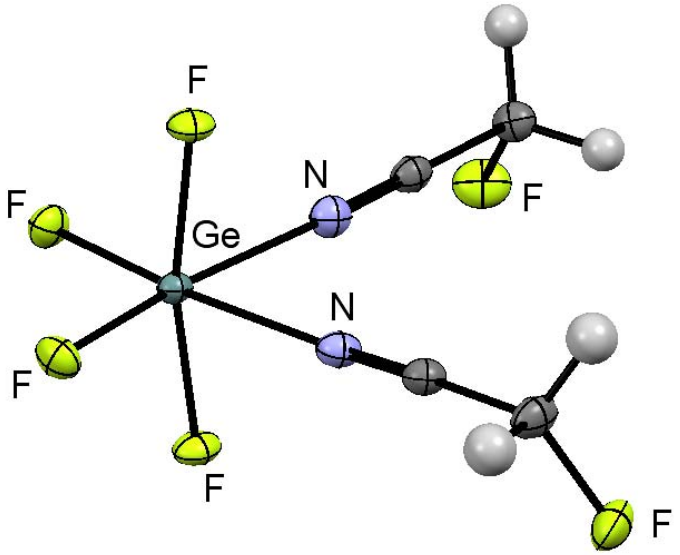

Figure 3.1 – Showing the *cis* arrangement of ligands in the crystal structure of $[GeF_4(NCCH_2F)_2]$. Redrawn for Ref 1.

The reaction of germanium tetra-ethoxide, aqueous HPF_6 and pyridine under solvothermal conditions leads to the formation of $[GeF_4(py)_2]$; this complex, unlike the *cis*-nitrile complex discussed previously, has the nitrogen donor ligands *trans* to each other (shown in **Figure 3.2** below).[2]

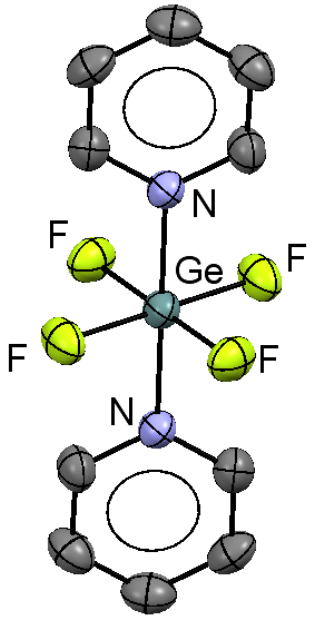

Figure 3.2 – The crystal structure of $[GeF_4(py)_2]$ showing the *trans* arrangement of the pyridine ligands. Redrawn from Ref. 2.

Polydentate nitrogen donor ligands can also be used to synthesise stable complexes of germanium fluoride. The reaction of 2,2-bipyridine, 1,10-phenanthroline, or $Me_2NCH_2CH_2NMe_2$ with $[GeF_4(MeCN)_2]$ in CH_2Cl_2 leads exclusively to the formation of the *cis*-isomer, with the neutral ligand chelating.[3,4] The reaction of Me_4cyclam with $[GeF_4(MeCN)_2]$ leads to the formation of $[GeF_4(\kappa^2\text{-}Me_4cyclam)]$, where the ligand binds in a bidentate fashion with the germanium centre being *exocyclic* to the ring. The structures of $[GeF_4(phen)]$ and $[GeF_4(\kappa^2\text{-}Me_4cyclam)]$ are shown below in **Figure 3.3**.

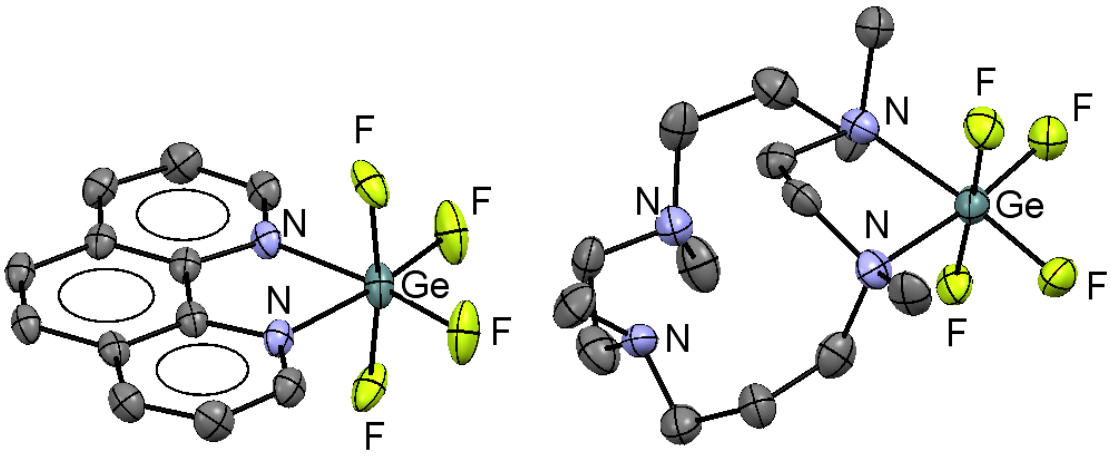

Figure 3.3 – (a) The crystal structure of $[GeF_4(phen)]$ and (b) the crystal structure of $[GeF_4(\kappa^2\text{-}Me_4cyclam)]$ showing the *cis* configuration. Both redrawn from Ref. 3.

Germanium fluoride can also form stable complexes with O-donor ligands; for example, the reaction of $[GeF_4(MeCN)_2]$ with two equivalents of OPR_3 (R = Me, Et, Ph) leads to the formation of $[GeF_4(OPR_3)_2]$. In the solution state, $^{19}F\{^1H\}$ NMR spectroscopy shows that these complexes exist as both *cis* and *trans* isomers. However, only the *trans* isomer has been determined crystallographically.[5] In contrast, for the bidentate phosphine oxides only the *cis* isomer is seen in solution.[6] When the heavier analogues, $GeCl_4$ or $GeBr_4$, are reacted with $OPMe_3$, depending on the ratio of germanium to ligand, one or two of the halides are displaced to form cationic or dicationic complexes of the form $[GeCl_3(OPMe_3)_3]_2[GeCl_6]$ and $[GeX_2(OPMe_3)_4][X]_2$ (X = Cl, Br); the structures of the chloride derivatives are shown below in **Figure 3.4**.[5] Presumably in the case of GeF_4, the stronger Ge-F bond precludes the phosphine oxide from displacing the fluorines from the germanium centre, and hence only the neutral complexes form.

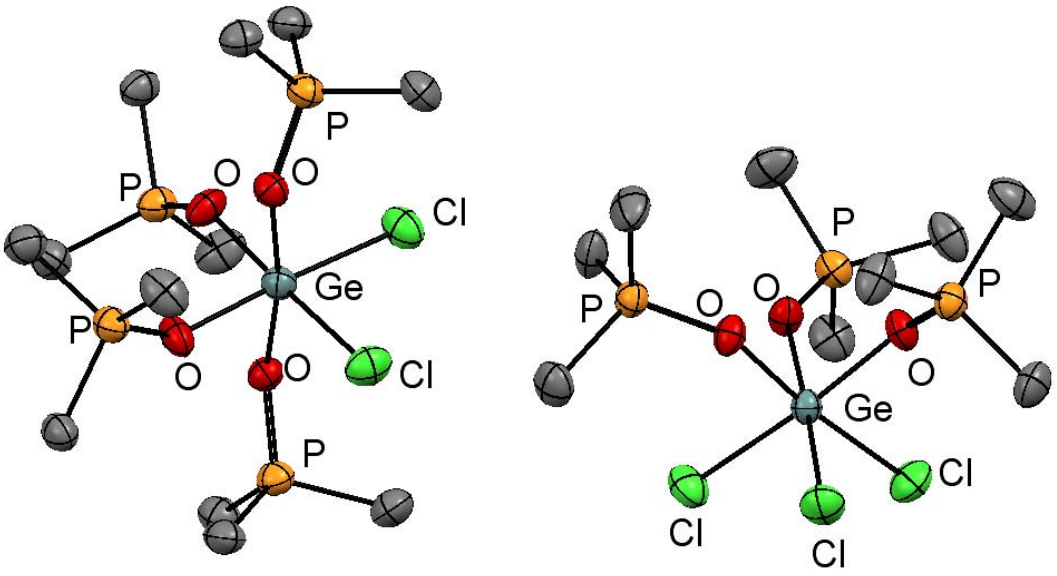

(a) (b)

Figure 3.4 – Crystal structures of (a) the dication in $[GeCl_2(OPMe_3)_4][Cl]_2$ and (b) the monocation in $[GeCl_3(OPMe_3)_3]_2[GeCl_6]$. Both redrawn from Ref. 5.

There are fewer reports of germanium fluoride complexes with softer donor ligands than there are for complexes with hard donor ligands. The reaction of $[GeF_4(MeCN)_2]$ with two equivalents of PMe_3 leads to the formation of *trans*-$[GeF_4(PMe_3)_2]$ as the sole product. Here multinuclear NMR spectroscopy can be used to suggest that the complex is *trans* in solution at 298 K, as a quintet is observed in the $^{31}P\{^1H\}$ NMR spectrum. The $^{19}F\{^1H\}$ NMR spectrum at 298 K shows a triplet, also consistent with the *trans* isomer being present. The reaction of $AsEt_3$ with $[GeF_4(MeCN)_2]$ forms a white unstable solid. In $[GeF_4(AsEt_3)_2]$, the arsine resonances are shifted to high frequency from 'free' ligand, and at low temperature two triplets are seen in the $^{19}F\{^1H\}$ NMR spectrum; this suggests that the *cis*-octahedral isomer forms in this case, but an analytically pure sample could not be obtained. However, the reaction of $AsEt_3$ with $GeCl_4$ leads to the formation of *trans*-$[GeCl_4(AsEt_3)_2]$, although this complex is not stable in solution and degrades into $AsEt_3Cl_2$ over time, presumably with concomitant formation of $GeCl_2$. There is spectroscopic evidence that $[GeCl_4(PMe_3)_2]$ can be isolated from a solvent-free reaction of $GeCl_4$ and PMe_3; although, if a solvent is employed, redox chemistry occurs and the product is $[GeCl_3][PMe_3Cl]$ exclusively.[7]

Diphosphine ligands can also react with $[GeF_4(MeCN)_2]$ to form stable complexes of the form $[GeF_4(diphosphine)]$ (diphosphine = *o*-$C_6H_4(PR_2)_2$ (R = Me, Ph), $R_2P(CH_2)_2PR_2$ (R = Me, Et, Cy, Ph). Low-temperature multinuclear NMR spectroscopy can be used to assign the geometry in these complexes. In the $^{19}F\{^1H\}$ NMR spectra, the fluorides *trans* to the phosphine ligand appear as a doublet of doublet of triplets; the two doublet couplings come from coupling to the magnetically inequivalent phosphorus' and the triplet coupling is due to coupling with the axial fluorines. A triplet of triplets is also seen in the $^{19}F\{^1H\}$ NMR spectrum due to the axial fluorines coupling to the phosphorus' and the equatorial fluorines. In the $^{31}P\{^1H\}$ NMR spectra of these complexes, a triplet of doublets of doublets is seen for each. Two of these complexes have been structurally characterised and have a *cis* geometry. The structure of the complex $[GeF_4\{o\text{-}C_6H_4(PMe_2)_2\}]$ is shown in **Figure 3.5** below.[7]

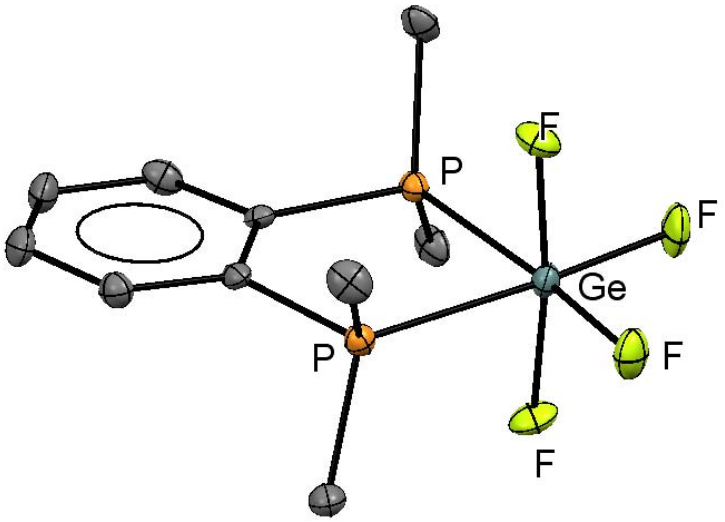

Figure 3.5 – The crystal structure of $[GeF_4\{o\text{-}C_6H_4(PMe_2)_2\}]$. Redrawn from Ref. 7.

3.1.2 Cationic germanium fluoride complexes

There are very few reports of cationic germanium fluoride complexes in the literature. The reaction of $[GeF_4(MeCN)_2]$ with $Me_3[9]aneN_3$ in CH_2Cl_2 leads to the formation of $[GeF_3(Me_3[9]aneN_3)]_2[GeF_6]$, showing that the tridentate macrocyclic N-donor ligand is a strong enough donor to displace one of the fluoride ligands. The cation found in this complex has been structurally characterised as its chloride salt in the solid state (shown in **Figure 3.6** below). In contrast, the reaction with Me_4cyclam does not lead to the formation of a cationic complex, as discussed above. The weaker S-donor macrocycle $[9]aneS_3$ is not strong enough to displace fluoride and so does not form an analogous complex; the low-temperature $^{19}F\{^1H\}$ NMR spectrum shows two sets of triplets, which suggests that this ligand forms a complex with κ^2-coordination, $[GeF_4(\kappa^2\text{-}[9]aneS_3)]$; however, this complex could not be isolated cleanly.[3]

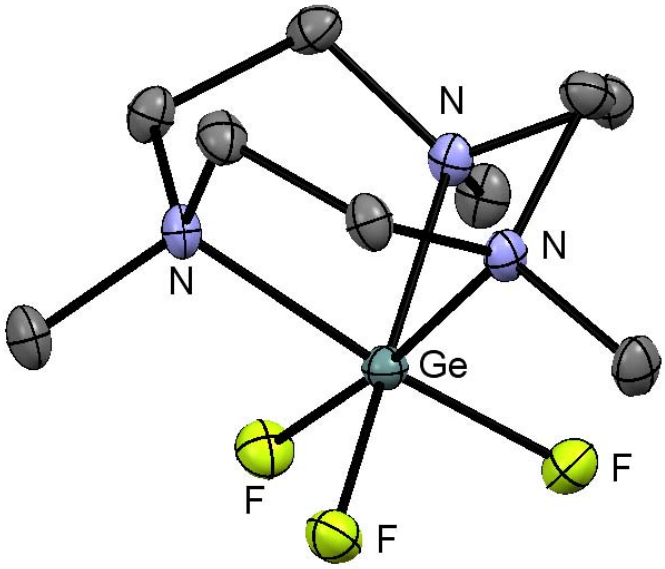

Figure 3.6 – Structure of the cation $[GeF_3(Me_3[9]aneN_3)]^+$ showing the *fac* geometry. Redrawn from Ref. 3.

Dicationic germanium fluoride complexes can also be synthesised by the treatment of Ge(II) complexes with a fluorinating agent. The reaction of $[Ge(BIMEt_3)][OTf]_2$ (BIMEt = tris(1-ethyl-benzoimidazol-2-ylmethyl)amine) with the oxidising agent XeF_2 leads to the clean formation of $[GeF_2(BIMEt_3)][OTf]_2$. This reaction is driven by the formation of Xe gas. The reaction of this difluoride complex with one equivalent of TMSOTf leads to $[GeF(OTf)(BIMEt_3)][OTf]_2$; this reaction can be reversed by the addition of one equivalent of $NaBF_4$. The structures of both of these complexes are shown in **Figure 3.7** below.[8]

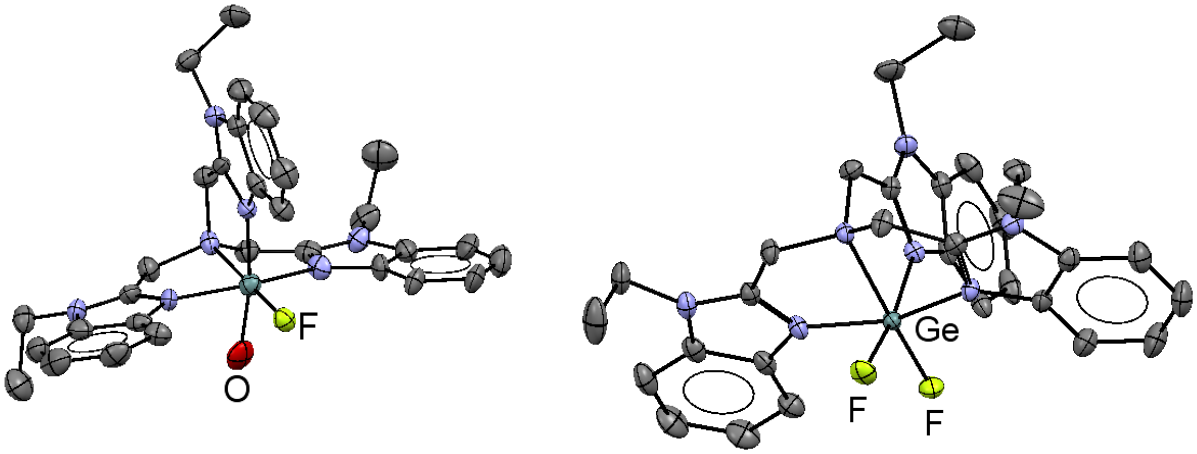

(a) (b)

Figure 3.7 – Showing the structure of the (a) the dication in $[GeF(OTf)(BIMEt_3)][OTf]_2$ showing the coordinated triflate oxygen atom and (b) the dication in $[GeF_2(BIMEt_3)][OTf]_2$. Both redrawn from Ref. 8

3.2 Aims

This chapter aims to develop the coordination chemistry of GeF_4 with soft donor ligands. Investigating the effect of changing ligand denticity as well as exploring the possibility of generating cationic complexes through halide abstraction and changing steric bulk of the ligand.

3.3 Results and discussion

3.3.1 Neutral germanium fluoride complexes

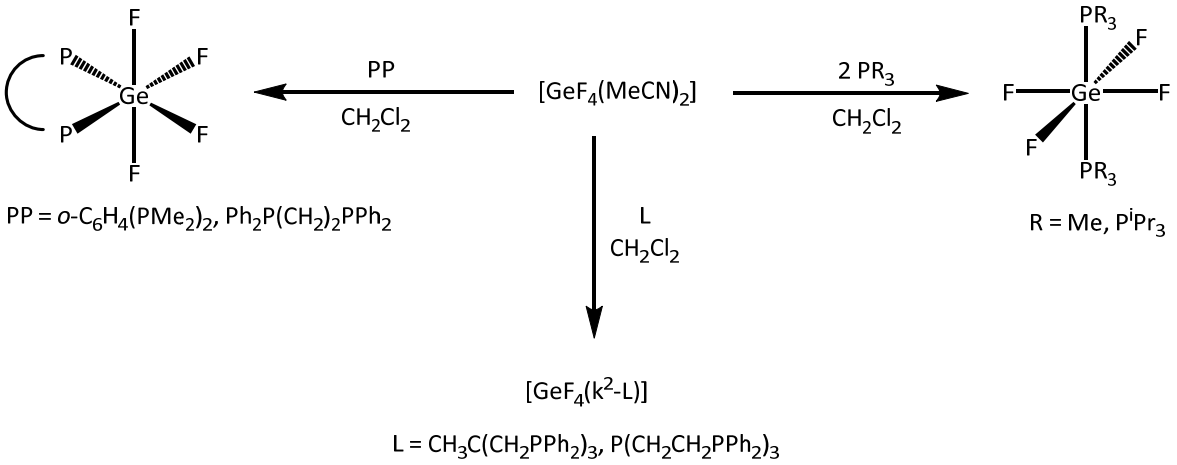

Scheme 3.1 – Synthesis of neutral germanium tetrafluoride phosphine complexes.

The reaction of $[GeF_4(MeCN)_2]$ with two equivalents of PMe_3 in CH_2Cl_2 leads to the formation of *trans*-$[GeF_4(PMe_3)_2]$ as described previously (See **Scheme 3.1**).[7] Weakly coordinating solvents are required for synthesis and NMR spectroscopy to prevent ligand displacement, because of this CH_2Cl_2 is usually chosen as the preferred solvent. At room temperature, a doublet is seen in the ^1H NMR spectrum at δ = 1.48 ($^2J_{PH}$ = 12 Hz), which compares favourably with the literature, where they report it at δ = 1.46, albeit in a different solvent (CD_2Cl_2 *vs.* $CDCl_3$).[7] The $^{31}P\{^1H\}$ NMR spectrum shows a broad singlet at δ = -14.5 at 298K, which is different to the expected quintet, which suggests at room temperature an exchange process is going on in solution.[7] At 298 K, the $^{19}F\{^1H\}$ NMR showed a broad singlet at δ = -96.6, which compares to the triplet reported in the literature at δ = -96.9; again this can be explained by fast ligand exchange.[7]

Slow evaporation of a CH_2Cl_2 solution of $[GeF_4(PMe_3)_2]$ led to the deposition of crystals suitable for single-crystal X-ray analysis. The crystal structure is shown in **Figure 3.8** below. This complex is the first structurally characterised monodentate phosphine complex of germanium fluoride, and there are no other examples of structurally characterised germanium(IV) halide phosphine complexes with which to compare. The lack of structurally authenticated complexes of this type is primarily due to their instability and their tendency to undergo redox chemistry in solution.[7] This is in stark contrast to tin(IV) halides, where phosphine complexes are known for all halides.[9] The

crystal structure demonstrates that the *trans*-octahedral geometry is retained in the solid-state.

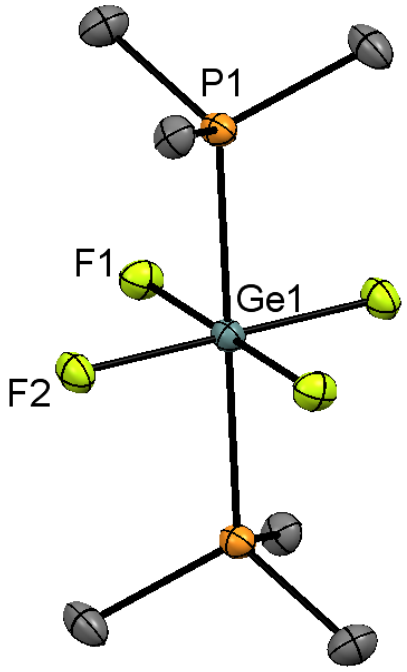

Figure 3.8 – The crystal structure of $[GeF_4(PMe_3)_2]$ showing the atom labelling scheme. The ellipsoids are drawn at the 50% probability level and H atoms are omitted for clarity. Selected bond lengths (Å) and angles (°) are: Ge1–P1 = 2.3718(5), Ge1–F1 = 1.8247(13), Ge1–F2 = 1.8146(13), F1–Ge1–F2 = 90.97(6). Symmetry operation: (-X,-Y,-Z).

To probe the effect of the ligand sterics on fluoride abstraction in this chemistry, the complex $[GeF_4(P^iPr_3)_2]$ was synthesised by the reaction of $[GeF_4(MeCN)_2]$ with two equivalents of $^iPr_3P$ in CH_2Cl_2. The ^1H NMR spectrum shows a doublet of doublets resonance at δ = 1.40 assigned to the methyl protons of the complex and a multiplet at δ = 2.55 corresponding to the CH protons, with the expected 6:1 ratio. The $^{31}P\{^1H\}$ and $^{19}F\{^1H\}$ NMR spectra contain broad resonances at δ = +34.3 and δ = -107.2, respectively, indicating fast exchange at room temperature on the NMR time scale. As part of this study, the diphosphine complexes $[GeF_4\{o\text{-}C_6H_4\{PMe_2\}_2\}]$ and $[GeF_4\{Ph_2P(CH_2)_2PPh_2\}]$ were also prepared according to literature procedures, and their purity confirmed by NMR spectroscopy.[7]

To expand the range of multidentate phosphine complexes of germanium fluoride, the triphosphine ligand, $CH_3C(CH_2PPh_2)_3$, was chosen. $CH_3C(CH_2PPh_2)_3$ reacts with $[GeF_4(MeCN)_2]$ in a 1:1 ratio to form $[GeF_4(\kappa^2\text{-}CH_3C\{CH_2PPh_2\}_3)]$, crystals of which were grown by layering a CH_2Cl_2 solution of the compound with hexane. The structure is shown in **Figure 3.9** below. The ligand coordinates in a bidentate fashion to the germanium centre, forming a puckered 6-membered ring with every atom of the ring being approximately coplanar (other than the bridgehead atom which is out of the plane). The pendent phosphine arm is uncoordinated and has no close contacts with neighbouring molecules and there is no evidence that the pendent arm can directly displace a fluoride from the germanium centre to generate a cation and κ^3-triphosphine coordination.

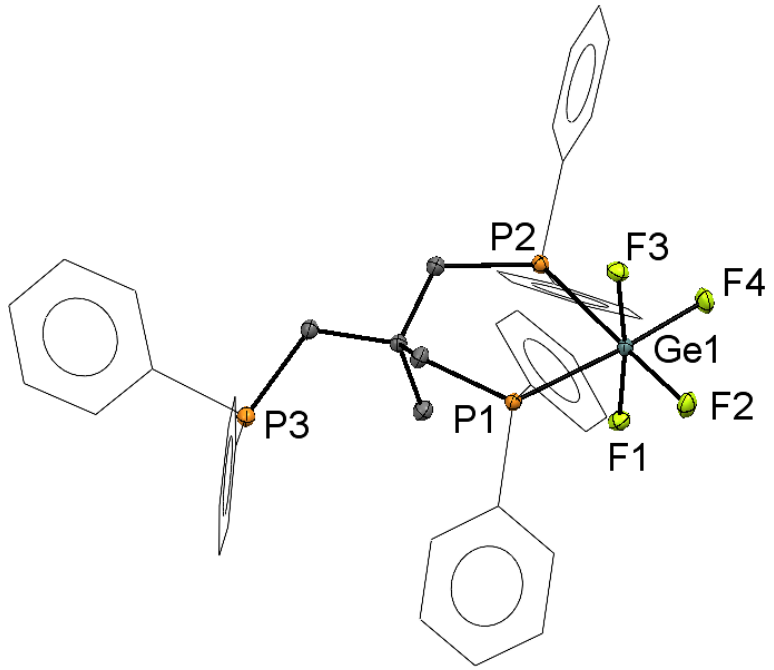

Figure 3.9 – The crystal structure of $[GeF_4(\kappa^2\text{-}CH_3C\{CH_2PPh_2\}_3)]$ showing the atom labelling scheme. The ellipsoids are drawn at the 50% probability level and H atoms and CH_2Cl_2 solvent molecule are omitted, and phenyl rings are displayed as wireframe for clarity. Selected bond lengths (Å) and angles (°) are: Ge1–P1 = 2.4732(4), Ge1–P2 = 2.5030(4), Ge1–F1 = 1.7871(9), Ge1–F2 = 1.7780(9), Ge1–F3 = 1.7977(9), Ge1–F4 = 1.7736(9), P1–Ge1–P2 = 92.886(13), F1–Ge1–F3 = 172.44(4), F2–Ge1–F4 = 92.47(4), P1–Ge1–F4 = 174.90(3), P2–Ge1–F2 = 178.75(3).

In the $^{19}F\{^{1}H\}$ NMR spectrum at room temperature, two broad resonances of equal intensity are seen at δ = -72.2 and δ = -108.6, which correspond to the two fluorine environments in the complex above. There is another sharper resonance at δ = -137.7, which corresponds to free GeF_4. In the room temperature $^{31}P\{^{1}H\}$ NMR spectrum, a broad resonance is seen at δ = 4.0 and another corresponding to uncoordinated phosphine appears at δ = -23.5, suggesting that the system is dynamic in solution at room temperature, and the phosphine ligand is weakly bound, since both 'free' phosphine and free GeF_4 are seen in the NMR spectra.

If the solution of the complex is cooled to 183 K, the $^{31}P\{^{1}H\}$ NMR spectrum shows a triplet of doublets of doublets at δ = -4.5 and a singlet at δ = -27.9 in a ratio of 2:1. This is consistent with the formation of a complex with two phosphine arms coordinated and one free arm. 'Free' phosphine also appears in the NMR spectrum. The $^{19}F\{^{1}H\}$ spectrum at 183 K shows resonances with intensities with a 1:1 ratio. Both resonances appear as broad multiplets at δ = -77.7 and δ = -110.3, similar to those found in other *cis* coordinated germanium tetrafluoride phosphine complexes.[7] At 243 K, the couplings of the resonances are more defined, and the resonance at δ = - 74.4 appears as two overlapping multiplets due to the axial fluorines being in similar but not identical environments. The resonance at δ = -109.3 appears as a doublet of doublet of triplets.

At room temperature in the ^{1}H NMR spectrum of this compound, there is a broad methylene resonance at δ = 2.69 and a methyl resonance at δ = 0.87 in a 6:3 ratio; this is consistent with fast exchange of the phosphine arms at this temperature. In the low temperature (183 K) ^{1}H NMR spectrum, there are three sets of methylene resonances at δ = 2.01, 2.79, and 2.90. The first of these corresponds to the methylene group of the free arm (H_c), the other two correspond to the methylenes on the coordinated arms; in each methylene group, one hydrogen points towards the other (H_b) and the second points away (H_a) (see **Figure 3.10**). In the spectrum some 'free' phosphine is also evident.

The molecule has approximately C_{2v} symmetry at germanium, so group theory predicts four IR active Ge-F stretching vibrations. However, in these systems it is common for some of the peaks to overlap, and in this case only one strong, broad peak is seen at 603 cm^{-1}. Elemental analysis data is consistent with the formation of the 1:1 complex.

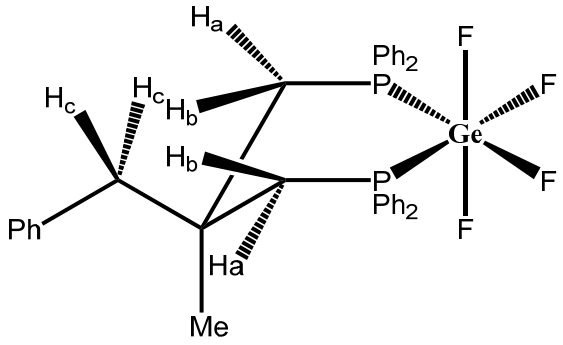

Figure 3.10 – Structure of $[GeF_4(\kappa^2\text{- } CH_3C\{CH_2PPh_2\}_3)]$ showing the different methylene H environments.

Following the successful formation of $[GeF_4(\kappa^2\text{- } CH_3C\{CH_2PPh_2\}_3)]$, the tetraphosphine ligand, $P(CH_2CH_2PPh_2)_3$, was investigated. This ligand can exhibit a range of possible coordination modes; the two possible *cis* isomers are shown in **Figure 3.11** below. The reaction of $[GeF_4(MeCN)_2]$ with $P(CH_2CH_2PPh_2)_3$ leads to the formation of the complex $[GeF_4\{\kappa^2\text{- } P(CH_2CH_2PPh_2)_3\}]$ as a white solid in good yield. In the room temperature ^1H spectrum, there are two broad singlets in the methylene region at δ = 2.03 and 2.28 and broad resonances in the aromatic region with a 1:1:6 integration, consistent with a dynamic process occurring, which exchanges the terminal arms at room temperature. This is also consistent with the room temperature $^{19}F\{^1H\}$ NMR spectrum, where two broad resonances are seen at δ = -94.8 and -114.2. The room temperature $^{31}P\{^1H\}$ NMR spectrum shows broad ill-defined multiplets to high frequency of the 'free' ligand.

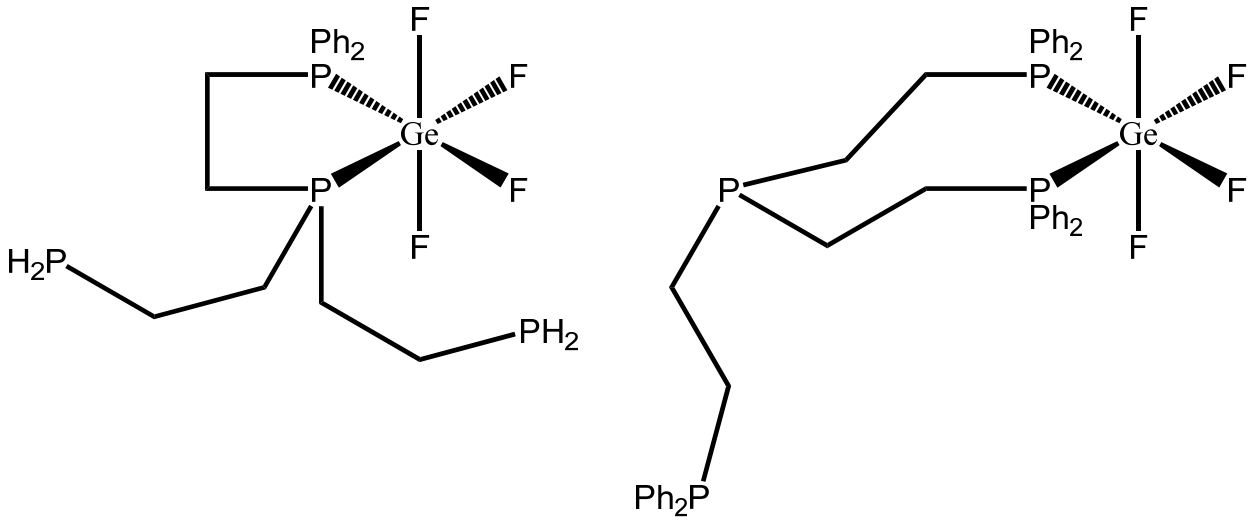

(a) (b)

Figure 3.11 – Two possible cis isomers of $[GeF_4\{\kappa^2\text{-}P(CH_2CH_2PPh_2)_3\}]$.

If the sample is cooled down to 183 K then the methylene resonances split into four broad resonances which is consistent with κ^2 ligand coordination. At 183 K, the ill-defined multiplets in the $^{31}P\{^1H\}$ NMR spectrum sharpen into three multiplets at δ = 3.2, -12.4, -17.6 in a ratio of 1:2:1, as shown in **Figure 3.12** below, and suggesting that at this temperature exchange is slow, and one isomer dominates. This isomer has one terminal and the apical phosphine groups coordinated as shown in **Figure 3.11a**. The $^{31}P\{^1H\}$ NMR spectrum was also simulated using the SPINACH software package[10] to confirm the coupling scheme (with the spin system labelling in **Figure 3.14**); the simulated spectrum is shown in **Figure 3.13** below.

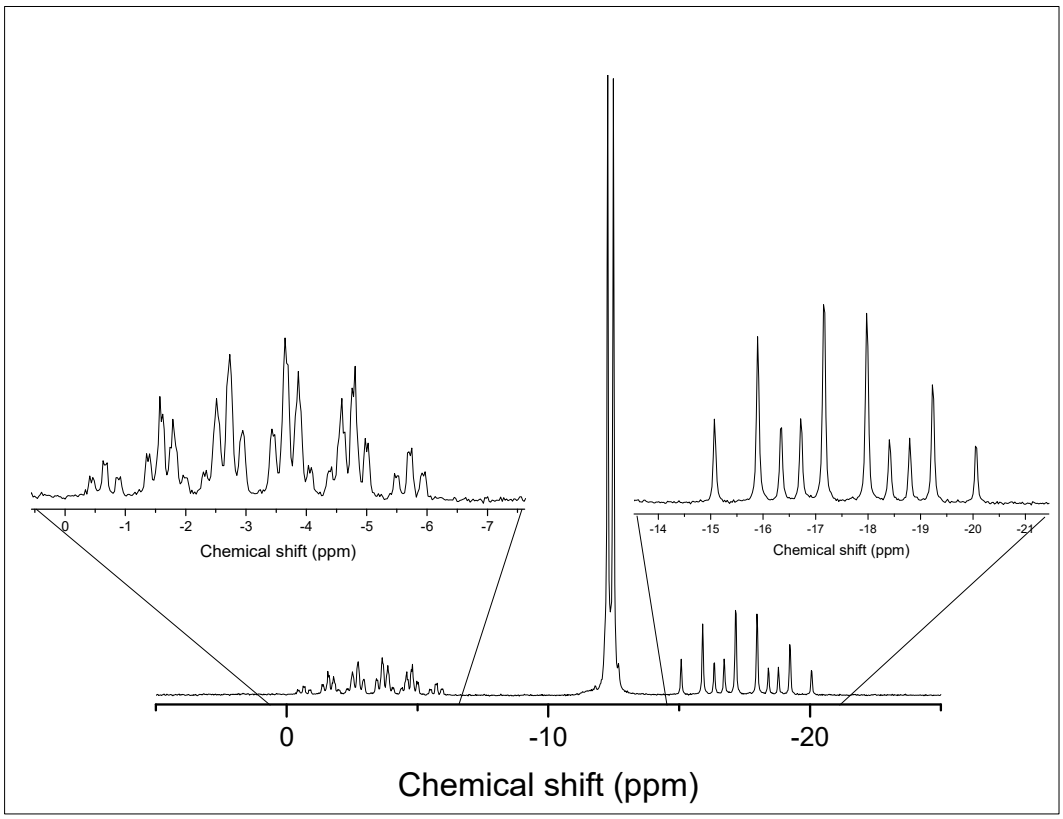

Figure 3.12 – $^{31}P\{^{1}H\}$ NMR spectrum of $[GeF_4(\kappa^2\text{-}P\{CH_2CH_2PPh_2\}_3)]$ at 183 K in CD_2Cl_2.

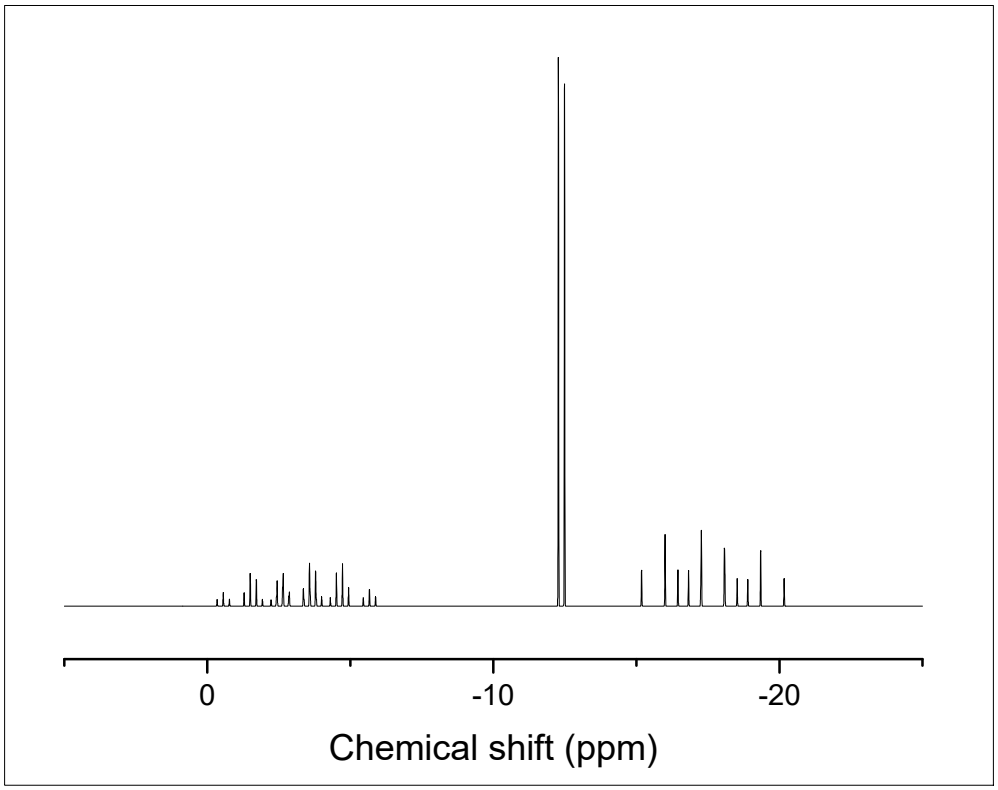

Figure 3.13 – $^{31}P\{^{1}H\}$ NMR spectrum of $[GeF_4(\kappa^2\text{-}P\{CH_2CH_2PPh_2\}_3)]$ simulated using the SPINACH package. Spin system: $J_{P1P3} = J_{P12P3} = 35$ Hz; $J_{P3P4} = 336$ Hz; $J_{P4F1} = J_{P4F2} = 133$ Hz; $J_{P3F1} = J_{P3F2} = 153$ Hz; $J_{F1F3} = J_{F1F4} = 54$ Hz; $J_{F2F3} = J_{F2F4} = 54$ Hz; $J_{F3F4} = 54$ Hz; $J_{P3F4} = 188$ Hz; $J_{P4F3} = 207$ Hz.

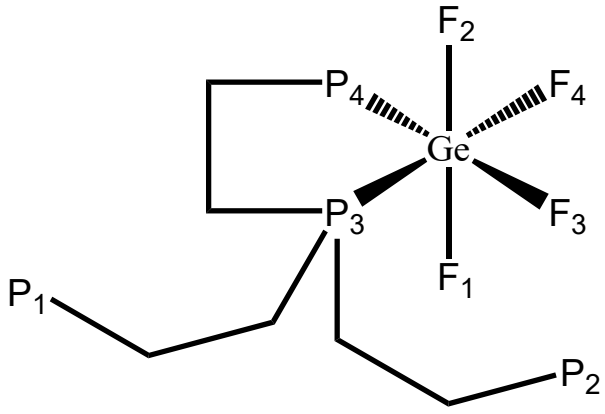

Figure 3.14 – Illustration of the labelling for the spin system.

The $^{19}F\{^{1}H\}$ NMR spectrum at 213 K (shown in **Figure 3.15** below) corroborates this picture. There are three main resonances in the spectrum with a relative ratio of 2:1:1, the first is a set of triplet of triplets at δ = -80.4 and two sets of what appear to be doublets of quartets, but which are most probably doublet of doublet of triplets, at δ = -108.4 and -114.1.

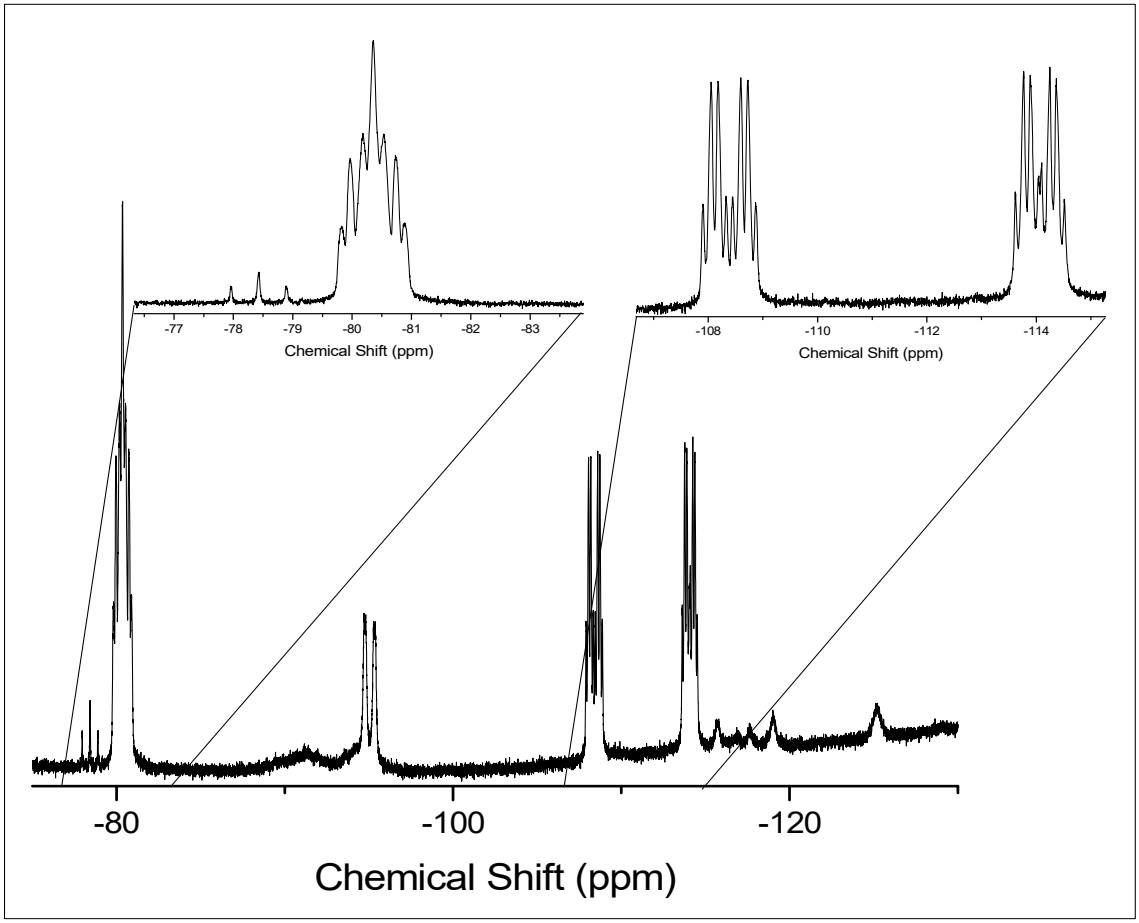

Figure 3.15 – $^{19}F\{^{1}H\}$ NMR spectrum of $[GeF_4\{\kappa^2\text{-}P(CH_2CH_2PPh_2)_3\})]$ at 213 K in CD_2Cl_2.

$[GeF_4(\kappa^2\text{-}P\{CH_2CH_2PPh_2\}_3)]$ has C_s symmetry, so group theory would predict four IR active Ge-F stretching vibrations (3A' +A''), these are seen at 508, 517, 589 and 608 cm^{-1}. Elemental analysis data are also consistent with the formation of the 1:1 complex as formulated.

3.3.2 Reactivity of $[GeF_4(PMe_3)_2]$ with TMSOTf

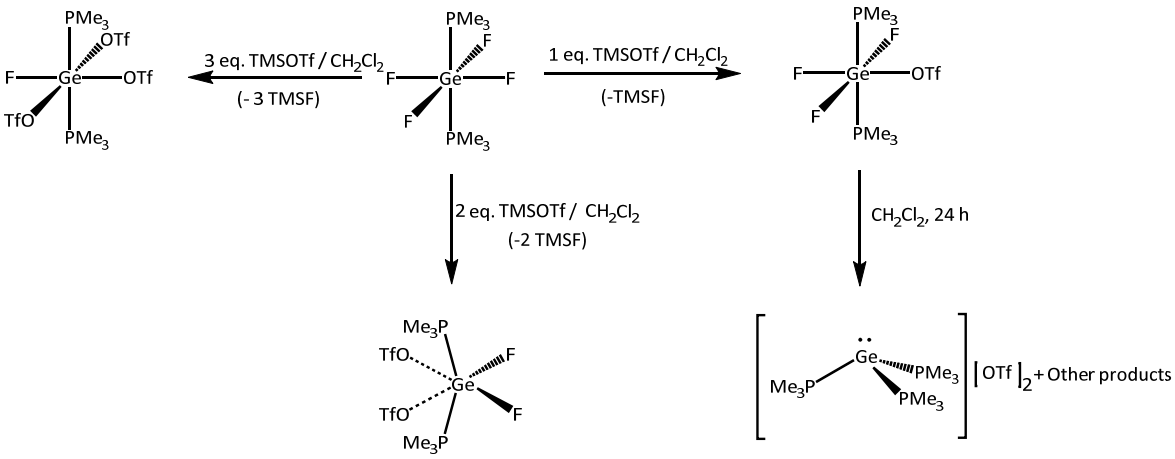

Scheme 3.2 – Reactivity of $[GeF_4(PMe_3)_2$ with TMSOTf.

Following the success of generating triflate complexes with tin(IV) chlorides in Chapter 2, the reactivity of $[GeF_4(PMe_3)_2]$ with TMSOTf was investigated (see **Scheme 3.2**). The reaction of $[GeF_4(PMe_3)_2]$ with one equivalent of TMSOTf in CH_2Cl_2 leads to the formation of $[GeF_3(PMe_3)_2(OTf)]$ as a white powder when isolated (structure shown in **Figure 3.16**).

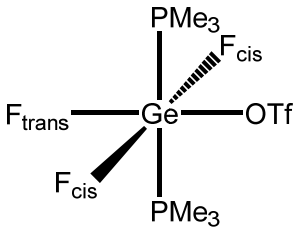

Figure 3.16 – Geometry of the complex $[GeF_3(PMe_3)_2(OTf)]$ showing the *cis* and *trans* fluorines (relative to OTf).

At room temperature, the ^1H NMR spectrum shows a doublet at δ = 1.68, which constitutes a shift of Δδ = +0.20 from $[GeF_4(PMe_3)_2]$, while the $^{31}P\{^1H\}$ NMR spectrum shows a broad singlet at δ = +3.1, which is a shift of Δδ = +17.6 from the neutral complex. At 183 K, the singlet shifts to δ = +5.2 and splits into a triplet of doublets ($^2J_{PF}$ = 192, 134 Hz) as shown in **Figure 3.17** below. This suggests that at low temperature the triflate is bound to germanium, since if it were not, a quartet would be expected (assuming a trigonal bipyramidal geometry, like in $[SnCl_3(PMe_3)_2]^+$).[11]

In the room temperature $^{19}F\{^{1}H\}$ NMR spectrum of this compound, a sharp triflate peak is seen at δ = -78.7, as well as a very broad singlet at δ = -94.0. Cooling to 183 K, a triplet of triplets is seen at δ = -123.5 ($^{2}J_{PF}$ = 134, $^{2}J_{FF}$ = 41 Hz) with an integral of one (corresponding to the fluorine *trans* to the triflate). A triplet of doublets is seen at δ = -85.9 ($^{2}J_{PF}$ = 192, $^{2}J_{FF}$ = 41 Hz) with an integral of two, corresponding to the fluorines *cis* to the triflate and a singlet at δ = -78.9 with an integral of three, corresponding to the triflate fluorines. The *trans* influence of the ligands can be seen here, with the $^{2}J_{PF}$ coupling constant being much smaller for F_{trans} *vs.* F_{cis}, and the chemical shift is much more positive for F_{cis} than F_{trans}. In the $^{19}F\{^{1}H\}$ NMR spectrum there are also resonances corresponding to $[FPMe_3]^+$ at δ = -135.7 ($^{1}J_{PF}$ = 936 Hz),[12] which indicates that some redox process must be occurring in solution.

The P-F coupling is only resolved for the fluorine resonances at low temperature. As the temperature is raised above 210 K, the coupling disappears, and the peaks broaden significantly. Eventually, the peaks merge, indicating fast exchange between the different fluorine environments (shown by the VT $^{19}F\{^{1}H\}$ NMR spectroscopy plot in **Figure 3.18**). The exchange of the fluorine environments is probably due to triflate dissociation and association in solution with the probable formation of a 5-coordinate cationic intermediate ($[GeF_3(PMe_3)_2]^+$).

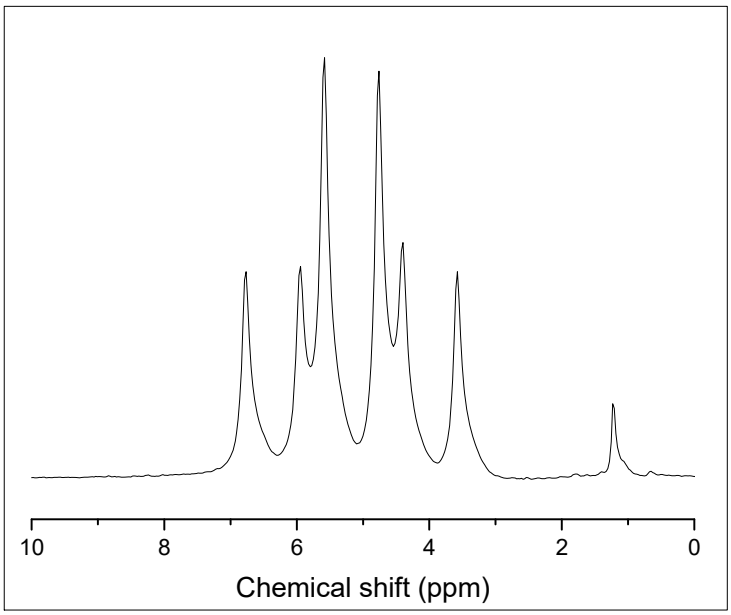

Figure 3.17 – $^{31}P\{^{1}H\}$ NMR spectrum of $[GeF_3(PMe_3)_2(OTf)]$ at 183 K (CH_2Cl_2) (as well as an unidentified impurity at *ca*. 1 ppm).

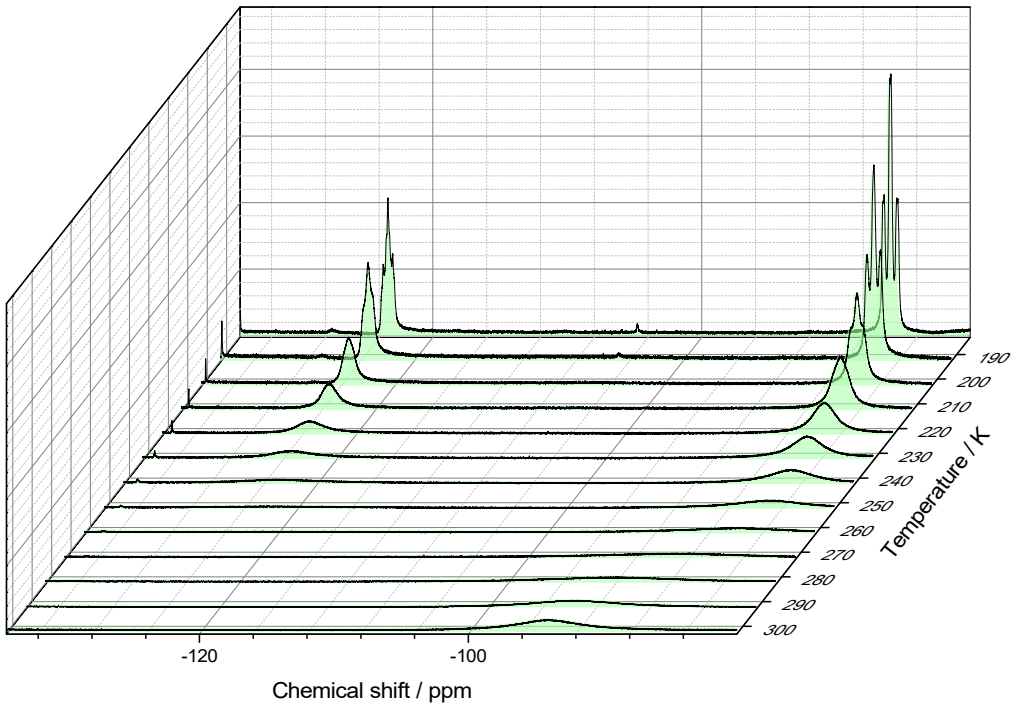

Figure 3.18 – Stacked VT $^{19}F\{^{1}H\}$ NMR spectra of $[GeF_3(PMe_3)_2(OTf)]$ in CD_2Cl_2 (triflate resonances omitted).

Even though the $[GeF_3(PMe_3)_2(OTf)]$ complex can be isolated as a white powder, it is unstable under inert atmosphere conditions. Over a period of 24 hours, the colour turns from white to a dark brown, and the resulting product is insoluble in CH_2Cl_2, which contrasts with the freshly prepared complex, which is freely soluble. Therefore all spectroscopic data were measured from a freshly synthesised sample. The compound is also unstable in solution; a CH_2Cl_2 solution of the compound left to evaporate overnight led to the deposition of crystals of the Ge(II) dication salt, $[Ge(PMe_3)_3][OTf]_2$ (see Chapter 4) formed by reduction of the mono-triflate complex from Ge(IV) to Ge(II), and presumably the oxidation of PMe_3 to $[FPMe_3]^+$. This can be compared to the reaction of $GeCl_4$ with PMe_3 in CH_2Cl_2, which also undergoes a redox process forming $[GeCl_3][PMe_3Cl]$,[7] although clearly in the $[GeF_3(PMe_3)_2(OTf)]$ case, a different process must be occurring to completely defluorinate the germanium centre. The specifics of $[Ge(PMe_3)_3][OTf]_2$ will be discussed further in Chapter 4. It should also be noted that germanium tetrafluoride phosphine complexes appear to have no tendency to undergo redox chemistry in solution.

A CH_2Cl_2 solution of $[GeF_3(PMe_3)_2(OTf)]$ layered with hexane and stored at -78 ˚C allowed for the isolation of crystals suitable for X-ray structure determination; the structure is shown in **Figure 3.19** below. As in the tin chloride analogue (chapter 2), the triflate is bound in the solid-state to give an octahedral geometry, this is consistent with the geometry predicted from the low temperature NMR data. Comparing $[GeF_3(PMe_3)_2(OTf)]$ with the related tetrafluoride complex there is a significant contraction of the d(Ge-P) bond distances (2.3656(3), 2.3546(3) *vs.* 2.3718(5)) as well as a contraction in the d(Ge-F) bond distances (1.8155(8), 1.7751(8),1.8014(8) *vs.* 1.8243(13), 1.8146(13)) which could indicate that the germanium is more Lewis acidic in the monotriflate case. Notably, the (Ge-F) distance is much shorter for F2 than for F1 and F3 due to the weaker *trans* effect of the triflate ligand compared to fluorine.

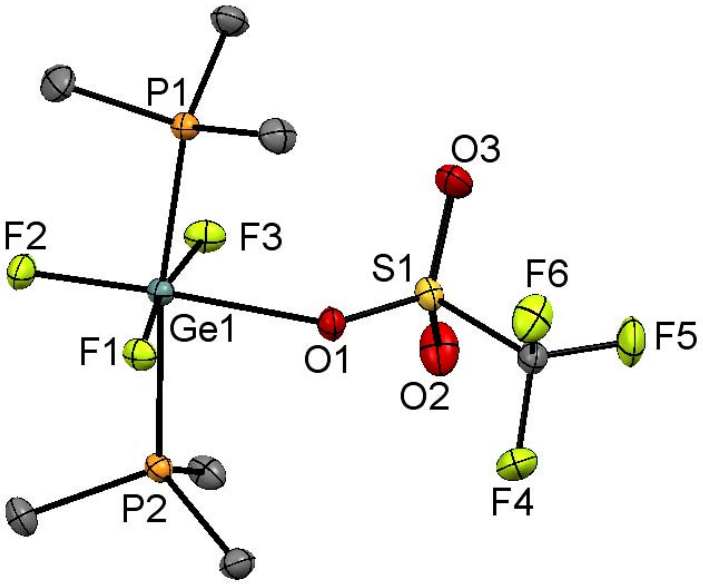

Figure 3.19 – The crystal structure of $[GeF_3(PMe_3)_2(OTf)]$ showing the atom labelling scheme. The ellipsoids are drawn at the 50% probability level and H atoms are omitted for clarity. Selected bond lengths (Å) and angles (°) are: Ge1–P1 = 2.3546(3), Ge1–P2 = 2.3656(3) Ge1–F1 = 1.8155(8), Ge1–F2 = 1.7751(8), Ge1–F3 = 1.8014(8), Ge1–O1 = 2.1882(9) P1–Ge1–P2 = 171.119(13), F1–Ge1–F3 = 170.46(4), O1–Ge1–F2 = 177.49(4).

The molecule has approximate C_{2v} symmetry, so group theory would predict three IR active Ge-F stretching modes (2 A_1 + B_1), however in the IR data, only two are seen with

one of the symmetric stretches (A_1) occurring at 515 cm^{-1}, there is a broader peak at around 572 cm^{-1} attributed to the concurrent remaining symmetric stretch (A_1) and the asymmetric stretch (B_1).

To try to form a genuine $[GeF_n(PR_3)_2]^+$ cation where the triflate is not coordinated, one approach is to use a bulkier phosphine ligand. P^iPr_3 was chosen for this purpose, it has a larger Tolman cone angle than PMe_3 (160˚ vs 118˚),[13] which may create a more crowded environment at Ge(IV) and therefore hinder OTf coordination. The reaction of $[GeF_4(^iPr_3P)_2]$ with one equivalent of TMSOTf leads to the formation of $[GeF_3(^iPr_3P)_2][OTf]$. In the room temperature $^{31}P\{^1H\}$ NMR spectrum a quartet is seen at δ = 46.8 ($^2J_{PF}$ = 152 Hz) (see **Figure 3.20**), which suggests that all the fluorides are in the same environment, suggesting that the triflate is not bound in solution. The quartet remains at low temperature (183K) which suggests that the triflate is not bound at this temperature. It is likely that in solution the $[GeF_3(^iPr_3P)_2]^+$ cation has a trigonal bipyramidal geometry (see **Figure 3.21**) based on the $^{31}P\{^1H\}$ NMR data. In the $^{19}F\{^1H\}$ NMR spectrum, a triplet is seen at δ = -56.7, a significant shift from the tetrafluoride complex of Δδ = +50.3, as well as a sharp singlet at δ = -79.0 (OTf) in a ratio of 1:1. The large positive shift of the fluorine resonance suggests a large increase in positive charge in the GeF_3 unit, consistent with the presence of discrete $[GeF_3(^iPr_3P)_2]^+$ cations and [OTf] anions in solution.

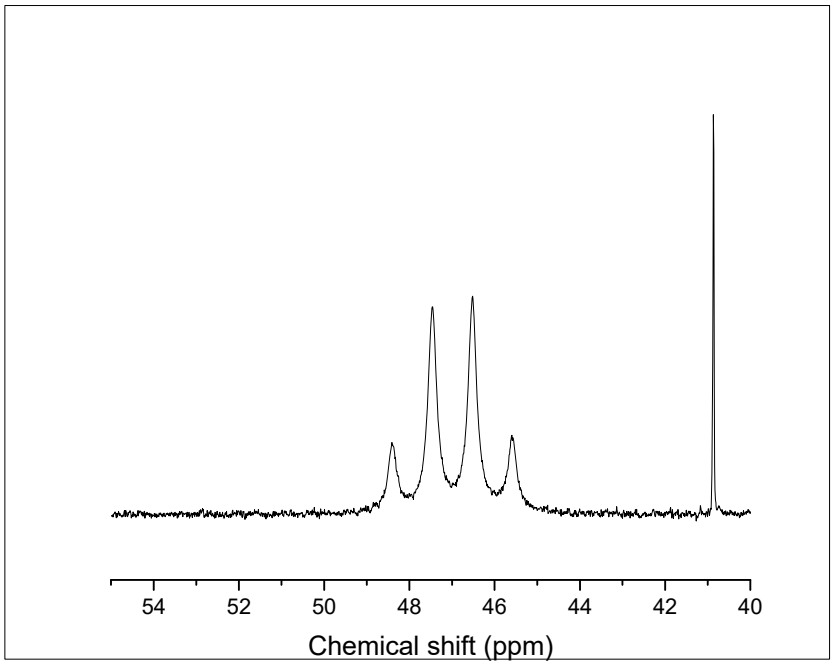

Figure 3.20 – $^{31}P\{^{1}H\}$ NMR spectrum of $[GeF_3(^{i}Pr_3P)_2][OTf]$ showing the quartet resonance due to the $[GeF_3(^{i}Pr_3P)_2]^+$ cation at 298 K in CD_2Cl_2., The impurity at *ca.* 41 ppm is due to protonated phosphine.

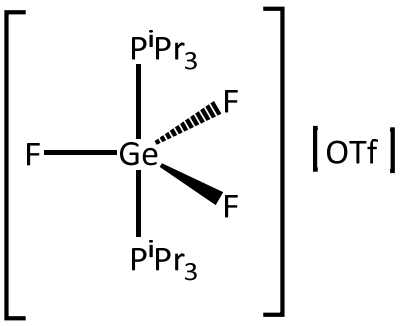

Figure 3.21 – Proposed product of the reaction of $[GeF_4(P^{i}Pr_3)_2]$ with TMSOTf.

Another possible approach to generate cationic complexes is the removal of further equivalents of fluorine. The addition of two equivalents of TMSOTf to $[GeF_4(PMe_3)_2]$ in CH_2Cl_2 results in the formation of $[GeF_2(PMe_3)_2(OTf)_2]$, which can be isolated as a white powder which is stable for several weeks under inert atmosphere conditions. The ^{1}H NMR spectrum shows a doublet resonance at $\delta = 1.98$, a shift of $\Delta\delta = +0.5$ from the tetrafluoride complex. The room temperature $^{31}P\{^{1}H\}$ NMR spectrum shows a broad peak at $\delta = +25.8$, which constitutes a shift of $\Delta\delta = +22.7$ from the monocation. At 233 K, this peak shifts to $\delta = +27.8$ and splits into a triplet ($^{2}J_{PF} = 83$ Hz).

In the $^{19}F\{^{1}H\}$ NMR room temperature spectrum, two resonances are seen, one at δ = -78.3 corresponding to triflate and a broad peak at δ = -119.5 ppm corresponding to the germanium bound fluorines. At 233 K the broad resonance at δ = -119.5 sharpens into a triplet at δ = -122.3 ($^{2}J_{PF}$ = 83 Hz). These results are consistent with the formation of a complex with the formulation $[GeF_2(PMe_3)_2(OTf)_2]$, although the NMR spectra do not allow differentiation between the different isomers possible with bound and unbound triflates.

Slow evaporation of a concentrated CH_2Cl_2 solution of $[GeF_2(PMe_3)_2(OTf)_2]$ leads to the deposition of colourless X-ray quality crystals. In the asymmetric unit of the crystal structure, there are three distinct $[GeF_2(PMe_3)_2(OTf)_2]$ units, the parameters of which are shown in **Table 3.1** below. The structure of one of the units (Ge1-centred) is shown in **Figure 3.22**. It has a pseudo-octahedral coordination environment with two relatively long contacts to the oxygen atoms of the κ^1-triflates, with d(Ge-O) = 2.375(3) Å and 2.396(3) Å, which are ~0.3 Å longer than the Ge-OTf bond in $[GeF_3(PMe_3)_2(OTf)]$. The P-Ge-P bond angle is 150.29(5)˚, which deviates significantly from the 180˚ that would be expected for an octahedral complex. This, together with the large F-Ge-F bond angle of 97.38(15)˚, suggests that the core $GeF_2(PMe_3)_2$ unit could be described as pseudo-tetrahedral, with the triflates only interacting weakly. The Ge2 and Ge3 centred molecules have similar geometrical parameters within error, although the Ge1-centred molecule has a significantly different geometry, with the closest Ge-O interaction being ~0.1 Å longer. The longer Ge-O distance could indicate a weaker interaction between the oxygen and germanium in this unit compared with the others. This is also borne out by the decrease of the P-Ge-P bond angles by ~6.7˚ and the increase in F-Ge-F bond angle by ~2.6˚, which are consistent with the central GeF_2P_2 unit becoming more tetrahedral as the triflate interaction weakens. The different degrees of distortion could also be due to packing effects.

The molecule has an approximately C_{2v} symmetry in the solid-state, therefore two Ge-F bands would be expected in the IR spectrum ($A_1 + B_1$). Only one broad peak that could be due to a Ge-F stretch is seen, at 573 cm^{-1}, although it is possible that both of these peaks are coincident.

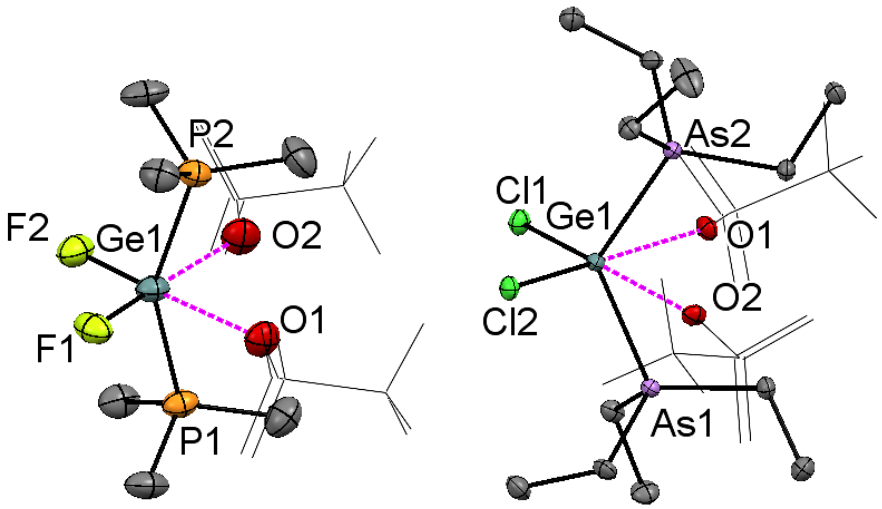

(a) (b)

Figure 3.22 – The crystal structures of (a) $[GeF_2(PMe_3)_2(OTf)_2]$ showing the atom labelling scheme (there are three independent molecules in the asymmetric unit). The ellipsoids are drawn at the 50% probability level and H atoms are omitted for clarity and only the closest oxygen of the triflate is drawn as an ellipsoid for clarity. Selected bond lengths (Å) and angles (°) are: Ge1–P1 = 2.3100(12), Ge1–P2 = 2.3074(12), Ge1–F1 = 1.747(3), Ge1–F2 = 1.748(3), Ge1···O1 = 2.374(3), Ge1···O2 = 2.396(3) P1–Ge1–P2 = 150.29(5), F1–Ge1–F2 = 97.40(14); (b) $[GeCl_2(AsEt_3)_2(OTf)_2]$ showing the atom labelling scheme. The ellipsoids are drawn at the 50% probability level and H atoms are omitted for clarity and only the closest oxygen of the triflate is drawn as an ellipsoid for clarity. Selected bond lengths (Å) and angles (°) are: Ge1–As1 = 2.4048(4), Ge1–As2 = 2.4169(4), Ge1–Cl1 = 2.1453(7), Ge1–Cl2 = 2.1602(7), Ge1···O1 = 2.6848(19), Ge1···O2 = 2.7436(19) , As1–Ge1–As2 = 125.186(16), Cl1–Ge1–Cl2 = 101.36(3).

Table 3.1 – Geometric parameters for the different units in the structure of $[GeF_2(PMe_3)_2(OTf)_2]$

$[GeF_2(PMe_3)_2(OTf)_2]$ units	Ge-1 centred	Ge-2 centred	Ge-3 centred
Ge-P	2.3074(12) 2.3100(12)	2.3154(12) 2.3173(12)	2.3126(12) 2.3146(12)
Ge-F	1.747(3) 1.748(3)	1.757(3) 1.762(2)	1.760(3) 1.759(3)
P-Ge-P	150.29(5)	156.92(5)	157.11(5)
F-Ge-F	97.40(14)	94.85(13)	94.78(13)
Ge-O	2.374(3) 2.396(3)	2.254(3) 2.301(4)	2.239(4) 2.309(3)

In a similar experiment the reaction of $GeCl_4$:2TMSOTf:2$AsEt_3$ in CH_2Cl_2 led to a mixture of products, when the mixture is layered with hexane colourless crystals of $[GeCl_2(AsEt_3)_2(OTf)_2]$ form. The structure of this complex is similar to that of $[GeF_2(PMe_3)_2(OTf)_2]$, although the contacts between the triflates and the germanium centre are significantly longer (2.7433(19) and 2.684(2) Å) than for the fluoride complex, indicating that the Ge-OTf interaction is even weaker in this complex. The As-Ge-As angle is 125.308(17)˚, and the Cl-Ge-Cl bond angle is 101.30(3), significantly closer to ideal angles for a tetrahedral molecule than an octahedral one. NMR data from these crystals suggest that a mixture of products form, including the redox products, $[AsEt_3Cl(OTf)]$ and $[AsEt_3(OTf)_2]$.

The addition of three equivalents of TMSOTf to $[GeF_4(PMe_3)_2]$ in CH_2Cl_2 leads to the formation of $[GeF(PMe_3)_2(OTf)_3]$ as a stable white solid. In the ^1H NMR spectrum, a doublet of doublets is seen at δ = 2.08, with Δδ = +0.6 from the tetrafluoride, consistent with the general trend of increasing chemical shift upon replacing fluorides with triflate and an increase of positive charge at the germanium centre. The room temperature $^{31}P\{^1H\}$ NMR spectrum shows a sharp doublet at δ = 32.4 ($^2J_{PF}$ = 75 Hz), confirming that only one fluorine is bound to the germanium centre. The room temperature $^{19}F\{^1H\}$ NMR spectrum shows a sharp triplet resonance at -107.2 ($^2J_{PF}$ = 75 Hz) as well as two broad triflate resonances. The relative ratio of the integrals for the germanium fluoride resonance to the triflate resonances is 1:9, consistent with the formulation of three triflate units per germanium. If all triflates remain coordinated in the solid-state and the phosphine ligands remain *trans* to each other, then the molecule can be assumed to have C_{2v} symmetry; this would mean in the IR, only one Ge-F stretching band would be expected with A_1 symmetry which is seen at 510 cm^{-1}.

Table 3.2 – Selected multinuclear data for complexes of the form $[GeF_{4-n}(PMe_3)_2(OTf)_n]$ for n = 0, 1, 2, 3 and $[GeF_{4-n}(P^iPr_3)_2][OTf]_n$ n = 0, 1)

Compound	δ $^{31}P\{^1H\}$/ppm	δ $^{19}F\{^1H\}$[a]/ppm	$^2J(^{31}P\text{-}^{19}F)$/Hz	$^2J(^{19}F\text{-}^{19}F)$/Hz
trans-$[GeF_4(PMe_3)_2]$[7] (298 K)	-12.4 (quintet)	-96.9 (t)	196	-
$[GeF_3(PMe_3)_2(OTf)]$ (183 K)	5.16 (td)	-85.9 (td), -123.5 (tt)	192, 134	41
$[GeF_2(PMe_3)_2(OTf)_2]$ (233 K)	27.4 (t)	-122.3 (t)	83	-
$[GeF(PMe_3)_2(OTf)_3]$ (298 K)	32.4 (d)	-107.2 (t)	75	-
$[GeF_4(P^iPr_3)_2]$ (183 K)	27.9 (quintet)	-107.2 (t)	160	-
$[GeF_3(P^iPr_3)_2][OTf]$ (298 K)	46.8 (q)	-56.7 (t)	152	-

[a] non-triflate resonances

There is a monotonic increase in the $^{31}P\{^1H\}$ chemical shift as the fluorides are replaced by triflates (see **Table 3.2**), which could indicate an increase of positive charge at the germanium centre, and there is also a monotonic decrease in the $^2J_{PF}$ coupling constant with increased triflate incorporation. Two main factors affect the fluorine chemical shifts; one is the *trans* influence of the ligand, with the fluorines *trans* to fluorine being much more deshielded compared to those *trans* to triflate (best exemplified by $[GeF_3(PMe_3)_2(OTf)]$). The second factor is the number of fluorines that have been exchanged for triflate; the more fluorines that have been exchanged, the more positive the chemical shift.

Table 3.3 – Selected geometric parameters for complexes of the form $[GeF_{4-n}(PMe_3)_2(OTf)_n]$ for n = 0, 1, 2 and $[GeCl_4(AsEt_3)_2]$ and $[GeCl_2(AsEt_3)_2][OTf]_2$

Complex	d(Ge-E) (E=P or As) / Å	d(Ge-X) (X=F or Cl) / Å	E-Ge-E angle / °	Range of C-E-C angles[a] / °
$[GeF_4(PMe_3)_2]$	2.3717(6)	1.8158(13) 1.8240(13)	180.0	105.83(13)-106.93(11)
$[GeF_3(PMe_3)_2(OTf)]$	2.3655(3) 2.3546(3)	1.8015(7)(*cis*) 1.8149(7) (*cis*), 1.7753(7) (*trans*)	171.122(11)	106.27(6)-109.00(6)
$[GeF_2(PMe_3)_2(OTf)_2]$	2.3074(12) 2.3100(12)	1.747(3) 1.748(3)	150.29(5)	107.0(2)-110.9(3)
$[GeCl_4(AsEt_3)_2]$ [13]	2.4904(9)	2.3233(19) 2.3296(19)	180.0	105.1(4)-106.4(4)
$[GeCl_2(AsEt_3)_2][OTf]_2$	2.4048(4) 2.4169(4)	2.1453(7) 2.1602(7)	125.186(16)	105.79(12)-113.81(12)

[a] C-P-C angle of free PMe_3 = 99.46˚, C-As-C angle of free $AsEt_3$ = 98.50˚

For the phosphine complexes, as the fluorides are replaced by triflates, there is a decrease in the Ge-P and Ge-F bond distances (see **Table 3.3**). This is consistent with an increase in positive charge and Lewis acidity at the germanium centre. This is also supported by the increase in the average C-P-C bond angle of the phosphine ligand going down the series, with the bond angle in the *bis*-triflate complex being almost 10˚ larger than in the free ligand and almost 3˚ larger than the neutral complex. The same trends are seen with the germanium chloride arsine complexes.

3.3.3 Reactivity of germanium fluoride complexes bearing multidentate phosphines with TMSOTf

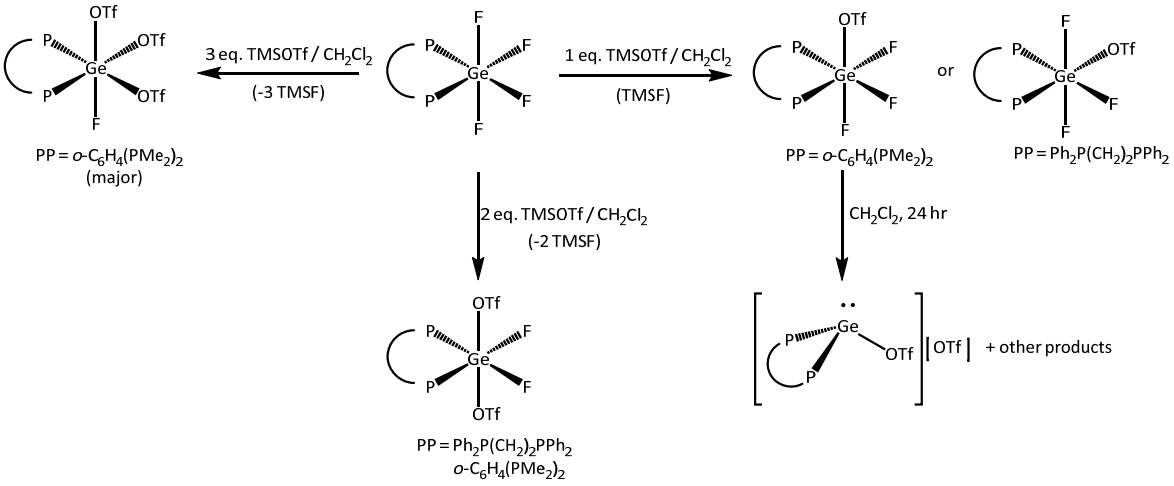

Scheme 3.3 – Reactivity of germanium fluoride complexes bearing bidentate phosphine ligands with TMSOTf.

The reaction of $[GeF_4\{o\text{-}C_6H_4(PMe_2)_2\}]$ with one equivalent of TMSOTf in CH_2Cl_2 leads to the formation of $[GeF_3\{o\text{-}C_6H_4(PMe_2)_2\}(OTf)]$ (see **Scheme 3.3**). In the ^1H NMR spectrum the methyl resonance appears at $\delta = 1.90$, with $\Delta\delta = +0.09$ from the tetrafluoride adduct. With one triflate bound, two isomers are possible, one where the fluorines are *mer* disposed and another where they are *fac* disposed (see **Figure 3.23** below). Multinuclear NMR spectroscopy can be used to differentiate these.

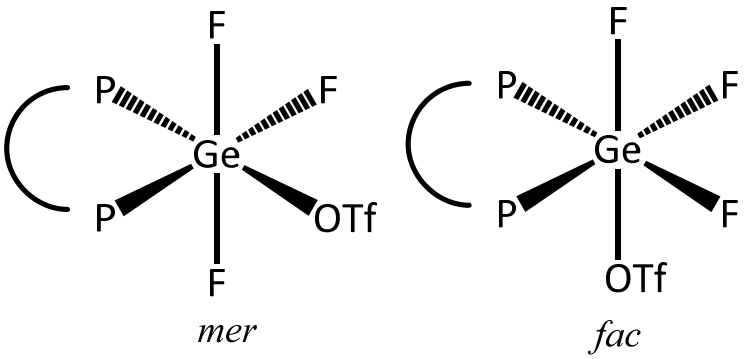

Figure 3.23 – The two possible isomers of the complex $[GeF_3\{o\text{-}C_6H_4(PMe_2)_2\}(OTf)]$ with the triflates bound.

The $^{19}F\{^{1}H\}$ NMR spectrum of [$GeF_3\{o\text{-}C_6H_4(PMe_2)_2\}$(OTf)] at 183 K (shown in **Figure 3.24** below) has a resonance at δ = -109.5, which appears as a doublet of doublet of doublets with two different $^{2}J_{PF}$ couplings and one $^{2}J_{FF}$ coupling, together with a triplet of triplets at δ = -123.7 with one $^{2}J_{PF}$ coupling and one $^{2}J_{FF}$. The $^{31}P\{^{1}H\}$ NMR spectrum at 183 K has a resonance at δ = -24.1, which is a doublet of doublet of doublets with three different $^{2}J_{PF}$ couplings. This indicates that there is only one phosphorus chemical environment (though they are magnetically inequivalent). These data are consistent with the *fac* isomer being the predominant species in solution at this temperature.

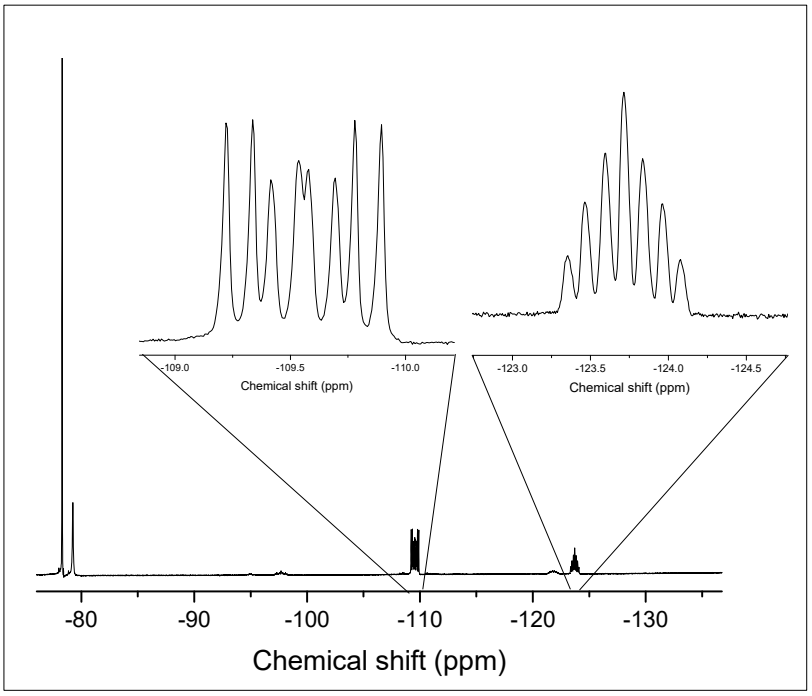

Figure 3.24 – $^{19}F\{^{1}H\}$ NMR spectrum of [$GeF_3\{o\text{-}C_6H_4(PMe_2)_2\}$(OTf)] at 183 K ($CD_2Cl_2$).

A CH_2Cl_2 solution of this complex layered with hexane led to the deposition of single crystals of the Ge(II) species, [$Ge\{o\text{-}C_6H_4(PMe_2)_2\}$(OTf)][OTf]. The reduction of the germanium centre from Ge(IV) to Ge(II), with concomitant complete defluorination, also occurred with the PMe_3 system. It should be noted that there is no propensity for the neutral tetrafluoride complexes to undergo the same reactivity.

The structure of [$Ge\{o\text{-}C_6H_4(PMe_2)_2\}$(OTf)][OTf] is shown below in **Figure 3.25**; one of the triflates is coordinated to the germanium centre with a bond length of 2.092(2) Å, well within the expected distance for a Ge-OTf bond. There are two longer contacts to weakly interacting triflates at 2.650 Å and 2.974 Å, completing an approximately five-coordinate

geometry around the germanium. The complex exists as a weakly associated dimer in the solid-state and appears to have a similar geometry to the previously reported complex, [GeCl($Me_2P(CH_2)_2PMe_2$)][OTf], although the crystal data for this has not been published, so more detailed comparisons cannot be made.[14]

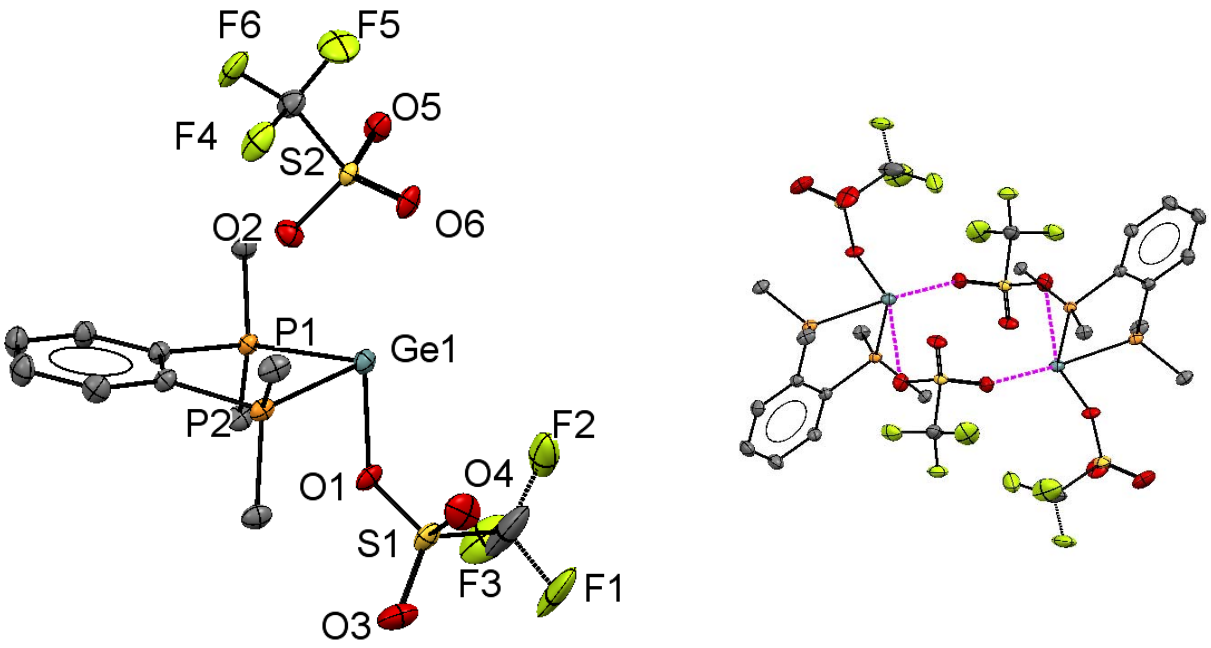

(a) (b)

Figure 3.25 – (a) The structure of [Ge{*o*-$C_6H_4(PMe_2)_2$}(OTf)][OTf] showing the atom labelling scheme and (b) the weakly associated dimer arrangement. The ellipsoids are drawn at the 50% probability level and H atoms and a CH_2Cl_2 solvent molecule are omitted for clarity. Selected bond lengths (Å) and angles (°) are: Ge1–P1 = 2.4321(5), Ge1–P2 = 2.4580(6), Ge1–O1 = 2.0968(15), Ge1···O2 = 2.6438(17), P1–Ge1–P2 = 81.469(18).

The addition of two equivalents of TMSOTf to [GeF_4{*o*-$C_6H_4(PMe_2)_2$}] in CH_2Cl_2 led to the formation of the complex, [GeF_2{*o*-$C_6H_4(PMe_2)_2$}$(OTf)_2$]. Here the methyl resonance shifts to δ = 2.03, i.e. Δδ = +0.13 from the monotriflate complex. In this system, there are three possible isomers if the triflates are bound, shown in **Figure 3.26** below.

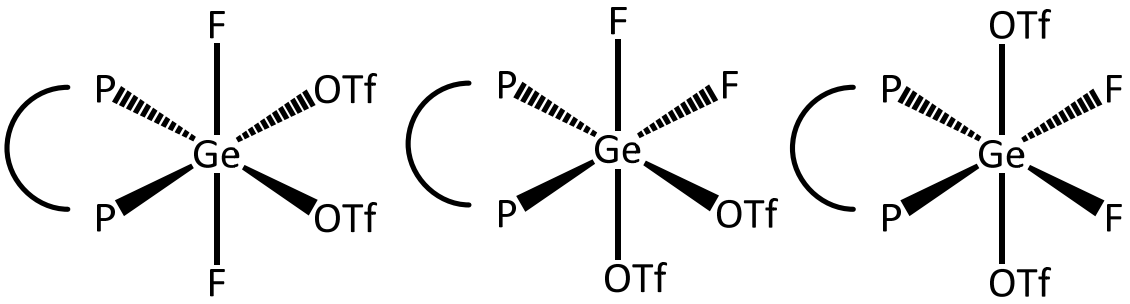

Figure 3.26 – The three possible isomers of $[GeF_2\{o\text{-}C_6H_4(PMe_2)_2\}(OTf)_2]$.

The room temperature $^{19}F\{^1H\}$ NMR spectrum shows a doublet of doublets at δ = -100.6, while correspondingly, the room temperature $^{31}P\{^1H\}$ NMR spectrum shows a doublet of doublets at δ = -23.2, with the same coupling constants ($^2J_{PF}$ = 121, 74). This is consistent with the third isomer being present in solution at room temperature. However, there is also another species in the $^{31}P\{^1H\}$ NMR spectrum appearing as a broad triplet at δ = -19.8, which could be either isomer 1 or 2 depending on the magnitudes of $^2J_{PF}$. At 183 K, another set of resonances appear in the $^{19}F\{^1H\}$ NMR spectrum at δ = -111.0, which appears as a triplet of doublets, which would be consistent with the second isomer being present at this temperature, although there is no corresponding doublet of doublet of doublets. There is however a broad doublet of doublets at δ = -96.7, which is in a 1:1 ratio with the doublet of triplets. The broadness of both these multiplets, suggest that the couplings may not be fully resolved at these temperatures and hence a definitive assignment is not possible.

Crystals of $[GeF_2\{o\text{-}C_6H_4(PMe_2)_2\}(OTf)_2]$ were grown from a CH_2Cl_2 solution of the complex layered with hexane, the structure of which is shown in **Figure 3.27** below. In the structure, the triflates are *trans* to each other and the fluorines are *cis*; this is consistent with the room temperature $^{31}P\{^1H\}$ and $^{19}F\{^1H\}$ NMR data.

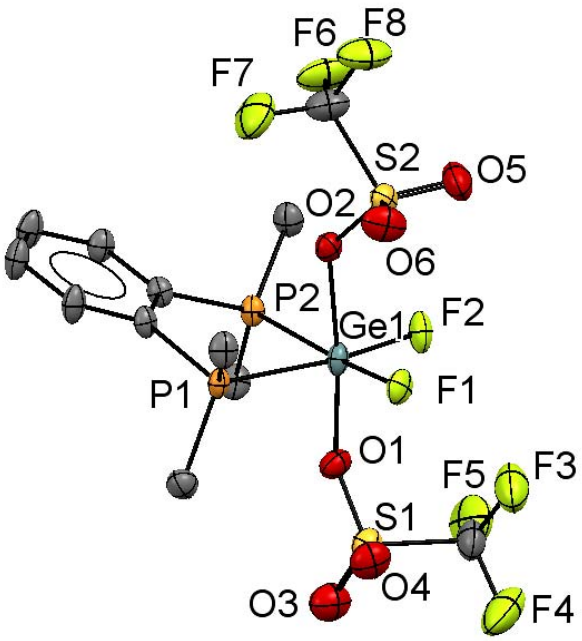

Figure 3.27 – The structure of $[GeF_2\{o\text{-}C_6H_4(PMe_2)_2\}(OTf)_2]$ showing the atom labelling scheme. The ellipsoids are drawn at the 50% probability level and H atoms are omitted for clarity. Selected bond lengths (Å) and angles (°) are: Ge1–P1 = 2.4033(16), Ge1–P2 = 2.3814(17) Ge1–F1 = 1.751(4), Ge1–F2 = 1.766(4), Ge1–O1 = 1.949(5), Ge1–O2 = 2.018(5), P1–Ge1–P2 = 86.33(6), O1–Ge1–O2 = 172.4(2), F1–Ge1–F2 = 92.51(14).

Addition of three equivalents of TMSOTf to $[GeF_4\{o\text{-}C_6H_4(PMe_2)_2\}]$ in CH_2Cl_2 leads predominately to the formation of $[GeF\{o\text{-}C_6H_4(PMe_2)_2\}(OTf)_3]$. There are two possible isomers in which the triflates are bound, shown in **Figure 3.28** below.

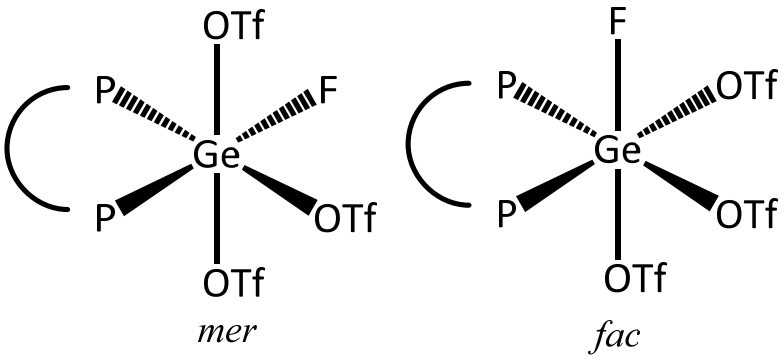

Figure 3.28 – The two possible isomers of $[GeF\{o\text{-}C_6H_4(PMe_2)_2\}(OTf)_3]$.

In the room temperature $^{19}F\{^1H\}$ NMR spectrum, there is a triplet at δ = -94.0 ($^2J_{PF}$ = 73 Hz), and in the $^{31}P\{^1H\}$ NMR spectrum, there is a doublet at δ = -13.5 ($^2J_{PF}$ = 73 Hz), this is consistent with the *fac* isomer being the major product in solution. There are also a

number of smaller doublets seen in the NMR spectrum, one of them being close to the main peak at δ = -12.5 ($^2J_{PF}$ = 69 Hz). For this compound the speciation in solution is complex with several forms present. In the $^{19}F\{^1H\}$ NMR spectrum, another triplet is also seen at δ = -91.1 ($^2J_{PF}$ = 69 Hz), which could indicate the presence of a species of the form $[GeF\{C_6H_4(PMe_2)_2\}(OTf)_n][OTf]_{3-n}$), the ratio of the minor and major species is 1:10. The ^1H NMR spectrum is complicated in the methyl region, again indicating that several species are present; this is unsurprising, as based on the geometry of the complex below, each methyl group is in a slightly different environment, though the ratio of methyl:aromatic resonances is still 12:4 as expected. A CH_2Cl_2 solution of the complex layered with hexane leads to the deposition of crystals. X-ray structure determination (shown in **Figure 3.29**) of one of these crystals shows that the solution geometry of the major product is maintained in the solid state, found to be $[GeF\{o\text{-}C_6H_4(PMe_2)_2\}(OTf)_3]$.

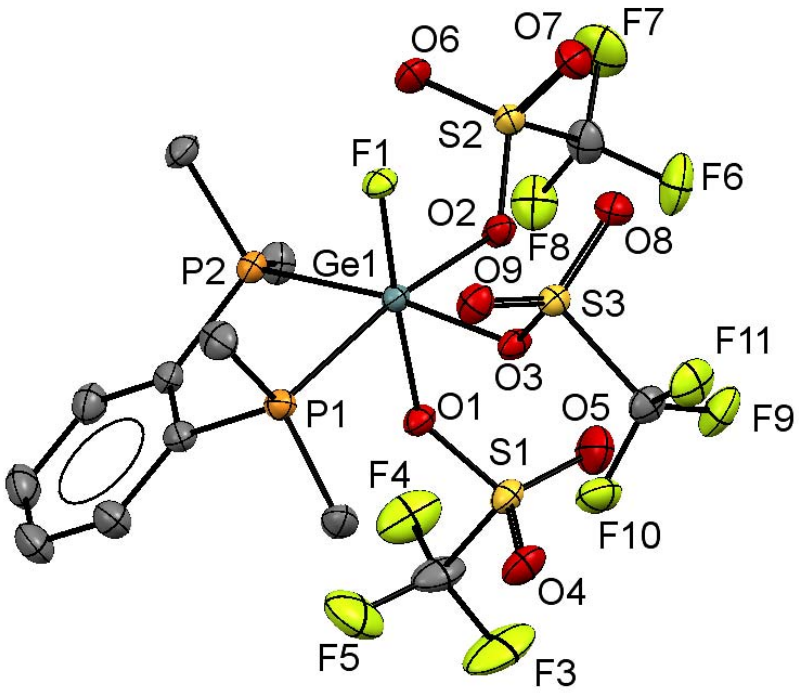

Figure 3.29 – The crystal structure of $[GeF\{o\text{-}C_6H_4(PMe_2)_2\}(OTf)_3]$ showing the atom labelling scheme. There are two $[GeF\{o\text{-}C_6H_4(PMe_2)_2\}(OTf)_3]$ in the asymmetric unit and only one is shown. The ellipsoids are drawn at the 50% probability level and H atoms and a CH_2Cl_2 solvent molecule are omitted for clarity. Selected bond lengths (Å) and angles (°) are: Ge1–P1 = 2.3900(9), Ge1–P2 = 2.3840(9) Ge1–F1 = 1.7681(18), Ge1–O1 = 1.948(2), Ge1–O2 = 1.939(2), Ge1–O3 = 1.917(2), P1–Ge1–P2 = 86.54(3), O2–Ge1–O3 = 83.67(10), O1–Ge1–F1 = 176.27(9).

The reaction of $[GeF_4\{Ph_2P(CH_2)_2PPh_2\}]$ with one equivalent of TMSOTf in CH_2Cl_2 leads to the formation of $[GeF_3\{Ph_2P(CH_2)_2PPh_2\}(OTf)]$. In the ^1H NMR spectrum of the complex, there is a singlet resonance in the methylene region at δ = 2.95; this constitutes a shift of Δδ = +0.24 from the neutral complex, and as expected, the ratio of methylene:aromatic integrals is 1:5. The multinuclear NMR data show that there is a complicated mixture of isomers or other reaction products, possibly due to greater lability and poorer donor power as compared to *o*-$C_6H_4(PMe_2)_2$ discussed above, so the discussion will focus on crystallographic data.

Crystals of this compound were grown from layering a CH_2Cl_2 solution of the complex with hexane, the structure of the complex is shown in **Figure 3.30** below.

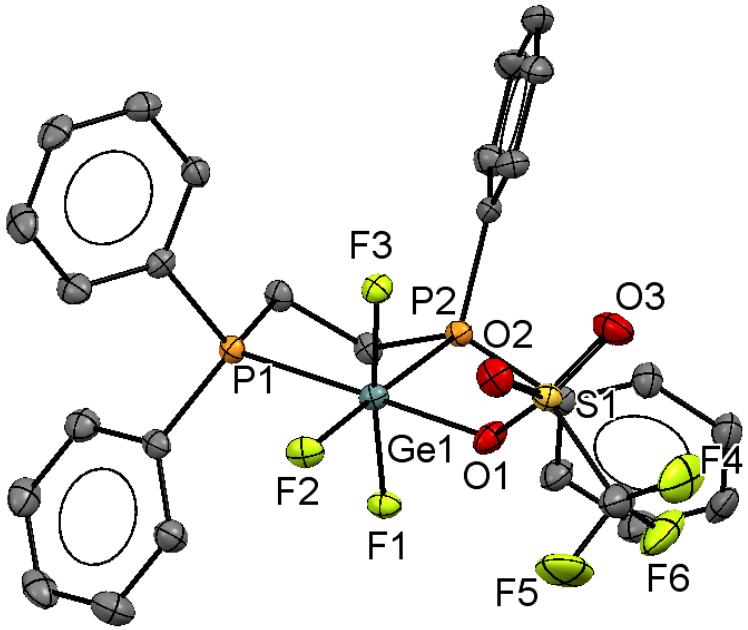

Figure 3.30 – The crystal structure of $[GeF_3\{Ph_2P(CH_2)_2PPh_2\}(OTf)]$ showing the atom labelling scheme. The ellipsoids are drawn at the 50% probability level and H atoms are omitted for clarity. Selected bond lengths (Å) and angles (°) are: Ge1–P1 = 2.4294(10), Ge1–P2 = 2.4321(11), Ge1–F1 = 1.791(2), Ge1–F2 = 1.762(2), Ge1–F3 = 1.775(2), Ge1–O1 = 1.966(3), P1–Ge1–P2 = 85.48(3), F1–Ge1–F3 = 173.68(10), P1–Ge1–O1 = 177.74(8), P2–Ge1–F2 = 173.04(8).

In the structure of [GeF_3{$Ph_2P(CH_2)_2PPh_2$}(OTf)], the diphosphine ligand is bonded in a *cis* configuration, and the fluorines are arranged in *mer* configuration. This is in contrast to [GeF_3{*o*-$C_6H_4(PMe_2)_2$}(OTf)] where the solution NMR data suggest that the configuration in this compound is *fac*.

From the same batch of crystals, a crystal of [GeF_2{$Ph_2P(CH_2)_2PPh_2$}$(OTf)_2$] was also found. The structure of this complex is shown in **Figure 3.31** below. The geometry of the compound is analogous to the *o*-$C_6H_4(PMe_2)_2$ complex above, with the fluorides *trans* to the phosphine ligand and the triflates *trans* to each other. In an attempt to prepare a bulk sample of this complex, [GeF_4{$Ph_2P(CH_2)_2PPh_2$}] was reacted with two equivalents of TMSOTf, which led to the formation of a white precipitate that was insoluble in chlorocarbon solvents, precluding useful NMR data from being obtained. However, in the IR spectrum of the compound, there are two peaks in the Ge-F region at 502 and 527 cm^{-1}, as well as peaks corresponding to triflate, which suggests the target complex has indeed formed. Elemental analysis supports the formulation as [GeF_2{$Ph_2P(CH_2)_2PPh_2$}$(OTf)_2$].

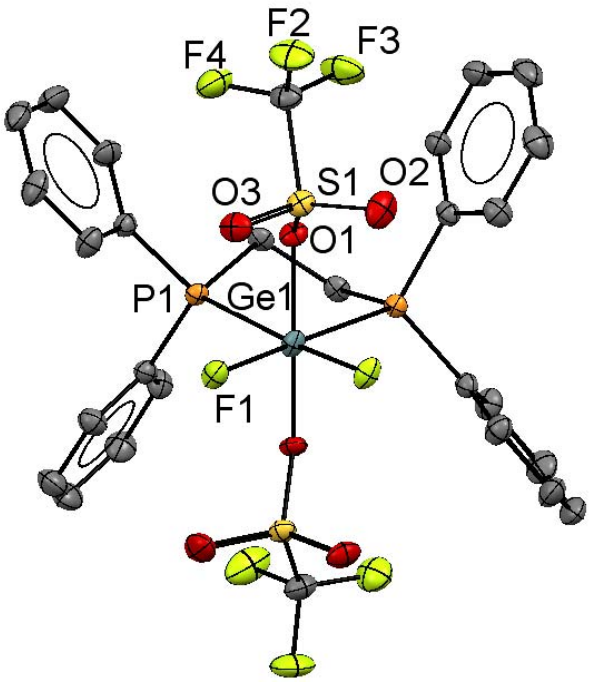

Figure 3.31 – The structure of [GeF_2{$Ph_2P(CH_2)_2PPh_2$}$(OTf)_2$] showing the atom labelling scheme. The ellipsoids are drawn at the 50% probability level and H atoms and a CH_2Cl_2 solvent molecule are omitted for clarity. Selected bond lengths (Å) and angles (°) are: Ge1–P1 = 2.4249(9), Ge1–F1 =

1.768(2), Ge1–O1 = 1.948(2), P1–Ge1–P1 = 86.29(4), F1–Ge1–F1 = 91.57(15), O1–Ge1–O1 = 173.30(14); symmetry operation: (3/2-X,3/2-Y,+Z).

Table 3.4 – Selected geometric parameters for complexes with bidentate phosphines

	Ge-P / Å	Ge-F / Å	P-Ge-P / °	Ge-O / Å
$[GeF_4\{o\text{-}C_6H_4(PMe_2)_2\}]$	2.4273(12) 2.4273(11)	1.815(2) 1.809(2) (*cis*) 1.765(2) 1.772(2) (*trans*)	85.61(4)	-
$[GeF_2\{o\text{-}C_6H_4(PMe_2)_2\}(OTf)_2]$	2.4033(16) 2.3814(17)	1.751(4) 1.776(4)	86.33(6)	1.949(5) 2.018(5)
$[GeF\{o\text{-}C_6H_4(PMe_2)_2\}(OTf)_3]$	2.3900(9) 2.3840(9)	1.7681(18)	86.54(3)	1.948(2) 1.939(2) 1.917(2)
$[GeF_4\{Ph_2P(CH_2)_2PPh_2\}]$	2.4636(7) 2.4822(7)	1.7692(14) (*trans*) 1.7731(14) 1.7829(13) (*cis*) 1.7987(14)	84.08(2)	-
$[GeF_3\{Ph_2P(CH_2)_2PPh_2\}\ (OTf)]$	2.4294(10) 2.4321(11)	1.791(2) 1.775(2) (*cis*) 1.762(2) (*trans*)	85.49(3)	1.965(3)
$[GeF_2\{Ph_2P(CH_2)_2PPh_2\}(OTf)_2]$	2.4217(6)	1.7641(11)	86.25(2)	1.934(7)

As **Table 4.3** shows, there is a decrease in d(Ge-P) as more fluorides are replaced by triflates, whereas d(Ge-F) does not vary much with the number of fluorides present. A small increase in the P-Ge-P bond angles occurs as fluoride are sequentially removed. The d(Ge-O) are much shorter for the bidentate phosphine complexes when compared to the monodentate phosphine complexes, indicating that the triflates are bound more strongly in the former.

3.4 Conclusions

The chapter shows that neutral phosphine complexes of GeF_4 can be extended to the higher denticity $CH_3C(CH_2PPh_2)_2$ and $P(CH_2CH_2PPh_2)_3$ ligands. In both cases, the pendent phosphines were not sufficiently strongly basic to displace fluoride from the germanium centre and therefore remained uncoordinated.

$[GeF_4(PMe_3)_2]$ was shown to react with n equivalents of TMSOTf to form a new series of complexes $[GeF_{4-n}(PMe_3)_2][OTf]_n$ (n = 0, 1, 2, 3), all of which could be isolated in high yield. $[GeF_3(PMe_3)_2(OTf)]$ was shown to be unstable in solution with respect to reductive defluorination to form the Ge(II) dication, $[Ge(PMe_3)_3][OTf]_2$. Using the bulkier $^iPr_3P$ allows the formation of $[GeF_3(^iPr_3P)_2][OTf]$, containing a germanium trifluoride *bis*-phosphine mono cation.

The diphosphine complex $[GeF_4\{o\text{-}C_6H_4(PMe_2)_2\}]$ was shown to react with n equivalents of TMSOTf to generate the series $[GeF_{4-n}\{o\text{-}C_6H_4(PMe_2)_2\}][OTf]_n$ (n = 0, 1, 2, 3), but here the diphosphine occupies mutually *cis* coordination sites. The complex $[GeF_3\{o\text{-}C_6H_4(PMe_2)_2\}(OTf)]$ was shown to be unstable in solution and from a CH_2Cl_2 solution of this complex, crystals of $[Ge\{(o\text{-}C_6H_4(PMe_2)_2\}(OTf)][OTf]$ deposited featuring a Ge(II) monocation, which is thought to proceed through a reductive defluorination mechanism. The reaction of $[GeF_4\{Ph_2P(CH_2)_2PPh_2\}]$ with TMSOTf leads to the formation of the complexes $[GeF_3\{Ph_2P(CH_2)_2PPh_2\}(OTf)]$ and $[GeF_2\{Ph_2P(CH_2)_2PPh_2\}(OTf)_2]$ which were characterised by X-ray crystallography.

3.5 X-Ray Crystallographic Data

Table 3.5 – X-ray crystallographic data[a]

Complex	$[GeF_4(PMe_3)_2]$	$[GeF_4\{CH_3C(CH_2PPh_2)_3\}]\cdot CH_2Cl_2$	$[GeF_3(PMe_3)_2(OTf)]$	$[GeF_2(PMe_3)_2(OTf)_2]$
Formula	$C_6H_{18}F_4GeP_2$	$C_{42}H_{41}Cl_2F_4GeP_3$	$C_7H_{18}F_6GeO_3P_2S$	$C_{24}H_{54}F_{24}Ge_3O_{18}P_6S_6$
M	300.73	858.15	430.84	1682.725
Crystal system	monoclinic	monoclinic	orthorhombic	triclinic
Space group (no.)	$P2_1/n$ (14)	$P2_1/n$ (14)	Pbca (61)	P-1 (2)
a /Å	6.1467(2)	13.9614(2)	11.3324(1)	9.3701(3)
b /Å	10.1678(4)	12.9040(2)	11.7241(1)	15.5931(6)
c /Å	9.5754(3)	21.6728(3)	23.5687(3)	21.5703(7)
α /°	90	90	90	93.050(3)
β /°	91.210(3)	96.8620(10)	90	94.382(3)
γ /°	90	90	90	91.974(3)
U /Å^3	598.31(4)	3876.56(10)	3131.39(6)	3135.60(19)
Z	2	4	8	2
μ(Mo-K_α) /mm^{-1}	2.838	1.102	2.359	1.909
F(000)	305	1760	1734	1685
Total number reflns	6990	48266	80977	57396
R_{int}	0.033	0.029	0.041	0.067
Unique reflns	1509	13630	5222	19099
No. of params, restraints	64, 0	470, 0	187, 0	849, 0
GOF	1.036	1.029	1.060	1.026
R_1, wR_2 $[I > 2\sigma(I)]$[b]	0.030, 0.069	0.039, 0.076	0.021, 0.049	0.071, 0.190
R_1, wR_2 (all data)	0.037, 0.074	0.055, 0.081	0.027, 0.050	0.113, 0.217

Complex	$[GeCl_2(AsEt_3)_2][OTf]_2$	$[GeF_2(o\text{-}C_6H_4(PMe_2)_2)(OTf)_2]$	$[GeF(o\text{-}C_6H_4(PMe_2)_2)(OTf)_3]\cdot 0.3CH_2Cl_2$
Formula	$C_{14}H_{30}As_2Cl_2F_6GeO_6S_2$	$C_{12}H_{16}F_8GeO_6P_2S_2$	$C_{52.6}H_{65.2}Cl_{1.2}F_{40}Ge_4O_{36}P_8S_{12}$
M	765.83	606.90	2998.82
Crystal system	triclinic	orthorhombic	monoclinic
Space group (no.)	P-1 (2)	$P2_12_12_1$ (19)	I2 (5)
a /Å	9.6136(3)	8.49904(14)	17.7401(2)
b /Å	9.7490(4)	15.8315(3)	9.08810(10)
c /Å	15.2210(5)	16.3349(4)	33.6730(3)
α /°	104.887(3)	90	90
β /°	101.440(3)	90	100.2150(13)
γ /°	97.269(3)	90	90
U /Å^3	1327.35(8)	2197.90(8)	5342.84(10)
Z	2	4	2
μ(Mo-K_α) /mm^{-1}	4.057	1.823	1.642
F(000)	760	1208	2978
Total number reflns	22109	71065	72764
R_{int}	0.060	0.071	0.039
Unique reflns	8925	6832	15790
No. of params, restraints	304, 0	284, 0	707, 1
GOF	1.029	1.131	1.037
R_1, wR_2 $[I > 2\sigma(I)]^b$	0.042, 0.081	0.061, 0.143	0.032, 0.066
R_1, wR_2 (all data)	0.059, 0.088	0.069, 0.146	0.038, 0.068

Compound	$[GeF_3\{Ph_2P(CH_2)_2PPh_2\}(OTf)]\cdot CH_2Cl_2$	$[GeF_2\{Ph_2P(CH_2)_2PPh_2\}(OTf)_2]\cdot CH_2Cl_2$	$[Ge\{o\text{-}C_6H_4(PMe_2)_2\}(OTf)][OTf]\cdot 1/3CH_2Cl_2$
Formula	$C_{28}H_{26}Cl_2F_6GeO_3P_2S$	$C_{29}H_{26}Cl_2F_8GeO_6P_2S_2$	$C_{12.34}H_{16.66}Cl_{0.67}F_6GeO_6P_2S_2$
M	761.98	892.05	597.210
Crystal system	monoclinic	orthorhombic	triclinic
Space group (no.)	Pn (7)	Pccn (56)	P-1 (2)
a /Å	10.22780(19)	11.5994(2)	8.5322(2)
b /Å	12.3841(2)	20.7200(4)	12.5345(4)
c /Å	12.2598(2)	14.7520(2)	12.6057(3)
α /°	90	90	64.833(3)
β /°	94.8064(16)	90	70.313(3)
γ /°	90	90	71.230(3)
U /Å^3	1547.39(5)	3545.49(10)	1123.35(7)
Z	2	4	2
μ(Mo-K_α) /mm^{-1}	1.400	1.327	1.847
F(000)	768	1766	598
Total number reflns	21335	105333	30424
R_{int}	0.042	0.093	0.053
Unique reflns	8585	6229	7059
No. of params, restraints	388, 2	271, 0	318, 0
GOF	1.015	1.163	1.035
R_1, wR_2 [$I > 2\sigma(I)$][b]	0.039, 0.065	0.048, 0.100	0.038, 0.084
R_1, wR_2 (all data)	0.049, 0.069	0.062, 0.105	0.049, 0.088

[a] Common items: T = 100 K; wavelength (Mo-K_α) = 0.71073 Å; θ(max) = 27.5°; [b] $R_1 = \Sigma||F_o|-|F_c||/\Sigma|F_o|$;

$wR_2=[\Sigma w(F_o^2-F_c^2)_2/\Sigma wF_o^4]^{1/2}$

CCDC Numbers: $[GeF_4(PMe_3)_2]$ (2113230), $[GeF_3(PMe_3)_2(OTf)]$ (2113231), $[GeF_2(PMe_3)_2(OTf)_2]$ (2113232), $[GeF_2\{o\text{-}C_6H_4(PMe_2)_2\}(OTf)_2]$ (2113233), $[GeF\{o\text{-}C_6H_4(PMe_2)_2\}(OTf)_3]$ (2113234), $[GeCl_2(AsEt_3)_2][OTf]_2$ (2113235), $[Ge\{o\text{-}C_6H_4(PMe_2)_2\}(OTf)][OTf]$ (2113236), $[GeF_3\{Ph_2P(CH_2)_2PPh_2\}(OTf)]$ (2113237), $[GeF_4\{\kappa^2\text{-}CH_3(CH_2PPh_2)_3\}]$ (2113415), $[GeF_2\{Ph_2P(CH_2)_2PPh_2\}(OTf)_2]$ (2113416)

3.6 Experimental

Refer to appendix A for sources of reagents, solvents and drying procedures, instrument specifications and references for NMR spectroscopy. $[GeF_4(PMe_3)_2]$, $[GeF_4\{o\text{-}C_6H_4(PMe_2)_2\}]$ and $[GeF_4(Ph_2P(CH_2)_2PPh_3\}]$ were made using literature methods.[7]

$[GeF_4(P^iPr_3)_2]$: To a suspension of $[GeF_4(MeCN)_2]$ (0.540 g, 2.34 mmol) in CH_2Cl_2 (5 mL) P^iPr_3 (0.750 g, 4.68 mmol) was added as a solution in CH_2Cl_2 (2 mL) and the reaction mixture stirred for 2 h to yield a clear colourless solution. The volatiles were removed *in vacuo* to leave a white solid which was washed with hexane (3 x 10 mL) and dried *in vacuo.* Yield: 0.941 g (76%). Satisfactory analytical data could not be obtained despite repeated attempts on different samples, with the elemental compositions varying from sample to sample. IR (Nujol/cm^{-1}): *v* = 590s (Ge-F). ^{1}H NMR (CD_2Cl_2, 298 K): δ = 1.33 (dd, $^3J_{HH}$ = 15 Hz, $^3J_{PH}$ = 7 Hz, [6H], CH_3), 2.38 (m, [1H], CH), ^{19}F{^{1}H} NMR (CD_2Cl_2, 298 K): δ = –65.0 (s, GeF); (183 K): δ = - 62.9 (t, $^2J_{PF}$ = 162 Hz, GeF) ^{31}P{^{1}H} NMR (CD_2Cl_2, 298 K): δ = 24.6 (s); (183 K): δ = 24.9 (quint, $^2J_{PF}$ = 162 Hz).

$[GeF_3(PMe_3)_2(OTf)]$: To a solution of $[GeF_4(PMe_3)_2]$ (0.100 g, 0.33 mmol) in CH_2Cl_2 (2 mL), a solution of TMSOTf (0.074 g, 0.33 mmol) in CH_2Cl_2 (2 mL) was added dropwise to form a clear solution. The reaction was stirred for 2 h, when the volatiles were removed *in vacuo* leaving a solid that was washed with hexane (3 x 10 mL) and dried *in vacuo* to form a white powder. Yield: 0.080 g (56%). Required for $C_7H_{18}F_6GeO_3P_2S$ (430.86): C, 19.5; H, 4.2. Found: C, 19.6; H, 4.3%. IR (Nujol/cm^{-1}): *v* = 572m, 515m (Ge-F). ^{1}H NMR (CD_2Cl_2, 298 K): δ = 1.68 (d, $^2J_{HP}$ = 13.2 Hz, CH_3). ^{19}F{^{1}H} NMR (CD_2Cl_2, 298 K): δ = –94.7 (br, [3F], GeF), –78.76 (s, [3F], OTf); (183 K): δ = –123.4 (tt, $^2J_{PF(trans\text{-}OTf)}$ = 134 Hz, $^2J_{FF}$ = 41 Hz, [F] GeF), –85.9 (td, $^2J_{PF(cis\text{-}OTf)}$ = 192 Hz, $^2J_{FF}$ = 41 Hz, [2F], GeF), –78.9 (s, [3F], OTf). ^{31}P{^{1}H} NMR (CD_2Cl_2, 298 K): δ = 3.1 (br s); (183 K): δ = 5.2 (td, $^2J_{PF(cis\text{-}OTf)}$ = 192 Hz, $^2J_{PF(trans\text{-}OTf)}$ = 134 Hz).

$[GeF_2(PMe_3)_2(OTf)_2]$: Method as above using $[GeF_4(PMe_3)_2]$ (0.100 g, 0.33 mmol) and TMSOTf (0.148 g, 0.66 mmol). White solid. Yield: 0.140 g (75%). Required for $C_8H_{18}F_8GeO_6P_2S_2$ (560.63): C, 17.1; H, 3.2. Found: C, 17.0; H, 3.3%. IR (Nujol/cm^{-1}): *v* = 573m (Ge-F). ^{1}H NMR (CD_2Cl_2, 298 K): 1.96 (m); (233 K): δ = 1.98 (d, $^2J_{HP}$ = 12 Hz, CH_3). ^{19}F{^{1}H} NMR (CD_2Cl_2, 298 K): δ = -119.5 (br s, [2F], GeF), -78.3 (s, [6F], OTf); (233 K): δ = –122.3 (t, $^2J_{PF}$ = 83 Hz, [2F], GeF), –78.3 (br, [6F], OTf). ^{31}P{^{1}H} NMR (CD_2Cl_2, 298 K): δ = 25.8 (br); (233 K): δ = 27.8 (t, $^2J_{PF}$ = 83 Hz).

[GeF(PMe$_3$)$_2$(OTf)$_3$]: Method as above using [GeF$_4$(PMe$_3$)$_2$] (0.100 g, 0.33 mmol) and TMSOTf (0.222 g, 1.00 mmol). White solid. Yield: 0.175 g (76%). Required for $C_9H_{18}F_{10}GeO_9P_2S_3$ (691.00): C, 15.6; H, 2.6. Found: C, 15.8; H, 2.6%. IR (Nujol/cm^{-1}): ν = 583m (Ge-F). ^{1}H NMR (CD_2Cl_2, 298 K): δ = 2.03 (dd, $^2J_{HP}$ = 13.8 Hz, $^4J_{FH}$ = 1 Hz. CH_3). ^{19}F{^{1}H} NMR (CD_2Cl_2, 298 K): δ = –107.2 (t, $^2J_{PF}$ = 75 Hz, [F], Ge-F), –77.6 (br s, OTf), –78.1 (br s, OTf, total OTf integral [9F]),. ^{31}P{^{1}H} NMR (CD_2Cl_2, 298 K): δ = 32.3 (d, $^2J_{PF}$ = 75 Hz).

[GeF$_3$(P^{i}Pr$_3$)$_2$][OTf]: Method as above using [GeF$_4$(P^{i}Pr$_3$)$_2$] (0.100 g, 0.33 mmol) and TMSOTf (0.074 g, 0.33 mmol). White powder. Yield: 0.188 g (48%). Required for $C_{18}H_{42}F_6GeO_3P_2S{\cdot}1/2CH_2Cl_2$ (629.63): C, 35.3; H, 6.9. Found: C, 35.3; H, 6.9%. IR (Nujol/cm^{-1}): ν = 572m (Ge-F). ^{1}H NMR (CD_2Cl_2, 298 K): δ = 1.43 (dd, $^3J_{HH}$ = 16 Hz, $^3J_{PH}$ = 7 Hz, [6H], CH_3), 2.69 (m, [1H], CH). ^{19}F{^{1}H} NMR (CD_2Cl_2, 298 K): δ = –79.0 (s, [3F], OTf), –56.7 (t, $^2J_{PF}$ = 153 Hz, [3F], GeF). ^{31}P{^{1}H} NMR (CD_2Cl_2, 298 K): δ = 46.8 (q, $^2J_{PF}$ = 153 Hz).

[GeF$_3${*o*-C$_6$H$_4$(PMe$_3$)$_2$}(OTf)]: Method as above using [GeF$_4${*o*-C$_6$H$_4$(PMe$_3$)$_2$}] (0.100 g, 0.29 mmol) and TMSOTf (0.064 g, 0.29 mmol) and stirring for 30 mins. White solid. Yield: 0.084 g (61%). Required for $C_{11}H_{16}F_6GeO_3P_2S$ (476.86): C, 27.7; H, 3.4. Found: C, 27.5; H, 3.6%. IR (Nujol/cm^{-1}): ν = 518m, 579m, 602m (Ge-F). ^{1}H NMR (CD_2Cl_2, 298 K): δ = 1.90 (m, [12H], CH_3), 7.84 (m, [4H], ArH). ^{19}F{^{1}H} NMR (CD_2Cl_2, 298 K): δ = -113.3 (br s, GeF), -78.3 (s, OTf); (183 K): δ = –123.7 (tt, $^2J_{PF}$ = 94 Hz; $^2J_{FF}$ = 43 Hz, [1F], GeF), –109.5 (ddd, $^2J_{PF}$ = 135, 76 Hz; $^2J_{FF}$ = 43 Hz, [2F], GeF), -78.3 (s, [3F], OTf). ^{31}P{^{1}H} NMR (CD_2Cl_2, 298 K): δ = –24.1 (br s); (183 K): δ = –23.1 (ddd, $^2J_{PF}$ = 135, 94, 76 Hz).

[GeF$_2${*o*-C$_6$H$_4$(PMe$_3$)$_2$}(OTf)$_2$]: Method as above using [GeF$_4${*o*-C$_6$H$_4$(PMe$_3$)$_2$}] (0.100 g, 0.29 mmol) and TMSOTf (0.128 g, 0.58 mmol) and stirring for 30 mins. White solid. Yield: 0.102 g (58%). Required for $C_{12}H_{16}F_8GeO_6P_2S_2{\cdot}CH_2Cl_2$ (691.84): C, 22.6; H, 2.6. Found: C, 22.7; H, 3.1%. IR (Nujol/cm^{-1}): ν = 637m (Ge-F). ^{1}H NMR (CD_2Cl_2, 298 K): δ = 2.03 (m, [12H], CH_3), 7.91 (m, [4H], ArH). ^{19}F{^{1}H} NMR (CD_2Cl_2, 298 K): δ = –100.5 (dd, $^2J_{PF}$ = 121 Hz, 74 Hz, GeF), -78.2 (s, OTf), -77.5 (s, OTf); (183 K): δ = -77.7 (s, OTf), -78.0 (s, OTf), -78.3 (s, OTf), -79.1 (s, OTf), -101.1 (dd, $^2J_{PF}$ = 126, 72 Hz, GeF), ^{31}P{^{1}H} NMR (CD_2Cl_2, 298 K): δ = –23.2 (dd, $^2J_{PF}$ = 121 Hz, 74 Hz); (183 K): δ = -19.9 (dd, $^2J_{PF}$ = 126, 72 Hz).

[GeF{*o*-$C_6H_4(PMe_3)_2$}$(OTf)_3$]: Method as above using [GeF_4{*o*-$C_6H_4(PMe_3)_2$}] (0.100 g, 0.29 mmol) and TMSOTf (0.192 g, 0.86 mmol) and stirring for 30 mins., then the solution was layered with hexane (10 mL) . After 3 days at -18 ˚C the product crystallised. Crystals were collected by filtration, washed with hexane (3 x 10 mL), and dried *in vacuo*. Yield: 0.086 g (40%). Required for $C_{13}H_{16}F_{10}GeO_9P_2S_3$ (736.98): C, 21.2; H, 2.2. Found: C, 22.1; H, 3.8%. IR (Nujol/cm^{-1}): ν = 633m (Ge-F). ^{1}H NMR (CD_2Cl_2, 298 K): δ = 2.03 (m, CH_3), 2.16 (m, CH_3), 2.25 (m, CH_3) (sum of methyl resonances [12H]), 7.97 (m, [4H], ArH). ^{19}F{^{1}H} NMR (CD_2Cl_2, 298 K): δ = -77.1 (s, OTf), -77.3 (s, OTf), -77.6 (s, OTf), -78.2 (br, OTf), -81.8 (t, $^2J_{PF}$ = 82 Hz, GeF)$^+$, -91.9 (t, $^2J_{PF}$ = 69 Hz, GeF)$^+$, –94.0 (t, $^2J_{PF}$ = 73 Hz, GeF)*. ^{31}P{^{1}H} NMR (CD_2Cl_2, 298 K): δ = –13.5 (d, $^2J_{PF}$ = 73 Hz)*, -8.53 (d, $^2J_{PF}$ = 69 Hz); (*= major species; $^+$= minor species).

[GeF_3{$Ph_2P(CH_2)_2PPh_2$}(OTf)]: Method as above using [GeF_4{$Ph_2P(CH_2)_2PPh_2$}] (0.100 g, 0.18 mmol) and TMSOTf (0.041 g, 0.18 mmol). White solid. Yield: 0.045 g (36%). Required for $C_{27}H_{24}F_6GeO_3P_2S$ (677.12): C, 47.9; H, 3.6 Found: C, 47.7; H, 3.7%. IR (Nujol/cm^{-1}): ν = 519m, 526m, 573m (Ge-F). The product was not sufficiently soluble in CH_2Cl_2 or CD_3NO_2 to obtain reliable solution NMR data

[GeF_2{$Ph_2P(CH_2)_2PPh_2$}$(OTf)_2$]: Method as above using [GeF_4{$Ph_2P(CH_2)_2PPh_2$}] (0.100 g, 0.18 mmol) and TMSOTf (0.081 g, 0.36 mmol). White solid. Yield: 0.119 g (81%). Required for $C_{28}H_{24}F_8GeO_6P_2S_2{\cdot}1/2CH_2Cl_2$ (849.60): C, 40.3; H, 3.0. Found: C, 39.9; H, 3.0%. IR (Nujol/cm^{-1}): ν = 502m, 527m (Ge-F). The product was not sufficiently soluble in CH_2Cl_2 or CD_3NO_2 to obtain reliable solution NMR data.

[GeF_4{κ^2-$CH_3C(CH_2PPh_2)_3$}]: To a suspension of [$GeF_4(MeCN)_2$] (0.200 g, 0.87 mmol) in CH_2Cl_2 (2 mL), $CH_3C(CH_2PPh_2)_3$ (0.541 g, 0.87 mmol) was added as a solid and the resulting solution is stirred for 2 h forming a clear colourless solution. Volatiles were removed *in vacuo* to yield a white solid, which was washed with hexane (3 x 10 mL) and dried *in vacuo*. Yield: 0.413 g (62%) Required for $C_{41}H_{39}F_4GeP_3{\cdot}1/2\ CH_2Cl_2$ (815.70): C, 61.1; H, 4.9. Found: C, 61.2; H, 5.1%. IR (Nujol/cm^{-1}): ν = 517br, 603br (Ge-F). ^{1}H NMR (CD_2Cl_2, 298 K): δ = 0.87 (s, [3H] CH_3), 2.69 (br s, [6H], CH_2), 7.28-7.58 (m, ArH); (183 K): δ = 0.73 (s, [3H], CH_3), 2.01 (br m, [2H], CH_2), 2.79 (br s, [2H], CH_2), 2.90 (br s, [2H], CH_2), 7.28-7.58 (m, ArH). ^{19}F{^{1}H} NMR (CD_2Cl_2, 298 K): δ = –108.6 (br s, GeF), –72.2 (br s, GeF); (243 K): δ = –74.4 (overlapping multiplets, [2F], GeF), –109.3 (ddt, $^2J_{PF}$ = 125, 67 Hz, $^2J_{FF}$ = 62 Hz, [2F], GeF); (183 K): δ = –77.7 (br m, [2F], GeF), –110.3 (br m, [2F], GeF). ^{31}P{^{1}H} NMR (CD_2Cl_2, 298 K): δ = –4.0 (br s), -23.5(s); (183 K): δ = –4.5 (tdd, $^2J_{PF}$ = 142, 125, 67 Hz, [2P], $P_{coordinated}$), –27.9 (s, [1P], P_{free}).

[$GeF_4\{\kappa^2$-$P(CH_2CH_2PPh_2)_3\}$]: To a suspension of [$GeF_4(MeCN)_2$] (0.200 g, 0.87 mmol) in CH_2Cl_2 (2 mL), $P(CH_2CH_2PPh_2)_3$ (0.581 g, 0.87 mmol) was added as a solid and the resulting solution was stirred for 2 h to give a clear colourless solution, from which volatiles were removed *in vacuo* to yield a white solid. The resulting solid was washed with hexane (3 x 10 mL) and dried *in vacuo*. Yield 0.408 (57%). Required for $C_{42}H_{42}F_4GeP_4$ (819.25): C, 61.6; H, 5.2. Found: C, 62.1; H, 5.5%. IR (Nujol/cm^{-1}): ν = 508m, 517m, 589m, 608m (Ge-F).^{1}H NMR (CD_2Cl_2, 298 K): δ = 2.03 (br s, [6H], CH_2), 2.28 (br s, [6H], CH_2), 7.38-7.48 (br m, [30H], ArH). $^{19}F\{^1H\}$ NMR (CD_2Cl_2, 298 K): δ = –94.8 (br s), –114.2 (br s); (213 K): δ = –80.4 (ddt, $^2J_{PF}$ = 153, 133 Hz, $^2J_{FF}$ = 54 Hz, [2F], GeF), –108.4 (ddt, $^2J_{PF}$ = 205, $^2J_{FF}$ = 54, 54 Hz, [F], GeF), –114.1 (ddt, $^2J_{PF}$ = 188 Hz, $^2J_{FF}$ = 54, 54 Hz, [F], GeF), $^{31}P\{^1H\}$ NMR (CD_2Cl_2, 183 K): δ = –3.2 (ddtt, $^2J_{PP}$ = 336, $^2J_{PF}$ = 188, 153,$^3J_{PP}$ = 35 Hz, [1P], P_{apical}), –12.4 (d, $^3J_{PP}$ = 35 Hz, [2P], $P_{free\ arm}$), –17.6 (ddt, $^2J_{PF}$ = 336, 207, 133 Hz, [1P], $P_{coordinated\ arm}$).

Reaction of $GeCl_4$ two eq. of $AsEt_3$ and two eq. of TMSOTf

To a solution of $GeCl_4$ (0.134 g, 0.625 mmol) in CH_2Cl_2 (2 mL), $AsEt_3$ (0.200 g, 1.23 mmol) was added as a solution in CH_2Cl_2 (2 mL). To this mixture TMSOTf (0.274 g, 1.23 mmol) was added as a solution in CH_2Cl_2 (2 mL), the reaction mixture was stirred for 1 h and the solution remained colourless. The solution was concentrated to 1 mL and layered with hexane (3 mL) and stored at -18 ˚C, after a number of days a colourless crystalline material formed which was collected by filtration and dried in vacuo to yield a white powder. Yield 0.261 g. IR (Nujol/cm^{-1}): ν = 397s, 408s (Ge-Cl), 1151m (OSO_2), 1213m, 1261m (CF_3). ^{1}H NMR (CD_2Cl_2, 298 K): δ = 1.34 (br s), 1.47 (br s), 1.52 (t, $^3J_{HH}$ = 7.7 Hz), 2.15 (br s), 2.51 (br s), 2.97 (br s), 3.09 (q, $^3J_{HH}$ = 7.7 Hz), 3.12 (q, $^3J_{HH}$ = 7.7)

3.7 References

1 A. W. Waller, N. M. Weiss, D. A. Decato and J. A. Phillips, J. Mol. Struct., 2017, 1130, 984–993.

2 D. T. Tran, P. Y. Zavalij and S. R. J. Oliver, Acta Crystallogr. Sect. E Struct. Reports Online, 2002, 58, m742–m743.

3 F. Cheng, M. F. Davis, A. L. Hector, W. Levason, G. Reid, M. Webster and W. Zhang, Eur. J. Inorg. Chem., 2007, 2007, 4897–4905.

4 A. D. Adley, P. H. Bird, A. R. Fraser and M. Onyszchuk, Inorg. Chem., 1972, 11, 1402–1409.

5 F. Cheng, M. F. Davis, A. L. Hector, W. Levason, G. Reid, M. Webster and W. Zhang, Eur. J. Inorg. Chem., 2007, 2488–2495.

6 K. George, A. L. Hector, W. Levason, G. Reid, G. Sanderson, M. Webster and W. Zhang, Dalton Trans., 2011, 40, 1584–1593.

7 M. F. Davis, W. Levason, G. Reid and M. Webster, Dalton Trans., 2008, 2261–2269.

8 R. Suter, A. Swidan, C. L. B. Macdonald and N. Burford, Chem. Commun., 2018, 54, 4140–4143.

9 J. Burt, W. Levason and G. Reid, Coord. Chem. Rev., 2014, 260, 65–115.

10 H. J. Hogben, M. Krzystyniak, G. T. P. Charnock, P. J. Hore and I. Kuprov, J. Magn. Reson., 2011, 208, 179–194.

11 E. MacDonald, L. Doyle, S. S. Chitnis, U. Werner-Zwanziger, N. Burford and A. Decken, Chem. Commun., 2012, 48, 7922–7924.

12 A. M. Forster and A. J. Downs, Polyhedron, 1985, 4, 1625–1635.

13 C. A. Tolman, Chem. Rev., 1977, 77, 313–348.

14 E. MacDonald, PhD Thesis, Dalhousie University, Halifax, Canada, 2013.

Chapter 4 Dicationic germanium(II) complexes with pnictine ligands

4.1 Introduction

4.1.1 Phosphine and arsine germanium(II) complexes

The first reported complexes of germanium(II) halides with secondary or tertiary phosphine ligands came in 1963. It was demonstrated that GeI_2 would react with equimolar amounts of secondary (e.g. $PHPh_2$) or tertiary phosphines (e.g. PPh_2Me, P^nPr etc.) in a mixture of boiling ethylcyclohexane and xylene to form 1:1 adducts (as determined by elemental analysis).[1] However, the structures of these complexes were not determined until later, in 1975, when the structure of $[GeCl_2(PPh_3)]$ was determined by single-crystal X-ray diffraction, revealing a pyramidal geometry around the germanium centre.[2] Later structural determinations of related complexes with different halides or different phosphines have shown that this structure type is general for these 1:1 adducts, e.g. the structure of $[GeCl_2(PPh_3)]$ shown in **Figure 4.1** below.[3] There are also a few examples of Ge(II) complexes with monodentate arsine ligands, $[GeCl_2(AsR_3)]$ (R = Ph, ^{t}Bu), although their crystal structures have not been determined.[4]

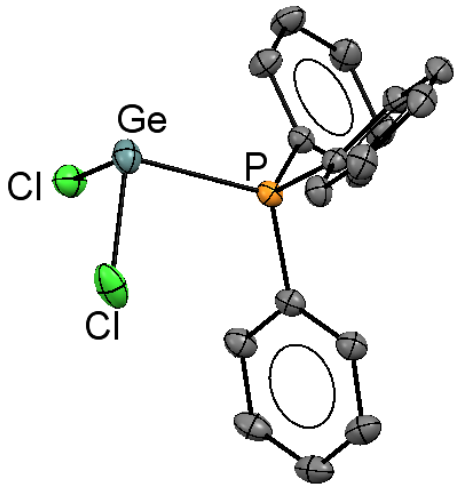

Figure 4.1 – The structure of $[GeCl_2(PPh_3)]$ showing the pyramidal coordination geometry. Redrawn from Ref. 3

Bidentate pnictine ligands can also form complexes with Ge(II) halides. Here the choice of ligand strongly affects the structure of the resulting product. The ligand *o*-$C_6H_4(PPh_2)_2$ reacts with [$GeCl_2$(dioxane)] or GeX_2 (X = Br, I) to form [GeX_2{*o*-$C_6H_4(PPh_2)_2$}] (X = Cl, Br, I). The structures are very similar for this set of complexes and feature asymmetric coordination of the bulky diphosphine ligand; the primary coordination environment can be said to be pyramidal, e.g. for X = Cl, shown in **Figure 4.2** (with a Ge-P distance of 2.5153(13)), with only a weak interaction (3.1958(15) Å) with the second phosphine group (Σr_{cov} = 2.27 Å,[5] Σr_{vdW} = 3.91 Å[6]). However, if the more strongly donating and less sterically demanding *o*-$C_6H_4(PMe_2)_2$ ligand is used, the ligand bonds in a symmetric manner, so the complexes [GeX_2{*o*-$C_6H_4(PMe_2)_2$}] (X = Cl, Br, I) are instead four-coordinate around germanium with the halides *trans*. Examples of both these structure types are shown in **Figure 4.2** below.[7]

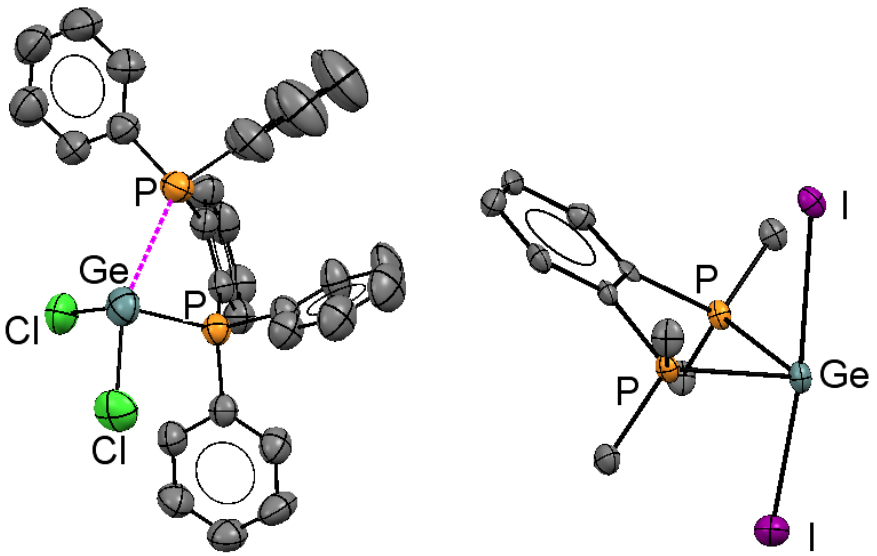

(a) (b)

Figure 4.2 – Structure of (a) [$GeCl_2${*o*-$C_6H_4(PPh_2)_2$}] (purple dashed line indicates weak interaction) and (b) [GeI_2{*o*-$C_6H_4(PMe_2)_2$}] showing the different structure types. Redrawn from Ref. 7

Bidentate arsine ligands also form complexes with germanium(II) halides. Here the specific halide dictates the product of the reaction. The reaction of GeI_2 with *o*-$C_6H_4(AsMe_2)_2$ in CH_2Cl_2 leads to the formation of [GeI_2{*o*-$C_6H_4(AsMe_2)_2$}], which has a structure analogous to the phosphine complex in **Figure 4.2b**. However, the reaction of [$GeCl_2$(dioxane)] with *o*-$C_6H_4(AsMe_2)_2$ forms [GeCl{*o*-$C_6H_4(AsMe_2)_2$}][$GeCl_3$], which

features a discrete $[GeCl\{o\text{-}C_6H_4(AsMe_2)_2\}]^+$ monocation, the first example of such a species.[7]

Recently, analogous related monocationic complexes $[GeCl\{Ph_2P(CH_2)_3PPh_2\}][X]$ (X = OTf^- or $GeCl_3^-$) have been synthesised; the structure of the cation is shown in **Figure 4.3**. [8] Clearly, in these systems the outcome of the reaction is strongly dependant on the conditions used and the properties of the ligands; sterics and ligand architecture have more of an influence in p-block chemistry compared to electronic effects.

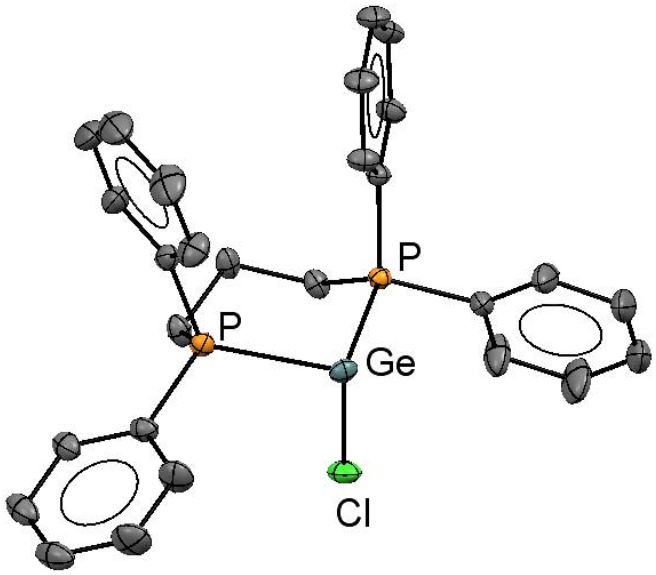

Figure 4.3 – The structure of the monocation in $[GeCl\{Ph_2P(CH_2)_3PPh_2\}][GeCl_3]$. Redrawn from Ref. 8.

4.1.2 Dicationic germanium(II) complexes

The discovery of the dication $[Ge(2,2,2\text{-crypt})]^{2+}$ (2,2,2-crypt = 4,7,13,16,21,24-hexaoxa-1,10-diazabicyclo[8.8.8]hexacosane) by Baines *et al.* spearheaded research in this area (see **Figure 4.4**). It was the first example of a mononuclear p-block element carrying a positive charge to be encapsulated within a cryptand. $[Ge(2,2,2\text{-crypt})][OTf]_2$ was synthesised through the reaction of [GeCl(OTf)(NHC)] (NHC = 1,3-diisopropyl-4,5-dimethylimidazol-2-ylidene) with 2,2,2-crypt in THF yielding $[Ge(2,2,2\text{-crypt})][OTf]_2$ as a white solid. In this complex, the nitrogen and oxygen atoms of the cryptand only interact weakly with the germanium centre with calculated bond orders of ~0.10 (with 1.0 being a

classical single covalent bond); the lone pair present on this cation resides in a 4s type orbital on germanium.[9]

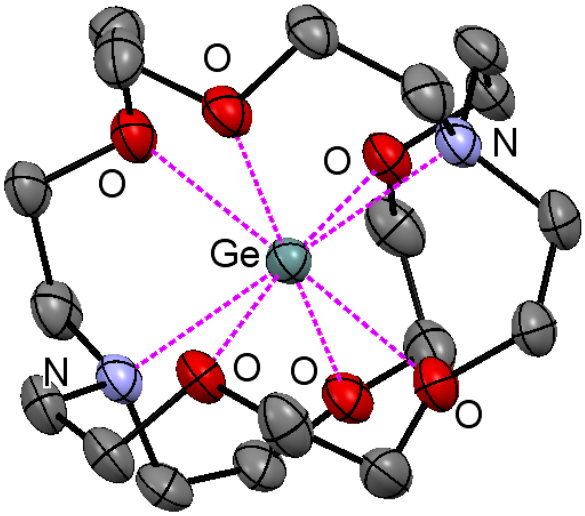

Figure 4.4 – Structure of the dication $[Ge(2,2,2\text{-crypt})]^{2+}$ Ge···O = 2.4856(16), Ge···N = 2.524(3). Redrawn from Ref. 9.

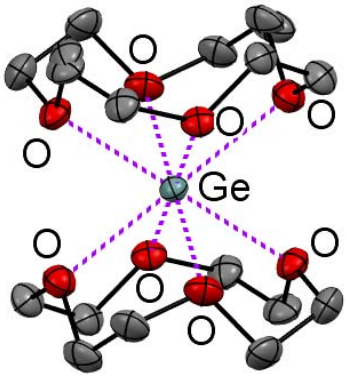

Figure 4.5 – Structure of the dication $[Ge(12\text{-crown-}4)_2]^{2+}$ Redrawn from Ref. 10.

Crown ethers and aza-macrocycles have also been shown to stabilise "naked" germanium(II) centres. The resulting geometries of these complexes are strongly dependant on the macrocycle ring size and denticity. With 12-crown-4, as shown in **Figure 4.5** above, a sandwich complex forms with the germanium being 8-coordinate with a square prismatic geometry. In contrast, for 15-crown-5, the germanium is located in the centre of the ring. However, in this case, the triflate anions are associated with the germanium, so the complex is not cationic. With 18-crown-6, the germanium is located to

one side of the ring with only four sequential crown oxygens coordinating to the germanium centre, with the coordination sphere completed by two triflates.[10,11] $[GeCl_2(dioxane)]$ reacts with Me_4cyclam (1,4,8,11-tetramethyl-1,4,8,11-tetraazacyclotetradecane) or Me_4cyclen (1,4,7,10-tetramethyl-1,4,7,10-tetraazacyclododecane) to form $[Ge(Me_4cyclam)][GeCl_3]_2$ and $[Ge(Me_4cyclen)][GeCl_3]_2$, which both have a distorted 4-coordinate geometry at germanium. In $[Ge(Me_4cyclam)][GeCl_3]_2$ there are two short and two long Ge-N bonds (see **Figure 4.6b**). The reaction of $GeBr_2$ with Me_3tacn (1,4,7-trimethyl-1,4,7-triazacyclononane) leads to the isolation of $[Ge(Me_3tacn)][GeBr_3]_2$; here the dication has a pyramidal structure at germanium (see **Figure 4.6a**). In the Me_3tacn, Me_4cyclam and Me_4cyclen complexes, there are no close anion contacts, so they can be regarded as truly ionic species. The electronic structure of these complexes has not been investigated.[11,12]

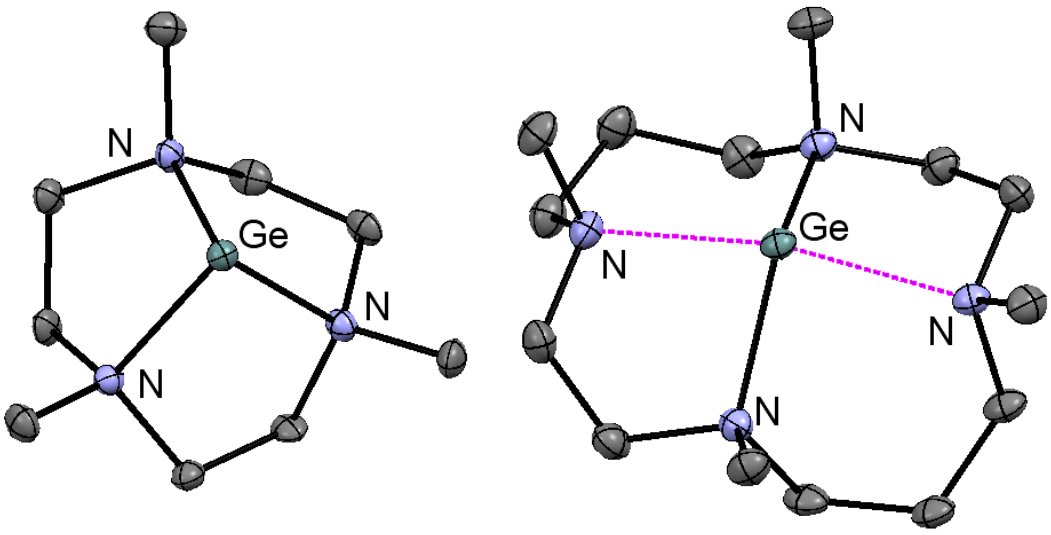

(a) (b)

Figure 4.6 – The crystal structures of the dications (a) $[Ge(Me_3tacn)]^{2+}$ and (b) $[Ge(Me_4cyclam)]^{2+}$, the purple dashed line indicating weak secondary contacts. Both redrawn from Ref. 11.

Dicationic germanium(II) complexes can also be synthesised with monodentate ligands, the reaction of $[GeI_2(NHC)]$ (NHC = 1,3-diisopropyl-4,5-dimethylimidazol-2-ylidene) with excess NHC leads to the displacement of the iodide ligands to form the salt $[Ge(NHC)_3][I]_2$ featuring a pyramidal dication with no close contacts to the iodides.[6] DFT calculations on this complex suggest that the HOMO is a lone pair on the germanium centre.[13] More

recently, a four-coordinate germanium(II) dication was isolated with isocyanide ligands. When three equivalents of $[GeCl_2(dioxane)]$ are reacted with four equivalents of isocyanide L (L = 2,6-dimethylphenylisocyanide) the resulting product is $[GeL_4][GeCl_3]_2$. The $[GeL_4]^{2+}$ unit has a distorted tetrahedral geometry with no close contacts with the counter anions. This is in stark contrast to the carbene complexes, where even with an excess of ligand only three ligands are bonded. In the isocyanide complex, the lone pair is stereochemically inactive, which also contrasts with the carbene analogue.[14]

Interestingly, it has also been shown that germanium(II) dications that bear a lone pair can be used as ligands towards transition metal centres. Manjumdar *et al.* have shown that the dicationic complex $[GeL][OTf]_2$, where L = 2,7-bis(2-pyridyl)-3,6-diazaota-2,6-diene (shown in **Figure 4.7**), can react with AgOTf or AuOTf to form the tetracation $[Ag(GeL)_2(OTf)][OTf]_4$ or the pentacation $[Au(GeL)_2][OTf]_5$, respectively. In the case of silver, one of the triflates also remains coordinated to the metal centre. This work shows that germanium(II) dications may see further use in stabilising highly charged metal centres.[15]

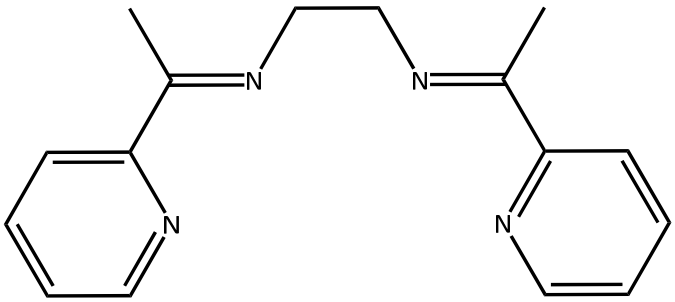

Figure 4.7 – The structure of the ligand 2,7-bis(2-pyridyl)-3,6-diazaota-2,6-diene.

4.1.3 Pyramidal main group *tris*-phosphine complexes

There are only a few examples of *tris*-monophosphine complexes of main group elements. In group 13, two examples are known, one for gallium and one for indium, both of the form $[M(PPh_3)_3]^+$ (M = Ga, In). In both cases, the large, diffuse and weakly coordinating $[Al\{OC(CF_3)_3\}_4]^-$ anion is used to balance the charge. The complexes are synthesised by reaction of the requisite metal and $Ag[Al\{OC(CF_3)_3\}_4]$ in *o*-$C_6H_4F_2$ and toluene to isolate $[M(toluene)_x][Al(OC(CF_3)_3)_4]$, which then react with three equivalents of PPh_3 to yield the complexes $[M(PPh_3)_3][Al(OC(CF_3)_3)_4]$. The structure for M = Ga is shown in **Figure 4.8b** below and reveals the pyramidal geometry around the gallium centre.[16,17]

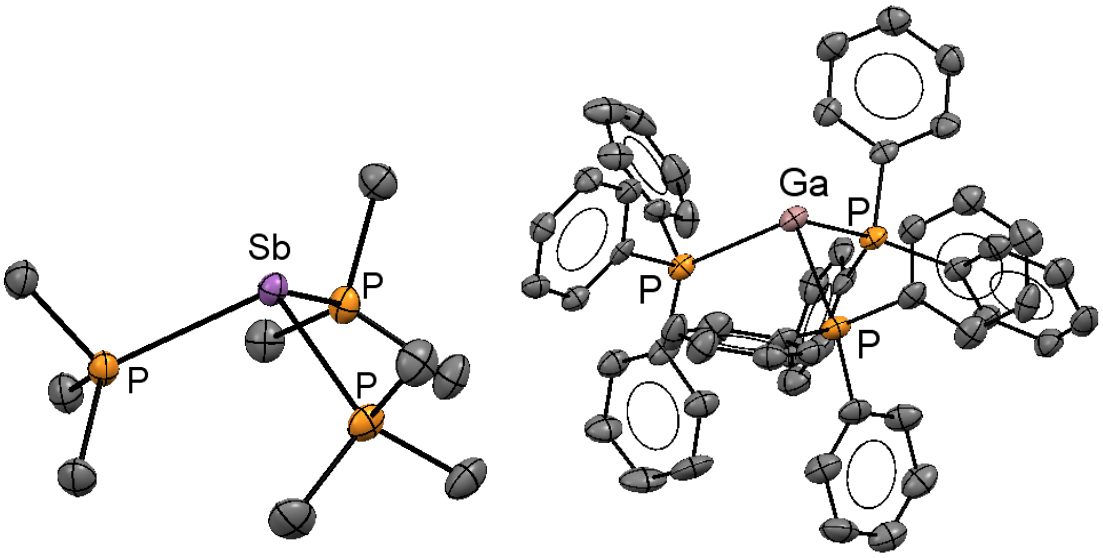

(a) (b)

Figure 4.8 – The structure of (a) $[Sb(PMe_3)_3]^{3+}$ from a co-crystal of $[Sb(PMe_3)_3][OTf]_3$ and $[Me_3PPMe_3][OTf]$ redrawn from Ref. 18 and (b) $[Ga(PPh_3)_3]^+$ from $[Ga(PPh_3)_3][Al(OC(CF_3)_3)_4]\cdot 1.5\ C_6H_4F_2$ redrawn from Ref. 16.

A group 15 trication can also be synthesised by the reaction of SbF_3 with three equivalents of PMe_3 and three equivalents of TMSOTf in MeCN, which leads to the formation of $[Sb(PMe_3)_3][OTf]_3$ (the cation is shown above in **Figure 4.8a**), which can be co-crystallised with $[Me_3PPMe_3][OTf]_2$. This complex is unstable and reduces to the tetracationic $[Sb_4(PMe_3)_4][OTf]_4$ with reductive elimination of $[Me_3PPMe_3]^{2+}$.[18]

There are also some examples that utilise triphosphine ligands, but in these cases, the negatively charged P_3B ligands are used (P_3B = $RB(CH_2PR'_2)_3$, where R and R' are aryl groups). Many complexes with these types of ligands have been reported for thallium(I).[19–21] This ligand type has also been used to synthesise a neutral tin(II) $[SnCl(P_3B)]$ complex. From this, the monocationic complex, $[Sn(P_3B)][PF_6]$, could be synthesised by reaction with the halide abstraction agent $Tl[PF_6]$.[22]

4.2 Aims

The aim of this chapter is to further develop the chemistry of Ge(II) with phosphine and arsine ligands, specifically using the less strongly coordinating nature of the OTf anion to explore new structural motifs.

4.3 Results and discussion

4.3.1 Synthesis of dicationic germanium(II) phosphine and arsine complexes

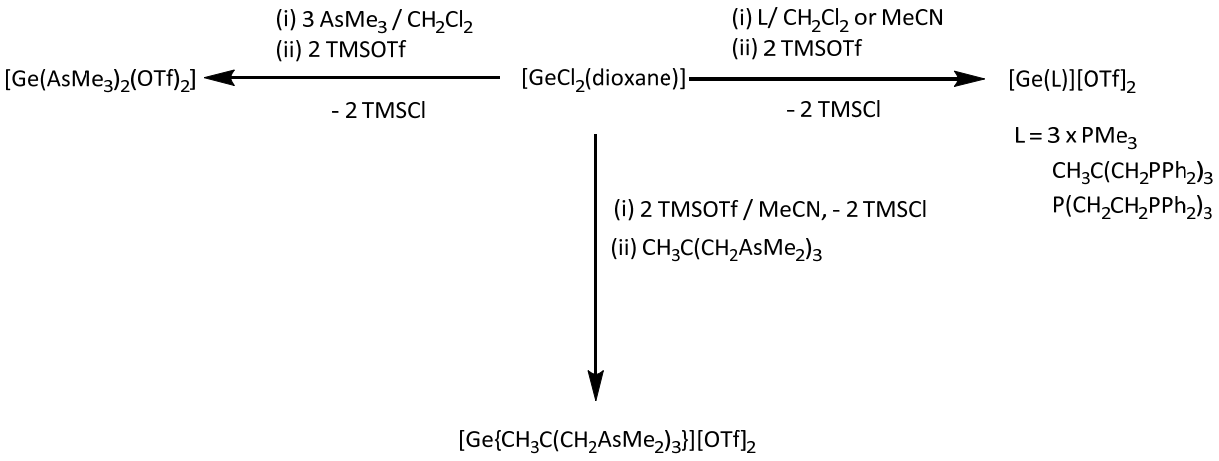

Scheme 4.1 – Routes to the complexes described in this chapter

The syntheses of the complexes described in the chapter are detailed in **Scheme 4.1**. Following the discovery of $[Ge(PMe_3)_3][OTf]_2$ from the decomposition of $[GeF_3(PMe_3)_2(OTf)]$ in CH_2Cl_2 solution (see **Chapter 3**), we sought to determine if this compound could be synthesised directly. $[GeCl_2(dioxane)]$ was selected as the source of Ge(II), and the reaction of this with two equivalents of TMSOTf and three equivalents of PMe_3 in MeCN gave a clear solution. The white powder isolated from this reaction by removing the solvent *in vacuo,* however, was identified as $[Ge(PMe_3)_2(OTf)_2]$ by microanalysis; this neutral complex has been structurally characterised previously.[23] This suggests that under the reaction conditions used, one of the PMe_3 groups is removed *in vacuo*. To combat this, instead of removing the solvent *in vacuo,* the reaction was performed in CH_2Cl_2 to yield a white precipitate. MeCN was then added until the solution went clear, and this solution was layered with hexane and left to crystallise for three days at -18 ˚C. At this point, the solvent was decanted, and the crystalline product was dried

under a stream of dry nitrogen (removing the solvent and drying *in vacuo* again led to the loss of one PMe_3). Crystals from this batch were examined by single-crystal X-ray diffraction and proved to be $[Ge(PMe_3)_3][OTf]_2$. The crystal structure of this compound is shown below in **Figure 4.9**.

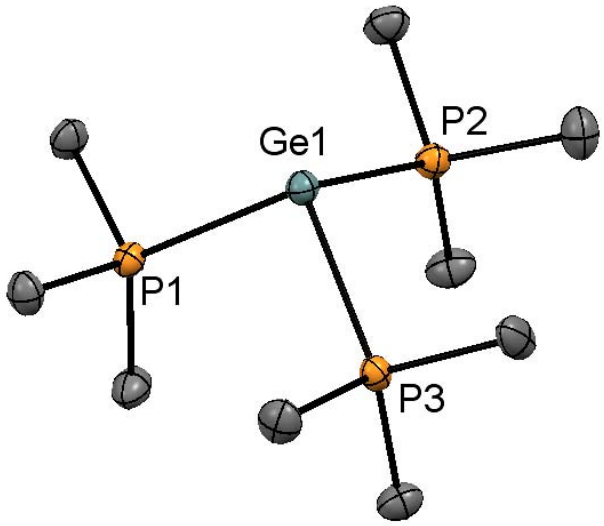

Figure 4.9 – The structure of the dication in $[Ge(PMe_3)_3][OTf]_2$ with the triflates and H atoms omitted for clarity and showing the atom labelling scheme. Ellipsoids are drawn at the 50% probability level. Selected bond lengths (Å) and angles (˚) are: Ge1-P1 = 2.3747(5), Ge1-P2 = 2.3828(5), Ge1-P3 = 2.3970(5), Ge1···O3 (closest oxygen to Ge) = 4.2853(17). P1-Ge1-P2 = 100.509(18), P1-Ge1-P3 = 98.085(17), P2-Ge1-P3 = 99.276(18).

The dication, $[Ge(PMe_3)_3]^{2+}$, has a trigonal pyramidal structure with the three phosphines stabilising the germanium centre, with the P-Ge-P angles being within the range 98.085(17)-100.507(18)˚. This is the first known example of P_3 homoleptic coordination for germanium(II) dications. There are no close contacts between the germanium centre and the triflate anions, with the closest approach being 4.2853(17) Å, well outside the expected range for Ge-OTf bonds (1.91-2.58 Å). This can be compared to the previously reported $[Ge(PMe_3)_2(OTf)]_2$, where the shortest Ge···O distance is 2.239 Å, the triflates in this case should be regarded as bound in the solid state. The d(Ge-P) distances fall within the range 2.4160(11)-2.4191(12) Å for the *bis*-phosphine complex, significantly longer than for the tris-complex (2.3747(5)-2.3970(5) Å). This contraction of the bond length reflects the increased Lewis acidity of the dication compared to the triflate-bound neutral species.

The ^{1}H NMR spectrum of $[Ge(PMe_3)_3][OTf]_2$ shows one doublet resonance at 1.88 ppm ($^{2}J_{PH}$ = 12 Hz), which indicates in solution there is still only one PMe_3 environment, which is consistent with the structure above in **Figure 4.9**; the coordination shift of the resonance is Δδ = +0.91 from the 'free' ligand. There is also a sharp singlet resonance in the $^{31}P\{^{1}H\}$ spectrum at δ = -12.8, i.e. Δδ = +47.7 from the 'free' ligand, which can be explained by a large increase in positive charge at the phosphorus centre. A sharp singlet at δ = -79.3 in the $^{19}F\{^{1}H\}$ NMR spectrum indicates that the triflate is ionic in solution, consistent with the solid-state data.

Peaks corresponding to the Ge-Cl stretches (found between 275-314 cm^{-1} in $[GeCl_2(dioxane)]$) are absent in the IR spectrum, indicating that all the $[GeCl_2(dioxane)]$ has been consumed; there are new peaks at 1156, 1123, and 1261 cm^{-1} corresponding to vibrations in the triflate anion.

The reaction of $[GeCl_2(dioxane)]$ with two equivalents of TMSOTf and three equivalents of $AsMe_3$ leads to the formation of the *bis*-arsine complex, $[Ge(AsMe_3)_2(OTf)_2]$, which can be crystallised by layering a CH_2Cl_2 solution with hexane. This *bis*-$AsMe_3$ complex has a distorted tetrahedral structure (**Figure 4.10** below), which contrasts with the reported structure of $[Ge(PMe_3)_2(OTf)_2]$, which has a disphenoidal structure. The Ge-OTf distances fall within the expected range for OTf coordination (2.0170(15) Å). In the solid state, there are also weak intermolecular interactions with neighbouring molecules through Ge···OTf interactions (2.994 Å) forming a polymeric chain in the *c*-direction and completes a distorted octahedral geometry at Ge(II) (see **Figure 4.11**).

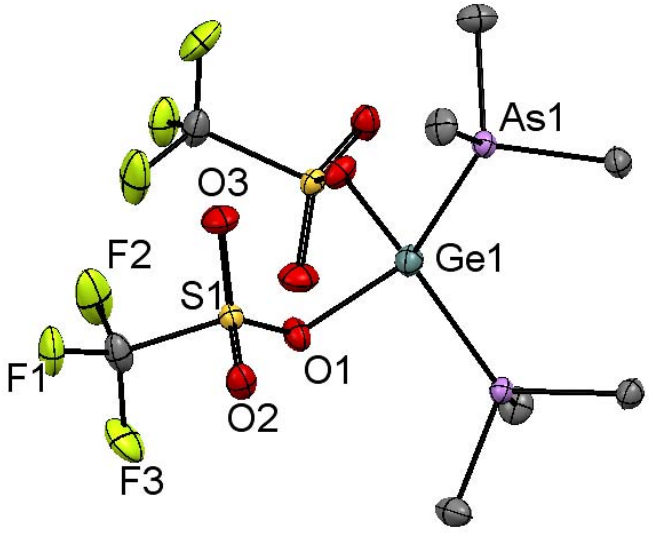

Figure 4.10 – The structure of $[Ge(AsMe_3)_2(OTf)_2]$ showing the atom labelling scheme. Ellipsoids are drawn at the 50% probability level, and H atoms are omitted for clarity. Selected bond lengths (Å) and angles (˚) are: Ge1-As1 = 2.4287(2), 3(9), Ge1-O1 = 2.0170(15). As1-Ge1-As1 = 119.600(15), O1-Ge1-O1 = 98.30(9). Symmetry operation: (1-X, +Y, 3/2 –Z).

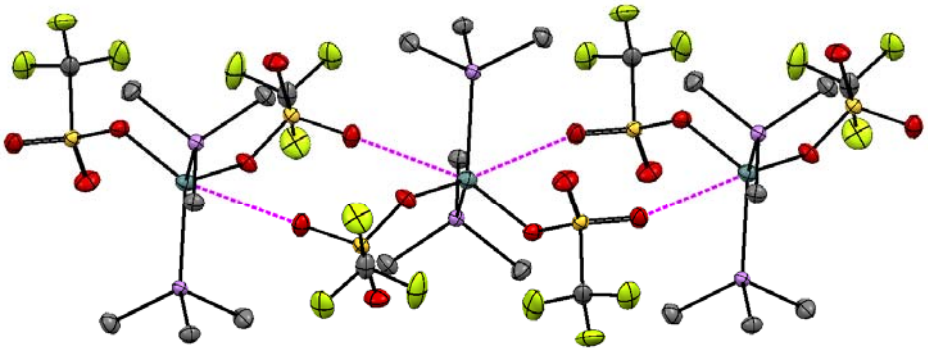

Figure 4.11 – The extended structure of $[Ge(AsMe_3)_2(OTf)_2]$ in the c-direction (purple dashed lines indicate long interactions d(Ge···O) = 2.994 Å).

With the aim of synthesising a more stable *tris*-phosphine dication of Ge(II), the triphosphine ligand $CH_3C(CH_2PPh_2)_3$ was used. The reaction of $[GeCl_2(dioxane)]$ with two equivalents of TMSOTf and one equivalent of $CH_3C(CH_2PPh_2)_3$ in MeCN leads to the formation of $[Ge\{\kappa^3\text{-}CH_3C(CH_2PPh_2)_3\}][OTf]_2$ in good yield as a light pink solid. In the aliphatic region of the ^1H NMR spectrum of this complex, there are two resonances, one

at δ = 2.61 corresponding to the bridgehead methyl group, split into a quartet by the three P atoms, which indicates that either the bonding environment at germanium must be highly symmetric or there is a fast exchange process occurring at the germanium centre. The other aliphatic resonance at δ = 3.48 corresponds to the methylene protons; this is split into a doublet by the neighbouring P atom. The ratio of methyl:methylene:aromatic protons is 1:2:10 as expected, consistent with a symmetrically bound ligand. The $^{31}P\{^{1}H\}$ NMR spectrum contains a sharp singlet at δ = -3.7, a substantial shift from 'free' ligand (δ = -26.3).

Crystals of this complex were grown by layering a CH_2Cl_2 solution of the complex with hexane and the structure is shown in **Figure 4.12** below. The $[Ge\{\kappa^3\text{-}CH_3C(CH_2PPh_2)_3\}]^{2+}$ dication has a similar coordination environment to the *tris*-PMe_3 complex described earlier, and is consistent with the solution state data. However, the locations of some of the anions in the structure proved difficult to determine, so only information about the geometry around the germanium centre could be gained from the structure. Because of the incomplete structure solution, no metrical parameters are included.

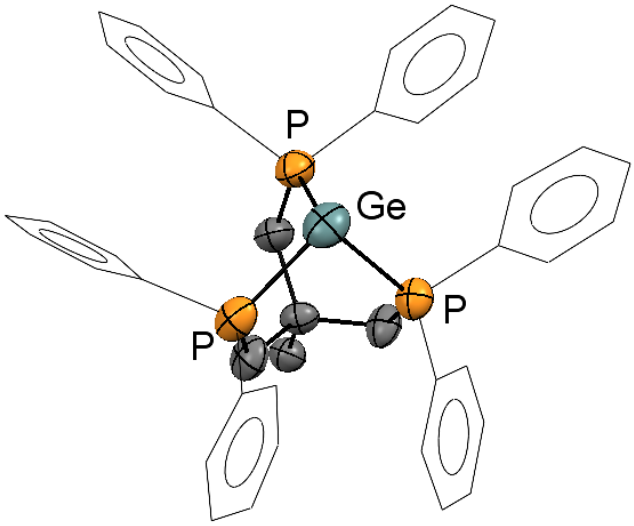

Figure 4.12 – The structure of the dication in $[Ge\{\kappa^3\text{-}CH_3C(CH_2PPh_2)_3\}][OTf]_2$ showing the pyramidal geometry. Ellipsoids are drawn at the 50% probability level, H atoms are omitted for clarity, and the Ph rings are drawn in wireframe from clarity.

Following the failure to isolate a *tris*-$AsMe_3$ dication with Ge(II) and the successful isolation of $[Ge\{\kappa^3\text{-}CH_3C(CH_2PPh_2)_3\}][OTf]_2$, the tripodal triarsine, $CH_3C(CH_2AsMe_2)_3$, was used with the idea that the multidentate nature of the ligand might confer more stability to the complex and allow the isolation of a dication with an As_3-donor set. The reaction of $[GeCl_2(dioxane)]$ with two equivalents of TMSOTf and $CH_3C(CH_2AsMe_2)_3$ in MeCN indeed leads to the formation of $[Ge\{\kappa^3\text{-}CH_3C(CH_2AsMe_2)_3\}][OTf]_2$ as a yellow solid. The ^1H NMR spectrum shows three resonances in a 3:18:6 ratio, consistent with the formation of a three-fold symmetric dication.

A CH_2Cl_2/MeCN solution of $[Ge\{\kappa^3\text{-}CH_3C(CH_2AsMe_2)_3\}][OTf]_2$ layered with hexane produced crystals. The structure of the dication is shown in **Figure 4.13** below. Similar to the complex with $CH_3C(CH_2PPh_2)_3$, the geometry is pyramidal with three-fold symmetry around the germanium, and with no close OTf contacts. Here the closest approach is 2.804 Å, which is outside the range of typical Ge-OTf bonds (1.917-2.582 Å) and represents only a very weak Ge···OTf interaction. Comparing this complex to the $[GeCl\{o\text{-}C_6H_4(AsMe_2)_2\}]^+$ monocation, the d(Ge-As) bond distances are shorter in the dication (2.5096(9)-2.5577(9) Å) compared to the monocation (2.5647(5) Å), reflecting the greater Lewis acidity in the dication. However, ligand architecture must also play a role, as the d(Ge-As) distance in the neutral complex $[Ge(AsMe_3)_2(OTf)_2]$ (2.4287(2) Å) is shorter than

in both the mono- and dicationic complexes. The compound $[Ge\{CH_3C(CH_2AsMe_2)_3\}][OTf]_2$ represents the only structurally characterised κ^3-coordinated arsine complex of any of the main group elements. This shows that even the more weakly donating arsine is sufficient to stabilise a germanium(II) dication.

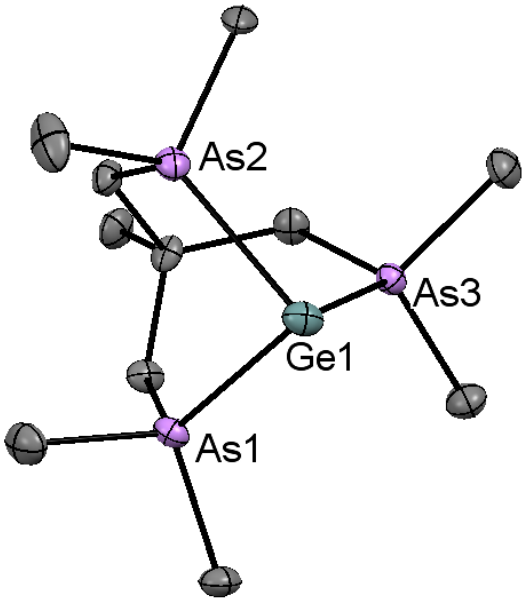

Figure 4.13 – The structure of the dication in $[Ge\{\kappa^3\text{-}CH_3C(CH_2AsMe_2)_3\}][OTf]_2$ showing the atom labelling scheme. Ellipsoids are drawn at the 50% probability level. Only one of the two $[Ge(CH_3C(CH_2AsMe_2)_3)]^{2+}$ in the asymmetric unit is shown and H atoms and triflates are omitted for clarity. Selected bond lengths (Å) and angles (˚) are: Ge1-As1 = 2.5578(9), Ge1-As2 = 2.5543(9), Ge1-As3 = 2.5096(9), As1-Ge1-As2 = 81.56(3), As1-Ge1-As3 = 83.16(3), As2-Ge1-As3 = 82.40(3) Ge1-O5 (closest O-Ge approach) = 2.804.

With tetradentate nitrogen donor ligands, Ge(II) dications can commonly become four coordinate, for example in $[Ge(Me_4cyclam)][GeCl_3]_2$ and $[Ge(BIMEt_3)][OTf]_2$ ($BIMEt_3$ = tris(1-ethyl-benzoimidazol-2-ylmethylamine)).[11,24] To test whether this could be extended to phosphorus, the tetraphosphine ligand $P(CH_2CH_2PPh_2)_3$ was chosen. The reaction of this ligand with $[GeCl_2(dioxane)]$ in CH_2Cl_2 leads to the dissolution of the germanium precursor and a change from a colourless to purple solution. The addition of two equivalents of TMSOTf does not lead to any further change of appearance for the solution. Following removal of the solvent *in vacuo*, a light purple powder was isolated. The $^{31}P\{^1H\}$ (**Figure 4.14**) spectrum shows two broad resonances with a 1:3 ratio at 64.5 ppm and 15.2 ppm, respectively; the broadness suggests there is a fast exchange of the pendant arms in solution rather than κ^4-coordination in solution. This is further

corroborated by the solid-state structure of the compound shown in **Figure 4.15** below, showing that the germanium(II) centre is three-coordinate via two terminal phosphines and the bridgehead phosphine. The uncoordinated phosphorus has no close contacts with any germanium centres. The d(Ge-P) distances in $[Ge(PMe_3)_3]^{2+}$ (2.3747(5)-2.3970(5) Å) are shorter than those in $[Ge\{\kappa^3\text{-}P(CH_2CH_2PPh_2)_3\}]^{2+}$ (2.4280(9)-2.4583(9) Å). This could be due to a combination of the weaker donor power of the tetradentate ligand and the greater steric demand of the ligand.

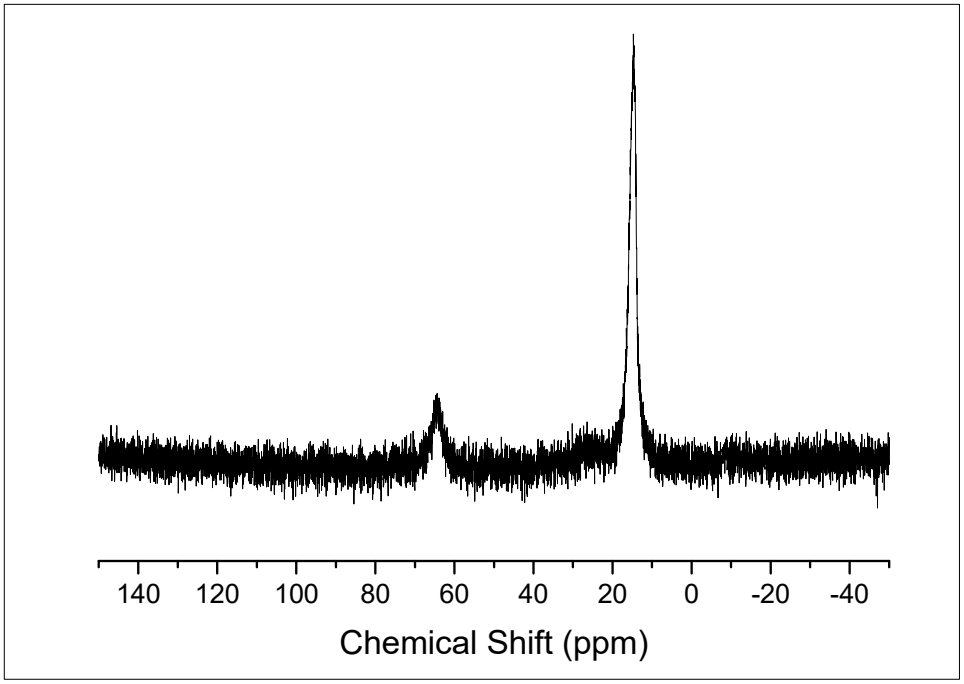

Figure 4.14 – The $^{31}P\{^1H\}$ spectrum of $[Ge\{\kappa^3\text{-}P(CH_2CH_2PPh_2\}][OTf]_2$ in CD_2Cl_2 at 298 K.

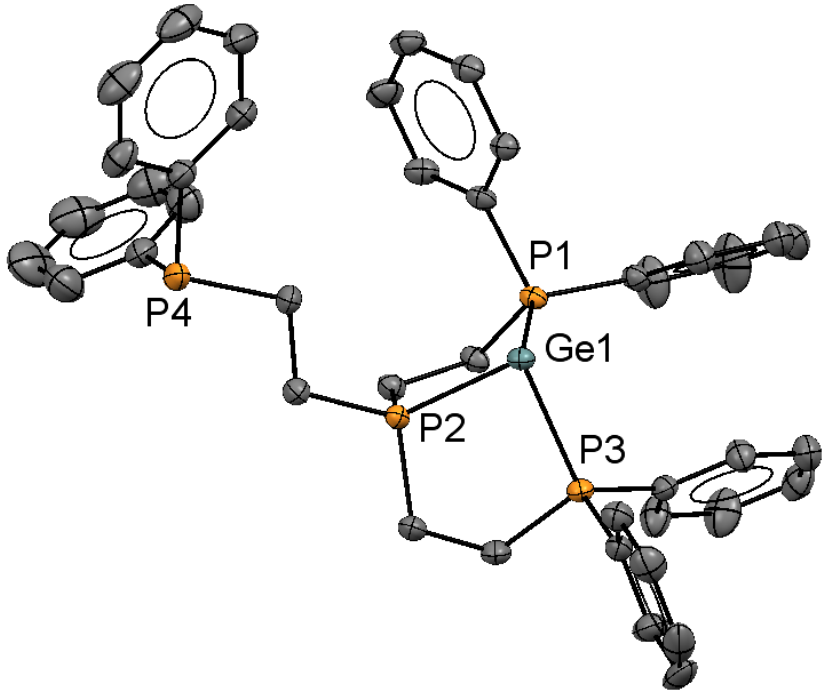

Figure 4.15 – The structure of the dication in $[Ge\{\kappa^3\text{-}P(CH_2CH_2PPh_2\}_3][OTf]_2$ showing the atom labelling scheme. Ellipsoids are drawn at the 50% level and H atoms, CH_2Cl_2 and triflates are omitted for clarity. Selected bond lengths (Å) and angles (˚) are: Ge1-P1 = 2.4280(9), Ge1-P2 = 2.4298(9), Ge1-P3 = 2.4583(9), Ge1-P4 = 5.7051(3), Ge1-O6 (closest O to Ge) = 3.151(3). P1-Ge1-P2 = 80.55(3), P1-Ge1-P3 = 91.14(3), P2-Ge1-P3 = 81.08(3).

The reaction of $[GeCl_2(dioxane)]$ with TMSOTf and $SbEt_3$ in MeCN led to the formation of a mixture of products evident by the ^1H NMR spectroscopy of the isolated waxy solid. By layering a CH_2Cl_2 solution of the mixture with hexane then a few crystals of $[EtSb(SbEt_3)_2]$ formed, the crystal structure is shown in **Figure 4.16** below. It is clear that under these conditions Sb-C bond cleavage occurs, with the central antinomy losing two of its ethyl groups, possibly through alkyl/halide exchange with $GeCl_2$, although more detailed investigation would be needed to elucidate the mechanism through which this product forms. The instability of the stibine ligand precluded the formation of any Ge(II) stibine complexes.

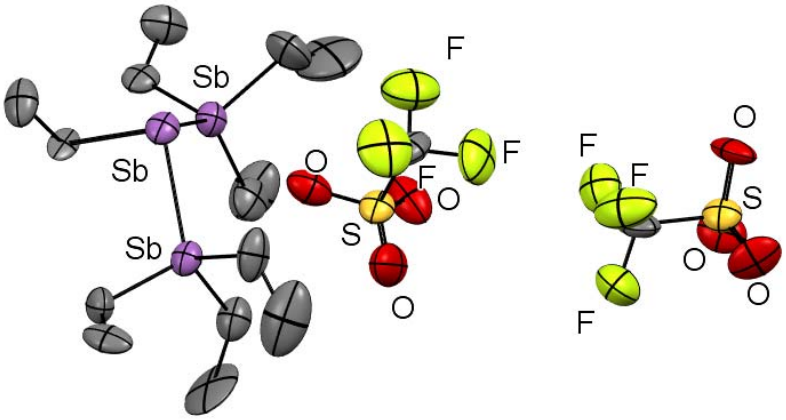

Figure 4.16 – Crystal structure of $[EtSb(SbEt_3)_2][OTf]_2$. Bond lengths and angles are not quoted due to poor quality data; the structure, however, confirms the identity of the complex.

4.3.2 DFT studies on germanium(II) dications

DFT (density functional theory) studies on the Ge(II) dications were performed to understand their structure and electronic properties better. The computed geometries of the complexes were optimised, and these parameters were compared to experimental (X-ray structural) parameters where possible to show that the basis sets used were appropiate. In this Chapter, all of the calculations involving $[Ge(PMe_3)_3]^{2+}$ were performed by Dr Victoria Greenacre, while I performed the calculations on all the other complexes.

Selected HOMO's and LUMO's are shown for $[Ge(PMe_3)_3]^{2+}$ in **Figure 4.17** below. The HOMO is a lone pair based orbital on the germanium centre. HOMO-1 and HOMO-2 are a pair of almost degenerate bonding orbitals consisting of the lone pairs from the phosphines interacting with empty p_x and p_y orbitals on germanium. LUMO and LUMO+1 are a pair of almost degenerate molecular orbitals that have mostly empty p_x and p_y characters and are Ge-P antibonding. Using the geometry of $[Ge(PMe_3)_3]^{2+}$ as a starting point calculations were performed on the dication $[Ge(AsMe_3)_3]^{2+}$ (subsituting P for As). The complex optimised to a pyramidal structure with no imaginary frequencies which suggests that this is ground state structure, which in principal means that the species could exist.

HOMO (-13.57630 eV)	LUMO (-7.97912 eV)
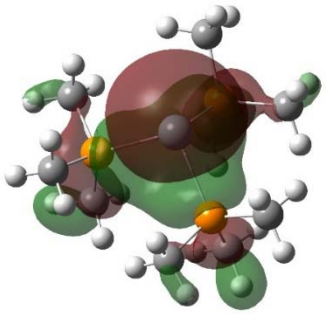	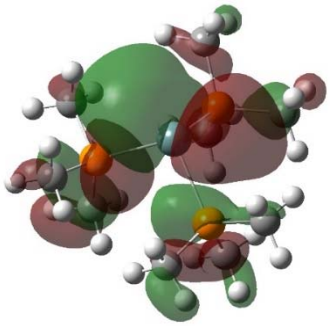
HOMO-1 (-15.17633 eV)	LUMO+1 (-7.97702 eV)
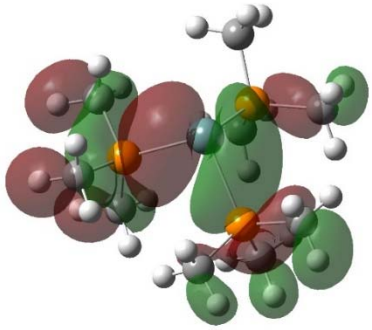	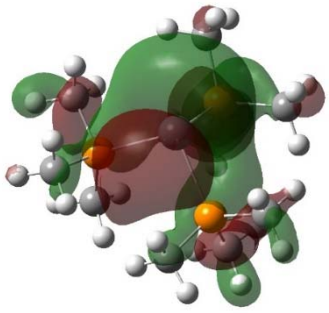
HOMO-2 (-15.17714 eV)	LUMO+2 (-0.70088 eV)
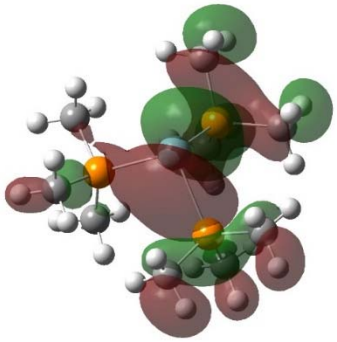	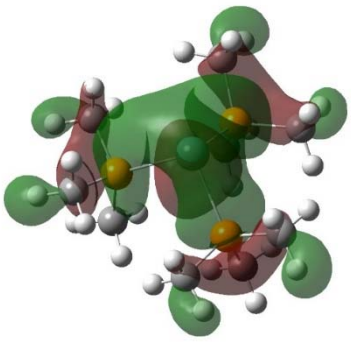

Figure 4.17 – Selected HOMO and LUMO representations for $[Ge(PMe_3)_3]^{2+}$.

Notably, the X-ray crystal structure of $[Ge(PMe_3)_3][OTf]_2$ shows that in all the PMe_3 groups there is a P-C bond *anti* to the lone pair on germanium. NBO (natural bond order) calculations reveal that the lone pair on the germanium donates into the P-C σ* orbital of the *anti* P-C bond; for $[Ge(PMe_3)_3]^{2+}$ the strength of this interaction is 10.67 kJ/mol per bond, totalling 32.01 kJ/mol over the whole molecule. This type of back donation is rare for p-block phosphine complexes, but the presence of the lone pair on Ge and the geometry of the complex allows this interaction to occur as shown in **Figure 4.18** below. This type of interaction is present in all of the pyramidal complexes in this chapter (see **Table 4.1**). For the complexes featuring tripodal ligands, the geometric constraints of the ligands mean the complexes are prearranged for this type of interaction. For the tetraphos complex, none of the P-C bonds on the apical phosphorous are *anti* to the lone pair, with one of the bonds being *syn* to the lone pair, and as such, there are no strong lone pair/P-C σ* interactions in this species.

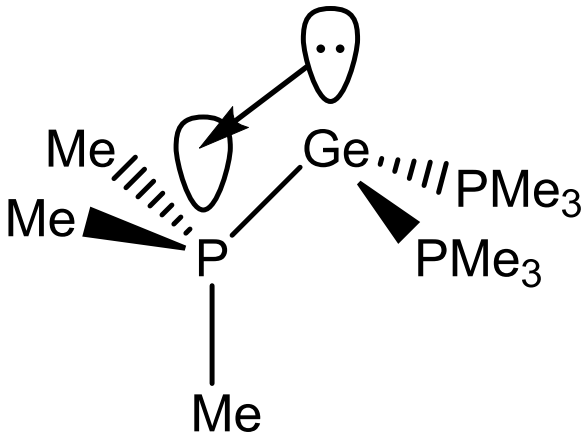

Figure 4.18 – A schematic of the interaction of the lone pair on germanium with the empty P-C σ* orbital on one of the phosphine ligands.

Table 4.1 – The energy associated with the germanium lone pair to E-C σ* interaction and the natural charge on Ge.

	$[Ge(PMe_3)_3]^{2+}$	$[Ge(AsMe_3)_3]^{2+}$	$[Ge\{CH_3C(CH_2PPh_2)_3\}]^{2+}$	$[Ge\{CH_3C(CH_2AsMe_2\}]^{2+}$	$[Ge\{P(CH_2CH_2PPh_2\}]^{2+}$
LP to E-C σ* interaction (kJ/mol)	10.67	12.10	11.33	6.82	5.19, 4.8, 3.60, 3.39, 2.38
Interaction over whole molecule (kJ/mol)	32.01	36.30	33.99	20.46	19.36
Natural Charge on Ge	+0.16	+0.21	+0.26	+0.29	+0.21

DFT calculations can also give an indication how the charge is distributed in these dicationic complexes. There are two extremes (shown in **Figure 4.19** below), one where all the charge is located on the germanium and the other where each of the three ligands takes a unit of positive charge, leaving the germanium centre negatively charged.

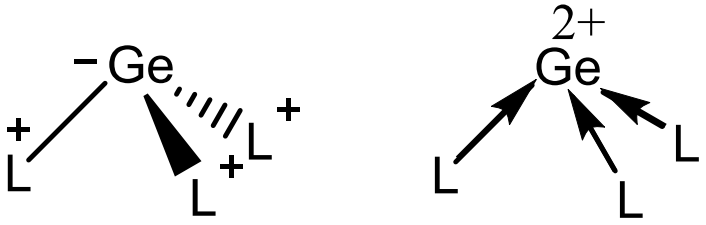

Figure 4.19 – The two extreme cases for where the charge is located in the complex.

For the dicationic complexes studied in this chapter the natural charge on germanium ranges from +0.16 to +0.29, this means the pnictine ligands take on a significant portion of the positive charge. This can be contrasted with $[Ge(2,2,2\text{-crypt})]^{2+}$ in which the residual charge on the germanium centre is +1.38, indicating in this dication most of the charge is located on the germanium. The complex $[Ge(Me_3tacn)]^{2+}$ is more similar structurally to the systems studied in this Chapter; the natural charge calculated for this dication at germanium (with the starting geometry taken from a published crystal structure[11]) is +1.34, this indicates that the donor atom type is important for determining where the charge is located in the complex, with the charge on germanium being much higher for the hard donor complexes compared to the soft donor complexes.

Table 4.2 – Orbital contributions (average) for the Ge-P/As bonds for Ge(II) dications.

	Atom	$[Ge(PMe_3)_3]^{2+}$	$[Ge(AsMe_3)_3]^{2+}$	$[Ge\{CH_3C(CH_2PPh_2)_3\}]^{2+}$	$[Ge\{CH_3C(CH_2AsMe_2)_3\}]^{2+}$	$[Ge\{P(CH_2CH_2PPh_2)_3\}]^{2+}$
Contribution (%)	Ge	31.41	30.51	29.93	29.20	30.62
	P/As	68.58	69.44	70.07	70.08	69.38
Orbital contribution Ge (%)	s	5.19	4.54	6.15	3.96	6.04
	p	93.47	94.92	92.92	95.45	93.04
Orbital contribution P/As (%)	s	23.87	25.42	23.54	24.87	22.57
	p	75.91	74.44	76.38	74.49	77.30
Orbital contribution LP	s	82.26	86.36	81.57	88.13	82.99 (Ge), 51.14(P)
	p	17.08	13.60	18.35	11.84	16.92 (Ge), 48.85 (P)

For all the dicationic complexes above, the pnictine atom (E) contributes most to the Ge-E bond (av. 69.51 %) (see **Table 4.2** above). In all cases, the orbital contribution from germanium to the Ge-E bond is mostly of p-character. For all the dications, the lone pairs have mostly s character but also have a reasonable amount of p character, presumably from the P_z orbital on germanium. This is in contrast to $[Ge(2,2,2\text{-crypt}))]^{2+}$ where the lone pair occupies a completely symmetric 4s type orbital on germanium.[9]

4.4 Conclusions

The work in this Chapter extends the set of ligands known to stabilise dicationic germanium centres to phosphines and arsines. These ligands are much softer than those previously used, which mostly featured N- or O-donor atoms or were organic in nature (carbene/isocyanide). The work also demonstrates that the ligands required to stabilise Ge(II) centres do not necessarily need to have a large amount of steric bulk, as shown by the formation of $[Ge(PMe_3)_3][OTf]_2$. In the case of arsine ligands, a multidentate tripodal ligand was needed to displace all triflates from the germanium centre, this reflects the weaker donor power of arsine compared to phosphines. DFT calculations suggest that the ligands take on a significant portion of the positive charge, which could aid in the stability of the complexes formed. Calculations suggest that there is a lone pair on germanium as well as empty p_x and p_y orbitals, which suggests that these complexes might be able to act as both Lewis acids and bases, though the reactivity of these complexes was not explored. Finally, back-donation from the germanium lone pair into E-C σ* orbitals was shown to stabilise these complexes.

4.5 X-ray Crystallographic Data

Table 4.3 – X-ray crystallographic data[a]

Compound	$[Ge(PMe_3)_3][OTf]_2$	$[Ge\{P(CH_2)_2PPh_2\}_3)][OTf]_2 \cdot CH_2Cl_2$	$[Ge(AsMe_3)_2(OTf)_2]$	$[Ge\{MeC(CH_2AsMe_2\}][OTf]_2$
Formula	$GeP_3C_{11}H_{27}F_6O_6S_2$	$GeP_4C_{45}H_{44}Cl_2F_6O_6S_2$	$GeAs_2C_8H_{18}F_6O_6S_2$	$GeAs_3C_{13}H_{27}F_6O_6S_2$
M	598.94	1126.29	610.77	754.81
Crystal system	monoclinic	triclinic	monoclinic	monoclinic
Space group (no.)	$P2_1/c$ (no. 14)	$P\bar{1}$ (no. 2)	C2/c (no. 15)	$P2_1/n$ (no. 14)
a /Å	6.3351(2)	10.9685(4)	14.3439(2)	13.7970(3)
b /Å	21.9849(6)	13.8745(5)	11.6424(2)	17.9667(3)
c /Å	17.2271(6)	17.4629(5)	12.6472(2)	20.4948(5)
α /°	90	82.599(3)	90	90
β /°	90.523(3)	83.283(3)	105.623(2)	90.430(2)
γ /°	90	69.756(3)	90	90
U /Å^3	2399.23(13)	2465.12(15)	2034.02(6)	5080.24(19)
Z	4	2	4	8
μ(Mo-K_α) /mm^{-1}	1.721	1.013	5.013	5.319
F(000)	1216	1148	1192	2960
Total no. reflns	74306	28986	27758	77036
R_{int}	0.075	0.036	0.036	0.114
Unique reflns	8642	12137	3379	12883
No. of params, restraints	271, 0	618, 0	117, 0	610, 516
GOF	1.021	1.054	1.055	1.070
R_1, wR_2 [$I > 2\sigma(I)$][b]	0.042, 0.092	0.053, 0.141	0.026, 0.056	0.063, 0.119
R_1, wR_2 (all data)	0.073, 0.092	0.074, 0.152	0.032, 0.061	0.095,0.130

[a] Common items: T = 100 K; wavelength (Mo-K_α) = 0.71073 Å; θ(max) = 27.5°; [b] $R1 = \Sigma||F_o|-|F_c||/\Sigma|F_o|$; $wR_2=[\Sigma w(F_o^2-F_c^2)_2/\Sigma wF_o^4]^{1/2}$

$[Ge(AsMe_3)_2(OTf)_2]$ (2080944), $[Ge(PMe_3)_3][OTf]_2$ (2080945), $[Ge\{P(CH_2CH_2PPh_2\}_3)][OTf]_2 \cdot CH_2Cl_2$ (2080946), $[Ge(CH_3(CH_2AsMe_2)_3][OTf]_2$ (2080947)

4.6 Experimental

For general experimental details, sources of reagents, solvents and purification methods, instrument specifications and NMR solvent references see appendix A.

$[Ge(PMe_3)_3][OTf]_2$: To a suspension of $[GeCl_2(dioxane)]$ (0.200 g, 0.86 mmol) in CH_2Cl_2 (5 mL), PMe_3 (0.264 g, 3.47 mmol) was added as solution in CH_2Cl_2 (2 mL) and stirred for 10 mins. to yield a slightly cloudy solution. To this was added TMSOTf (0.384 g, 1.73 mmol) as a solution in CH_2Cl_2, resulting in the precipitation of a white solid. MeCN is added until the solution became clear, it was then layered with hexane and cooled to -18˚C for 3 days, yielding colourless crystals. The solid was collected by filtration and this was then dried under a gentle stream of nitrogen. Unit cell determinations on several different crystals from this batch proved to be $[Ge(PMe_3)_3][OTf]_2$. Required for 1:3 $C_{11}H_{27}F_6GeO_6P_3S_2$ (598.97): C, 22.1, H, 4.5 %. Required for 1:2 $C_8H_{18}F_6GeO_6P_2S_2$ (522.90): C, 18.4, H, 3.5. Found: C, 19.0, H, 4.4%. For sample held at vacuum Found: C, 18.2, H, 3.60% Yield: 0.281 g (54%). IR (Nujol/cm^{-1}): 1156m (OSO_2), 1223w, 1261m (CF_3). ^1H NMR (d-MeCN, 298 K): δ = 1.88 (d $^2J_{H\text{-}P}$ = 12.1, CH_3). $^{19}F\{^1H\}$ NMR (d-MeCN, 298 K): δ = -79.3 (s, OTf). $^{31}P\{^1H\}$ NMR (d-MeCN, 298 K): δ = -12.7 (s).

$[Ge\{\kappa^3\text{-}CH_3(CH_2PPh_2)_3\}][OTf]_2$: To a suspension of $[GeCl_2(dioxane)]$ (0.222 g, 0.96 mmol) in MeCN (5 mL) was added $CH_3(CH_2PPh_2)_3$ (0.600 g, 0.96 mmol), causing the solution turned to cloudy pink. To this was added TMSOTf (0.426 g, 1.92 mmol) as a solution in MeCN and the reaction mixture was stirred for 2 h. Volatiles were removed *in vacuo* to yield a light pink powder, which was washed with hexane (3 x 10 mL) and dried *in vacuo*. Crystals suitable for single crystal X-ray diffraction could be grown from layering a CH_2Cl_2 solution of the complex with hexane. Yield: 0.816 g (85%). Required for $C_{43}H_{39}F_6GeO_6P_3S_2{\cdot}0.5CH_2Cl_2$ (1037.84): C, 50.3, H, 3.9. Found: C, 50.3, H, 4.2%. IR (Nujol/cm^{-1}): 1148m (OSO_2), 1223w, 1260m (CF_3). ^1H NMR (CD_2Cl_2, 298 K): δ = 2.61 (q, $^4J_{H\text{-}P}$ = 4 Hz, [3H], CH_3), 3.48 (d, $^2J_{H\text{-}P}$ = 12 Hz, [6H], CH_2), 7.17-7.85 (m, [30H], ArH). $^{19}F\{^1H\}$ NMR (CD_2Cl_2, 298 K): δ = -78.3 (s, OTf). $^{31}P\{^1H\}$ NMR (CD_2Cl_2, 298 K): δ = -3.7 (s).

[Ge{κ^3-CH$_3$(CH$_2$AsMe$_2$)$_3$}][OTf]$_2$: To a suspension of [GeCl$_2$(dioxane)] (0.181 g, 0.78 mmol) in MeCN (5 mL) was added TMSOTf (0.347 g, 1.56 mmol) as a solution in MeCN (2 mL) and the reaction mixture was stirred for 10 mins. to yield a clear solution. CH$_3$(CH$_2$AsMe$_2$)$_3$ (0.300 g, 0.78 mmol) was then added as a solution in MeCN (2 mL) to yield a clear solution. Volatiles were removed *in vacuo* to leave a yellowish solid, which was then washed with hexane (3 x 10 mL) and dried *in vacuo* to yield a yellowish powder. Crystals suitable for single crystal X-ray diffraction could be grown from layering a MeCN+CH$_2$Cl$_2$ solution of the complex with hexane. Yield: 0.391 g (66%). Required for C$_{13}$H$_{27}$As$_3$F$_6$GeO$_6$S$_2$ (754.84): C, 20.7, H, 3.6. Found: C, 20.1, H, 3.6%. IR (Nujol/cm^{-1}): ν = 1151m (–OSO$_2$), 1223w, 1261m (CF$_3$). ^{1}H NMR (d-MeCN, 298 K): δ = 1.33 (s, [3H] C-CH$_3$), 1.84 (s, [18H], As-CH$_3$), 2.23 (s, [6H], CH$_2$). ^{19}F{^{1}H} NMR (d-MeCN, 298 K): δ = -79.4 (s, OTf).

[Ge(P(CH$_2$CH$_2$PPh$_2$)$_3$)][OTf]$_2$: To a suspension of [GeCl$_2$(dioxane)] (0.069 g, 0.30 mmol) in CH$_2$Cl$_2$ (2 mL), was added tetraphos (0.200 g, 0.30 mmol) and the resulting pale purple solution was stirred for 5 mins. TMSOTf (0.133 g, 0.60 mmol) in 1 mL of CH$_2$Cl$_2$ was added and the reaction was stirred for *ca.* 1 h. Volatiles were removed *in vacuo* to yield a pale purple solid, which was then washed with hexane (3 x 10 mL) and dried *in vacuo*. Crystals suitable for single crystal X-ray diffraction could be grown from layering a CH$_2$Cl$_2$ solution of the complex with hexane. Yield: 0.207 g (66%). Required for C$_{44}$H$_{42}$F$_6$GeO$_6$P$_4$S$_2$·0.5CH$_2$Cl$_2$ (1083.84): C, 49.3, H, 4.0. Found: C, 48.8, H, 3.6%. IR (Nujol/cm^{-1}): ν = 1152m (–OSO$_2$), 1222w, 1259m (CF$_3$). ^{1}H NMR (CD$_2$Cl$_2$, 298 K): δ = 2.81-3.00 (br, [12H], CH$_2$), 7.35-7.94 (m, [30H], ArH). ^{19}F{^{1}H} NMR (CD$_2$Cl$_2$, 298 K): δ = -78.8 (s, OTf). ^{31}P{^{1}H} NMR (CD$_2$Cl$_2$, 298 K): δ = 15.2 (s, [3P], PPh$_2$), 64.5 (s, [1P], P$_{apical}$).

[Ge(AsMe$_3$)$_2$(OTf)$_2$]: To a suspension of [GeCl$_2$(dioxane)] (0.194 g, 0.84 mmol) in CH$_2$Cl$_2$ (5 mL) was added AsMe$_3$ (0.300 g, 2.50 mmol)as a solution in CH$_2$Cl$_2$ (2 mL), followed by TMSOTf (0.390, 1.75 mmol) as a solution in CH$_2$Cl$_2$ (2 mL) to yield a clear colorless solution, which was stirred for 2 h. The solution was then layered with hexane cooled to -18˚C for 3 months after which a white, crystalline solid had formed, which was dried under a stream of N$_2$ gas. Crystals suitable for single crystal X-ray diffraction could be grown from layering a CH$_2$Cl$_2$ solution of the complex with hexane. Yield: 0.234 g, (46%). Required for C$_8$H$_{18}$As$_2$F$_6$GeO$_6$S$_2$ (610.80): C, 15.7, H, 3.0. Found: C, 16.2, H, 3.2%. IR (Nujol/cm^{-1}): ν = 1155m (OSO$_2$), 1221w, 1261m (CF$_3$). ^{1}H NMR (CD$_2$Cl$_2$, 298 K): δ = 1.63 (s, CH$_3$). ^{19}F{^{1}H} NMR (CD$_2$Cl$_2$, 298 K): δ = -78.40 (s, OTf).

Reaction of $[GeCl_2(dioxane)]$, $SbEt_3$ and TMSOTf

To a suspension of $[GeCl_2(dioxane)]$ (0.074 g, 0.319 mmol) in MeCN (2 mL) TMSOTf (0.142 g, 0.639 mmol) was added as a solution in MeCN (1 mL), the mixture was stirred until it went clear. Then $SbEt_3$ (0.200 g, 0.957 mmol) was added as a solution in MeCN (2 mL) the resulting mixture turned a yellow color and was stirred for 1 h before volatiles were removed *in vacuo* leaving a yellow sticky oily solid. ^1H NMR (CD_2Cl_2, 298 K): 1.41 (t, [18H], $^3J_{HH}$ = 7.8, CH_3), 1.52 (t, [3H], $^3J_{HH}$ = 7.9, CH_3), 2.01 (q, [12H], $^3J_{HH}$ = 7.8, CH_2), 2.24 (q, [2H], $^3J_{HH}$ = 7.9, CH_2). $^{19}F\{^1H\}$ NMR (CD_2Cl_2, 298 K): δ = -78.3 (s, OTf). Although the NMR data clearly indicate a mixture of products, a few crystals of one of these, $[EtSb(SbEt_3)_2][OTf]_2$, were obtained by cooling a CH_2Cl_2 solution of the mixture and layering with hexane.

DFT Calculations

The electronic structure of these complexes was investigated using DFT calculations using Gaussian 16W.[25] The density functional chosen was B3LYP-D3[26] with the basis set 6-311G(d).[27] For $[Ge(PMe_3)_3]^{2+}$, $[Ge\{CH_3C(CH_2PPh_2)_3\}]^{2+}$, $[Ge\{CH_3C(CH_2AsMe_2)_3\}]^{2+}$ and $[Ge\{P(CH_2CH_2PPh_2)_3\}]^{2+}$ the initial geometries were taken from their crystal structures, for $[Ge(AsMe_3)_3]^{2+}$ the initial geometry was taken from the structure of $[Ge(PMe_3)_3]^{2+}$ and the phosphorus atoms changed to arsenic. In all cases the structures converged to a stable geometry with no imaginary frequencies. For all dications, except $[Ge(AsMe_3)_3]^{2+}$, their geometrical parameters were compared with the parameters from the crystal structures and were found to match closely.

4.7 References

1 R. B. King, Inorg. Chem, 1963, 2, 199–200.

2 N. G. Bokii, Y. T. Struchkov, S. P. Kolesnikov, I. S. Rogozhin and O. M. Nefedov, Bull. Acad. Sci. USSR Div. Chem. Sci., 1975, 24, 732–735.

3 L. A. Leites, A. V. Zabula, S. S. Bukalov, A. A. Korlyukov, P. S. Koroteev, O. S. Maslennikova, M. P. Egorov and O. M. Nefedov, J. Mol. Struct., 2005, 750, 116–122.

4 W. W. du Mont and G. Rudolph, Z. Naturforsch., B Chem. Sci., 1986, 36b, 1215–1218.

5 F. Cheng, A. L. Hector, W. Levason, G. Reid, M. Webster and W. Zhang, Inorg. Chem., 2010, 49, 752–760.

6 V. A. Béland, Z. Wang, C. L. B. Macdonald, T. Sham and P. J. Ragogna, Chem. – Eur. J., 2019, 25, 14790–14800.

7 A. N. Chrvkhlow, J. Struct. Chem., 2003, 44, 335–339.

8 P. A. Rupar, V. N. Staroverov and K. M. Baines, Science (80-.)., 2008, 322, 1360–1363.

9 P. A. Rupar, R. Bandyopadhyay, B. F. T. Cooper, M. R. Stinchcombe, P. J. Ragogna, C. L. B. Macdonald and K. M. Baines, Angew. Chem. Int. Ed., 2009, 48, 5155–5158.

10 F. Cheng, A. L. Hector, W. Levason, G. Reid, M. Webster and W. Zhang, Angew. Chem. Int. Ed., 2009, 48, 5152–5154.

11 M. Mantina, A. C. Chamberlin, R. Valero, C. J. Cramer and D. G. Truhlar, J. Phys. Chem. A, 2009, 113, 5806–5812.

12 P. A. Rupar, V. N. Staroverov, P. J. Ragogna and K. M. Baines, J. Am. Chem. Soc., 2007, 129, 15138–15139.

13 V. S. V. S. N. Swamy, S. Yadav, S. Pal, T. Das, K. Vanka and S. S. Sen, Chem. Commun., 2016, 52, 7890–7892.

14 R. K. Raut and M. Majumdar, Chem. Commun., 2017, 53, 1467–1469.

15 J. M. Slattery, A. Higelin, T. Bayer and I. Krossing, Angew. Chem., 2010, 49, 3228–3231.

16 A. Higelin, U. Sachs, S. Keller and I. Krossing, Chem. - Eur. J., 2012, 18, 10029–10034.

17 S. S. Chitnis, Y.-Y. Carpenter, N. Burford, R. McDonald and M. J. Ferguson, Angew. Chem. Int. Ed., 2013, 52, 4863–4866.

18 P. J. Fischer, S. Senthil, J. T. Stephan, M. L. Swift, M. D. Storlie, E. T. Chan, M. V. Vollmer and V. G. Young, Dalton Trans., 2018, 47, 6116–6176.

19 I. Arenas, M. A. Fuentes, E. Alvarez, Y. Diaz, A. Caballero, S. Castillion and P. J. Perez, Inorg. Chem, 2014, 53, 3991–3999.

20 I. R. Shapiro, D. M. Jenkins, J. C. Thomas, M. W. Day and J. C. Peters, Chem. Commun., 2001, 2152–2152.

21 A. A. Barney, A. F. Heyduk and D. G. Nocera, Chem. Commun., 1999, 2379–2380.

22 E. MacDonald, Dalhousie University, Canada, 2013.

23 R. Suter, A. Swidan, C. L. B. Macdonald and N. Burford, Chem. Commun., 2018, 54, 4140–4143.

24 F. Cheng, A. L. Hector, W. Levason, G. Reid, M. Webster and W. Zhang, Angew. Chemie, 2009, 121, 5254–5256.

25 D. J. Frisch, M. J.; Trucks, G. W.; Schlegel, H. B.; Scuseria, G. E.; Robb, M. A.; Cheeseman, J. R.; Scalmani, G.; Barone, V.; Petersson, G. A.; Nakatsuji, H.; Li, X.; Caricato, M.; Marenich, A. V.; Bloino, J.; Janesko, B. G.; Gomperts, R.; Mennucci, B.; Hratch, 2016.

26 C. Lee, W. Yang and R. G. Parr, Phys. Rev. B, 1988, 37, 785–789.

27 R. Krishnan, J. S. Binkley, R. Seeger and J. A. Pople, J. Chem. Phys., 1980, 72, 650–654.

Chapter 5 Synthesis of neutral and cationic complexes of tin(IV) fluoride and tin(II) complexes with pnictine ligands

5.1 Introduction

5.1.1 Neutral complexes of tin(IV) fluoride

Compared to the heavier halides (covered in Chapter 2), there are remarkably few examples of structurally characterised tin(IV) fluoride complexes with neutral ligands; this is also true of other main group fluorides more generally.[1,2] Most of the early work in this area focused on IR, NMR or elemental analysis studies. The first reported structure of a SnF_4 complex with a neutral ligand was $[SnF_4(bipy)]$ in 1972; the complex has the expected *cis*-octahedral coordination.[3] Later, the structure of $[SnF_4(phen)]$ was determined and also showed the same *cis*-octahedral coordination (shown in **Figure 5.1** below).[4]

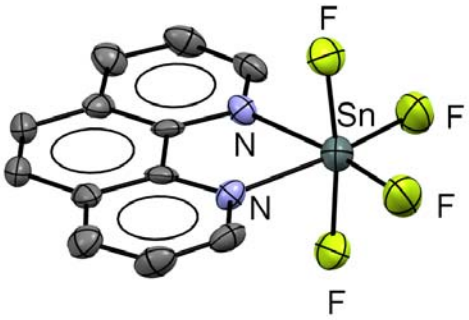

Figure 5.1 – The structure of $[SnF_4(phen)]$ showing the *cis*-octahedral geometry. Redrawn from Ref.4.

Complexes of SnF_4 with oxygen-donor ligands can also be synthesised. Two equivalents of monodentate phosphine and arsine oxides react with $[SnF_4(MeCN)_2]$ to form the complexes $[SnF_4(OEMe_3)_2]$ (E = P, As) and $[SnF_4(OPPh_3)_2]$. The solution NMR spectroscopic data ($^{19}F\{^1H\}$ and $^{31}P\{^1H\}$) indicate that these complexes are dynamic in solution with both *cis* and *trans* isomers present; structure determination showed that for $[SnF_4(OPMe_3)_2]$, the geometry is *trans* in the solid state. For bidentate phosphine oxide ligands, only the

cis-octahedral geometry is present in the solution, and solid states.[5] Phosphine oxide ligands bearing amide and fluoride groups have also been shown to react with $[SnF_4(MeCN)_2]$ to form 2:1 adducts, again here *cis* and *trans* isomers are seen with the exact ratio depends on the particular ligand.[6]

Recently, SnF_4 complexes with softer donor atom (S- or P-) ligands have been synthesised. In the case of sulfur, dithioether complexes have been synthesised by reacting $[SnF_4(MeCN)_2]$ in CH_2Cl_2 with the appropriate dithioether in a 1:1 ratio. A $^{19}F\{^1H\}$ NMR study on $[SnF_4\{^iPrS(CH_2)_2S^iPr\}]$ demonstrated that this complex is dynamic in solution at room temperature, with the expected pair of triplets (expected for a *cis*-coordinated complex) only observable at -50˚C, this dynamic behaviour is due to the weak donor power of sulfur and the hard-soft mismatch of the ligand and metal centre. The structures of some of the dithioether adducts have been determined by X-ray crystallography showing *cis* coordination in the solid state. The $^{19}F\{^1H\}$ NMR spectrum of a mixture of 1:2 ratio of $[SnF_4(MeCN)_2]$ and SMe_2 displays no resonances at room temperature, but if the solution is cooled to -60˚C then two triplets and a singlet are seen, which confirms adduct formation, with both *cis* and *trans* adducts present, however, in this case, a pure sample could not be isolated.[7]

The reaction of $[SnF_4(MeCN)_2]$ with two equivalents of the monodentate phosphines PMe_3 or PCy_3 leads to the isolation of the complexes $[SnF_4(PR_3)_2]$ (R = Me, Cy); unlike for the phosphine oxides, only the *trans* complexes are detected in solution (evidenced by multinuclear spectroscopy) and the solid state. *Cis*-octahedral phosphine complexes can be synthesised by reacting a 1:1 ratio of $[SnF_4(MeCN)_2]$ and a diphosphine ligand (for example $Et_2P(CH_2)_2PEt_2$). Examples of complexes with both geometries are shown **Figure 5.2** below.[4]

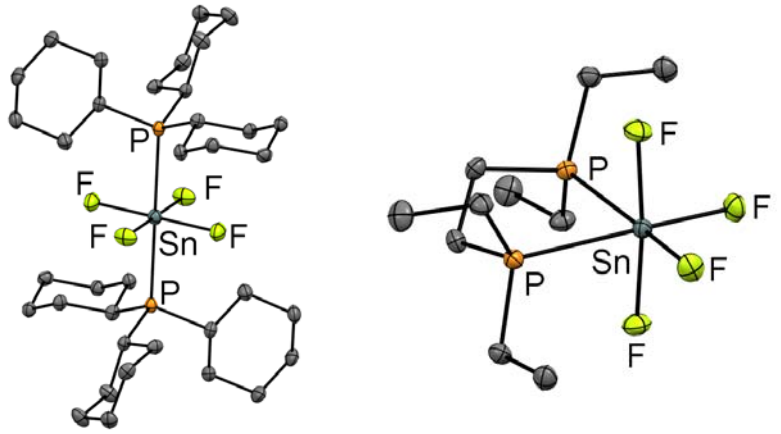

(a) (b)

Figure 5.2 – Crystal structures of (a) *trans*-$[SnF_4(PCy_3)_2]$ and (b) *cis*-$[SnF_4\{Et_2P(CH_2)_2PEt_2\}]$. Both redrawn from Ref. 4.

There are more limited examples of tin(II) fluoride complexes with neutral ligand coordination. This is probably due to the lack of a suitable molecular synthon and the limited solubility of SnF_2 in organic solvents. However, the reaction of Me_3PO with SnF_2 in methanol leads to the formation of $[SnF_2(Me_3PO)]$ as a white solid. Other oxygen donor ligands can also form 1:1 complexes with SnF_2, including DMSO and pyNO; the structure of the DMSO complex has been structurally determined. The structure has a dimeric Sn_2F_4 core with two coordinated DMSO ligands, and these dimers are associated together in a 1-D chain in the solid state through weak Sn-F interactions. The reaction of 2,2'-bipy or phen with SnF_2 in MeOH also forms Sn(II) fluoride complexes; in the case of phen $[SnF(phen)]_2[SnF_4]\cdot 2MeOH$ resulted which features two SnF_2(phen) units bridged by a SnF_2 unit, forming weakly associated 1-D chains in the solid state. In the case of 2',2'-bipy, the complex isolated was $[SnF(bipy)]_2[SnF_6]$, which features two SnF(bipy) units bridged by an $[SnF_6]^{2-}$ suggesting that Sn(II) had been oxidised to Sn(IV), presumably through air oxidation. There have been no examples of complexes with softer donor atoms accessed through this route.[8]

Neutral tin(IV) fluoride complexes can also be synthesised by the reaction of a cationic tin(IV) centre with a fluoroanion. The reaction of $[Me_3Sn]^+$ with $[BF_4]^-$ leads to the formation of the compound $[Me_3SnFBF_3]$ of which the *o*-anisaldehyde (*o*-C_6H_4(OMe)CHO) adduct has been structurally characterised.[9] The reaction of 5-chloro-1-aza-5-

stannabicyclo[3.3.3]undecane (see **Figure 5.3**) with the fluoroanion salts $Ag[BF_4]$ or $Ag[SbF_6]$ leads to the formation of the complexes $[N\{(CH_2)_3\}_3Sn(BF_4)]$ and $[N\{(CH_2)_3\}_3Sn(SbF_6)]$ respectively driven by the formation of AgCl. These complexes have Sn-F bonds in the solid state but in solution the complex exists as a separated ion-pair as determined by NMR spectroscopy. The reaction of 5-chloro-1-aza-5-stannabicyclo[3.3.3]undecane with $Na[BAr^F]$ with leads to the formation of a separated ion pair both in solution and in the solid state. Comparison of the ^{119}Sn NMR of the BAr^F salt with the fluoroanion salts demonstrate that the fluoroanion salts exist as separated ions in solution.[10]

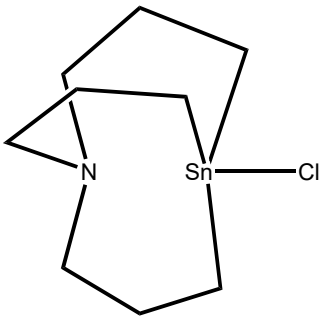

Figure 5.3 – The structure of 5-chloro-1-aza-stannabicyclo[3.3.3]undecane[10]

5.1.2 Cationic tin fluoride complexes

There are few examples of cationic tin fluoride complexes, especially non-organotin complexes, though there are examples containing both Sn(II) and Sn(IV) centres predominantly involving hard O- and N-donor ligands. There are examples of organotin fluoride cations,[11,12] though this section will focus on cations which do not contain a tin-carbon bond. There is an example of an inorganic tin fluoride cation where $[SnF_3]^-$ acts as a ligand and is coordinated to a Pt_3 fragment forming the complex $[Pt_3(\mu_3\text{-}SnF_3)(\mu_3\text{-}CO)(Ph_2PCH_2PPh_2)_3][PF_6]$.[13] The reaction of $Sn(PF_6)_2$, 18-crown-6, and KF in a mixture of MeCN and H_2O led to the formation of the complex $[Sn(18\text{-crown-}6)F][PF_6]$ as a white solid. The structure of this complex is shown in **Figure 5.4** below. The structure contains a seven-coordinate tin(II) monocation with a fluorine coordinated to the tin centre. [14]

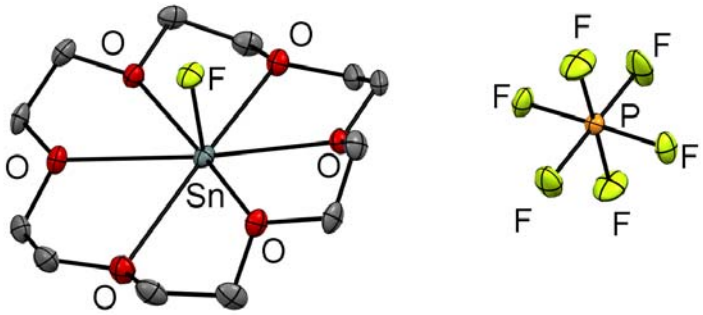

Figure 5.4 – The structure of [Sn(18-crown-6)F][PF_6]. Redrawn from Ref. 14.

Unlike for the germanium analogue (see Chapter 3), the reaction of [Sn(BIMEt)][OTf]$_2$ (BIMEt = tris(1-ethyl-benzoimidazol-2-ylmethyl)amine) with XeF_2 leads to a mixture of products, whereas for germanium the exclusive product was [GeF_2(BIMEt)][OTf]$_2$. So, as an alternative route to the tin(IV) fluoride cations, SnF_4 was reacted with one equivalent of BIMEt and TMSOTf in MeCN, forming [SnF_3(BIMEt)][OTf], which was confirmed by the presence of a quartet in the ^{119}Sn NMR spectrum at δ = -763.6 and a singlet in the ^{19}F{^{1}H} NMR spectrum flanked by tin satellites.[7] This complex can be reacted further with one or two equivalents of TMSOTf to generate the complexes [SnF_2(BIMEt)][OTf]$_2$ and [SnF(BIMEt)(OTf)][OTf]$_2$. There is a stepwise high-frequency shift in the ^{119}Sn NMR resonances going from the *mono*- to *bis*- to *tris*-triflate complexes, which is also accompanied by an increase in the $^1J_{119Sn\text{-}F}$ coupling constant.[15]

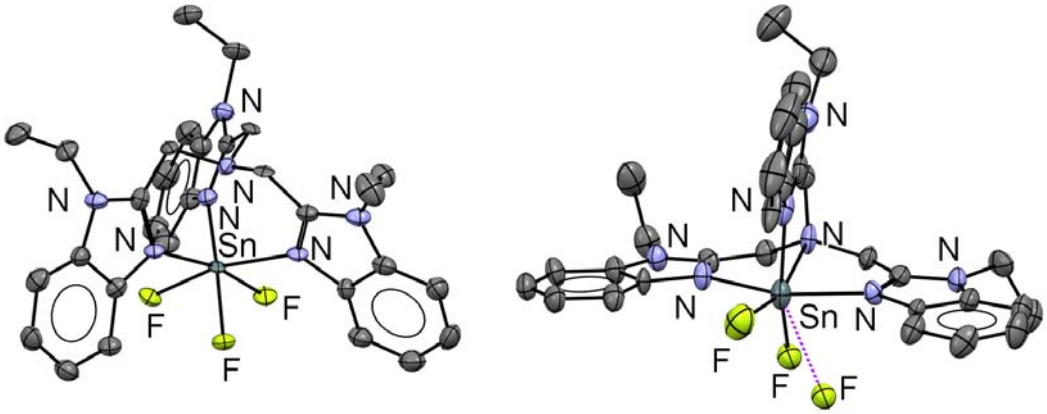

(a) (b)

Figure 5.5 – The structures of (a) the $[SnF_3(BIMEt)]^+$ monocation and (b) the $[SnF_2(BIMEt)]^{2+}$ dication (which forms dimers through a long fluoride contact shown by the purple dashed line). Both redrawn from Ref. 15.

As shown in **Figure 5.5** above, for the *mono*- and *bis*-triflate complexes, the triflates are not bound to the tin centre; this is in contrast to the *tris*- and *tetrakis*-triflate complexes where one triflate is bound in the first case and two in the second (shown in **Figure 5.6** below) with the remaining triflates balancing the charge. In both cases, in the solid-state, they are best regarded as dicationic complexes. In the ESI^+ mass spectrum of $[SnF(BIMEt)(OTf)][OTf]_2$, there are signals corresponding to the trication, $[SnF(BIMEt)]^{3+}$, which suggests that under these conditions the triflate is labile enough to be removed. However, even in this case, the most abundant species is the triflate bound $[SnF(BIMEt)(OTf)]^{2+}$; $[SnF_2(BIMEt)]^{2+}$ is also seen in the mass spectrum. For $[Sn(BIMEt)(OTf)_2][OTf]_2$ no signals for the tetracation $[Sn(BIMEt)]^{4+}$ could be detected by ESI^+ mass spectrometry, but triflate-bound species, including $[Sn(BIMEt)(OTf)]^{3+}$ were observed.[15]

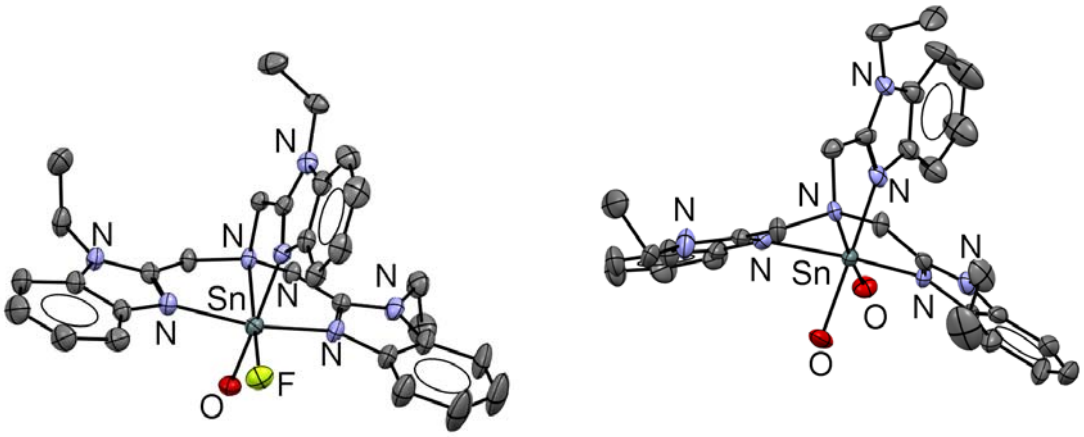

(a) (b)

Figure 5.6 – The structure of (a) $[SnF(BIMEt)(OTf)]^{2+}$ and (b) $[Sn(BIMEt)(OTf)_2]^{2+}$, only the coordinating O-atom of the triflate is shown. Both redrawn from Ref. 10. [15]

The reaction of the *tris*-triflate complexes prepared *in situ* with one equivalent of $OPEt_3$ leads to the isolation of the complex $[SnF(BIMEt_3)(OPEt_3)][OTf]_3$, as a tricationic tin fluoride complex, this also demonstrates that in these systems, triflates can be displaced from the tin centre by appropriate ligands to generate cationic species.[15]

5.2 Aims

The aim of this chapter is to develop the chemistry of SnF_4 with soft phosphine donors and explore fluoride abstraction chemistry with TMSOTf with the aim of developing cationic complexes.

5.3 Results and discussion

5.3.1 Synthesis of neutral complexes of tin(IV) fluoride with phosphine ligands

As part of this study, the complex $[SnF_4(PMe_3)_2]$ was synthesised by the reaction of $[SnF_4(MeCN)_2]$ with two equivalents of PMe_3 in CH_2Cl_2. In the ^1H NMR spectrum of this complex, a doublet is seen at δ = 1.60 in CD_2Cl_2, the choice of solvent influences the position of the resonance, with the resonance occurring at δ = 1.68 in $CDCl_3$.[4] In the $^{19}F\{^1H\}$ NMR spectrum, there is a triplet at δ = -134.4, which is close to the reported literature value, δ = -132.8, in both cases the coupling constant is the same at $^2J_{PF}$ = 155

Hz. In the $^{31}P\{^{1}H\}$ NMR spectrum, there is a quintet resonance at δ = -18.4, which compares to δ = -19.1 from the literature report.[4]

To test the effect of increased steric bulk on fluoride abstraction chemistry, the new complex $[SnF_4(P^iPr_3)_2]$ was synthesised by the reaction of two equivalents of P^iPr_3 with $[SnF_4(MeCN)_2]$ in CH_2Cl_2, yielding a white solid. In the ^{1}H NMR spectrum, there is a doublet of doublets at δ = 1.41 corresponding to the methyl protons and a septet of doublets at δ = 2.55 from the CH proton, this is a significant shift from the 'free' ligand of Δδ = +0.35 and Δδ = +0.86. A greater shift is seen for the CH protons due to them being closer to the metal centre and thus most affected by coordination. In the $^{31}P\{^{1}H\}$ NMR spectrum, there is a sharp quintet at δ = 30.6, indicative of *trans* phosphine coordination, which is consistent with previously reported monodentate phosphine complexes, with a coupling constant of $^{2}J_{PF}$ = 124 Hz (cf. δ = +22.2, $^{2}J_{PF}$ = 124 in $[SnF_4(PCy_3)_2]$).[4] Well-defined tin satellites are seen with magnitudes of $^{1}J_{119SnP}$ = 2477 Hz and $^{1}J_{117SnP}$ = 2363 Hz, similar to the couplings in the related complex, $[SnF_4(PCy_3)_2]$ ($^{1}J_{119SnP}$ = 2530 Hz).[4] In the $^{19}F\{^{1}H\}$ NMR spectrum (shown in **Figure 5.7** below) there is triplet at δ = -99.1 ppm with a coupling constant of $^{2}J_{PF}$ = 124 Hz ($^{1}J_{119Sn-F}$ = 2920 Hz, $^{1}J_{117Sn-F}$ = 2792 Hz), also similar to those reported for $[SnF_4(PCy_3)_2]$ (δ = -98.4, $^{2}J_{PF}$ = 124 Hz, $^{1}J_{119SnF}$ = 2993 Hz). Finally, the ^{119}Sn NMR spectrum of this complex shows a resonance at δ = -622.0 and appears as a quintet of triplets, which confirms the formation of the complex *trans*-$[SnF_4(P^iPr_3)_2]$. As part of this study, the complex $[SnF_4\{o\text{-}C_6H_4(PMe_2)_2\}]$ was also synthesised, spectroscopic data were consistent with literature reports.[4]

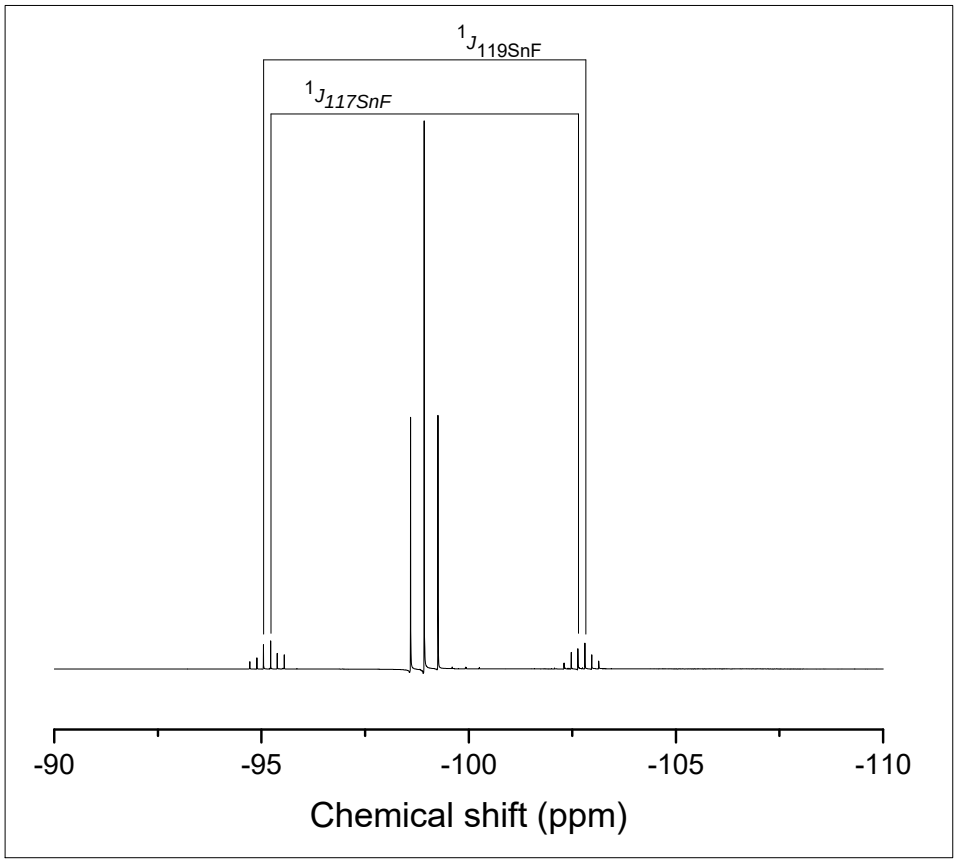

Figure 5.7 – $^{19}F\{^1H\}$ NMR spectrum of $[SnF_4(P^iPr_3)_2]$ showing the tin satellites at 298 K in CD_2Cl_2.

The reaction of $[SnF_4(MeCN)_2]$ with the tripodal triphosphine, $CH_3C(CH_2PPh_2)_3$, in CH_2Cl_2 leads to the formation of $[SnF_4\{\kappa^2\text{-}CH_3C(CH_2PPh_2)_3\}]$ as a white solid. In the ^1H NMR spectrum, there are three resonances for the methylene protons, two broad resonances at δ = 2.95 and 3.11 of equal intensity corresponding to the methylene environments of the coordinated phosphine arms, and another also of equal intensity at δ = 2.28 corresponding to the uncoordinated arm. The resonance at δ = 0.87 ppm corresponds to the methyl protons and broad multiplets in the aromatic region. The ratio of the methyl:methylene:aromatic integrals is as expected 3:6:30. In the $^{31}P\{^1H\}$ NMR spectrum there are two main resonances, a singlet at δ = -27.1 corresponding to the 'free' arm and a doublet of triplets of doublets at δ = -6.9 ($^2J_{PF}$ = 121, 98, 51 Hz) corresponding to the coordinated arms. In the $^{19}F\{^1H\}$ NMR spectrum, there are two resonances, one at δ = -144.2, where a doublet of doublet of triplets is seen corresponding to fluorines *trans* to the phosphine ligands ($^2J_{PF}$ = 98, 51, $^2J_{FF}$ = 45 Hz). The other signal seen at δ = -109.7 ppm is two overlapping multiplets which correspond to the axial fluorines, which are in

two slightly different environments due to the bridgehead. The ratio of these resonances is consistent with the formulation of the complex [$SnF_4\{\kappa^2$-$CH_3C(CH_2PPh_2)_3\}$]

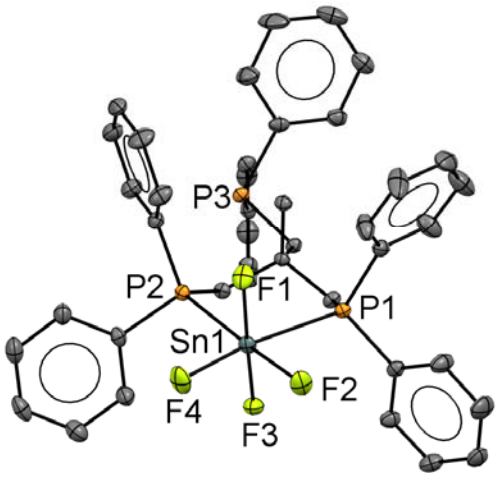

Figure 5.8 – The structure of [$SnF_4\{\kappa^2$-$CH_3C(CH_2PPh_2)_3\}$] showing the atom labelling scheme. The ellipsoids are drawn at the 50% probability level and H atoms are omitted for clarity. Selected bond lengths (Å) and angles (°) are: Sn1–P1 = 2.6302(5), Sn1–P2 = 2.6314(5) Sn1–F1 = 1.9670(12), Sn1–F2 = 1.9488(12), Sn1–F3 = 1.9791(12), Sn1–F4 = 1.9307(12), P1–Sn1–P2 = 91.245(14), P1–Sn1–F4 = 172.46(4), P2–Sn1–F2 = 174.74(4), F1–Sn1–F3 = 173.44(5).

Crystals of [$SnF_4\{\kappa^2$-$CH_3C(CH_2PPh_2)_3\}$] were grown by layering a CH_2Cl_2 solution of the complex with hexane. The crystal structure (see above in **Figure 5.8**) shows that this complex is monomeric in the solid state, consistent with the solution state data. The complex features a six-membered chelate ring which has a chair-like conformation; this is in contrast to [$GeF_4\{\kappa^2$-$CH_3C(CH_2PPh_2)_3\}$] (see Chapter 3), which has an envelope-like conformation. There is no evidence that the third arm can displace a fluorine from the tin centre to form a cation.

The reaction of [$SnF_4(MeCN)_2$] with the tetraphosphine ligand, $P(CH_2CH_2PPh_2)_3$, in CH_2Cl_2 leads to the formation of a mixture of products, two of them identifiable, which are [$SnF_4\{\kappa^2$-$P(CH_2CH_2PPh_2)_3\}$] and [$SnF_4\{\kappa^1$-$P(CH_2CH_2PPh_2)_3\}_2$]. In the $^{31}P\{^1H\}$ NMR spectrum at 183 K there are multiplets corresponding to [$SnF_4\{\kappa^2$-$P(CH_2CH_2PPh_2)_3\}$], the complex gives rise to three resonances which are observed as a doublet, a doublet of doublet of triplets and a doublet of doublet of triplet of triplet of doublets in 2:1:1 ratio (shown in **Figure 5.9**), this is consistent with the complex being present in the mixture (shown in **Figure 5.10** below). In [$SnF_4\{\kappa^2$-$P(CH_2CH_2PPh_2)_3\}$] the apical phosphorus and one of the terminal arms is coordinated to the tin centre, with the other two terminal arms remaining ‘free’.

There is also a second product, $[SnF_4\{\kappa^1\text{-}P(CH_2CH_2PPh_2)_3\}_2]$, that displays a quintet of quartets in the low-temperature phosphorus NMR spectrum as well as a doublet, and in the low-temperature $^{19}F\{^1H\}$ spectrum, a triplet is seen, this is consistent with κ^1 coordination of two equivalents of the tetraphosphine ligand to the tin centre. This is an unusual coordination mode for $P(CH_2CH_2PPh_2)_3$, with no structurally authenticated examples in the CCDC database of this coordination mode in the solid state. Both of the identified products are shown in **Figure 5.10** below; NMR spectroscopy suggests there is also at least one other unidentified product.

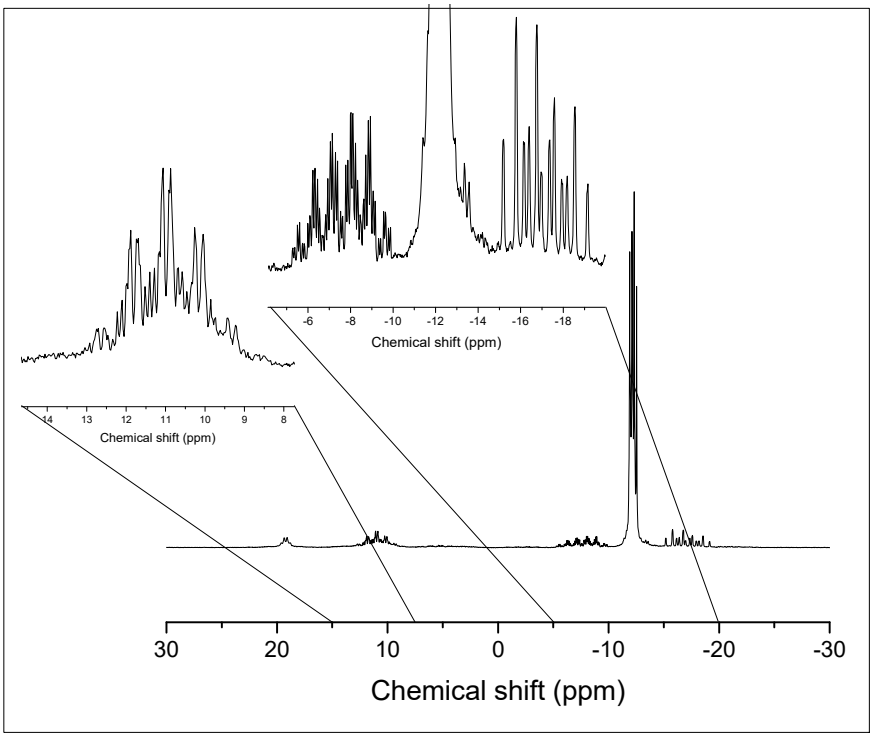

Figure 5.9 – $^{31}P\{^1H\}$ NMR spectrum of the product of the reaction of $[SnF_4(MeCN)_2]$ with $P(CH_2CH_2PPh_2)_3$ in CD_2Cl_2 at 183 K.

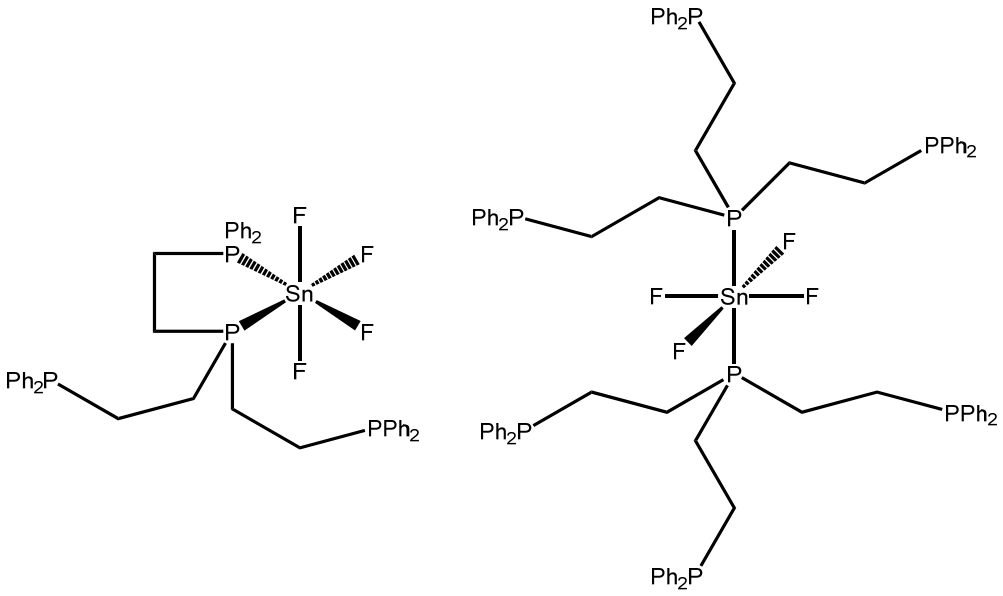

(a) (b)

Figure 5.10 – The two major products of the reaction of $[SnF_4(MeCN)_2]$ with $P(CH_2CH_2PPh_2)_3$. (a) $[SnF_4(\kappa^2\text{-}P\{CH_2CH_2PPh_2\}_3)]$ and (b) $[SnF_4(\kappa^1\text{-}P\{CH_2CH_2PPh_2\}_3)_2]$.

5.3.2 Reactions of monodentate phosphine tin(IV) fluoride complexes with TMSOTf

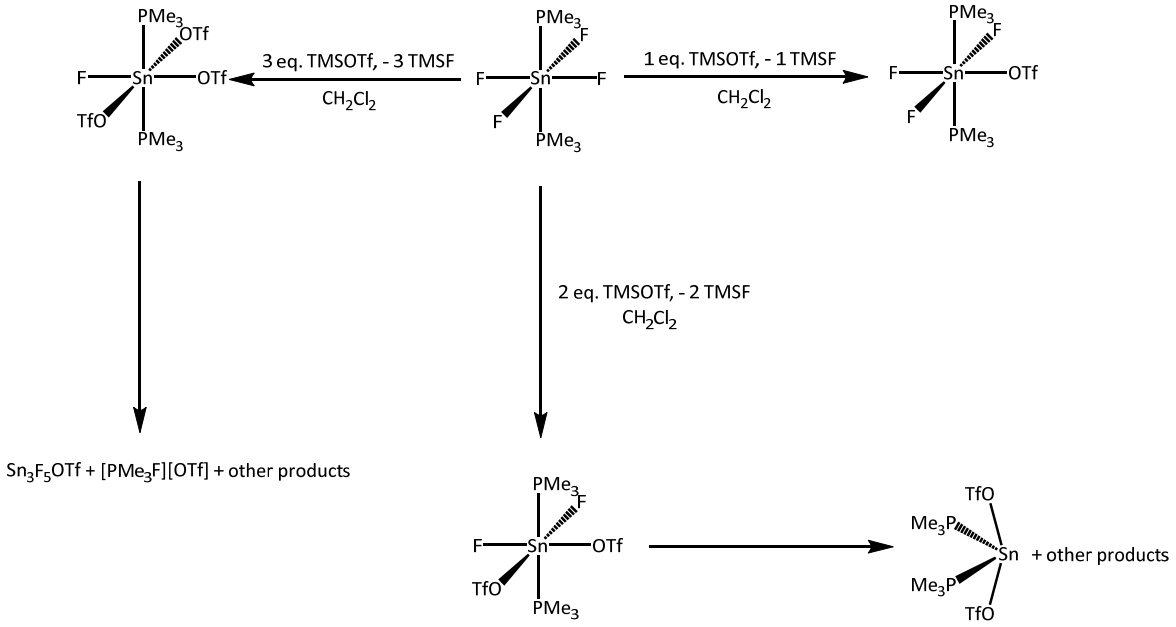

Scheme 5.1 – Reactions of $[SnF_4(PMe_3)_2]$ with TMSOTf.

The reaction of $[SnF_4(PMe_3)_2]$ with one equivalent of TMSOTf in CH_2Cl_2 leads to the isolation of $[SnF_3(PMe_3)_2(OTf)]$ (see **Scheme 5.1**). In the ^{1}H NMR spectrum of this complex, there is doublet at δ = 1.70, which is a shift of Δδ = +0.02 from the parent tetrafluoride complex. The resonances in $^{19}F\{^1H\}$ and $^{31}P\{^1H\}$ NMR spectra at 298 K are broad, indicating that the complex is dynamic at this temperature. At 183 K the $^{31}P\{^1H\}$ NMR spectrum shows a triplet of doublets at δ = -3.2, which is a shift of Δδ = +15.9 from the tetrafluoride complex, indicating an increase in charge at the tin centre. There is also an increase in the $^1J_{119Sn\text{-}31P}$ coupling constant from 2975 Hz to 3412 Hz; this is a similar trend seen for the triflate complexes in chapter 2, where the replacement of a halide with triflate increases the coupling constant. In the corresponding low-temperature $^{19}F\{^1H\}$ NMR spectrum (shown in **Figure 5.11** below), there are two resonances corresponding to the Sn-F fluorines in the compound; there is a triplet of triplets at δ = -151.4 and a triplet of doublets at δ = -127.9. This is consistent with the complex having the same structure as the germanium analogue (**Figure 3.19**). The $^1J_{119Sn\text{-}F}$ coupling constant for the fluorine *trans* to the triflate is smaller than for the fluorines *cis* to the triflate (3013 Hz vs 3253 Hz), but both are larger than the coupling for the tetrafluoride (2745 Hz). In the low temperature (183 K) ^{119}Sn NMR spectrum, there is an ill-defined multiplet at δ = 559.9, a high-frequency shift from the tetrafluoride by Δδ = +28.1, which suggests that the triflate

is bound (a truly cationic complex would be expected to have a much more positive chemical shift (see chapter 2)).

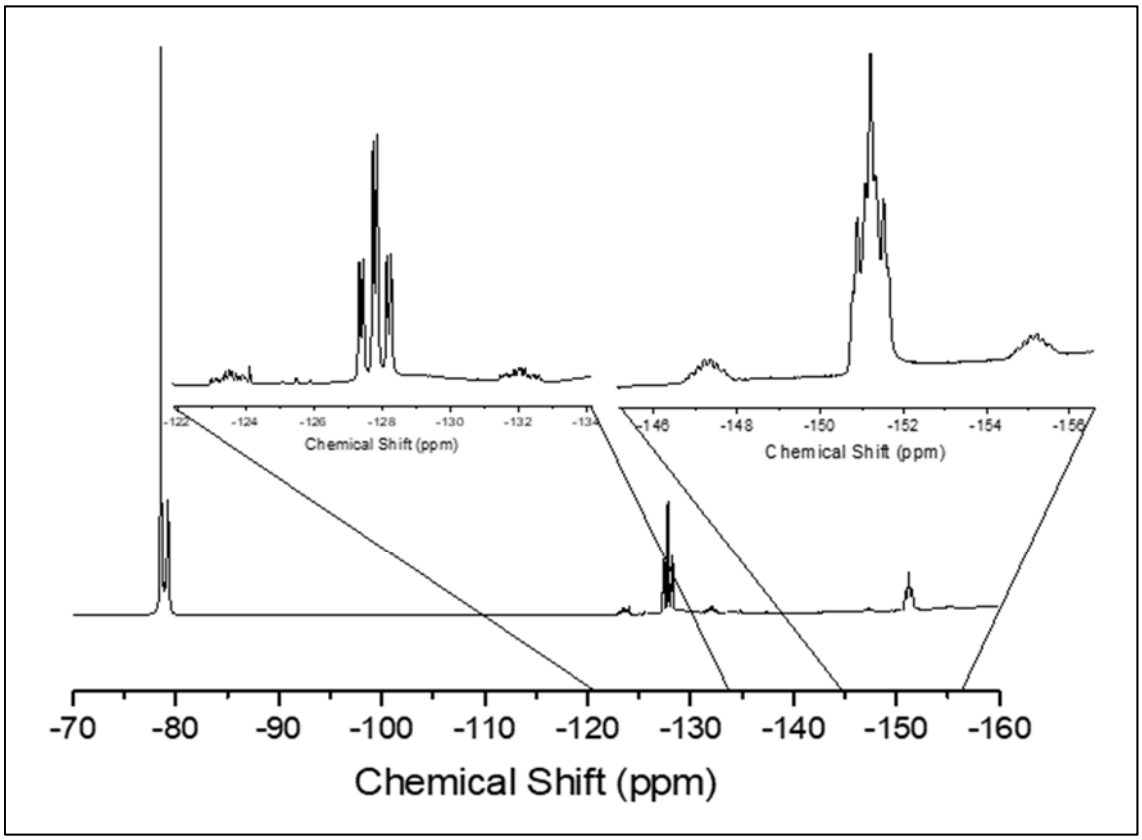

Figure 5.11 – $^{19}F\{^{1}H\}$ NMR spectrum of $[SnF_3(PMe_3)_2(OTf)]$ at 183 K in CD_2Cl_2.

Crystals of this compound were grown by layering a CH_2Cl_2 solution of the complex with hexane, and the structure was determined by X-ray crystallography (see **Figure 5.12**). The geometry around the tin centre is approximately octahedral, with the triflate coordinated to the tin centre, this is consistent with the low-temperature NMR data, and with the germanium analogue in chapter 3 and the tin chloride analogue in chapter 2. Comparing this structure with $[SnF_4(PCy_3)_2]$ the only other structurally characterised mono-dentate phosphine complex of SnF_4, the d(Sn-P) distance is shorter in the triflate complex (2.5778(4), 2.5405(4) *vs*. 2.6538(11)Å), although this could be due to the smaller steric requirement of PMe_3 *vs.* PCy_3 or the increased charge on the tin centre. The d(Sn-F) are broadly similar in the two complexes (1.9761(9), 1.9595(10), 1.9871(9) *vs.* 1.959(2), 1.980(2) Å). The molecule has approximate C_{2v} symmetry, therefore three Sn-F stretching bands ($2A_1 + B_1$) would be expected in the IR spectrum; they are observed at 517, 547 and 573 cm^{-1}, together with peaks associated with the triflate.

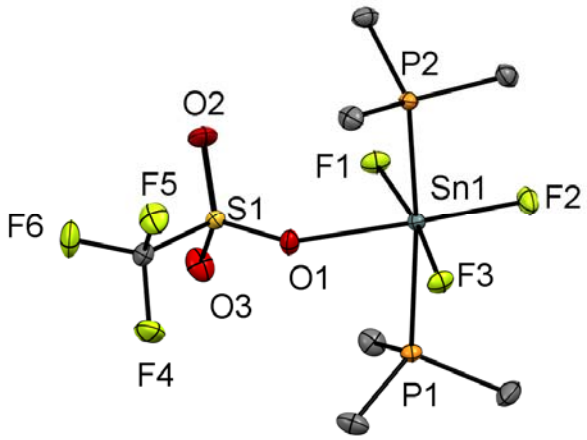

Figure 5.12 – The crystal structure of $[SnF_3(PMe_3)_2(OTf)]$ showing the atom labelling scheme. The ellipsoids are drawn at the 50% probability level and H atoms are omitted for clarity. Selected bond lengths (Å) and angles (°) are: Sn1–P1 = 2.5278(4), Sn1–P2 = 2.5405(4), Sn1–F1 = 1.9761(9), Sn1–F2 = 1.9595(10), Sn1–F3 = 1.9871(9), Sn1–O1 = 2.2445(12), P1–Sn1–P2 = 171.615(13), F1–Sn1–F3 = 171.00(4), O1–Sn1–F3 = 176.66(4)

The reaction of $[SnF_4(PMe_3)_2]$ with two equivalents of TMSOTf leads to the isolation of $[SnF_2(PMe_3)_2(OTf)_2]$. In the ^1H NMR spectrum there is a further shift of $\Delta\delta$ = +0.02 from the monotriflate (to δ = 1.88). In the low temperature (183 K) $^{31}P\{^1H\}$ NMR spectrum, there is a triplet at δ = 10.2, consistent with the formation of the complex, here the tin-119 satellites have a coupling constant of $^1J_{119Sn\text{-}31P}$ = 3654 Hz, which is a further increase from the *mono*-triflate. In the $^{31}P\{^1H\}$ NMR spectrum there is also a minor product which displays a triplet at δ = 4.5, which could be another isomer of the product of the form $[SnF_2(PMe_3)_2(OTf)_x][OTf]_{2-x}$, although in this case, the signal is too weak to observe tin satellites. The $^{19}F\{^1H\}$ NMR spectrum (at 183 K) showed a triplet resonance corresponding to the Sn-F fluorines appears at δ = -142.7, here the coupling constant is $^1J_{119Sn\text{-}19F}$ = 3393 Hz which also constitutes an increase from *mono*-triflate to *bis*-triflate. In the low temperature ^{119}Sn NMR spectrum, there is a resonance at δ = -609, which appears as a triplet of triplets; this is a shift of $\Delta\delta$ = +19 from the tetrafluoride complex. Assuming that the fluorides are *cis* to each other (and that the geometry is similar to $[GeF_2(PMe_3)_2][OTf]_2$), then the molecule would be expected to have approximate C_{2v} symmetry, so two bands associated with Sn-F stretching modes would be expected (A_1 and B_1); these are seen at 517 and 531 cm^{-1}.

This complex is not indefinitely stable in solution. If a CH_2Cl_2 solution of the complex is layered with hexane, crystals of the complex $[Sn(PMe_3)_2(OTf)_2]$ deposit, here the tin centre has been reduced to Sn(II). This demonstrates that replacing fluorine with triflate can induce redox chemistry in these systems. The structure is shown in **Figure 5.13** below – the geometry is approximately disphenoidal at tin. There are long contacts with neighbouring triflates to form a weakly associated chain in the b-direction; the additional contact completes an approximately five-coordinate square pyramidal geometry at tin, shown in **Figure 5.14** below. The structure seems to be analogous to the known $[Ge(PMe_3)_2(OTf)_2]$.[16]

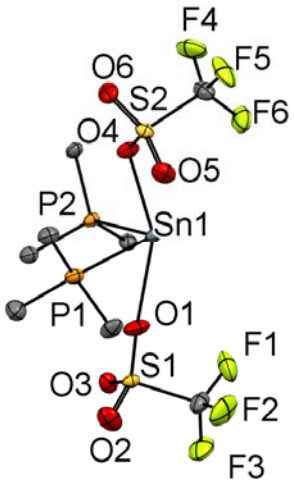

Figure 5.13 – The structure of $[Sn(PMe_3)_2(OTf)_2]$ showing the atom labelling scheme. The ellipsoids are drawn at the 50% probability level, and H atoms are omitted for clarity. Selected bond lengths (Å) and angles (°) are: Sn1–P1 = 2.7796(10), Sn1–P2 = 2.6610(8), Sn1–O1 = 2.523(3), Sn1–O1 = 2.342(3) P1–Sn1–P2 = 96.27(3), O1–Sn1–O4 = 154.39(10).

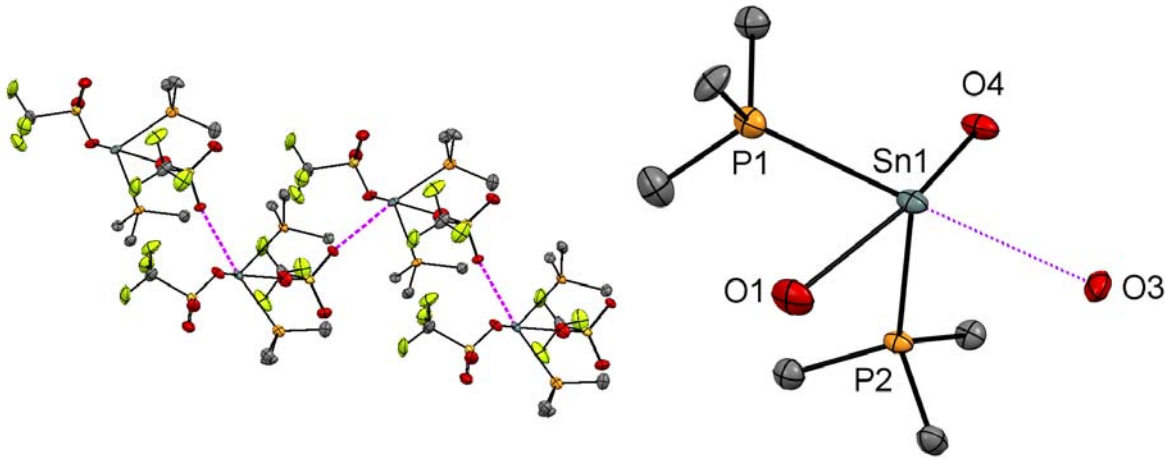

(a) (b)

Figure 5.14 – (a) The extended structure of $[Sn(PMe_3)_2(OTf)_2]$ in the b-direction showing tin triflate contacts (purple dashed lines) (b) the geometry around the tin centre with only the coordinated oxygens from the triflates shown (Sn1···O3 = 3.044 Å).

The reaction of $[SnF_4(PMe_3)_2]$ with three equivalents of TMSOTf leads to the formation of $[SnF(PMe_3)_2(OTf)_3]$. In the ^1H NMR spectrum there is a doublet resonance at δ = 2.0, which is a change of Δδ = +0.32 from the tetrafluoride complex. The $^{19}F\{^1H\}$ NMR spectrum of this complex consists of a triplet resonance at δ = -132.9 (corresponding to the Sn-F fluorine) and singlet at δ = -77.6 (corresponding to the triflate anion) in a 1:9 ratio, here $^1J_{119SnF}$ = 3557 Hz, which is a further increase from the *bis*-triflate. In the $^{31}P\{^1H\}$ NMR spectrum, there is doublet at δ = 18.3, which is a shift of Δδ = +37.4 from the tetrafluoride complex, here the tin-phosphorus coupling constant is $^1J_{119SnP}$ = 3740 Hz, which is 765 Hz larger than the tetrafluoride complex. In the low temperature ^{119}Sn NMR spectrum, there is a resonance at δ = -617, which appears as a broad quartet; this can be explained by the fact that $^1J_{119SnP} \approx {}^1J_{119SnF}$, leading to the expected triplet of doublets overlapping to form a *pseudo*-quartet.

Making the assumption that the phosphines are still *trans* to each other and the triflate are still bound, the geometry would be C_{2v}, one Sn-F peak (A_1) would be expected in the IR spectrum, which is seen at 510 cm^{-1}. This complex is not stable in CH_2Cl_2 and over the course of a couple of hours, crystals of the polymeric $Sn_3F_5(OTf)$ form (the structure of which is shown in **Figures 5.15** below), resonances corresponding to $[SnF(PMe_3)_2(OTf)_3]$

disappear, and resonances corresponding to $[PMe_3F]^+$ appear in the $^{19}F\{^1H\}$ NMR spectrum.[8] It is clear that some of the phosphine ligands are being oxidised and fluorinated, and the tin(IV) centre is being reduced to tin(II). This reduction from tin(IV) to tin(II) is also seen in $[SnF_2(PMe_3)_2(OTf)_2]$, but here the outcome of the reduction is different (the product in that system is $[Sn(PMe_3)_2(OTf)_2]$).

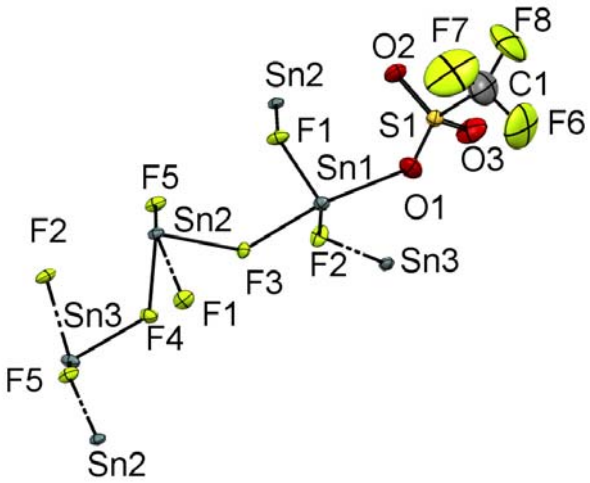

Figure 5.15 – The asymmetric unit of $[Sn_3F_5(OTf)]$ showing the atom labelling scheme. The ellipsoids are drawn at the 50% probability level. Selected bond lengths (Å) and angles (°) are: Sn1–F1 = 2.055(2), Sn1–F2 = 2.143(3), Sn1–F3 = 2.148(3), Sn2–F1 = 2.385(2), Sn2–F3 = 2.165(2), Sn2–F4 = 2.175(3), Sn2–F5 = 2.268, Sn3–F2 = 2.183(3), Sn3–F4 = 2.156(3), Sn3–F5 = 2.083(2).

Figure 5.16 below shows the extended structure of this compound along both the c and b directions. The compound has an infinite two-dimensional structure in the b and c directions, with the layers stacking in the 'a' direction. The layers are capped with triflates bonded to Sn1. There are three distinct tin environments in the structure; two four-coordinate tin centres, with Sn1 connected to F1-3 and a triflate and Sn2 connected to F1 and F3-5. There is also a three coordinate tin centre Sn3 which is connected to F2, F4, and F5. Each Sn1 unit is connected to two Sn2 centres, one through F1 and another through F3 and to a Sn3 centre through F2. Each Sn2 unit is connected to two Sn3 units, one through F3 and one through F4. This compound is an unusual example of a 2-D tin fluoride layered polymer.

(a)

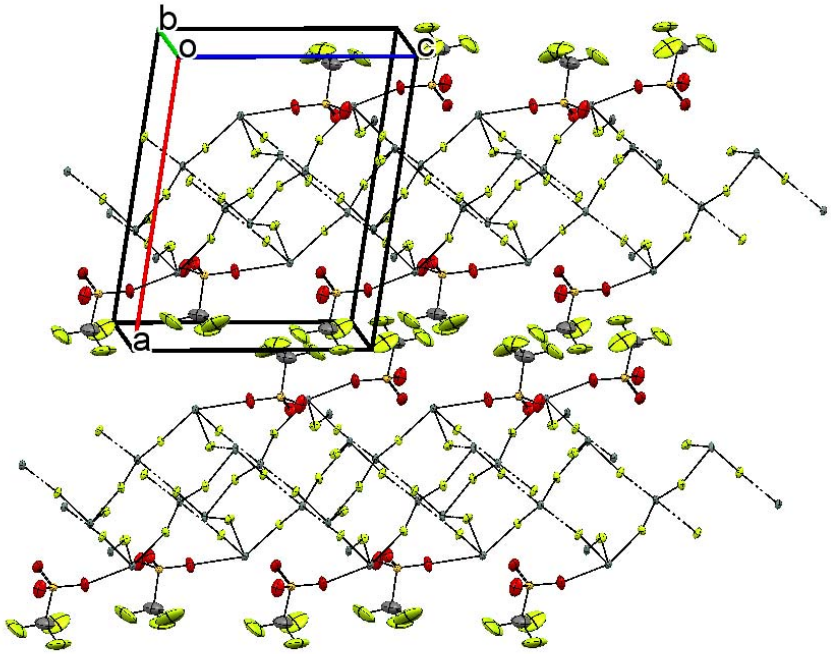

(b)

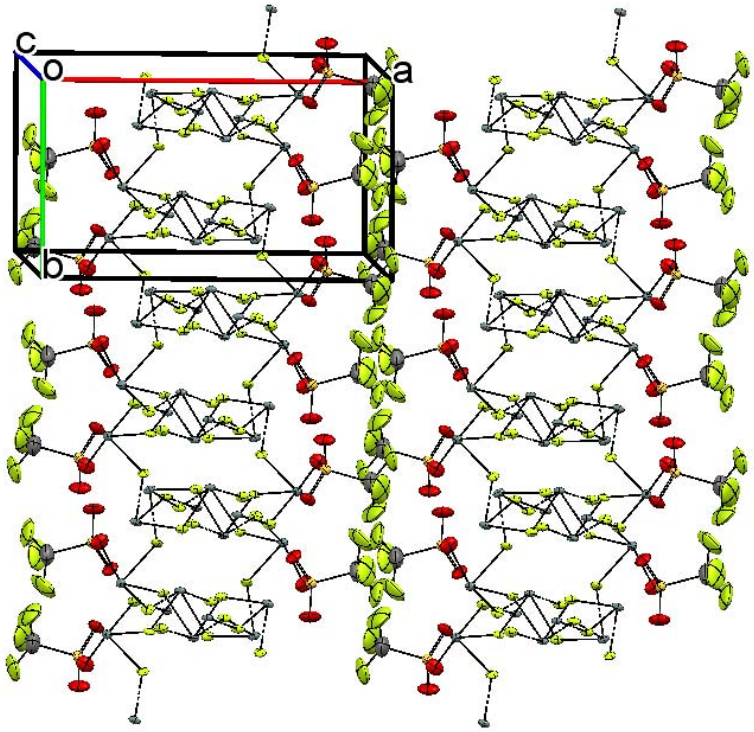

Figure 5.16 – The extended structure of $[Sn_3F_5(OTf)]$ in the (a) c-direction, (b) b-direction.

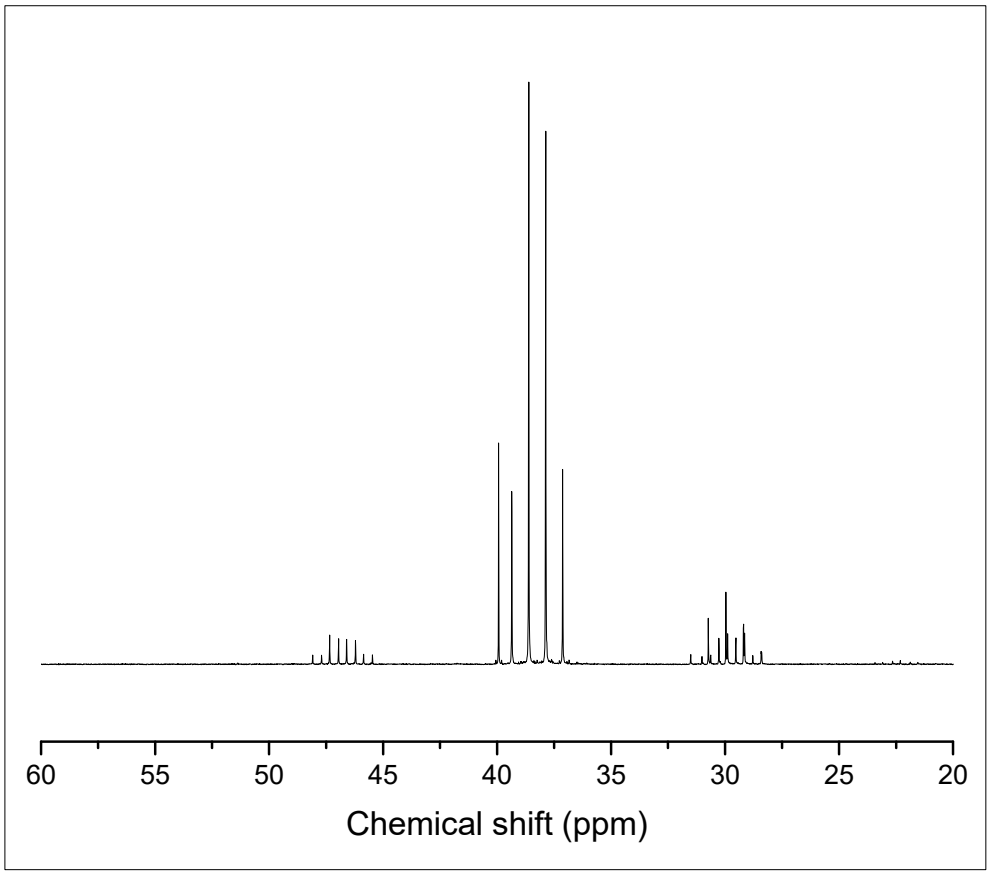

Figure 5.17 – $^{31}P\{^{1}H\}$ spectrum of $[SnF_3(^{i}Pr_3P)_2][OTf]$ in CD_2Cl_2 at 298 K (there is also a small amount of $[HP^{i}Pr_3]^+$ present in the NMR as well as a small amount of $[SnF_4(P^{i}Pr_3)_2]$.

In the complex $[SnF_3(PMe_3)_2(OTf)]$, the triflate is strongly associated with the tin centre (see **Figure 5.12**). A more sterically crowded phosphine may be able to exclude the triflate from the tin coordination sphere. To this end, $P^{i}Pr_3$ was chosen due to its larger cone angle than PMe_3 (160˚ *vs.* 118˚).[17] The reaction of $[SnF_4(P^{i}Pr_3)_2]$ with one equivalent of TMSOTf in CH_2Cl_2 leads to the formation of $[SnF_3(P^{i}Pr_3)_2(OTf)]$. In the ^{1}H spectrum of this complex, a doublet of doublets is seen at δ = 1.45 ppm, Δδ = +0.04 from the tetrafluoride complex. The resonance for the C*H* is at δ = 2.77, which constitutes a shift of Δδ = +0.22. This is much larger than that seen for the PMe_3 derivative. The $^{31}P\{^{1}H\}$ NMR spectrum at room temperature is a sharp quartet (shown above in **Figure 5.17**) at δ = 38.2 (Δδ = +7.6 from the tetrafluoride), this suggests that at this temperature the triflate is not bound to the tin centre, as all the three fluorines are in equivalent environments on the ^{31}P NMR timescale, but at low temperature, there are signs of the multiplet splitting into a triplet

of doublets although it is not well resolved. In the room temperature $^{19}F\{^{1}H\}$ NMR spectrum, there is a broad resonance at around δ = -73.8 and a second, broader resonance around δ = -116.9, both of which sharpen at 183 K, but the couplings are still not resolved at this temperature. The resonance at δ = -73.8 has tin satellites with $^{1}J_{SnF}$ = 3518 Hz, and the resonance at δ = -116.9 has $^{1}J_{SnF}$ = 3244 Hz. The ^{119}Sn NMR spectrum at 183 K shows a resonance at δ = -611.1, which appears as a triplet of doublets of triplets, consistent with the triflate being coordinated at this temperature. The 18 line pattern has been simulated using the SPINACH software package[18]; based on the coupling constants extracted from the phosphorus and fluorine spectra, the pattern matches closely with the experimental data, which supports the assignment of the triflate being coordinated to the tin centre (see **Figure 5.18** and **Figure 5.19**). In summary, these data suggest that at low temperature the triflate coordinates to the tin centre, but at room temperature, it is closer to the high-temperature limit where $[SnF_3(^{i}Pr_3P)_2]^+$ predominates in solution. The addition of two equivalents of TMSOTf to $[SnF_4(P^{i}Pr_3)_2]$ leads to the formation of $[SnF_2(P^{i}Pr_3)_2(OTf)_2]$, in the $^{31}P\{^{1}H\}$ NMR spectrum of this product there is a triplet and in the $^{19}F\{^{1}H\}$ NMR there is a broad resonance at δ = -56.9 which is flanked by tin satellites. In the ^{119}Sn NMR spectrum there is a triplet of triplets at -630 ppm, which is consistent with the formation of the product.

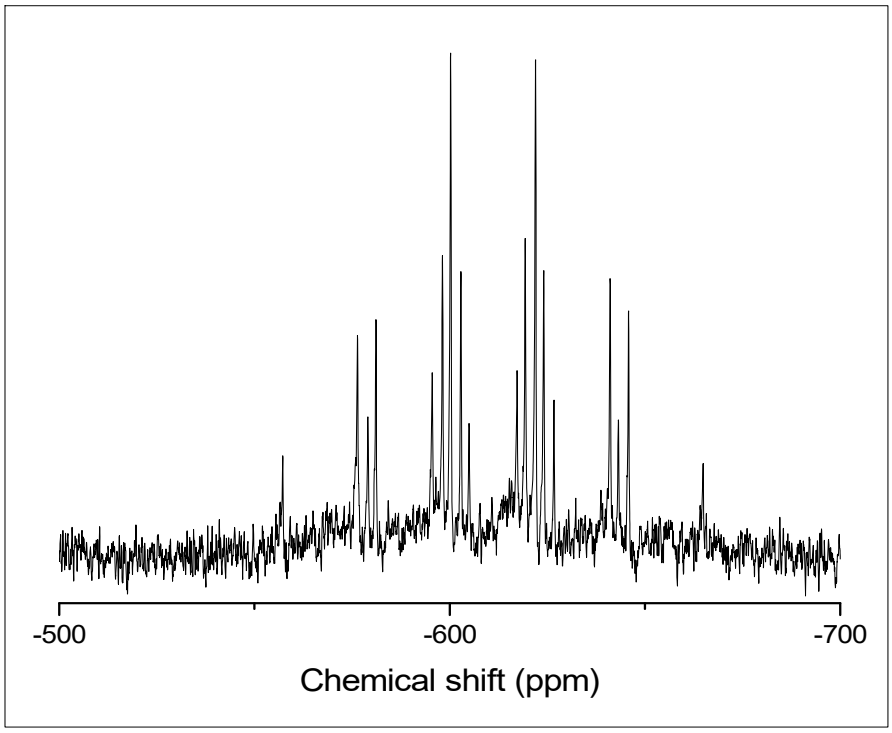

Figure 5.18 – ^{119}Sn spectrum of [$SnF_3(^iPr_3P)_2(OTf)$] at 183 K in CD_2Cl_2.

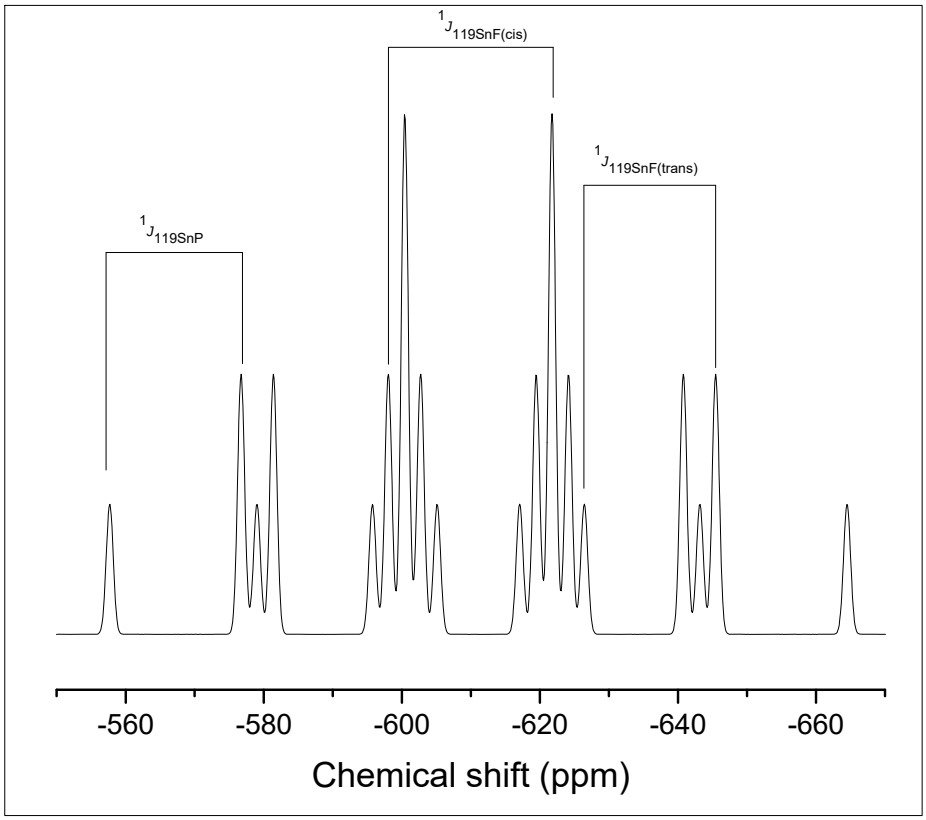

Figure 5.19 – Simulation of the ^{119}Sn spectrum of [$SnF_3(P^iPr_3)_2(OTf)$] using SPINACH.[18]

Table 5.1 – Selected multinuclear NMR data for complexes of the form $[SnF_{4-n}(PMe_3)_2(OTf)_n]$ for n = 0, 1, 2, 3 and $[SnF_{4-n}(P^iPr_3)_2(OTf)_n]$ for n = 0, 1, 2.

Compound	$\delta(^{31}P\{^1H\})$ (ppm)	$\delta(^{19}F\{^1H\})$ (ppm)	$\delta(^{119}Sn)$[a] (ppm)	$^2J(^{31}P\text{-}^{19}F)$ (Hz)	$^2J(^{19}F\text{-}^{19}F)$ (Hz)	$^1J(^{119}Sn\text{-}^{31}P)$ (Hz)	$^1J(^{119}Sn\text{-}^{19}F)$ (Hz)
trans-$[SnF_4(PMe_3)_2]$[4]	-19.1 (quin)	-132.8 (t)	-628.0 (t of quin)	155	-	2975	2745
$[SnF_3(PMe_3)_2(OTf)]$	-3.2 (td)[a]	-127.9 (td)[a] -151.4 (tt)[a]	-599.9 (m)	153 121	41	3412	3253 3013
$[SnF_2(PMe_3)_2(OTf)_2]$	10.2 (t)[a]	-142.7 (t)[a]	-609 (tt)	107	-	3654	3393
$[SnF(PMe_3)_2(OTf)_3]$	18.3 (d)	-132.9(t)	-617 (m)	88	-	3740	3557
trans-$[SnF_4(P^iPr_3)_2]$	30.6 (quin)	-99.1 (t)	-622.0 (quin of t)	124	-	2477	2920
$[SnF_3(P^iPr_3)_2(OTf)]$	38.2 (q)	-73.5 (br) -116.9 (br)	-611.1 (tdt)	121	-	2856	3518[b] 3244[b]
$[SnF_2(P^iPr_3)_2(OTf)_2]$	49.4 (t)	-56.9 (br)	-630 (tt)	117	-	2971	4082[b]

[a] Recorded at 183 K, [b] Average $^{119/117}$Sn satellites

Table 5.1 summarises the multinuclear data for the trimethylphosphine and triispropylphosphine complexes. Like the analogous germanium systems (see Chapter 3), as fluoride is replaced by triflate, there is an increase in the $^{31}P\{^1H\}$ NMR chemical shift, indicating an increase in charge at metal centre. Two main factors affect the $^{19}F\{^1H\}$ chemical shift in these systems, the first being the ligand *trans* to the fluorine in question; the *trans* effect of the fluoride leads to much more positive chemical shifts than those that are *trans* to a triflate. The other factor is the number of fluorides that have been removed, and the more fluorides removed, the more positive the chemical shift. As fluorides are removed there is a decrease in the $^2J_{PF}$ coupling constant, with the coupling constant for the *tris*-triflate complex being almost half that of the tetrafluoride complex in the case of the trimethylphosphine complexes. There is also a substantial increase in the $^1J_{119SnP}$ and $^1J_{119SnF}$ coupling constants as the fluorides are replaced by triflates for both series of phosphine complexes. Low temperature ^{119}Sn chemical shifts for these complexes all occur within a narrow range, consistent with 6-coordinate neutral complexes.

The reaction of [SnF_4{*o*-$C_6H_4(PMe_3)_2$}] with TMSOTf in CH_2Cl_2 leads to the formation of a mixture of products as identified by $^{31}P\{^1H\}$ NMR spectroscopy, the only identifiable one being the Sn(II) reduction product [Sn{*o*-$C_6H_4(PMe_3)_2$}$(OTf)_2$], which was identified by single crystal X-ray analysis. The $^{31}P\{^1H\}$ NMR spectrum contains a singlet at δ = -18.0 ppm, flanked by tin satellites ($^1J_{119Sn\text{-}31P}$ = 1879 Hz, $^1J_{117Sn\text{-}31P}$ = 1792 Hz), the coupling constants are consistent with those seen in previously reported tin(II) diphosphine complexes.[19]

Crystals of [Sn{*o*-$C_6H_4(PMe_2)_2$}$(OTf)_2$] were grown by layering a CH_2Cl_2 solution of the complex with hexane and the structure is shown in **Figure 5.20a**. The triflates remain coordinated to the tin centre. Interactions with nearby molecules give rise to loosely associated trimers (**Figure 5.20b**); this is in contrast to the germanium analogue, which forms dimers in the solid state (see chapter 3). The long Sn···OTf contacts complete a distorted octahedral coordination environment around the tin centres; however, if the lone pair on the tin is included, then the geometry could be said to be distorted pentagonal bipyrimidal instead (**Figure 5.21**). The higher coordinate geometry in the tin analogue probably reflects the larger ionic radius of tin(II) compared to germanium(II).

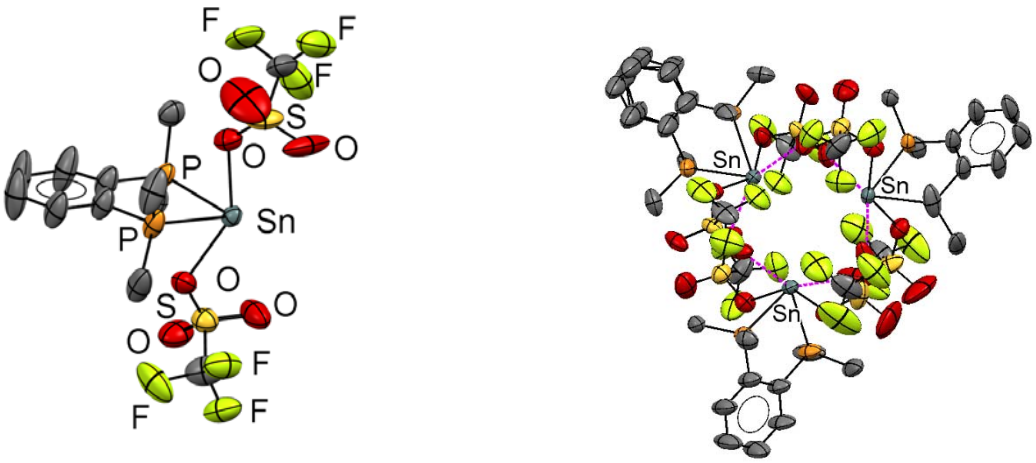

(a) (b)

Figure 5.20 – (a) The structure of [Sn{*o*-$C_6H_4(PMe_2)_2$}$(OTf)_2$]; note that the poor data quality means the structure refinement is poor. Therefore, only the connectivity is shown and not any structural parameters (b) the trimeric structure with long triflate contacts as purple dashed lines.

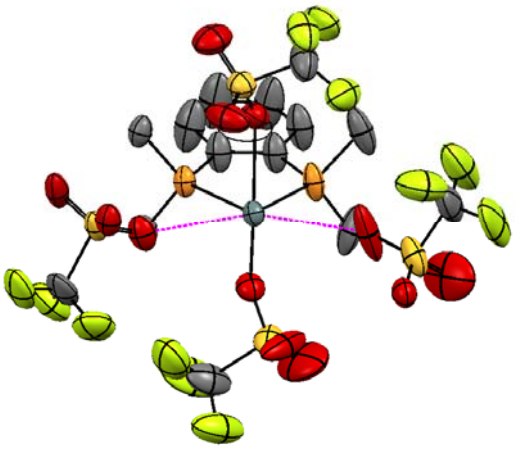

Figure 5.21 – View of the distorted pentagonal bipyramidal geometry around the tin centre in [Sn{*o*-$C_6H_4(PMe_2)_2$}$(OTf)_2$].

5.4 Conclusions

In this chapter, the reactivity of tin(IV) fluoride phosphine complexes with TMSOTf is explored. It was shown that the fluorides can be sequentially removed from [$SnF_4(PMe_3)_2$] by adding n equivalents of TMSOTf in CH_2Cl_2, forming [$SnF_{4-n}(PMe_3)_2(OTf)_n$] (n = 1, 2, 3). These complexes were characterised by multinuclear NMR spectroscopy, which revealed that there are systematic trends as you go down the series (increase in both the ^{31}P and ^{19}F chemical shifts), which are similar to the germanium analogues described in chapter 3. The complexes with n = 2 and 3 were shown to be unstable in solution, leading to the Sn(II) reduction products, [$Sn(PMe_3)_2(OTf)_2$] and the 2-D polymeric solid $Sn_3F_5(OTf)$, crystallising from their respective solutions. Thus, removing fluoride and replacing it with triflate promotes redox chemistry in these systems, which is not seen in the tetrafluoride complexes, and indeed for tin is not seen with chlorides or bromides, but does occur for iodides.[20] The reaction of the bulkier phosphine complex [$SnF_4(P^iPr_3)_2$] with one equivalent of TMSOTf leads to the formation of [$SnF_3(P^iPr_3)_2$][OTf], for which solution state evidence suggests that this complex is ionic with an ion separated $[SnF_3(P^iPr_3)_2]^+$ monocation and $[OTf]^-$ at room temperature, but at low temperature, the triflate remains bound. The reaction of [$SnF_4(P^iPr_3)_2$] with two equivalents of TMSOTf leads to the formation of [$SnF_2(P^iPr_3)_2(OTf)_2$]. The reaction of [SnF_4{*o*-$C_6H_4(PMe_2)_2$}] with TMSOTf leads to a mixture of products, with the only one identifiable being the Sn(II) reduction product, [Sn{*o*-$C_6H_4(PMe_2)_2$}$(OTf)_2$], which is evident in the NMR spectra of this complex and also in a crystal structure, which shows that it exists as a loosely associated trimer in the solid

state. The reaction of $[SnF_4(MeCN)_2]$ with $CH_3C(CH_2PPh_2)_3$ was shown to form $[SnF_4(\kappa^2\text{-}CH_3C(CH_2PPh_2)_3)]$ with no evidence of direct displacement of fluoride by the third phosphine function. The reaction of $[SnF_4(MeCN)_2]$ with the tetraphosphine ligand $P(CH_2CH_2PPh_2)_3$ was also explored and was shown to form a mixture of products including $[SnF_4\{\kappa^2\text{-}P(CH_2CH_2PPh_2)_3\}]$ and $[SnF_4\{\kappa^1\text{-}P(CH_2CH_2PPh_2)_3\}_2]$.

5.5 X-Ray Crystallographic Data

Table 5.2 – X-ray crystallographic data[a]

Compound	$[SnF_3(PMe_3)_2(OTf)]$	$[Sn(PMe_3)_2(OTf)_2]$	$Sn_3F_5(OTf)$	$[SnF_4\{\kappa^2\text{-}CH_3C(CH_2PPh_2)_3\}]$
Formula	$C_7H_{18}F_6O_3P_2SSn$	$C_8H_{18}F_6O_6P_2S_2Sn$	$CF_8O_3SSn_3$	$C_{41}H_{39}F_4P_3Sn$
M	476.90	568.97	600.14	819.32
Crystal system	orthorhombic	monoclinic	monoclinic	monoclinic
Space group (no.)	Pbca (61)	$P2_1/n$ (14)	$P2_1/n$ (14)	$P2_1/n$ (14)
a /Å	11.4007(2)	12.9043(3)	13.4971(4)	13.8624(2)
b /Å	11.84650(10)	10.9889(3)	7.6953(2)	12.9086(2)
c /Å	23.9749(3)	15.1867(6)	10.7894(30	20.5379(4)
α /°	90	90	90	90
β /°	90	110.338(3)	97.810(2)	98.7350(17)
γ /°	90	90	90	90
U /Å^3	3238.01(7)	2019.27(11)	1110.24(5)	3632.50(11)
Z	8	4	4	4
μ(Mo-K_α) /mm^{-1}	1.967	1.704	6.983	0.886
F(000)	1872	1120	1072	1664
Total number reflns	85205	15141	29342	59518
R_{int}	0.079	0.049	0.122	0.044
Unique reflns	5553	6008	3642	11707
No. of params, restraints	187, 0	232, 0	145, 0	443, 0
GOF	1.014	1.052	1.030	1.035
R_1, wR_2 $[I > 2\sigma(I)]$[b]	0.024, 0.052	0.043, 0.098	0.036, 0.075	0.033, 0.072
R_1, wR_2 (all data)	0.031, 0.055	0.061, 0.103	0.052, 0.080	0.048, 0.077

[a] Common items: T = 100 K; wavelength (Mo-K_α) = 0.71073 Å; θ(max) = 27.5°; [b] $R1 = \Sigma||F_o|-|F_c||/\Sigma|F_o|$; $wR_2=[\Sigma w(F_o^2-F_c^2)_2/\Sigma wF_o^4]^{1/2}$

CCDC Numbers: $[SnF_3(PMe_3)_2(OTf)]$ (2104492), $[Sn(PMe_3)_2(OTf)_2]$ (2104490), $Sn_3F_5(OTf)$ (2104491), $[SnF_4\{\kappa^2\text{-}CH_3C(CH_2PPh_2)_3\}]$ (2104493)

5.6 Experimental

$[SnF_4(PMe_3)_2]$[4] and $[SnF_4(C_6H_4\{PMe_2\})]$[4] were made by literature methods; the identity and purity of the products were determined by NMR spectroscopy comparing with published literature data. Refer to appendix A for sources of reagents, drying of solvents, instrument specifications and standard references for NMR.

$[SnF_3(PMe_3)_2(OTf)]$: To a solution of $[SnF_4(PMe_3)_2]$ (0.100 g, 0.29 mmol) in CH_2Cl_2 (2 mL) a solution of TMSOTf (0.064 g, 0.29 mmol) in CH_2Cl_2 (2 mL) was added dropwise to form a clear solution. The reaction was stirred for 2 h, the volatiles were then removed *in vacuo* to leave a solid, which was washed with hexane (3 x 10 mL) and dried *in vacuo* to form a white powder. Crystals suitable for single crystal X-ray diffraction were made by layering a CH_2Cl_2 solution of the complex with hexane. Yield 0.083 g (60%). Required for $C_7H_{18}F_6P_2S_2Sn$ (476.91): C, 17.6; H, 3.8. Found: C, 17.5; H, 4.2%. IR (Nujol/cm^{-1}): ν = 517m, 546m, 573m (Sn-F), 1156 (-OSO_2), 1224, 1261 (CF_3). ^{1}H NMR (CD_2Cl_2, 298 K): δ = 1.70 (d, $^2J_{PH}$ = 12 Hz, CH_3). ^{19}F{^{1}H} NMR (CD_2Cl_2, 298 K): δ =-149.2 (br s, SnF), -126.9 (br s, SnF), -78.8 (s, OTf); (183 K): δ = -151.4 (tt, $^2J_{P\text{-}F(trans\text{-}OTf)}$ =121 Hz, $^2J_{FF}$ = 41, $^1J_{119SnF}$ = 3013 Hz, $^1J_{117SnF}$ = 2893 Hz, [1F], $SnF_{trans\text{-}OTf}$), -127.9 (td, $^2J_{PF(cis\text{-}OTf)}$ = 153 Hz, $^2J_{FF}$ = 41 Hz, $^1J_{119SnF}$ = 3253 Hz, $^1J_{117SnF}$ = 3108 Hz, [2F], $SnF_{cis\text{-}OTf}$), -78.5 (s, [3F], OTf). ^{31}P{^{1}H} NMR (CH_2Cl_2, 298 K): δ = -6.01 (s); (183 K): δ = -3.2 (td, $^2J_{PF(cis\text{-}OTf)}$ = 153 Hz; $^2J_{PF(trans\text{-}OTf)}$ = 121 Hz; $^1J_{119SnP}$ = 3412 Hz; $^1J_{117SnP}$ = 3263). ^{119}Sn NMR (CH_2Cl_2, 183 K): δ = -599.9 (m).

$[SnF_2(PMe_3)_2(OTf)_2]$: To a solution of $[SnF_4(PMe_3)_2]$ (0.100 g, 0.29 mmol) in CH_2Cl_2 (2 mL) a solution of TMSOTf (0.128 g, 0.58 mmol) in CH_2Cl_2 (2 mL) was added dropwise to form a clear solution. The reaction was stirred for 2 h. The volatiles were then removed *in vacuo* to leave a solid, which was washed with hexane (3 x 10 mL) and dried *in vacuo* to form a white powder. Yield 0.103 g (59%). Required for $C_8H_{18}F_8O_6P_2S_2Sn$ (606.98): C, 15.8; H, 3.0. Found: C, 15.7; H, 3.6%. IR (Nujol/cm^{-1}): ν = 531 (s) (Sn-F). ^{1}H NMR (CD_2Cl_2, 298 K): δ = 1.88 (d, $^2J_{PH}$ = 12 Hz, CH_3). ^{19}F{^{1}H} NMR (CD_2Cl_2, 298 K): δ = -140 (br s, [2F], SnF), -78.0 (s, [6F], OTf); (183 K): δ = -142.7 (t, $^2J_{P\text{-}}$ = 107 Hz, $^1J_{119SnF}$ = 3393 Hz, $^1J_{117SnF}$ = 3232, [2F], SnF), -78.4 (OTf), -77.8 (OTf, sum of OTf resonances [6F]). ^{31}P{^{1}H} NMR (CH_2Cl_2, 298 K): δ = 7.3 (br); (183 K): δ = 10.2 (t, $^2J_{PF}$ 107 Hz; $^1J_{119SnP}$ = 3654 Hz; $^1J_{117SnP}$ = 3484). ^{119}Sn NMR (CH_2Cl_2, 183 K): δ = -609 (tt, $^1J_{119SnP}$ = 3654 Hz, $^1J_{119SnF}$ = 3393 Hz).

[SnF(PMe$_3$)$_2$(OTf)$_3$]: To a solution of [SnF$_4$(PMe$_3$)$_2$] (0.100 g, 0.29 mmol) in CH_2Cl_2 (2 mL) a solution of TMSOTf (0.192 g, 0.86 mmol) in CH_2Cl_2 (2 mL) was added dropwise to form a clear solution. The reaction was stirred for 10 mins., the volatiles were then removed *in vacuo* to leave a solid, which was washed with hexane (3 x 10 mL) and dried *in vacuo* to form a white powder. Yield 0.137 g (64%). Required for $C_9H_{18}F_{10}O_9P_2S_3Sn$ (737.07): C, 14.7; H, 2.6. Found: C, 14.3; H, 3.7%. IR (Nujol/cm^{-1}): *v* = 510m (Sn-F), 1158m, 1164m (-OSO_2), 1191m, 1202m, 1237m, 1243m (CF_3). ^{1}H NMR (CD_2Cl_2, 298 K): δ = 2.0 (d, $^2J_{PH}$ = 13 Hz, CH_3). ^{19}F{^{1}H} NMR (CD_2Cl_2, 298 K): δ = -132.9 (t, $^2J_{PF}$ = 88 Hz, $^1J_{119SnF}$ = 3557 Hz, $^1J_{117SnF}$ = 3396 Hz, [1F], SnF), -77.6 (s, [9F], OTf). ^{31}P{^{1}H} NMR (CD_2Cl_2, 298 K): δ = 18.3 (d, $^2J_{PF}$ = 88 Hz, $^1J_{119SnP}$ = 3740 Hz; $^1J_{117SnP}$ = 3568 Hz). ^{119}Sn NMR (CH_2Cl_2, 183 K): δ = -617 (m).

[SnF$_4$(P^{i}Pr$_3$)$_2$]: To a suspension of [SnF$_4$(MeCN)$_2$] (0.648 g, 2.34 mmol) in CH_2Cl_2 (5 mL) a solution of P^{i}Pr$_3$ (0.750 g, 4.68 mmol) in CH_2Cl_2 was added to form a slightly cloudy solution. The reaction was stirred for 1 h, then the solution was filtered and the filtrate was concentrated *in vacuo* to yield a white solid, which was washed with hexane (3 x 10 mL) and dried *in vacuo*. Yield: 0.862 g (71%). $C_{18}H_{42}F_4P_2Sn{\cdot}3/4CH_2Cl_2$ (578.84): C, 38.9; H, 7.6. Found: C, 38.8 H, 8.1%. IR (Nujol/cm^{-1}): *v* = 535s (Sn-F). ^{1}H NMR (CD_2Cl_2, 298 K): δ = 1.41 (dd, $^3J_{PH}$ = 15Hz, $^3J_{HH}$ = 7 Hz, [18H], CH_3), 2.55 (septet of d, $^3J_{HH}$ = 7 Hz, $^2J_{PH}$ = 1 Hz, [3H], CH), ^{19}F{^{1}H} NMR (CD_2Cl_2, 298 K): δ = -99.1 (t, $^2J_{PF}$ = 124 Hz, $^1J_{119SnF}$ = 2920 Hz, $^1J_{117SnF}$ = 2792 Hz), ^{31}P{^{1}H} NMR (CD_2Cl_2, 298 K): δ = 30.6 (quint, $^2J_{PF}$ = 124, $^1J_{119SnP}$ = 2477 Hz, $^1J_{117SnP}$ = 2363 Hz). ^{119}Sn NMR (CH_2Cl_2, 183 K): δ = -622.0 (quin of t, $^1J_{119SnF}$ = 2920 Hz ,$^1J_{117SnP}$ = 2477 Hz).

[SnF$_3$(P^{i}Pr$_3$)$_2$(OTf)]: To a solution of [SnF$_4$(P^{i}Pr$_3$)$_2$] (0.100 g, 0.19 mmol) in CH_2Cl_2 (2 mL) a solution of TMSOTf (0.043 g, 0.19 mmol) was added dropwise to form a clear solution. The reaction was stirred for 1 h, volatiles were then removed *in vacuo* to yield a white solid, which was washed with hexane (3 x 10 mL) and dried *in vacuo*. Yield: 0.095 g (76%). Required for $C_{19}H_{42}F_6O_3P_2S{\cdot}1/2CH_2Cl_2$ (718.68): C, 32.6; H, 6.0. Found: C, 32.1; H, 6.7%. IR (Nujol/cm^{-1}): *v* = 540m, 558m, 571m (Sn-F). 1150m (-OSO_2) 1223, 1260 (CF_3). ^{1}H NMR (CD_2Cl_2, 298 K): δ = 1.45 (dd, $^3J_{PH}$ = 15Hz, $^3J_{HH}$ = 7 Hz, [18H], CH_3), 2.77 (septet of d, $^3J_{HH}$ = 7 Hz, $^2J_{PH}$ = 2 Hz, [3H], CH), ^{19}F{^{1}H} NMR (CD_2Cl_2, 298 K): δ = -116.9 (br s, $^1J_{SnF}$ = 3244 Hz, SnF), -78.5 (s, OTf), -73.5 (br s, $^1J_{SnF}$ = 3518 Hz, SnF). ^{31}P{^{1}H} NMR (CH_2Cl_2, 298 K): δ = 38.2 (q, $^2J_{PF}$ = 121 Hz, $^1J_{119SnP}$ = 2827 Hz, $^1J_{117SnP}$ = 2702 Hz), ^{119}Sn NMR (CH_2Cl_2, 183 K): -611.1 (tdt, $^1J_{119SnF}$ = 3558, 3200 Hz, $^1J_{119SnP}$ = 2856 Hz).

[$SnF_2(P^iPr_3)_2(OTf)_2$]: To a solution of [$SnF_4(P^iPr_3)_2$] (0.200 g, 0.39 mmol) in CH_2Cl_2 (2 mL) a solution of TMSOTf (0.173 g, 0.78 mmol) was added dropwise to form a clear solution. The reaction was stirred for 1hr, volatiles were removed *in vacuo* to yield a white solid which was washed with hexane (3 x 10 mL) and dried *in vacuo*. Yield: 0.231 g (77%). Required for $C_{20}H_{42}F_8O_6P_2S_2Sn{\cdot}CH_2Cl_2$ (860.20): C, 29.3; H, 5.2. Found: C, 29.1; H, 5.8%. IR (Nujol/cm^{-1}): *v* = 519w, 533w (Sn-F), 1150 (OSO_2), 1234w, 1261w (CF_3). ^{1}H NMR (CD_2Cl_2, 298 K): 1.49 (dd, $^3J_{PH}$ = 16Hz [8H], CH_3), 3.05 (septet of d, $^3J_{HH}$ = 8 Hz, $^2J_{PH}$ = 3 Hz, [3H], CH). ^{19}F{^{1}H} NMR (CD_2Cl_2, 298 K): -77.9 (s, OTf), -56.9 (br, $^1J_{SnF}$ = 4082 Hz). ^{31}P{^{1}H} NMR (CH_2Cl_2, 298 K): 49.4 (t, $^2J_{PF}$ = 117 Hz, $^1J_{119SnP}$ = 2971 Hz, $^1J_{117SnP}$ = 2839 Hz), ^{119}Sn NMR (CH_2Cl_2, 183 K): -630 (tt, $^1J_{119SnF}$ = 4013, $^1J_{119SnP}$ = 2941).

[$SnF_4\{\kappa^2$-$CH_3(CH_2PPh_2)_3\}$)]: To a suspension of [$SnF_4(MeCN)_2$] (0.200 g, 0.72 mmol) in CH_2Cl_2 (2 mL), triphos (0.451 g, 0.72 mmol) was added as a solid and the resulting solution was stirred for 2 h to yield a cloudy solution, which was then filtered. Volatiles were removed from the filtrate *in vacuo* to yield a white solid, which was washed with hexane (3 x 10 mL) and dried *in vacuo*. Crystals suitable for single crystal X-ray diffraction could be grown by layering a CH_2Cl_2 solution of the complex with hexane. Yield: 0.326 g (55%). Required for $C_{41}H_{39}F_4P_3Sn{\cdot}1/2CH_2Cl_2$ (861.78): C, 57.8; H, 4.7. Found: C, 58.2 H, 4.8%. IR (Nujol/cm^{-1}): *v* = 516m, 552m, 564m (Sn-F).^{1}H NMR (CD_2Cl_2, 298 K): δ = 0.87 (s, [3H], CH_3), 2.28 (s, [2H]), 2.91-2.95 (m, [2H]), 3.11 (m, [2H]), 7.1-8.1 (m, [30H], ArH). ^{19}F{^{1}H} NMR (CD_2Cl_2, 298 K): δ = -144.2 (tt, $^2J_{PF}$ = 98 Hz, $^2J_{FF}$ = 45, [2F], SnF), -109.7 (m, [2F], SnF). ^{31}P{^{1}H} NMR (CD_2Cl_2, 298 K): δ = -6.9 (dtd, $^2J_{PF}$ = 121, 98, 51, [2P]), -27.1 (s, [1P]).^{119}Sn NMR (CH_2Cl_2, 183 K): δ = -681.4 (m).

Reaction of [$SnF_4(MeCN)_2$] with $P(CH_2CH_2PPh_2)_3$

To a suspension of [$SnF_4(MeCN)_2$] (0.200 g, 0.72 mmol) in CH_2Cl_2 (2 mL) , $P(CH_2CH_2PPh_2)_3$ (0.485, 0.72 mmol) was added as a solid and the resulting solution was stirred for 2 h to yield a clear colourless solution. Volatiles were removed *in vacuo* to yield a white solid, which was washed with hexane (3 x 10 mL) and dried *in vacuo.* Yield: 0.254 g. Required for $C_{42}H_{42}F_4P_4Sn{\cdot}1/2\ CH_2Cl_2$ (907.79)): C, 56.2; H, 4.8. Found: C, 56.4 H, 5.0%. IR (Nujol/cm^{-1}): *v* = 508m, 541m, 564m (Sn-F). ^{1}H NMR (CD_2Cl_2, 298 K): δ = 1.43-2.50 (br, [12H], CH_2), 7.27-7.39 (br, [30H], ArH); ^{19}F{^{1}H} NMR (CD_2Cl_2, 298 K): -114.3(br m, [2F], SnF), -149.4 (br m, [2F], SnF); (183 K): -115.0 (t, $^2J_{PF}$ = 133 Hz, SnF)*, -118.7 (m, [2F], SnF)^, -146.3 (m, [1F])^, -148.2(m, [1F])^ (* minor product, ^ major product); ^{31}P{^{1}H} NMR (CD_2Cl_2, 298 K): δ = -12.2-14.0 (ill defined multiplets); (CD_2Cl_2, 183 K): δ = -16.8 (m), -12.13 (m), -7.05 (m), 11.0 (m), 10.1 (m).

Reaction of [SnF_4{*o*-$C_6H_4(PMe_2)_2$}] with TMSOTf

To a suspension of [SnF_4{*o*-$C_6H_4(PMe_2)_2$}] (0.100 g, 0.26 mmol) in CH_2Cl_2, TMSOTf (0.057 g, 0.26 mmol) was added as a solution in CH_2Cl_2 (2 mL) the resulting cloudy mixture was stirred for 2 hr, volatiles were removed in vacuo and the solid washed with hexane (3 x 10 mL) and dried in vacuo to yield a white solid. Yield: 0.102 g. ^{1}H NMR (CD_2Cl_2, 298 K): δ = 1.93 (m, [12H], CH_2), 7.80 (m, [12H], ArH); ^{19}F{^{1}H} NMR (CD_2Cl_2, 298 K): -78.5 (s, OTf) ^{31}P{^{1}H} (CD_2Cl_2, 298 K): δ = -18.0 (s, $^1J_{119SnP}$ = 1879 Hz, $^1J_{117Sn\text{-}31P}$ = 1792 Hz). (resonances correspond to [Sn{$C_6H_4(PMe_2)_2$}][OTf]$_2$ the only identifiable product)

5.7 References

1 W. Levason, F. M. Monzittu and G. Reid, Coord. Chem. Rev., 2019, 391, 90–130.

2 S. L. Benjamin, W. Levason and G. Reid, Chem. Soc. Rev., 2013, 42, 1460–1499.

3 A. D. Adley, P. H. Bird, A. R. Fraser and M. Onyszchuk, Inorg. Chem., 1972, 11, 1402–1409.

4 M. F. Davis, M. Clarke, W. Levason, G. Reid and M. Webster, Eur. J. Inorg. Chem., 2006, 14, 2773–2782.

5 M. F. Davis, W. Levason, G. Reid and M. Webster, Polyhedron, 2006, 25, 930–936.

6 M. A. Sanhoury, M. T. Ben Dhia and M. R. Khaddar, J. Fluorine Chem., 2011, 132, 865–869.

7 M. F. Davis, W. Levason, G. Reid, M. Webster and W. Zhang, Dalton Trans., 2008, 533–538.

8 C. Gurnani, A. L. Hector, E. Jager, W. Levason, D. Pugh and G. Reid, Dalton Trans., 2013, 42, 8364–8374.

9 J. M. Blackwell, W. E. Piers and R. McDonald, J. Am. Chem. Soc., 2002, 124, 1295–1306.

10 A. Kavoosi and E. Fillion, Angew. Chem. Int. Ed., 2015, 54, 5488–5492.

11 R. E. Marsh, Acta Crystallogr. Sect. B Struct. Sci., 2009, 65, 782–783.

12 W. Plass, J. Pinkas and J. G. Verkade, Inorg. Chem., 1997, 36, 1973–1978.

13 G. Douglas, M. C. Jennings, L. Manojlović-Muir, K. W. Muir and R. J. Puddephatt, J. Chem. Soc., Chem. Commun., 1989, 159–161.

14 C. Beattie, P. Farina, W. Levason and G. Reid, Dalton Trans., 2013, 42, 15183–15190.

15 R. Suter, A. Swidan, H. S. Zijlstra, C. L. B. Macdonald, J. S. McIndoe and N. Burford, Dalton Trans., 2018, 47, 16729–16736.

16 E. MacDonald, PhD Thesis, Dalhousie University, Halifax Canada, 2013.

17 C. A. Tolman, Chem. Rev., 1977, 77, 313–348.

18 H. J. Hogben, M. Krzystyniak, G. T. P. Charnock, P. J. Hore and I. Kuprov, J. Magn. Reson., 2011, 208, 179–194.

19 P. A. W. Dean, D. D. Phillips and L. Polensek, Can. J. Chem., 1981, 59, 50–61.

20 L. Apostolico, G. Kociok-Köhn, K. C. Molloy, C. S. Blackman, C. J. Carmalt and I. P. Parkin, Dalton Trans., 2009, 10486–10494.

Chapter 6 Synthesis, properties and electronic structure of neutral and cationic phosphine complexes of silicon(IV) halides

6.1 Introduction

6.1.1 Silicon halide phosphine complexes

As group 14 is descended the reorganisation energy required to distort the tetrahedral MX_4 unit into either a D_{4h} geometry (required for *trans* complexes) or a C_{2v} geometry (required for *cis* complexes) decreases therefore it is significantly easier to distort $SnCl_4$ compared to $SiCl_4$. The strength of metal-ligand interactions also decrease as the halides get heavier, which would suggest that tin fluoride complexes would be the most stable and silicon iodide would be the least stable.[1] Therefore it is imperative to see what the limits are for silicon halide coordination chemistry with phosphine ligands.

There have been few experimental studies on phosphine complexes of silicon tetrahalides in the literature. The first studies in the 1960s claimed to report monodentate phosphine adducts of $SiCl_4$ and $SiBr_4$; the complexes were characterised by partial microanalysis (halide content). However, this report was not reproducible, and it was suggested that they were likely to be phosphine oxide adducts rather than the intended phosphine adducts.[2,3] Later, it was demonstrated that the complexes $[SiX_4(PMe_3)_2]$ (X = Cl, Br) form instead, with IR data and a low-quality crystal structure (for the chloride) indicating that the *trans*-octahedral complex forms.[4,5] More recently, a higher quality crystal structure of $[SiCl_4(PMe_3)_2]$ has been determined, as well as the structure of $[SiBr_4(PMe_3)_2]$, demonstrating that they both have the expected *trans*-octahedral phosphine coordination (**Figure 6.1**).[6] The lack of evidence of adduct formation between SiF_4 and phosphine ligands in solution has been attributed to the energy cost associated with rearranging the tetrahedral SiF_4 unit into the geometry required for the target octahedral product; however, there is tensiometric titration evidence of the formation of a 1:1 and 1:2 adducts of SiF_4 and PMe_3 under solvent-free conditions at -78 ˚C .[5] There have been

no reports in the literature of phosphine adduct formation with the weakly Lewis acidic SiI_4.[6]

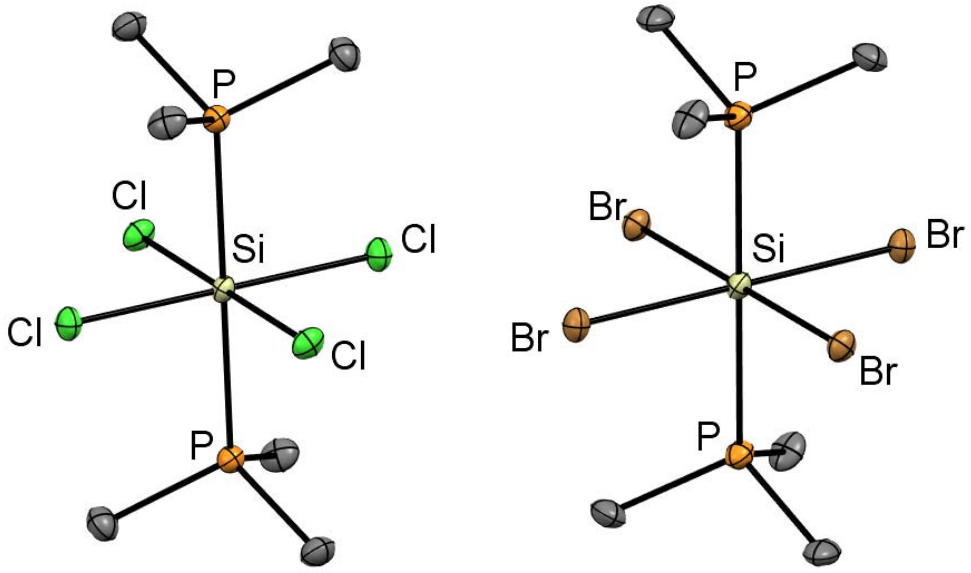

(a) (b)

Figure 6.1 – Crystal structures of (a) $[SiCl_4(PMe_3)_2]$ and (b) $[SiBr_4(PMe_3)_2]$. Both redrawn from Ref. 6.

Diphosphines (*o*-$C_6H_4(PMe_2)_2$ and $R_2P(CH_2)_2PR_2$ (R = Me, Et)) also react with $SiCl_4$ and $SiBr_4$ to form stable complexes; in most cases the expected *cis* coordination is observed, similar to the tin analogues. However, similar to germanium, but unlike the tin analogues, they do not form complexes with bidentate arsine ligands.[6] The reaction of $SiCl_4$ with the methylene-linked $Me_2PCH_2PMe_2$ leads to the formation of *trans*-$[SiCl_4(\kappa^1\text{-}Me_2PCH_2PMe_2)_2]$, irrespective of the ratio used; the different reactivity of this ligand compared to other bidentate phosphine ligands is no doubt due to the small bite angle of this ligand (forming a four-membered ring), which precludes bidentate ligand coordination; the structure of this complex is shown in **Figure 6.2** below.[6]

Dispite significant efforts, the reaction of $[SiCl_4(L)_2]$ with common reducing agents (C_8K, K, sodium naphthalide, $[(DiPPNacNac)Mg]_2$]) did not lead to the isolation of Si(II) phosphine adducts. Computational work does suggest that Si(II) phosphine adducts should be stable species (ΔG = -56.1 kJ mol^{-1} for $[SiCl_2(PMe_3)]$), and they are predicted to be even more stable than the Si(IV) adducts, which have already been synthesised,[6] but were predicted to be of borderline stability.[7]

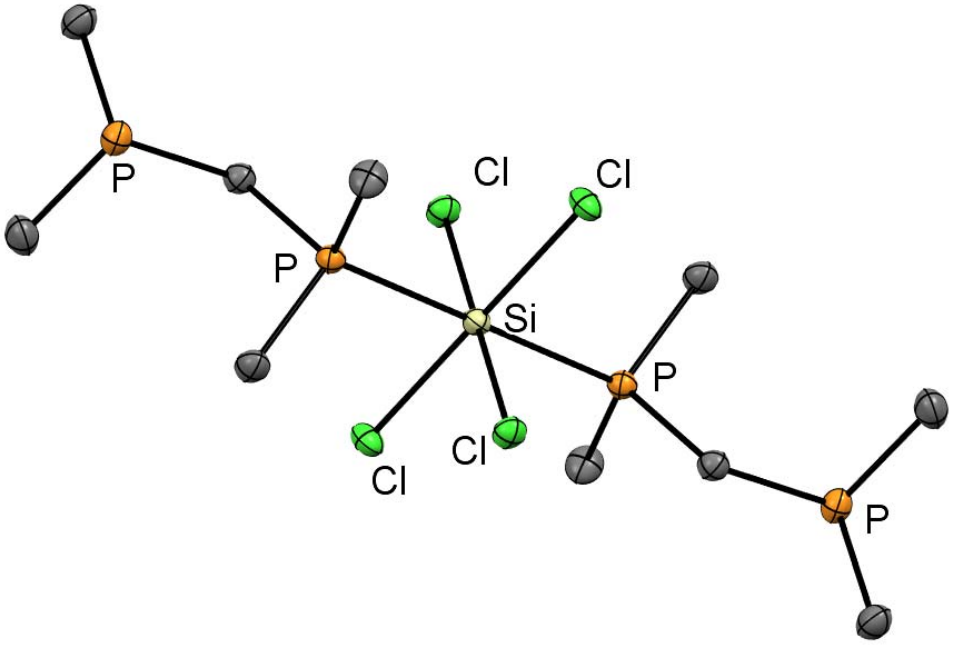

Figure 6.2 – Structure of $[SiCl_4(\kappa^1\text{-}Me_2PCH_2PMe_2)_2]$. Redrawn from Ref. 6.

The ionic compound $[SiCl_3(PMe_3)_2][ClO_4]$ was reported by Ozin in the 1960s, and can be formed from two different preparations, one by the reaction of $AgClO_4$ with $SiICl_3$ in benzene, followed by the separation of $[SiCl_3][ClO_4]$ from the precipitated AgI, followed by the distillation of two equivalents of PMe_3 into the reaction solution to form the product as a white solid. The second method is by reacting $[SiCl_3(NMe_3)_2][ClO_4]$ with two equivalents of PMe_3 in MeCN. The authors reported that this complex was characterised by partial microanalysis (halide content) and IR spectroscopy; however, the IR data were not reported in the paper, hence the evidence for this species is limited and very little is known about its properties.[5]

6.1.2 Cationic silicon halide complexes

The only known cationic silicon halide phosphine complex is $[SiCl_3(PMe_3)_2]^+$, isolated as discussed above, as its perchlorate salt. In contrast, there are many examples of carbene stabilised cationic silicon halide complexes. The reaction of NHC_1 (NHC_1 = 1,3-dimethylimidazolidin-2-ylidene) with $SiCl_4$ leads to the formation of the 1:1 adduct $[SiCl_4(NHC_1)]$. Two equivalents of this adduct can react with the electron-deficient silane,

$H_2Si(C_2F_5)_2$, to generate $[SiCl_2H(NHC_1)_2][SiCl_3(C_2F_5)_2]$. The cation in this complex is trigonal bipyramidal, with two NHC_1 ligands and a hydride in the equatorial positions and the two halides in the axial positions.[8] The reaction of $[SiCl_4(NHC_1)]$ with BCl_3 leads to the formation of the salt, $[SiCl_3(NHC_1)][BCl_4]$, containing a tetracoordinate silicon-based monocation. This can then be reacted with a further equivalent of $[SiCl_4(NHC_1)]$ to form $[SiCl_3(NHC_1)_2][BCl_4]$; here the $[SiCl_4(NHC_1)]$ acts as a carbene transfer reagent, with $SiCl_4$ as the by-product. In the $[SiCl_3(HNC_1)_2]^+$ cation, the carbenes occupy two of the equatorial positions, the third is taken up by a chloride, with the other two chlorides axial.[9]

The reaction of the heavier silicon tetrahalides with NHC_2 (NHC_2 = 1,2-bis(2,6-diisopropylphenyl)imidazole-2-ylidene) leads to the displacement of one of the halides from the silicon centre to form the salts $[SiX_3(NHC_2)][X]$ (X = Br, I) (see **Figure 6.4**). Remarkably, in the case of the bromide and iodide salts, they can be reduced with KC_8 to form the neutral Si(II) species $[SiX_2(NHC_2)]$, and are very rare examples of a monomeric Si(II) complexes. $[SiI_2(NHC_2)]$ can be reacted further in fluorobenzene with 3 equivalents of NHC_3 (NHC_3 = 1,3,4,5-tetramethyl-imidazol-2-ylidene) to form $[Si(NHC_3)_3][I]_2$ featuring a very unusual Si(II) dication (see **Figure 6.4**).[10] Structures of the various carbenes described in this chapter are shown in **Figure 6.3** below.

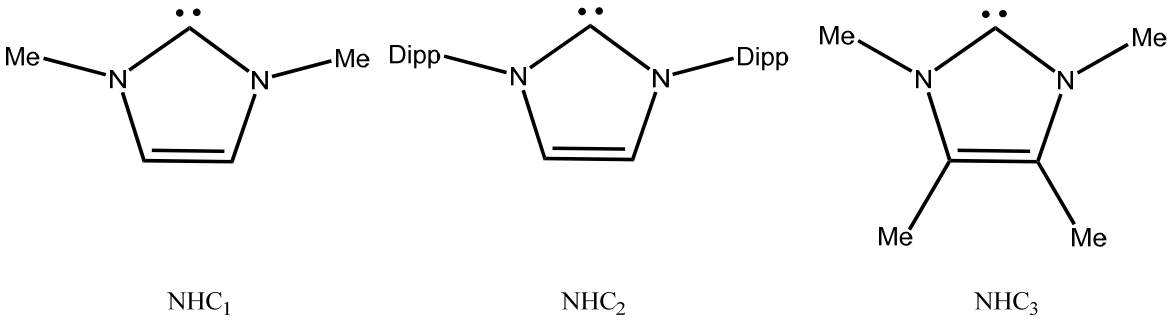

Figure 6.3 – Structures of the NHCs described in this chapter.

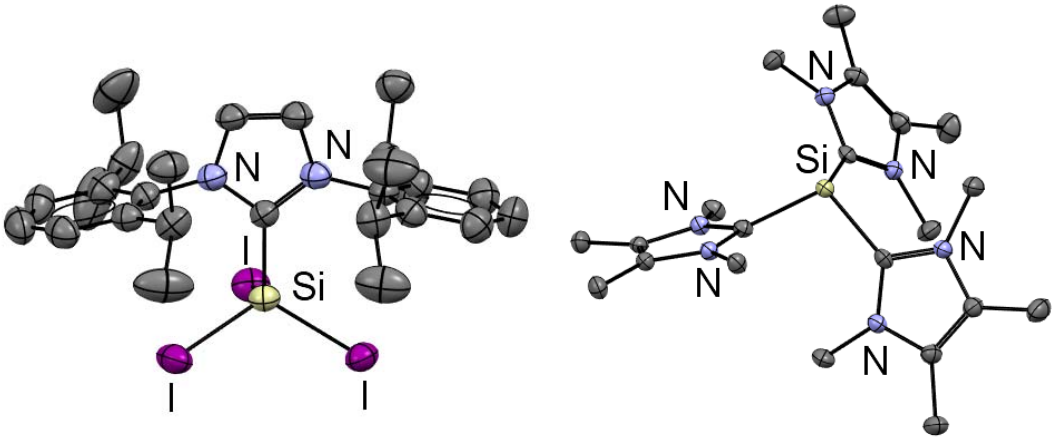

(a) (b)

Figure 6.4 – The structures of (a) the cation in $[SiI_3(NHC_2)][I]$ and (b) the dication in $[Si(NHC_3)_3][I]_2$ the iodide anions are removed for clarity.. Both redrawn from Ref. 8.

Cationic silicon(IV) halide complexes with N-donor ligands have been long known, although they remain quite few in number. The complex $[Si(bipy)_3]I_4$ can be synthesised by the reaction of SiI_4 with three equivalents of bipy; this compound features a tetracationic silicon species where all the halides have been displaced. Formation of the cation in this case is presumably driven by the weakness of the Si-I bond.[11] Reaction of nitrogen donor ligands with other silicon(IV) halides can also lead to the formation of cationic complexes. The reaction of the mixed halide $SiCl_2Br_2$ or $SiCl_4$ with the *N*-methylimidazole (NMI) leads to the displacement of two of the halides to form the salts, $[SiCl_2(NMI)_4]X_2$ (X= Cl, Br); these feature six-coordinate distorted octahedral silicon centres where the NMI ligands all lie in a plane.[12]

The reaction of the triamine ligand, pmdta, with $SiCl_4$ and $Na[BAr^F]$ in toluene leads to the formation of the complex $[SiCl_3(pmdta)][BAr^F]$, which features a *mer* coordinated triamine (see **Figure 6.5** (a)). Similarly, the reaction of the tridentate macrocyclic ligand, Me_3tacn, with $SiCl_4$ leads to the displacement of one of the chlorides to form the salt *fac*-$[SiCl_3(Me_3tacn)]Cl$ as one of the products, although through this route a clean sample could not be obtained. However, if $SiCl_4$, TMSOTf, and Me_3tacn are reacted in a 1:1:1 ratio in CH_2Cl_2, then the pure complex $[SiCl_3(Me_3tacn)][OTf]$ can be isolated. In these salts, the triaza macrocycle is *fac* coordinated (see **Figure 6.5** (b)).[13]

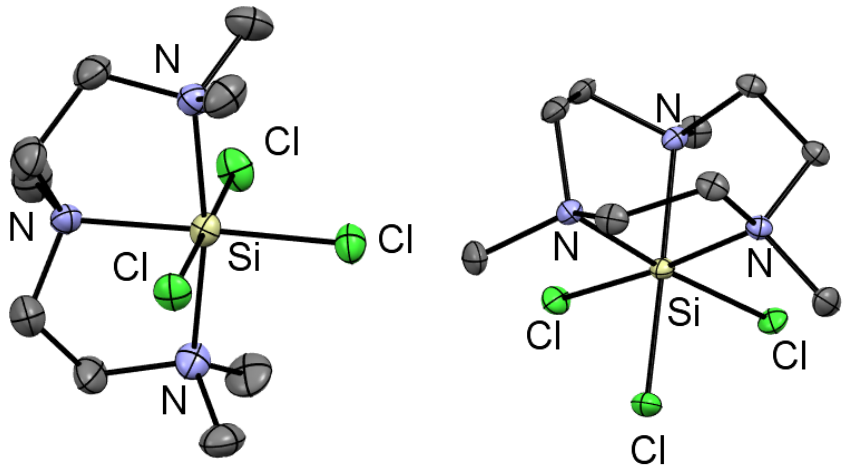

(a) (b)

Figure 6.5 – Crystal structures of the cations (a) $[SiCl_3(pmdta)]^+$ and (b) $[SiCl_3(Me_3tacn)]^+$. Both redrawn from Ref. 11.

Halide displacement by neutral N-donor ligands can also be extended to SiF_4, which is surprising considering Si-F bonds are the strongest single bonds of any group 14 halide (see section 1.4). The reaction of SiF_4 with Me_3tacn in toluene or CH_2Cl_2 leads to the formation of $[SiF_3(Me_3tacn)][SiF_5]$; the cation exhibits a sharp resonance at δ = -147.6 with ^{29}Si satellites ($^1J_{SiF}$ = 208 Hz) in the $^{19}F\{^1H\}$ NMR spectrum. Anion metathesis with $Na[BAr^F]$ leads to the clean isolation of $[SiF_3(Me_3tacn)][BAr^F]$. The reaction of SiF_4 with the acyclic di- or tri-amine, tmeda (N,N,N',N'-tetramethyl-1.2-diaminoethane) or pmdta, however, leads to κ^2-coordinated complexes with no fluoride displacement. Clearly, in these systems, the additional stabilising effect of the macrocycle is needed to liberate the fluoride.

Neutral O-donor ligands can also be used to generate silicon(IV) halide cations. The reaction of HMPA (hexamethylphosphoramide) with $SiCl_4$ leads to the formation of $[SiCl_3(HMPA)_2]Cl$, *trans*-$[SiCl_4(HMPA)_2]$, or *fac/mer*-$[SiCl_3(HMPA)_3]Cl$ depending on the ratio of $SiCl_4$:HMPA. This system was studied by both $^{31}P\{^1H\}$ and ^{29}Si NMR spectroscopy, as well as by X-ray crystallography. The ^{29}Si NMR spectral parameters for the various species are shown in **Table 6.1** below; it can be seen that the five-coordinate $[SiCl_3(HMPA)_2]^+$ cation has a much less negative chemical shift compared to both the

neutral six-coordinate complex and the two six-coordinate cations. $[SiCl_4(HMPA)_2]$ and *mer*-$[SiCl_3(HMPA)_3]Cl$ have also been structurally characterised.[14]

Table 6.1 – Selected NMR spectroscopic data for silicon chloride HMPA complexes.[14]

Complex	^{29}Si/ppm	$^2J_{SiP}$/Hz
$[SiCl_3(HMPA)_2]Cl$	-120.5	15
trans-$[SiCl_4(HMPA)_2]$	-205.5	9.7
mer-$[SiCl_3(HMPA)_3]Cl$	-206	-
fac-$[SiCl_3(HMPA)_3]Cl$	-210	5

6.2 Aims

The aim of this chapter is to develop the chemistry of silicon halides with phosphine ligands. With a focus on expanding the known chemistry to include silicon iodide and towards the generation of cationic complexes through halide abstraction.

6.3 Results and discussion

6.3.1 Reactions of silicon(IV) halides with phosphine ligands

This chapter invesigates the reactivty of phosphine ligands with silicon halides, with the main aim of generating phosphine-stabilised silicon-centred cations, which are rare. As part of this study, the complexes $[SiCl_4(PMe_3)_2]$ and $[SiBr_4(PMe_3)_2]$ were prepared according to literature procedures.[6] NMR data for these complexes match closely with the reported data. Previously, no ^{29}Si NMR resonances could be obtained for these complexes due to the reactivity of the complexes with the relaxation agents used which were either TEMPO or $[Cr(acac)_3]$. However, the bulkier relaxation agent tris(2,2,6,6-tetramethyl-3,5-heptanedionato)chromium(III), which has been used previously with the $SiCl_4$/HMPA systems discussed in section 6.1.2,[14] was found not to react with these complexes on the timescale necessary for NMR spectral acquisition and hence ^{29}Si NMR spectra could be recorded. For the complex $[SiCl_4(PMe_3)_2]$ in CD_2Cl_2, a triplet is seen in the ^{29}Si NMR spectrum (**Figure 6.6**) at δ = -210 ($^1J_{SiP}$ = 266 Hz), which is to low frequency of $SiCl_4$ (δ = -20 in C_6F_6)[15] and is consistent with the *trans*-octahedral geometry seen in the solid state being retained in solution. A triplet is also seen in the ^{29}Si NMR spectrum of

the bromo analogue, $[SiBr_4(PMe_3)_2]$ (δ = -284 $^1J_{SiP}$ = 227 Hz), with $\Delta\delta$ = -192 from $SiBr_4$. Large low-frequency shifts are also seen in the ^{119}Sn NMR spectra of the analogous tin(IV) halide complexes.[16]

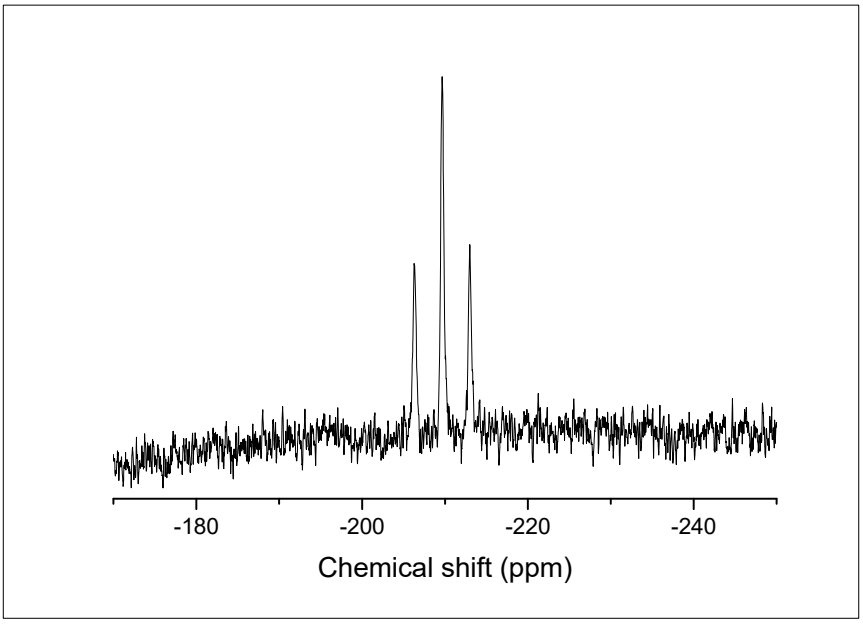

Figure 6.6 – ^{29}Si NMR spectrum of $[SiCl_4(PMe_3)_2]$ at 183 K in CD_2Cl_2.

Previously, it was shown that SiI_4 had no reactivity with phosphines in CH_2Cl_2 solution.[6] However, if two equivalents of PMe_3 are added to SiI_4 dissolved in a hydrocarbon solvent (see Scheme 6.1 below), precipitation of a yellow product occurs immediately. In the ^{1}H NMR spectrum of this solid, there is a broad singlet at δ = 1.66, which is +0.77 ppm from PMe_3 itself, indicating ligand coordination. In the $^{31}P\{^1H\}$ NMR spectrum, there is a broad singlet at δ = 3.2, with $\Delta\delta$ = + 65 from free PMe_3. This resonance cannot be due to ligand iodination, as the resonance for $[IPMe_3]^+$ comes at δ = 80.0.[17] Silicon-phosphorus coupling is resolved for this complex at 253 K with a magnitude of $^1J_{SiP}$ = 93 Hz.

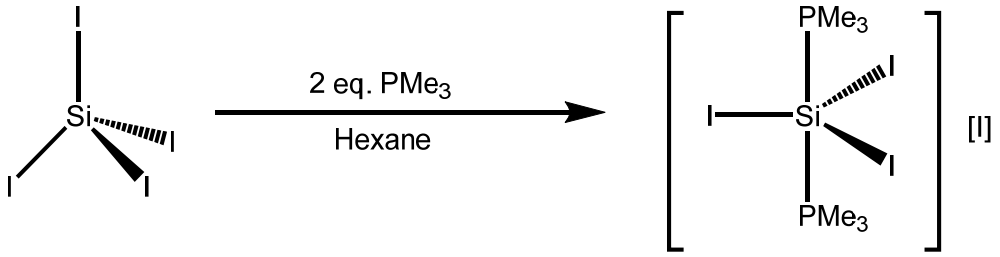

Scheme 6.1 – Reaction of SiI_4 with trimethylphosphine.

The yellow complex is stable in CH_2Cl_2 after synthesis, and crystals of the complex were grown by layering a CH_2Cl_2 solution of the complex with hexane. Rather unexpectedly, a single crystal structure determination of this product (**Figure 6.7**) shows that one of the iodides has been displaced spontaneously from the silicon centre to form a $[SiI_3(PMe_3)_2]^+$ cation. This does not occur in the bromide and chloride systems, which form six-coordinate *trans*-octahedral complexes exclusively. The difference in the reactivity of the iodides *vs.* the lighter halides probably reflects the small size of the silicon centre, together with the relative weakness of the Si-I bond (see section 1.4). The cation has a trigonal bipyramidal geometry with the PMe_3 ligands mutually *trans*. The I-Si-I bond angles are not significantly different from the expected 120˚. The P-Si-P bond angle deviates from the expected 180˚ by a few degrees (176.4(3) °), as appears to be common in these types of cations, for example, in the related complex $[SnCl_3(PMe_3)_2]^+$, where the P-Sn-P bond angle is 173˚, which was attributed to crystal packing effects.[18]

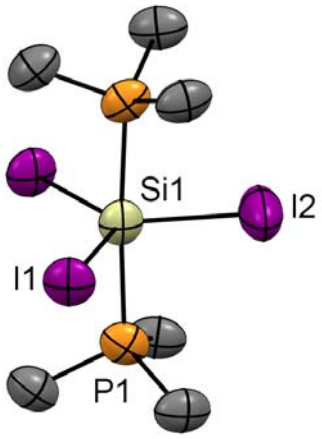

Figure 6.7 – The structure of the monocation in $[SiI_3(PMe_3)_2][I]$ showing the atom labelling scheme. Ellipsoids are drawn at the 50% probability level, H atoms, the I^- counter anion and lattice CH_2Cl_2 are omitted for clarity. Selected bond lengths (Å) and angles (˚) are: Si1-P1 = 2.380(5), Si1-I1 = 2.503(4), Si1-I2 = 2.471(7), P1-Si1-P1 = 176.3(4), I1-Si1-I2 = 119.92(14), I1-Si1-I1 = 120.2(3). symmetry operation: (1+Y-Z,+Y,3/2-Z).

The crystallographically equivalent Si-P bonds are slightly longer than the bond lengths in the tetrahalide complexes $[SiX_4(PMe_3)_2]$ (X = Cl, Br); this probably reflects the weaker Lewis acidity of silicon iodide *vs.* the lighter halides, even in the monocation.

The cation has D_{3h} symmetry, so group theory analysis predicts two Si-I stretching modes (A_1' and E') although only E' is IR active and this peak is seen at 379 cm^{-1}. Group theory also predicts two stretching bands for the Si-P bonds (A'_1 and A''_2); out of these, only the A''_2 stretch is IR active; this asymmetric stretch appears at 404 cm^{-1}.

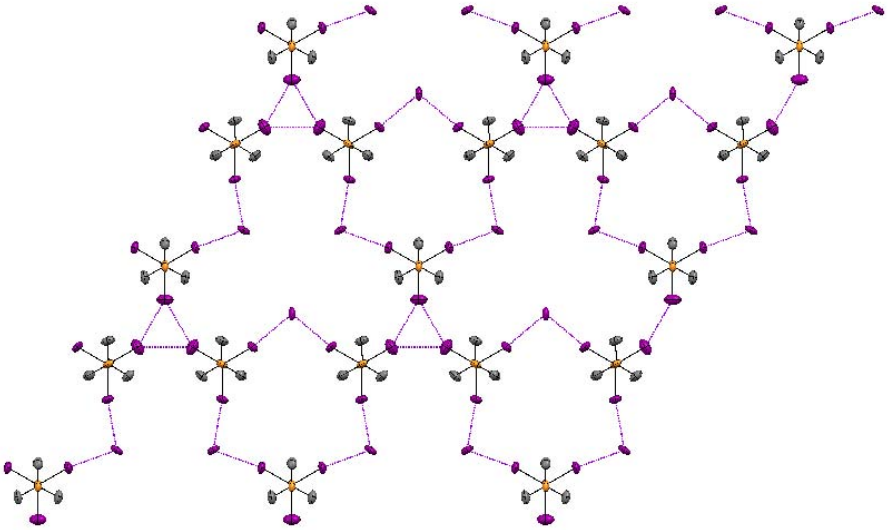

Figure 6.8 – Showing I···I interactions (purple dashes) between the $[SiI_3(PMe_3)_2]^+$ cations as well as between the $[SiI_3(PMe_3)_2]^+$ cations and I^-, looking down the P-P axis.

In the crystal structure of $[SiI_3(PMe_3)_2][I]$, there are long, weak I···I interactions that fall just within the sum of the van der Waals radii (4.08 Å)[19]; the cations and iodide anions form a 2-D network through these interactions as shown in **Figure 6.8**. Three $[SiI_3(PMe_3)_2]^+$ units form weakly associated triangles *via* the coordinated iodides, the shortest I···I distances are 3.933 Å. There are also cation-anion interactions between two of the iodine atoms in each $[SiI_3(PMe_3)_2]^+$ unit at two iodide counter anions, with d(I···I) = 3.685 Å, well within the sum of the van der Waals radii (4.08 Å). These interactions lead to the formation of a porous structure that contains void spaces which form pockets and channels in the structure aligned in the c direction and account for *ca.* 21% of the volume of the cell. These voids contain disordered CH_2Cl_2 solvent, which was accounted for in the structure refinement by using a solvent mask.[20]

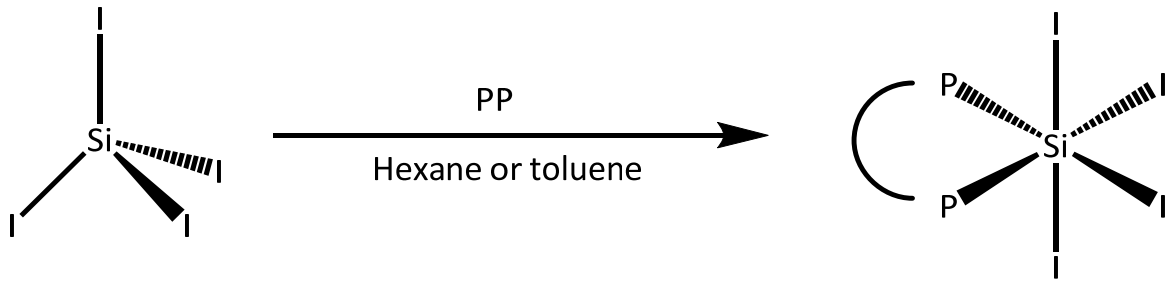

PP = $Et_2P(CH_2)_2PEt_2$
o-$C_6H_4(PMe_2)_2$

Scheme 6.2 – Reaction of SiI_4 with bidentate phosphines.

In order to investigate whether bidentate phosphines would also lead to iodide displacement, the reactions of SiI_4 with $Et_2P(CH_2)_2PEt_2$ and *o*-$C_6H_4(PMe_2)_2$ were explored (**Scheme 6.2**). The addition of the diphosphine to a solution of SiI_4 in hydrocarbon solvent leads to the immediate precipitation of orange solids, which were formulated as the neutral six coordinate complexes, $[SiI_4\{Et_2P(CH_2)_2PEt_2\}]$ and $[SiI_4\{o\text{-}C_6H_4(PMe_2)_2\}]$, respectively, on the basis of crystal structure determinations (*vide infra*).

In the ^1H NMR spectrum of $[SiI_4\{o\text{-}C_6H_4(PMe_2)_2\}]$, the methyl resonance occurs at δ = 1.99, +0.68 ppm to high frequency from the 'free' diphosphine. In the $^{31}P\{^1H\}$ NMR spectrum, there is a singlet resonance at δ = -33.6; this is a much smaller shift than seen in the analogous chloride or bromide complexes (0.7 and -2.1 ppm, respectively). The phosphine resonance is flanked by silicon satellites with $^1J_{SiP}$ = 26 Hz, which is much smaller than for the chloride and bromide complexes ($^1J_{SiP}$ = 137 and 103 Hz, respectively).[6] These data are consistent with the weaker Lewis acidity of SiI_4 compared to the lighter homologues.

In the ^1H NMR spectrum of $[SiI_4\{Et_2P(CH_2)_2PEt_2\}]$, three resonances are seen at δ = 1.41, 1.98, 2.36, with an integration ratio of 12:4:8, consistent with *cis*-bidentate coordination. The corresponding $^{31}P\{^1H\}$ NMR spectrum contains a singlet at δ = -25.6, some -7.4 ppm to low frequency from the diphosphine itself.

Crystals of $[SiI_4(o\text{-}C_6H_4\{PMe_2\}_2)]$ were grown by layering a CH_2Cl_2 solution with hexane, while crystals of $[SiI_4(PEt_2\{CH_2\}_2PEt_2)]$ came from slow evaporation of a CH_2Cl_2 solution of the complex. The structures (see **Figure 6.9** below) confirm the *cis*-octahedral coordination environment around the silicon centre with bidentate diphosphine coordination and retention of four coordinated iodides, similar to the bromide and

chloride analogues.[6] There is no evidence of displacement of the iodides from the silicon centre with these ligands, unlike the PMe_3 complex discussed earlier.

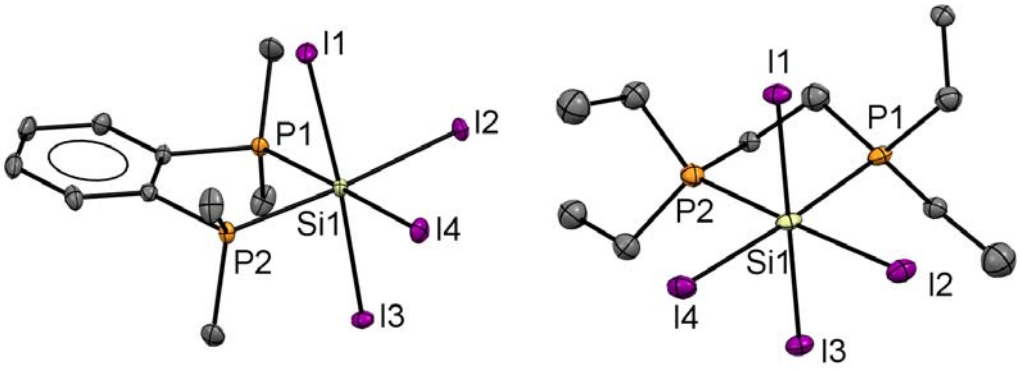

(a) (b)

Figure 6.9 – The crystal structures of (a) $[SiI_4\{o\text{-}C_6H_4(PMe_2)_2\}]$ showing the atom labelling scheme. Ellipsoids are drawn at the 50% probability level and H atoms are omitted for clarity. Selected bond lengths (Å) and angles (˚) are: Si1-P1 = 2.3707(9), Si1-P2 = 2.3678(9), Si1-I1 = 2.6812(7), Si1-I2 = 2.6326(7), Si1-I3 = 2.6266(7), Si1-I4 = 2.6371(7) P1-Si1-P2 = 86.14(3), I1-Si1-I3 = 175.81(3), I2-Si1-I4 = 93.47(2) and (b) $[SiI_4(PEt_2\{CH_2\}_2PEt_2]$ showing the atom labelling scheme. Ellipsoids are drawn at the 50% probability level and H atoms are omitted for clarity. Selected bond lengths (Å) and angles (˚) are: Si1-P1 = 2.391(8), Si1-P2 = 2.405(7), Si1-I1 = 2.647(7), Si1-I2 = 2.631(5), Si1-I3 = 2.670(7), Si1-I4 = 2.645(6) P1-Si1-P2 = 86.14(3), I1-Si1-3 =175.81(3), I2-Si1-I4 = 93.47(2).

The d(Si-I) are similar in the two $[SiI_4(diphosphine)]$ complexes, and all fall within the range of 2.6266(7)-2.6812(7) Å, i.e. elongated relative to SiI_4 itself (2.43 Å),[21] consistent with the higher coordination number in the former. The d(Si-I) in the bidentate phosphine complexes are also *ca.* 0.15 Å longer than for the five-coordinate $[SiI_3(PMe_3)_2]^+$ cation (2.471(7)-2.503(4) Å) and can also be explained by the lower coordination number (less steric crowding) in the PMe_3 complex, along with the presence of the positive charge strengthening the Si-I interaction.

$[SiI_3(PMe_3)_2][I]$, $[SiI_4\{Et_2P(CH_2)_2PEt_2\}]$ and $[SiI_4\{o\text{-}C_6H_4(PMe_2)_2\}]$ represent the first phosphine complexes of silicon iodide. For PMe_3, it has now been shown that complexes form with all the silicon halides (although for X = F, the only evidence is through tensiometric data), much like tin(IV) (see Chapter 5) and unlike germanium(IV) (see Chapter 3). The bidentate phosphine complexes represent the first structurally characterised complexes featuring the 'SiI_4' unit. This paucity of examples is due to the propensity of SiI_4 to auto-ionise, as demonstrated by the formation of the $[SiI_3(PMe_3)_2][I]$ salt with PMe_3 and by the cationic complexes formed with N-, O- and C-donor ligands discussed in section 6.1.2. In this case, the diphosphines are sufficiently good donors to form chelate complexes, but are sufficiently poor as not to cause auto-ionisation.

6.3.2 Reaction of GeI_4 with PMe_3

Tin(IV) iodide is known to react with some phosphine ligands in CH_2Cl_2 to produce iodinated phosphines rather than simple adducts, for example the reaction of PCy_3 and SnI_4 leads to the formation of $[IPCy_3][SnI_3]$.[22] However, phosphine adducts can be formed by the reaction of tin metal powder with diiodophosphines.[23] While previous work has shown that GeF_4 can form adducts with phosphines, there are no reports of adducts of GeI_4 with phosphine ligands, whereas previous work has shown that $GeCl_4$ and $GeBr_4$ react with phosphines in solution to form halophosphonium salts with GeX_3^- anions *via* redox chemistry.[24]

The reaction of GeI_4 with two equivalents of PMe_3 in toluene led to the formation of a red/brown solid, the ^1H NMR spectrum of which shows a doublet at δ = 1.81, i.e. Δδ = 0.84 *vs*. uncoordinated PMe_3, indicating adduct formation. In the $^{31}P\{^1H\}$ NMR spectrum, there is a singlet at δ = -41.3, which is only a modest shift (Δδ = +19.2) from 'free' PMe_3. This product is not iodinated phosphine, as $[PMe_3I]^+$ occurs as +80.0 ppm.[25]

Single crystal X-ray analysis of a crystal grown by layering a CH_2Cl_2 solution of the germanium product with hexane show that the germanium centre has, in fact, been reduced to Ge(II) and the phosphine ligand oxidised to form the complex, $[Ge(OPMe_3)_3][GeI_3]_2$ (see **Figure 6.10**). The dicationic part of the compound can be considered to be a phosphine oxide analogue of the dication $[Ge(PMe_3)_3]^{2+}$ described in Chapter 4. Notably, the O-Ge-O bond angles in the phosphine oxide complex are more acute than the P-Ge-P bond angles (91.03(12)° *vs*. 98.085(17)-100.507(18)°).

Using the crystal structure geometry of $[Ge(OPMe_3)_3]^{2+}$ as a starting geometry DFT calculations were performed on the dication using the B3LYP functional and 6-113G(d) basis set. NBO analysis on the ground state structure shows that the germanium centre has a natural charge of +1.34, which is much greater than in the corresponding phosphine complex (+0.16) (Chapter 4).

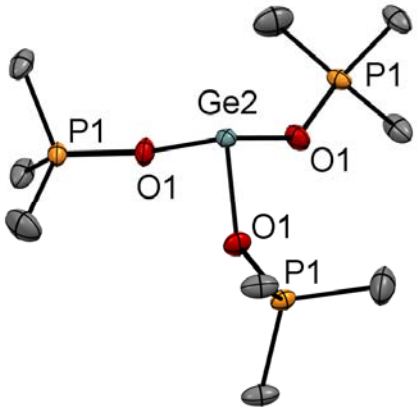

Figure 6.10 – The crystal structure of the dication in $[Ge(OPMe_3)_3][GeI_3]_2$ showing the atom labelling scheme. Ellipsoids are drawn at the 50% probability level, H atoms and the $[GeI_3]$ counter anions are omitted for clarity. Selected bond lengths (Å) and angles (˚) are: Ge2-O1 = 1.888(4), O1-P1 = 1.537(5), O1-Ge2-O1 = 91.03(12). Symmetry operations: (+Y-X, 1-X, Z), (1-Y,1+X-Y, ½-Z).

6.3.3 The reaction of silicon(IV) halide phosphine complexes with halide abstraction agents

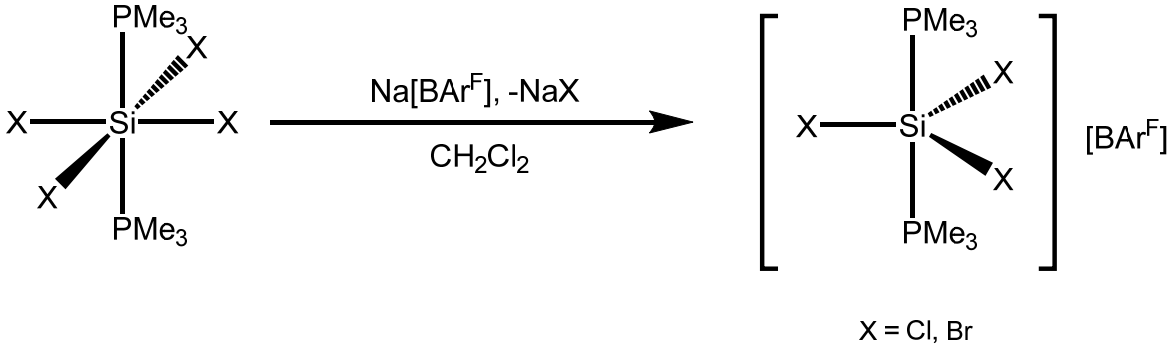

Scheme 3.3 – The reaction of $[SiX_4(PMe_3)_2]$ with $Na[BAr^F]$

Following the discovery of the $[SiI_3(PMe_3)_2]^+$ monocation discussed above, we sought to determine whether analogous cations could be generated with the lighter halide homologues. $Na[BAr^F]$ was chosen as the halide abstraction agent based upon the successful generation of tin(IV) cations (discussed in Chapter 2).

The reaction of $[SiCl_4(PMe_3)_2]$ with $Na[BAr^F]$ in CH_2Cl_2 leads to the precipitation of NaCl and the formation of the $[SiCl_3(PMe_3)_2][BAr^F]$ salt (**Scheme 3.3**). In the ^1H NMR spectrum of this complex there is a doublet at δ = 1.60, which is to low frequency of the neutral tetrachloride precursor complex. In the $^{31}P\{^1H\}$ NMR spectrum there is a sharp singlet resonance at δ = -3.5, is also to low frequency of the neutral complex, with the silicon-phosphorus coupling being $^1J_{SiP}$ = 211 Hz, (i.e. a decrease of 55 Hz from that for $[SiCl_4(PMe_3)_2]$. In the ^{29}Si NMR spectrum of this complex, a triplet is seen at δ = -105, a shift of +106 ppm from the tetrachloride complex, consistent with an increase of positive charge at silicon in the cation. In the IR spectrum of the complex, the Si-Cl E' stretch occurs at 527 cm^{-1}, and the Si-P A''$_2$ stretch at 484 cm^{-1}. Crystals of this complex were grown by layering a CH_2Cl_2 solution of the complex with hexane.

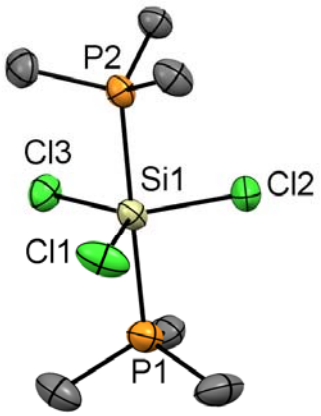

Figure 6.11 – The structure of the cation in $[SiCl_3(PMe_3)_2][BAr^F]$ showing the atom labelling scheme. Ellipsoids are drawn at the 50% probability level. H atoms and the BAr^F counter anion are omitted for clarity. Selected bond lengths (Å) and angles (˚) are: Si1-P1 = 2.3276(14), Si1-P2 = 2.3230(13), Si1-Cl1 = 2.0832(13), Si1-Cl2 = 2.0809(13), Si1-Cl3 = 2.0866(12), P1-Si1-P2 = 179.00(6), Cl1-Si1-Cl2 = 120.32(7), Cl2-Si1-Cl3 = 121.28(6), Cl1-Si1-Cl3 = 118.39(6),

The crystal structure of $[SiCl_3(PMe_3)_2][BAr^F]$ reveals a trigonal bipyramidal geometry (see **Figure 6.11**) at the silicon centre, similar to that seen in $[SnCl_3(PMe_3)_2][AlCl_4]$ (Chapter 2). In the Si cation, the PMe_3 groups are eclipsed with respect to each other and are staggered with respect to the chlorides; this contrasts with the neutral $[SiCl_4(PMe_3)_2]$, where the PMe_3 groups are staggered with respect to each other. There is a small decrease in the Si-P bond length upon going from the neutral tetrachloride complex to the monocation (see **Table 6.2**). This is accompanied by a substantial decrease in the d(Si-Cl) by *ca.* 0.14 Å upon formation of the monocation, indicating that most of the positive charge is taken up by the $SiCl_3$ unit. There is also a large increase in the average C-P-C bond angle (by ~ 2˚) upon forming the monocation; consistent with the $SiCl_3^+$ unit being a better Lewis acid towards phosphines compared to $SiCl_4$.

Table 6.2 – Selected geometric parameters for silicon halide PMe_3 complexes

	$[SiCl_4(PMe_3)_2]$	$[SiCl_3(PMe_3)_2][BAr^F]$	$[SiI_3(PMe_3)_2][I]$
d(Si-X) / Å	2.2069(3) 2.2296(3)	2.0832(13) 2.0809(13) 2.0866(12)	2.502(4) 2.478(8)
d(Si-P) / Å	2.3484(3)	2.3276(14) 2.3230(13)	2.385(6)
C-P-C angles / °	104.76(5)-105.94(5)	106.4(3)-108.2(3)	104.2(7)-109.1(9)

The corresponding bromo complex, $[SiBr_3(PMe_3)_2][BAr^F]$, can be synthesised by the reaction of $[SiBr_4(PMe_3)_2]$ with $Na[BAr^F]$ in CH_2Cl_2. The ^1H NMR spectrum of this complex shows a doublet resonance at δ = 1.62, with Δδ = -0.1 from the neutral $[SiBr_4(PMe_3)_2]$. The $^{31}P\{^1H\}$ NMR spectrum a broad singlet at δ = 3.5 (Δδ = +4.7). At 183 K, this resonance shifts to 6.3 ppm and the expected silicon satellites are resolved, with $^1J_{SiP}$ = 184 Hz, which is smaller than for the tetrabromide complex (227 Hz).[6] This is in line with the trend seen for the chloride analogues (257 Hz to 211 Hz). There is a triplet resonance in the ^{29}Si NMR of this complex at δ = -140, a shift of +144 ppm from the neutral $[SiBr_4(PMe_3)_2]$. The IR spectrum shows the Si-Br E' stretch at 433 cm^{-1} and the Si-P stretch at 474 cm^{-1}. A summary of the key NMR spectroscopic data is shown in **Table 6.3** below.

Table 6.3 – Selected spectroscopic data for neutral and cationic silicon(IV) phosphine complexes

Compound	$^{31}P\{^1H\}$/ ppm	^{29}Si / ppm[a]	$^1J_{SiP}$/ Hz	ν(Si-X)/ cm^{-1}
$[SiCl_4(PMe_3)_2]$[6]	2.3	-210	257	417
$[SiCl_3(PMe_3)_2][BAr^F]$	-3.5	-105	211	527
$[SiBr_4(PMe_3)_2]$[6]	-1.2	-284	227	321
$[SiBr_3(PMe_3)_2][BAr^F]$	3.5	-140	184	433
$[SiI_3(PMe_3)_2][I]$	3.2	-229	93	379

[a] recorded in CD_2Cl_2 at 183 K using $[Cr(TMHD)_3]$ as relaxation agent

Addition of a second equivalent of $Na[BAr^F]$ to $[SiCl_3(PMe_3)_2][BAr^F]$ did not abstract further halide, therefore, to attempt to generate dicationic complexes, the appropriate AlX_3 was used as an alternative halide abstractor (following the success of generating dicationic complexes of tin(IV) chlorides in chapter 2). However, in this case, the reaction

of $[SiX_4(PMe_3)_2]$ with two equivalents of AlX_3 in CH_2Cl_2 led to the formation of a mixture of species including $[AlX_3(PMe_3)]$ (X = Cl or Br) as indicated by distinctive multiplet resonances in their $^{31}P\{^1H\}$ NMR spectra.[26] This suggests that silicon halides are poorer Lewis acids towards phosphines than AlX_3, which can abstract a phosphine ligand from the silicon centre (or, if the phosphines are labile, can outcompete the silicon centre for coordination), and the silicon halides are more halophilic than the aluminium halides so the halide is not abstracted. The reaction of $Ag[BAr^F]$ with $[SiCl_4(PMe_3)_2]$ also leads to the abstraction of PMe_3 from the silicon centre.

As the addition of two equivalents of aluminium halides did not generate dications, effort moved to TMSOTf as an alternative halide abstractor. The reaction of $[SiCl_4(PMe_3)_2]$ with one or two equivalents of TMSOTf in CH_2Cl_2 generated the complexes $[SiCl_3(PMe_3)_2(OTf)]$ and $[SiCl_2(PMe_3)_2(OTf)_2]$. There is a small positive shift in the ^1H NMR resonance upon converting the tetrachloride to the *mono*- and *bis*-triflate derivatives. However, in the $^{31}P\{^1H\}$ spectrum, there is a negative shift to δ = -0.21 for the mono-triflate and a positive shift to δ = +3.2 for the *bis*-triflate. In the case of $[SiCl_2(PMe_3)_2(OTf)_2]$, silicon satellites are observed with $^1J_{SiP}$ = 211 Hz, which is a decrease from the parent tetrachloride complex.

A few crystals of $[SiCl_2(PMe_3)_2(OTf)_2]$ were grown by layering a CH_2Cl_2 solution of $[SiCl_3(PMe_3)_2(OTf)]$ with hexane; from these, the crystal structure of $[SiCl_2(PMe_3)_2(OTf)_2]$ could be determined (see **Figure 6.12**).

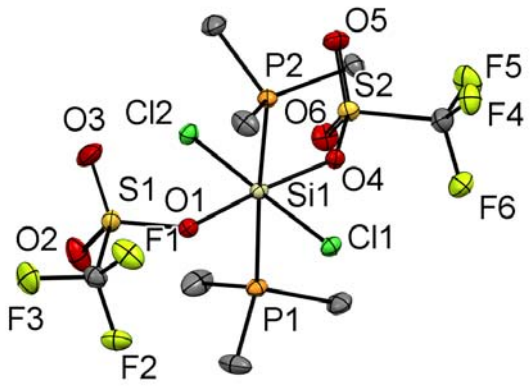

Figure 6.12 – The structure of $[SiCl_2(PMe_3)_2(OTf)_2]$ showing the atom labelling scheme. Ellipsoids are drawn at the 50% probability level and H atoms are omitted for clarity. Selected bond lengths (Å) and angles (˚) are: Si1-P1 = 2.3388(6), Si1-P2 = 2.3477(6), Si1-Cl1 = 2.1753(5), Si1-Cl2 = 2.1881(5), Si1-O1 = 1.8401(11), Si1-O4 = 1.8438(11), P1-Si1-P2 = 175.49(2), Cl1-Si1-Cl2 = 178.98(3), O1-Si1-O4 = 175.01(6).

The complex $[SiCl_2(PMe_3)_2(OTf)_2]$ exhibits a *trans*-octahedral geometry in the solid state, with both OTf groups coordinated and also mutually *trans*. This is in contrast to the $[GeF_2(PMe_3)_2(OTf)_2]$ analogue (Chapter 3), in which the triflates only interact weakly with the metal centre and are mutually *cis*. The difference in structure between the two complexes is surprising considering that the silicon is smaller than germanium and might be expected to form a lower coordinate species. The triflates are sufficiently small that the silicon centre can accommodate both of them; the short silicon-oxygen distances, d(Si-O) = 1.850(4), 1.846(4) Å, suggest that the interaction with the silicon centre is strong. The silicon-phosphorus bond lengths (2.3477(6), 2.3388(6) Å) are similar to those in $[SiCl_4(PMe_3)_2]$ (2.3484(3) Å), whereas the silicon-chloride bonds (2.1753(5), 2.1881(5) Å) are significantly shorter than those in $[SiCl_4(PMe_3)_2]$ (2.2296(3), 2.2069(3) Å), but longer than those in the $[SiCl_3(PMe_3)_2]^+$ cation. These data indicate that for the silicon complexes the positive charge is accommodated mostly by the silicon halide unit rather than the phosphine.

From a mixture of $SiCl_4$:PPr_3:TMSOTf in solution (CH_2Cl_2) crystals of the phosphonium salt, $[PPr_3H]_2[Si(OTf)_6]$, were isolated, which contained the unusual anion $[Si(OTf)_6]^{2-}$, which is shown in **Figure 6.13** below. This demonstrates that triflate is sufficiently small that even for silicon(IV), six triflate anions can fit within the coordination sphere.

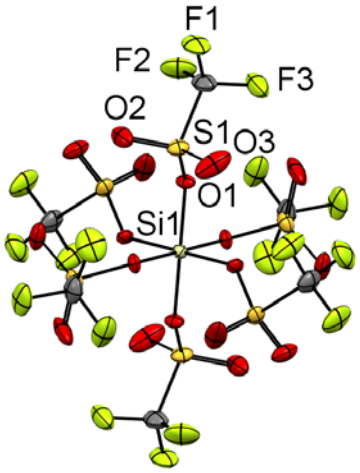

Figure 6.13 – The structure of the dianion $[Si(OTf)_6]^{2-}$ in $[HPPr_3]_2[Si(OTf)_6]$ showing the atom labelling scheme. Ellipsoids are drawn at the 50% probability level, and the cations are omitted for clarity. Selected bond lengths (Å) and angles (˚) are: Si1-O1 = 1.766(4), O1-Si-O1 = 88.7(2), 91.3(2), 180.0(3). Symmetry operations: (+Z, +Y, +X), (1-Y, 1-Z, 1-X), (1-X, 1-Y, 1-Z), (1-Z, 1-X, 1-Y), (+Y, +Z, +X).

6.3.4 DFT analysis of Si(IV) phosphine complexes

DFT calculations using the B3LYP-D3 functional were performed on the cations $[SiX_3(PMe_3)_2]^+$ (F, Cl, Br, I) in order to better understand their electronic structure. For $[SiCl_3(PMe_3)_2]^+$ and $[SiI_3(PMe_3)_2]^+$, their structures have been crystallographically determined, so the geometric optimisations started from the experimental geometries. For the $[SiF_3(PMe_3)_2]^+$ and $[SiBr_3(PMe_3)_2]^+$ cations, the experimental structures are unknown, so the geometry of $[SiCl_3(PMe_3)_2]^+$ was chosen as a starting point (with the chloride exchanged for the appropriate halide) and the structures were allowed to refine and optimise. In all cases, the calculations converged with no imaginary frequencies, showing that the optimised geometries are minima on the potential energy surface. To compare with their neutral counterparts, calculations were also performed on the tetrahalide complexes, $[SiX_4(PMe_3)_2]$ (X = F – I). For X = Cl, Br, the starting geometries were based on published crystal structures for these complexes,[6] while for X = F and I the structures were computed starting from the geometry of $[SiCl_4(PMe_3)_2]$ (changing the Cl to the appropriate halide).

Table 6.4 – Comparing computed and experimentally determined geometric parameters for $[SiCl_3(PMe_3)_2]^+$

$[SiCl_3(PMe_3)_2]^+$	X-ray data / Å	DFT (B3LYP-D3) / Å
Si-Cl	2.0832(13) 2.0809(13) 2.0866(12)	2.12782 2.12767 2.12785
Si-P	2.3276(14) 2.3230(13)	2.35909 2.35908
Cl-Si-Cl	120.32(7) 121.28(6) 118.39(6)	120.03881 119.99066 120.03881
P-Si-P	179.00(6)	179.97953

Table 6.5 – Comparing computed and experimentally determined geometric parameters for $[SiI_3(PMe_3)_2]^+$

$[SiI_3(PMe_3)_2]^+$	X-ray data / Å	DFT (B3LYP-D3) / Å
Si-I	2.503(4) 2.471(7)	2.57309 2.57336 2.57324
Si-P	2.380(5)	2.44975 2.44975
I-Si-I	119.92(14) 120.2(3)	119.98383 120.000888 120.01529
P-Si-P	176.3(4)	179.96224

Table 6.4 and **Table 6.5** above compare the geometric parameters from the experimental X-ray crystallographic data and the computed geometries for the $[SiCl_3(PMe_3)_2]^+$ and $[SiI_3(PMe_3)_2]^+$ cations. There is good agreement between the X-ray crystallographic geometries and the optimised geometries from the DFT calculations (although, of course the DFT calculations assume an isolated cation in the gas phase, whereas the X-ray crystallographic data are determined from the solid state and include the anions and packing effects).

Table 6.6 – Selected NBO data for the complexes $[SiX_4(PMe_3)_2]$ and $[SiX_3(PMe_3)_2]^+$

	$[SiF_4(PMe_3)_2]$	**$[SiCl_4(PMe_3)_2]$**	**$[SiBr_4(PMe_3)_2]$**	**$[SiI_4(PMe_3)_2]$**
Natural charge on Si	1.81	0.77	0.49	0.14
Natural charge on P	1.02	1.11	1.13	1.13
Natural charge on X (av.)	-0.68	-0.48	-0.41	-0.31
	$[SiF_3(PMe_3)_2]^+$	**$[SiCl_3(PMe_3)_2]^+$**	**$[SiBr_3(PMe_3)_2]^+$**	**$[SiI_3(PMe_3)_2]^+$**
Natural charge on Si	1.79	0.84	0.57	0.23
Natural charge on P	1.00	1.07	1.10	1.08
Natural charge on X (av.)	-0.64	-0.37	-0.29	-0.14

NBO calculations were performed on the complexes to determine how the charge is distributed in the various Si(IV) phosphine complexes. The NBO data are summarised in **Table 6.6**. In general, the positive charge on the silicon centre decreases upon going from F to I. Except for the case of X = F, the abstraction of a halide leads to an increase in positive charge on both the silicon centre and on the halides. For X = F there is a small decrease in natural charge on silicon upon fluoride abstraction. Overall, in the complexes there is only a moderate change in the charge on the phosphorus atoms, consistent with the $^{31}P\{^1H\}$ NMR shifts being similar across the halides and also with the ^{29}Si NMR shifts being much more sensitive to the specific halide present and the charge on the complex.

6.4 Conclusions

In this chapter, the chemistry of silicon (IV) halides with phosphine ligands were explored, with particular emphasis on developing a series of unusual cationic Si(IV)-phosphine species. The first examples silicon iodide phosphine complexes were synthesised and characterised; in the case of PMe_3, the reaction with SiI_4 led to spontaneous iodide displacement and the formation of the ionic complex, $[SiI_3(PMe_3)_2][I]$, contrasting with the chemistry of the other halides with PMe_3 (where only the neutral $[SnX_4(PMe_3)_2]$ complexes were observed).[6] Silicon(IV) iodide was also shown to react with the diphosphine ligands $Et_2P(CH_2)_2PEt_2$ and *o*-$C_6H_4(PMe_2)_2$ to form six-coordinate neutral complexes with *cis*-octahedral coordination, the first known complexes featuring the SiI_4 unit. Comparing these complexes with the known Si(IV) iodide complexes there are two

main differences to note, firstly, there are no known neutral silicon(IV) iodide complexes with NHC ligands (all known examples are cationic due to iodide displacement), whereas two are now known with phosphine ligands. Secondly, due to the bulkiness of the NHC ligands previously used, the coordination numbers of known NHC silicon(II)/(IV) complexes are four or fewer, whereas for phosphine ligands coordination numbers are found to be five or six. Less bulky NHCs may form complexes with higher coordination numbers.

The related $[SiX_3(PMe_3)_2]^+$ (X = Cl, Br) cations have been synthesised by the reaction of the tetrahalide complexes with $Na[BAr^F]$. In contrast, the reaction of $[SiCl_4(PMe_3)_2]$ with TMSOTf leads to the formation of neutral complexes $[SiCl_3(PMe_3)_2(OTf)]$ and $[SiCl_2(PMe_3)_2(OTf)_2]$ with the OTf remaining coordinated to the silicon centre, while the reactions of the tetrahalide complexes with AlX_3 or $Ag[BAr^F]$ led to the removal of the phosphine from the silicon centre.

DFT calculations suggest that the charge on the silicon centre in $[SiX_4(PMe_3)_2]$ and $[SiX_3(PMe_3)_2]^+$ increases in the series F > Cl > Br > I, in line with expectations based on the decreasing electronegativity going down group 17. Going from the tetrahalide to trihalide complexes the majority of the charge is accommodated by the 'SiX_3' with no significant change in the natural charge on the phosphorus atom.

The complexes described in this chapter are very rare examples of phosphine complexes of silicon halides, with some classes of complexes being completely unknown prior to this work.

6.5 X-ray crystallographic data

Table 6.7 – X-ray crystallographic data[a]

Compound	$[SiCl_3(PMe_3)_2][BArF]$	$[SiCl_2(PMe_3)_2(OTf)_2]$	$[Ge(OPMe_3)_3][GeI_3]$
Formula	$C_{38}H_{30}BCl_3F_{24}P_2Si$	$C_8H_{18}C_{12}F_6O_6P_2S_2Si$	$C_9H_{27}Ge_3I_6O_3P_3$
M	1149.81	549.27	1255.38
Crystal system	orthorhombic	monoclinic	hexagonal
Space group (no.)	Pbca (61)	$P2_1$ (4)	$P6_3/m$ (176)
a /Å	17.7948(7)	7.9858(2)	14.9724(2)
b /Å	19.5965(6)	12.3268(3)	14.9724(2)
c /Å	26.8774(11)	10.7399(2)	7.94029(14)
α /°	90	90	90
β /°	90	92.284(2)	90
γ /°	90	90	120
U /Å^3	9372.6(6)	1056.39(4)	1541.53(4)
Z	8	2	2
μ(Mo-K_α) /mm^{-1}	0.415	0.787	9.078
F(000)	4592	566	1128
Total number reflns	66260	29360	38440
R_{int}	0.063	0.041	0.062
Unique reflns	14048	6701	1907
No. of params, restraints	626, 3	250, 0	52, 0
GOF	1.012	1.037	1.313
R_1, wR_2 [$I > 2\sigma(I)$][b]	0.070, 0.180	0.026, 0.058	0.036, 0.082
R_1, wR_2 (all data)	0.138, 0.237	0.030, 0.060	0.040, 0.082

Compound	$[SiI_3(PMe_3)_2][I]\cdot CH_2Cl_2$	$[SiI_4\{o\text{-}C_6H_4(PMe_2)_2\}]$	$[SiI_4\{Et_2P(CH_2)_2PEt_2\}]$
Formula	$C_7H_{20}Cl_2I_4P_2Si$	$C_{10}H_{16}I_4P_2Si$	$C_{10}H_{24}I_4P_2Si$
M	772.76	733.889	741.953
Crystal system	hexagonal	monoclinic	monoclinic
Space group (no.)	$P6_3/mmc$ (194)	$P2_1/n$ (14)	Cc (9)
a /Å	18.1858(3)	7.22644(14)	12.8535(6)
b /Å	18.1858(3)	16.7515(3)	8.8973(3)
c /Å	13.4510(3)	17.0301(4)	17.8528(9)
α /°	90	90	90
β /°	90	101.887(2)	103.382(5)
γ /°	120	90	90
U /Å^3	3852.56(15)	2017.35(7)	1986.24(16)
Z	6	4	4
μ(Mo-K_α) /mm^{-1}	5.217	6.379	6.480
F(000)	2112	1323	1355
Total number reflns	167082	52055	10249
R_{int}	0.094	0.079	0.093
Unique reflns	2407	6706	3943
No. of params, restraints	52, 0	159, 0	158, 62
GOF	1.079	1.021	1.013
R_1, wR_2 [$I > 2\sigma(I)$][b]	0.097, 0.240	0.026, 0.059	0.079, 0.213
R_1, wR_2 (all data)	0.116, 0.252	0.029, 0.060	0.082, 0.215

[a] Common items: T = 100 K; wavelength (Mo-K_α) = 0.71073 Å; θ(max) = 27.5°; [b] $R_1 = \Sigma||F_o|-|F_c||/\Sigma|F_o|$;

$wR_2=[\Sigma w(F_o^2-F_c^2)_2/\Sigma wF_o^4]^{1/2}$

Compound	$[HP^nPr_3]_2[Si(OTf)_6]$
Formula	$C_{24}H_{32}F_{18}O_{18}P_2S_6Si$
M	1232.87
Crystal system	cubic
Space group (no.)	Pa-3 (205)
a /Å	17.1572(5)
b /Å	17.1572(5)
c /Å	17.1572(5)
α /°	90
β /°	90
γ /°	90
U /Å^3	5050.5(2)
Z	4
μ(Mo-K_α) /mm^{-1}	0.485
F(000)	2480
Total number reflns	12472
R_{int}	0.037
Unique reflns	2407
No. of params, restraints	114, 6
GOF	1.248
R_1, wR_2 [I > 2σ(I)][b]	0.131, 0.276
R_1, wR_2 (all data)	0.147, 0.284

[a] Common items: T = 100 K; wavelength (Mo-K_α) = 0.71073 Å; θ(max) = 27.5°; [b] $R_1 = \Sigma||F_o|-|F_c||/\Sigma|F_o|$; $wR_2=[\Sigma w(F_o^2-F_c^2)_2/\Sigma wF_o^4]^{1/2}$

6.6 Experimental

Refer to appendix A for sources of reagents, instrument specifications and references for NMR. $[SiCl_4(PMe_3)_2]$ and $[SiBr_4(PMe_3)_2]$ were made using published literature methods.[6]

$[SiI_3(PMe_3)_2][I]$: SiI_4 (0.500 g, 0.99 mmol) was dissolved hexane (5 mL), to this PMe_3 (0.142 g, 1.85 mmol) was added as a solution in hexane, causing a yellow powder to precipitate immediately, the reaction was stirred for 1 h. The supernatant was filtered away, and the solid was washed with hexane (3 x 10 mL) and was dried *in vacuo* to yield a yellow solid. Crystals of this complex suitable for X-ray crystallography were grown by layering a CH_2Cl_2 solution of the complex with hexane. The complex can also be synthesised using n-pentane as a solvent. Yield: 0.478 g (75%) Required for $C_6H_{18}I_4P_2Si.1/4C_6H_{14}$ (709.40): C, 12.7; H, 3.1. Found: C, 11.8; H, 3.6%. IR (Nujol/cm^{-1}): *v* = 379s (Si-I). ^1H NMR (CD_2Cl_2, 298 K): δ = 1.66 (d, $^1J_{PH}$ = 11 Hz, CH_3). $^{31}P\{^1H\}$ NMR (CD_2Cl_2, 298 K): δ = 3.2 (br s); (253 K): δ = 4.6 (s, $^1J_{SiP}$ = 93 Hz). ^{29}Si NMR (CD_2Cl_2, 298 K): δ = -233 (br s); (253 K): δ = -229

$[SiI_4\{o\text{-}C_6H_4(PMe_2)_2\}]$: SiI_4 (0.150 g, 0.28 mmol) was dissolved in hexane. To this *o*-$C_6H_4(PMe_2)_2$ (0.055 g, 0.28 mmol) was added as a solution in hexane, causing immediate precipitation of an orange powder. The reaction mixture was stirred for 1 h. The supernatant was filtered away, and the solid was washed with hexane (3 x 10 mL) and dried *in vacuo* to yield an orange solid. Crystals of this complex suitable for X-ray analysis were grown from layering a CH_2Cl_2 solution of this complex with hexane. The complex can also be synthesised using n-pentane as a solvent. Yield: 0.173 g (85%) Required for $C_{10}H_{16}I_4P_2Si{\cdot}1/2C_5H_{12}$ (769/94) : C, 19.5; H, 2.9 Found: C, 19.3; H, 2.7%. IR (Nujol/cm^{-1}): *v* = 281m, 310m (Si-I) ^1H NMR (CD_2Cl_2, 298 K): δ = 1.99 (m, [12H], CH_3), 7.69-7.90 (m, [4H], ArH). $^{31}P\{^1H\}$ NMR (CD_2Cl_2, 298 K): δ = -33.6 (s, $^1J_{SiP}$ = 25 Hz). ^{29}Si NMR (CD_2Cl_2, 298/183 K): n.o.

$[SiI_4\{Et_2P(CH_2)_2PEt_2\}]$: SiI_4 (0.300 g, 5.60 mmol) was dissolved in toluene (5 mL), to this $Et_2P(CH_2)_2PEt_2$ (0.116 g, 5.62 mmol) was added as a solution in toluene (2 mL), causing the precipitation of an orange solid. The reaction was stirred for 1 h. The supernatant was filtered away, and the solid was washed with hexane (3 x 10 mL) and dried *in vacuo* to yield an orange solid. Crystals of the complex suitable for X-ray crystallography were grown by layering a CH_2Cl_2 solution of the complex with hexane. Yield: 0.233 g (56%). for $C_{10}H_{24}I_4P_2Si{\cdot}1/2C_5H_{12}$ (766.99): C, 19.3; H, 3.8. Found: C, 19.2; H, 4.3%. IR (Nujol/cm^{-1}): *v* = 278m, 305m (Si-I). ^1H NMR (CD_2Cl_2, 298 K): δ = 1.41 (m, [12H], CH_3), 1.98(m, [4H], CH_2), 2.36 (br m, [8H], CH_2). $^{31}P\{^1H\}$ NMR (CD_2Cl_2, 298 K): δ = -25.6 (br s); (183 K): δ = -20.8 (br, s). ^{29}Si NMR (CD_2Cl_2, 298 K): -696 (br, s) ;(183 K): δ = -687 (br, s)

[$SiCl_3(PMe_3)_2$][BAr^F]: [$SiCl_4(PMe_3)_2$] (0.200 g, 0.62 mmol)) was dissolved in CH_2Cl_2 (5 mL) and Na[BAr^F] (0.550 g, 0.62 mmol) was added as a solid. The reaction mixture was stirred for 1 h during which a small amount of white precipitate formed (NaCl). The supernatant was filtered away and concentrated *in vacuo* to yield a white solid. Crystals of the complex suitable for X-ray crystallography were grown by layering a CH_2Cl_2 solution of the complex with hexane. Yield: 0.492 g (69%) Required for $C_{38}H_{30}BCl_3F_{24}P_2Si$ (1149.73): C, 39.7; H, 2.6. Found: C, 39.7; H, 3.1%. IR (Nujol/cm^{-1}): *v* = 527s (Si-Cl).^{1}H NMR (CD_2Cl_2, 298 K): δ = 1.60 (m, [18H], CH_3), 7.57 (s, [4H], ArH), 7.73 (s, [8H], ArH). $^{31}P\{^1H\}$ NMR (CD_2Cl_2, 298 K): δ = -3.5 ($^1J_{SiP}$ = 211 Hz); (183 K): δ = -2.4 ($^1J_{SiP}$ = 211 Hz). ^{29}Si NMR (CD_2Cl_2, 298 K): δ = -104 (t, $^1J_{SiP}$ = 211 Hz); (183 K): -105 (t, $^1J_{SiP}$ = 211 Hz).

[$SiBr_3(PMe_3)_2$][BAr^F]: [$SiBr_4(PMe_3)_2$] (0.100g, 0.20 mmol) was dissolved in CH_2Cl_2 (5 mL) to which Na[BAr^F] (0.177 g, 0.20 mmol) was added as a solid, the reaction mixture was stirred for 1 h, during which a small amount of white precipitate formed which was removed by filtration (NaBr). The supernatant was concentrated *in vacuo* to yield a white solid. Yield: 0.233 g (91%). Required for $C_{38}H_{30}BBr_3F_{24}P_2Si$ (1283.11): C, 35.6; H, 2.4. Found: C, 35.8; H, 2.7%. IR (Nujol/cm^{-1}): 433s (Si-Br). ^{1}H NMR (CD_2Cl_2, 298 K): δ = 1.62 (m, [18H], CH_3), 7.57 (s, [4H], ArH), 7.73 (s, [8H], Ar-H). $^{31}P\{^1H\}$ NMR (CD_2Cl_2, 298 K): δ = +3.5 (br s); (183 K): δ = +6.3 (s, $^1J_{SiP}$ = 184 Hz). ^{29}Si NMR (CD_2Cl_2, 298 K): n.o; (183 K): δ = -140 (t, $^1J_{SiP}$ = 184 Hz).

[$SiCl_3(PMe_3)_2$(OTf)]: [$SiCl_4(PMe_3)_2$] (0.100 g, 0.31 mmol) was dissolved in CH_2Cl_2 (5 mL) and TMSOTf (0.069, 0.31 mmol) was added as a solution in CH_2Cl_2 (2 mL), resulting in a colourless solution. The reaction was stirred for 1 h, after which the volatiles were removed *in vacuo* to yield a white solid, which was washed with hexane (3 x 10 mL) and dried *in vacuo*. Yield 0.119 g (88%). Required for $C_7H_{18}Cl_3F_3O_3P_2SSi$ (435.63): C, 19.3; H, 4.2. Found: C 19.3; H, 4.4%. IR (Nujol/cm^{-1}): *v* = 383m, 423m (Si-Cl). ^{1}H NMR (CD_2Cl_2, 298 K): δ = 1.67 (d, $^2J_{PH}$ = 12 Hz, CH_3). $^{31}P\{^1H\}$ NMR (CD_2Cl_2, 298 K): δ = -0.21 (s, $^1J_{SiP}$ = 248 Hz). ^{29}Si NMR (CD_2Cl_2, 298 K): -146 (t, $^1J_{SiP}$ = 248 Hz)

[$SiCl_2(PMe_3)_2$(OTf)$_2$]: [$SiCl_4(PMe_3)_2$] (0.200 g, 0.62 mmol) was dissolved in CH_2Cl_2 (5 mL) to which TMSOTf (0.216 g, 1.24 mmol) was added as a solution in CH_2Cl_2 (2 mL), resulting in a colourless solution. The reaction was stirred for 1 h and the reaction mixture was layered with hexane (10 mL) and stored at -18 ˚C, which after one day afforded a crop of colourless crystals, which were collected by filtration, washed with hexane (3 x 10 mL) and dried *in vacuo*. Yield: 0.231 g (68%). Required for $C_8H_{18}Cl_2F_6O_6P_2S_2Si{\cdot}1/4C_6H_{14}$ (570.79): C, 20.0; H, 3.8. Found: C, 19.6; H, 4.2%. Found: C, 19.6; H, 4.2%. IR (Nujol/cm^{-1}): 442m, 462m (Si-Cl). ^{1}H NMR (CD_2Cl_2, 298 K): δ = 1.67 (d, $^2J_{PH}$ = 12 Hz, CH_3). $^{31}P\{^1H\}$ NMR (CD_2Cl_2, 298 K): δ = 3.2 (s, $^1J_{SiP}$ = 211 Hz). ^{29}Si NMR (CD_2Cl_2, 298 K): -194 (t, $^1J_{SiP}$ = 311 Hz)

[$GeI_4(PMe_3)_2$]: GeI_4 (0.200 g, 0.34 mmol) was dissolved in toluene (2mL) to form a light yellow solution and PMe_3 (0.052 g, 0.68 mmol) was then added as a solution in toluene (2mL), causing the reaction mixture to turn a deeper yellow colour. After stirring for 1 h, volatiles were removed *in vacuo* and the resultant yellow-orange solid was washed with hexane (3 x 10 mL) and dried *in vacuo*. Yield: 0.160 g (64%). Required for $C_6H_{18}GeI_4P_2$ (732.39): C, 9.8; H, 2.5. Found: C, 10.2; H, 2.9%. IR (Nujol/cm^{-1}): 262m (Ge-I). ^1H NMR (CD_2Cl_2, 298 K): δ = 1.81 (d, $^2J_{PH}$ = 11 Hz, CH_3). $^{31}P\{^1H\}$ NMR (CD_2Cl_2, 298 K): δ = -41.3.

DFT Calculations

The electronic structure of these complexes was investigated using DFT calculations using the Guassian 16W software package.[27] The density functional chosen was B3LYP-D3[28] with the basis set 6-311G(d)[29] for all atoms except in species containing Br and I where the Lanl2dz basis set was used for these atoms.[30] For $[SiCl_4(PMe_3)_2]$,[6] $[SiBr_4(PMe_3)_2]$,[6] $[SiI_3(PMe_3)_2]^+$ and $[SiCl_3(PMe_3)_2]^+$ the initial geometries were taken from their crystal structures, For $[SiF_4(PMe_3)_2]$ and $[SiI_4(PMe_3)_2]$ the complex $[SiCl_4(PMe_3)_2]$ was chosen as the starting geometry, with the halide atoms exchanged as appropriate. For $[SiF_3(PMe_3)_2]^+$ and $[SiBr_3(PMe_3)_2]^+$ the $[SiCl_3(PMe_3)_2]^+$ cation was chosen as the starting geometry with the halide atoms exchanged as appropriate. In all cases the structures converged to a stable geometry with no imaginary frequencies. For the complexes with known geometries the DFT geometries were compared with the crystallographic geometries and were found to be in good agreement.

6.7 References

1 E. I. Davydova, A. Y. Timoshkin, T. N. Sevastianova, A. V. Suvorov and G. Frenking, J. Mol. Struct. , 2006, 767, 103–111.

2 K. Issleib and H. Reinhold, Z. Anorg. und Allg. Chemie, 1962, 314, 113–124.

3 G. Fritz, R. Wiemers and U. Protzer, Z. Anorg. und Allg. Chemie, 1968, 363, 225–232.

4 H. E. Blayden and M. Webster, Inorg. Nucl. Chem. Lett., 1970, 6, 703–705.

5 I. R. Beattie and G. A. Ozin, J. Chem. Soc. A, 1969, 2267–2269.

6 W. Levason, D. Pugh and G. Reid, Inorg. Chem., 2013, 52, 5185–5193.

7 D. J. D. Wilson, S. A. Couchman and J. L. Dutton, Inorg. Chem., 2012, 51, 7657–7668.

8 T. Böttcher, S. Steinhauer, B. Neumann, H.-G. Stammler, G.-V. Röschenthaler and B. Hoge, Chem. Commun., 2014, 50, 6204–6206.

9 T. Böttcher, S. Steinhauer, L. C. Lewis-Alleyne, B. Neumann, H.-G. Stammler, B. S. Bassil, G.-V. Röschenthaler and B. Hoge, Chem. Eur. J., 2015, 21, 893–899.

10 A. C. Filippou, Y. N. Lebedev, O. Chernov, M. Straßmann and G. Schnakenburg, Angew. Chem. Int. Ed., 2013, 52, 6974–6978.

11 H. L. Liu, Y. Ohmori, M. Kojima and Y. Yoshikawa, J. Coord. Chem., 1998, 44, 257–268.

12 K. Hensen, R. Mayr-Stein, T. Stumpf, P. Pickel, M. Bolte and H. Fleischer, J. Chem. Soc., Dalton Trans., 2000, 473–477.

13 M. Everett, A. Jolleys, W. Levason, M. E. Light, D. Pugh and G. Reid, Dalton Trans., 2015, 44, 20898–20905.

14 S. E. Denmark and B. M. Eklov, Chem. Eur. J., 2008, 14, 234–239.

15 U. Niemann and H. C. Marsmann, Z. Naturforsch. B, 1975, 30, 202–206.

16 M. F. Davis, M. Clarke, W. Levason, G. Reid and M. Webster, Eur. J. Inorg. Chem., 2006, 14, 2773–2782.

17 N. Bricklebank, S. M. Godfrey, A. G. Mackie, C. A. McAuliffe, R. G. Pritchard and P. J. Kobryn, J. Chem. Soc., Dalton Trans., 1993, 101.

18 E. MacDonald, L. Doyle, S. S. Chitnis, U. Werner-Zwanziger, N. Burford and A. Decken, Chem. Commun., 2012, 48, 7922–7924.

19 M. Mantina, A. C. Chamberlin, R. Valero, C. J. Cramer and D. G. Truhlar, J. Phys. Chem. A, 2009, 113, 5806–5812.

20 P. van der Sluis and A. L. Spek, Acta Crystallogr. Sect. A Found. Crystallogr., 1990, 46, 194–201.

21 M. Kolonits and M. Hargittai, Struct. Chem., 1998, 9, 349–352.

22 L. Apostolico, G. Kociok-Köhn, K. C. Molloy, C. S. Blackman, C. J. Carmalt and I. P. Parkin, Dalton Trans., 2009, 10486–10494.

23 N. Bricklebank, S. M. Godfrey, C. A. McAuliffe and R. G. Pritchard, J. Chem. Soc., Chem. Commun., 1994, 695.

24 M. F. Davis, W. Levason, G. Reid and M. Webster, Dalton Trans., 2008, 2261–2269.

25 S. Maria, F. Stoffelbach, J. Mata, J.-C. Daran, P. Richard and R. Poli, J. Am. Chem. Soc., 2005, 127, 5946–5956.

26 J. Burt, W. Levason, M. E. Light and G. Reid, Dalton Trans., 2014, 43, 14600–14611.

27 D. J. Frisch, M. J.; Trucks, G. W.; Schlegel, H. B.; Scuseria, G. E.; Robb, M. A.; Cheeseman, J. R.; Scalmani, G.; Barone, V.; Petersson, G. A.; Nakatsuji, H.; Li, X.; Caricato, M.; Marenich, A. V.; Bloino, J.; Janesko, B. G.; Gomperts, R.; Mennucci, B.; Hratch, 2016.

28 C. Lee, W. Yang and R. G. Parr, Phys. Rev. B, 1988, 37, 785–789.

29 R. Krishnan, J. S. Binkley, R. Seeger and J. A. Pople, J. Chem. Phys., 1980, 72, 650–654.

30 W. R. Wadt and P. J. Hay, J. Chem. Phys., 1985, 82, 284–298.

Chapter 7 Synthesis of salts of $[SbS_4]^{3-}$ towards the electrodeposition of Sb_2S_3

7.1 Introduction

Main group binary and ternary materials have a wide range of important applications. For example PbTe for infrared detectors,[1] GST (germanium antimony telluride) for phase change memory,[2] and SnSe for thermoelectric applications.[3] Within the ADEPT (Advanced Devices by ElectroPlaTing) Program Grant the electrodeposition of various main group materials has been investigated, mainly through the use of haloanion sources of the elements in question.[4,5] This work sought to expand the scope to the electrodeposition of sulfide-containing main group semiconductor materials, which were not accessible through the halide systems.

7.1.1 Antimony sulfide thin films

Sb_2S_3 is a V-VI material semiconductor. It has a layered structure consisting of $(Sb_4S_6)_n$ ribbon-like chains in the b-direction, which are held together by weak van der Waals interactions.[6] This material has a band gap of 1.7 eV, which is within the range for visible light, it also has a high absorption coefficient (10^5 cm^{-1}).[7,8] The material only has one stable phase, and Sb_2S_3 films can also be crystallised at temperatures at or lower than 350˚C.[9] Sulfur and antimony are relatively earth abundant elements which adds to the interest in this as a sustainable semiconductor material. Both p[10] and n[11] type semiconductor behaviour has been observed for this material. There are a wide variety of applications for Sb_2S_3, including thermoelectric devices,[11] solar cells,[12,13] microwave technologies,[11] photocatalysis,[11,14,15] and optoelectronics[16].

Various methods have been used to deposit thin films of Sb_2S_3, one of them being chemical bath deposition. Here the substrate is submerged in a solution containing the precursor materials, which then react with the surface of the substrate to deposit films. With this technique various parameters can be changed, including ion concentration, pH and complexation agents. Doped materials can also be formed by the introduction of other materials into the bath.[17] The first example of this technique used potassium

antimony tartrate ($K_2[Sb_2(C_4H_2O_6)_2]$), triethanolamine and thioacetamide, producing films of thickness ca. 1μm on SnO_2 coated glass slides over 92 h.[18]

Spray pyrolysis has also been used to deposit films of Sb_2S_3. Here a precursor mixture is sprayed onto a substrate at elevated temperature at a constant rate to form a polycrystalline thin film.[19] AACVD (aerosol assisted chemical vapour deposition) can be used to deposit films of Sb_2S_3 using antimony dithiocarbamates [$Sb\{S_2CN(Me)R\}_3$] (R = ^nBu, Hex, Bn) as the precursors.[20] LPCVD (low pressure chemical vapour deposition) can also be used to deposit Sb_2S_3 thin films using the precursors $Sb(SR)_3$ (R = ^tBu, CH_2CF_3).[21] However, it is notable that with both of these precursor types, contamination with oxygen or antimony was common, although the use of a tris(thiobenzoato)antimony(III) complex can mitigate these problems, with AACVD generating contaminant-free Sb_2S_3 films.[22]

Electrodeposition has also been used to deposit films of Sb_2S_3 onto FTO electrodes (fluorine doped tin oxide), using an aqueous solution of $SbCl_3$ and $Na_2S_2O_3$ under potentiostatic and galvanostatic conditions. The deposited films are polycrystalline and the crystallinity can be improved by annealing.[23] Pulsed electrodeposition using the same precursor mix has also been used[24] to give films with a thickness of 250 nm. Other materials such as Cu can be electrodeposited on top, which can then be heat treated to form $CuSbS_2$.[25] Prior to the work in this thesis, there were no examples of electrodeposition of Sb_2S_3 from a single source precursor. Here a single source precursor means that all the elements required for the target material are present in the same precursor molecule.

7.1.2 Non-aqueous electrodeposition

One advantage of non-aqueous electrodeposition is that the range of accessible potentials are usually larger than in aqueous electrolytes. This can be very useful, for example, in the electrodeposition of materials such as GST (germanium antimony telluride), where the potential for electrodeposition of germanium from aqueous solution is typically within the range for water reduction, whereas in CH_2Cl_2 it is well within the potential window of the solvent (-2.0 to +1.0 V) at -1.6 V.[26] GST is a ternary alloy containing germanium, antimony and tellurium, it can exist in both crystalline and amorphous forms. The amorphous phase is much less conducting than the crystalline

phase and the phase can be rapidly changed by heating the material. This switching behaviour means that GST can act as a phase change memory material.[2]

Other advantages of using non-aqueous solvents such as CH_2Cl_2 is their lower viscosity and surface tension (compared to water), which can allow better filling of small pores (on the nano-scale), which is advantageous for the deposition of material into small structures for device applications. Electrodeposition is also a non-line-of-sight technique, which allows for deposition into more complicated substrate architectures than possible via line-of-sight techniques like sputtering or chemical vapour deposition.

Previously within the ADEPT Programme Grant a set of electrodeposition precursors has been developed for the electrodeposition of a range of main group materials from non-aqueous media. The previously used precursors were based on tetrabutylammonium chlorometallates of the form $[N^nBu_4][MCl_4]$ (M = In, Ga, Bi, Sb) or $[N^nBu_4]_2[MCl_6]$ (M = Se, Te, Ge). It has been shown that these precursors can be used to deposit either the crystalline elemental material, as well as binary (InSb, Bi_2Te_3) and ternary (GST) materials.[24] There are however no analogous halometallate precursors suitable for the introduction of sulfur into the target materials, therefore the work in this study focuses on development of a different precursor system for the non-aqueous electrodeposition of main group sulfide materials. One possible solution to this challenge is to consider utilising thiometallate salts as single source precursors to deliver both the metal and the sulfur.

7.1.3 Electrodeposition from $[MS_4]^{n-}$ salts

Previously, single source precursors of the form $[MS_4]^{2-}$ (M = Mo or W) have been used to electrodeposit transition metal sulfide materials from aqueous and non-aqueous solvents.[15,28–30] Very recently it has been shown that the single source precursor $[N^nBu_4]_2[MoS_4]$ can be used to deposit MoS_2 from CH_2Cl_2 across an insulating SiO_2 surface using lateral growth from a TiN electrode. $[N^nBu_4]Cl$ was used as the supporting electrolyte and $[HNMe_3]Cl$ as a proton source to remove the excess sulfur (as H_2S).[31] This thiomolybdate anion can also be used for electrodeposition from aqueous solvents.[32] WS_2 has been deposited from acetonitrile solution using $[NH_4]_2[WS_4]$ as a single source precursor using either sodium or lithium perchlorate as the electrolyte.[15]

Antimony has an analogous tetrathioantimonate anion ($[SbS_4]^{3-}$), however, there have been no previous studies to explore the prospects of using this anion as a single source precursor for the electrodeposition of antimony sulfide thin films.

The voltammetric behaviour of this Sb(V) anion at an automatic controlling growth mercury electrode has been investigated and has been shown to be electrochemically active, though here HgS is deposited at the electode[27] The work in this chapter therefore explores the preparation and characterisation of salts of the $[SbS_4]^{3-}$ anion, and its corresponding tetraselenoantimonate anion ($[SbSe_4]^{3-}$) with a range of possible cations, and preliminary electrochemical studies to determine whether $[SbS_4]^{3-}$ can be used to grow Sb_2S_3 thin films by electrodeposition. The electrochemical studies were performed by Dr Shibin Thomas, Dr Alexander Wallace and Alexander Black.

7.2 Aims

The aim of this chapter is to develop precursors for the electrodepostion of Sb_2S_3 from a single source precursor. With secondary aims of developing precursors for non-aqueous electrodeposition as well as precursors for the electrodeposition of Sb_2Se_3.

7.3 Results and discussion

7.3.1 Synthesis and characterisation of $[SbS_4]^{3-}$ salts

The known salt $Na_3[SbS_4]\cdot 9H_2O$ was synthesised as part of this work. Sb_2S_3 was treated with six equivalents of elemental sulfur in concentrated sodium hydroxide solution. Boiling this solution for two hours caused the colour of the solution to change to orange-yellow. Cooling this solution overnight led to the deposition of yellow crystals of $Na3[SbS4]\cdot 9H_2O$.[33] $[SbS_4]^{3-}$ is a regular tetrahedral anion and group theory predicts only one IR active Sb-S stretch (T_2). The IR spectrum of the compound shows an intense peak at 388 cm^{-1} which is diagnostic of the $[SbS_4]^{3-}$ anion.[34] However, group theory predicts that both the A_1 and T_2 vibrations will be Raman active, and the Raman spectrum shows these peaks at 363 cm^{-1} 380 cm^{-1}, respectively.

^{121}Sb NMR spectroscopy of the compound in D_2O shows a resonance around δ = 1032 ppm, this is consistent with reported literature data for this anion,[35] although because of

the inherent characteristics of the quadrupolar antimony-121 nucleus (see chapter 1) only very symmetric species are expected to be seen in the NMR spectrum.

Using analogous methodology, salts of other alkali metals (K-Cs) with this anion were also synthesised, all of which show identical ^{121}Sb NMR chemical shifts confirming the presence of the same $[SbS_4]^{3-}$ anion in the salts. These also all feature the diagnostic IR band around 388 cm^{-1}.

In order to test whether these salts could be used for the non-aqueous electrodeposition of Sb_2S_3 their solubilities were tested. While they were all found to be soluble in H_2O, they were all found to be insoluble in common organic solvents such as CH_2Cl_2 and MeCN and decomposed by alcoholic solvents.

To overcome this problem of lack of solubility in organic solvents, salts with different counter cations were synthesised. Prior work has shown that $[NR_4]^+$ cations are good candidates for solubilising inorganic anions in solvents such as CH_2Cl_2.[36] However, tetraalkylammonium salts of $[SbS_4]^{3-}$ have not been reported in the literature, therefore, synthetic routes to these salts had to be developed.

Cation metathesis is commonly used to synthesise alkylammonium salts of thiometallates (e.g. $[MoS_4]^{2-}$),[37] but in this system attempts at metathesis led to decomposition of the anion. However, it was found that replacing the alkali metal hydroxides in the original synthesis with alkylammonium hydroxides allowed the direct formation of $[SbS_4]^{3-}$ salts (**Scheme 7.1**). Within this study $[NR_4]_3[SbS_4]$ (R = Me, Et, ^{n}Pr, ^{n}Bu) salts have been prepared and characterised. Like for the alkali metal salts, the tetraalkylammonium salts all have a peaks characteristic of $[SbS_4]^{3-}$ in their vibrational spectra and resonances consistent with the presence of the anion in their ^{121}Sb NMR spectra in D_2O (See **Figure 7.4**).

Scheme 7.1 – Synthesis of alkylammonium salts of tetrathioantimonate.

Crystals of $[N^nBu_4]_3[SbS_4]$ were grown from a saturated THF solution of the compound stored at -18 ˚C. The compound crystallises as the hexahydrate, $[N^nBu_4]_3[SbS_4]\cdot 6H_2O$. The anions in the structure are disordered over two independent positions with both

tetrahedra interpenetrating (shown in **Figure 7.1** below). The sites are occupied in a 1/3:2/3 ratio. Each of the $[SbS_4]^{3-}$ anions is surrounded by six H_2O molecules forming a hydrogen bonded network around the unit (shown in **Figure 7.2** below), forming an 18-membered ring, including three sulfurs from the anion; three water molecules also interact with the remaining sulfur. It seems that (adventitious) water is needed to grow crystals suitable for X-ray diffraction, but the powder initially formed was confirmed to be anhydrous (evidenced by IR spectroscopy and elemental analysis) and can be reformed by drying these crystals *in vacuo*.

The antimony-sulfur bond lengths, d(Sb-S), are similar to those reported before for this anion (~ 2.33 Å) and the S-Sb-S angles are also similar to those reported (~ 109.23 °).

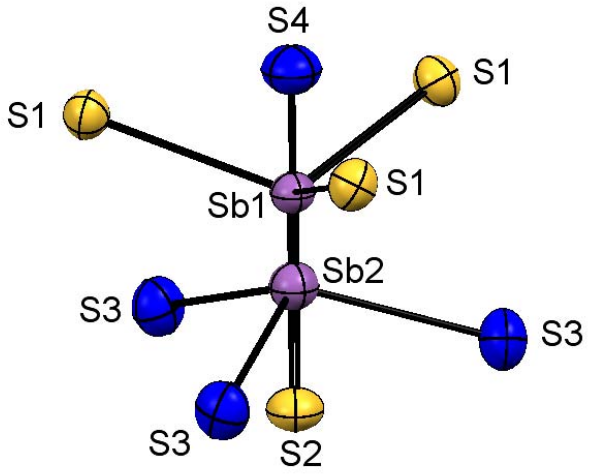

Figure 7.1 – View of the structure of the $[SbS_4]^{3-}$ anion disordered over two sites with the sulfur atoms associated with Sb1 in yellow (66% occupancy) and those associated with Sb2 in blue (33% occupancy). Selected bond lengths (Å) and angles (°) are: Sb1–S1 = 2.3148(10), Sb1–S2 = 2.3627(19), Sb2–S3 = 2.329(2), Sb2–S4 = 2.364(4), S1–Sb1–S1 = 110.918(12), S1–Sb1–S2 = 107.98(3), S3–Sb1–S3 = 110.88(6), S3–Sb1–S4 = 108.02(7). Symmetry operations: (½+Z, ½-X, 1-Y), (½-Y, 1-Z, ½+X).

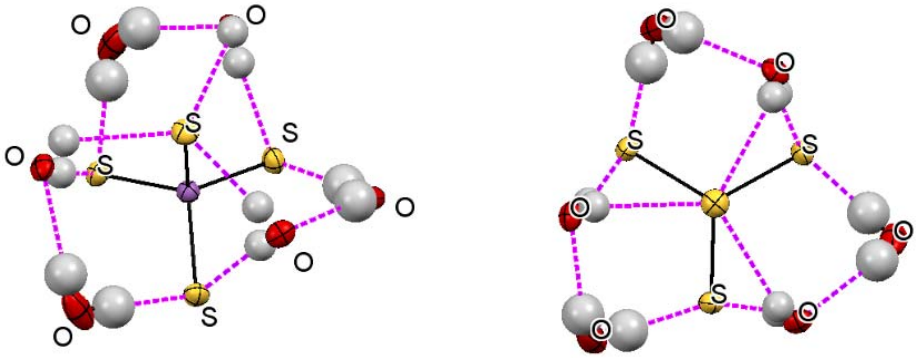

Figure 7.2 – View of the hydrogen bonding network around the $[SbS_4]^{3-}$ anion (Sb1) in $[N^nBu_4]_3[SbS_4]\cdot 6H_2O$.

Each of these $[SbS_4]^{3-}$ units are encapsulated in an octahedron of $[N^nBu_4]^+$ cations (shown in **Figure 7.3**), these octahedra are connected in a vertex-sharing fashion with a void at the centre of eight of these units remaining empty.

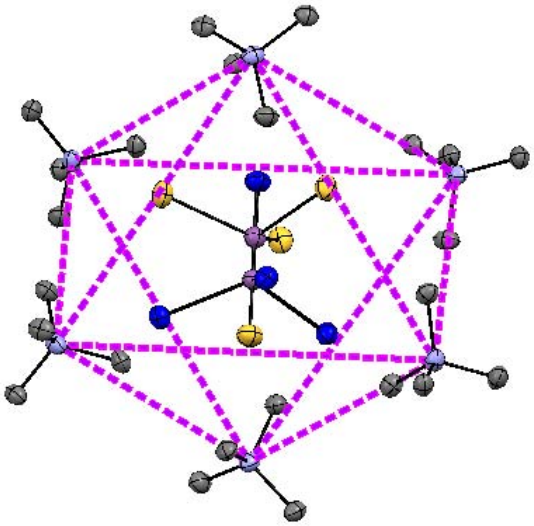

Figure 7.3 – The $[SbS_4]^{3-}$ anions inside a octahedron of $[N^nBu_4]^+$ cations (carbon chain truncated at the first carbon and H atoms omitted for clarity; purple dashed lines show the edges of the octahedron, not an interaction).

With these tetraalkylammonium salts in hand, further solubility studies were undertaken. $[Me_4N]_3[SbS_4]$ has similar solubility to the alkali metal salts, in that it is not soluble in non-alcoholic organic solvents. However, the longer chain alkylammonium salts were found to be soluble in a variety of organic solvents, including CH_2Cl_2 and MeCN. Unsurprisingly, the tetrabutylammonium salt is soluble in the widest range of organic solvents, even including THF, in which none of the other salts had any appreciable solubility. Hence, this salt was taken forward for further study in non-aqueous solvent systems.

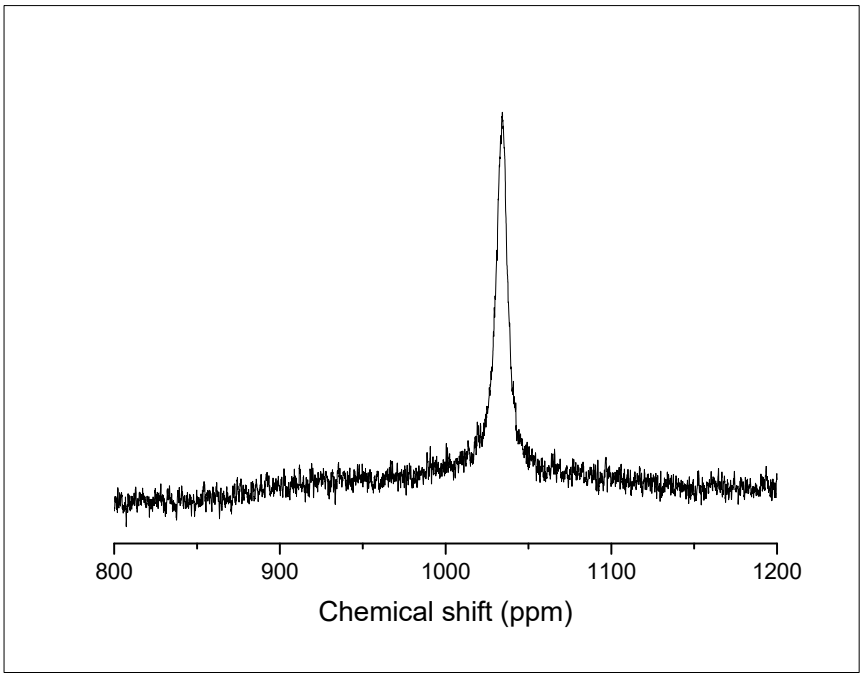

Figure 7.4 – ^{121}Sb NMR spectrum of $[N^nBu_4]_3[SbS_4]$ in D_2O at 298 K.

As already noted, one drawback of ^{121}Sb NMR spectroscopy is the large quadrupole moment associated with ^{121}Sb, which means that only highly symmetrical species with near zero electric field gradients (efgs) will be observed in the NMR spectrum. There is also no evidence of ^{121}Sb NMR signals in non-aqueous solvents, possibly as a result of ion-pairing in solution, which would be expected to reduce the symmetry of the anion, leading to a non-zero efg. To combat this, $Na_3[SbS_4]\cdot 9H_2O$ and $[N^nBu_4]_3[SbS_4]$ were also studied by solution Raman spectroscopy to probe the speciation in solution.

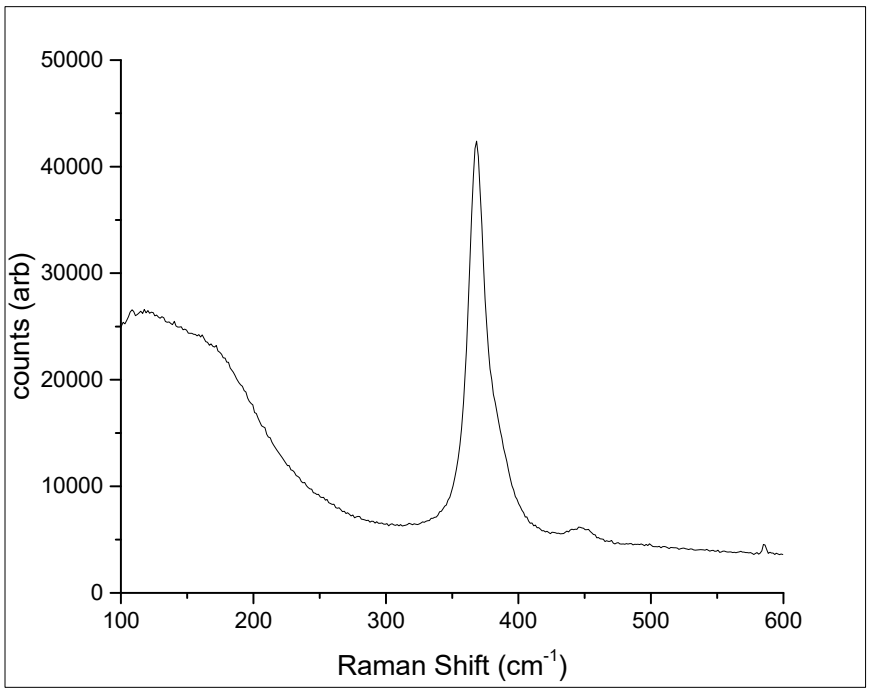

Figure 7.5 – Raman spectrum of $Na_3[SbS_4].9H_2O$ in aqueous solution.

The solution Raman spectrum of $Na_3[SbS_4]\cdot 9H_2O$ in aqueous solution (see **Figure 7.5** above) shows the expected peak at 366 cm^{-1}, which corresponds to the A_1 stretching mode in T_d symmetry (although the peak is quite broad and is likely to be coincident with the T_2 stretch). As the anion is no longer in the solid state it is in a highly symmetrical environment, so no splitting of the degenerate mode is seen. A solution Raman spectrum was also recorded for $[N^nBu_4]_3[SbS_4]$ to determine whether it would exhibit similar behaviour in water. This also shows a peak at 366 cm^{-1}, consistent with the presence of the $[SbS_4]^{3-}$ anion in solution.

Turning to the electrochemical properties, it has been shown that for the electrodeposition of MoS_2 from $[MoS_4]^{2-}$ a proton source is needed (for removal of the excess sulfur).[37] A similar situation occurs for $[SbS_4]^{3-}$, which contains a 1:4 Sb:S ratio, whereas the target Sb_2S_3 material requires only a 2:3 Sb:S ratio. Hence, the stability of $[SbS_4]^{3-}$ towards trialkylammonium proton sources was also explored. The addition of $[Me_3NH]Cl$ to an aqueous solution of $[N^nBu_4]_3[SbS_4]$ leads to the rapid precipitation of an orange powder. However, the addition of $[^nBu_3NH]Cl$ to a solution of $[N^nBu_4]_3[SbS_4]$ in CH_2Cl_2 does not cause any precipitate to form and the solution remains a yellow colour.

A mixture of $[N^nBu_4]_3[SbS_4]$ and $[Bu_3NH]Cl$ in THF stored for ~ 3 days at -18 ˚C (freezer) lead to the formation of some crystals of the decomposition product, $[N^nBu_4]_3[Sb(SSO_3)_3]\cdot 2THF$ (shown in **Figure 7.6**). The $[SSO_3]^{2-}$ anion is known to be generated in the reaction of sulfur with hydroxides in air.[38] This is an unusual homoleptic thiosulfate complex of antimony(V), the first such complex in the p-block.

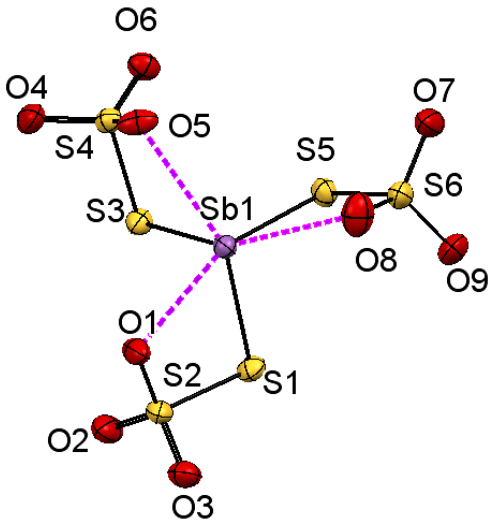

Figure 7.6 – The structure of $[N^nBu_4]_3[Sb(SSO_3)_3].2THF$ showing the atom labelling scheme. The ellipsoids are draw at the 50% probability level and H atoms, THF molecules, and cations are omitted for clarity. Selected bond lengths (Å) and angles (°) are: Sb1–S1 = 2.4539(9), Sb1–S3 = 2.4650(9), Sb1–S5 = 2.4518(9), Sb1–O1 = 2.706(3), Sb1–O5 = 2.816(3), Sb1–O8 = 2.911(4), S1–Sb1–S3 = 92.07(3), S3–Sb1–S5 = 90.92(3), S5–Sb1–S1 = 92.38(3).

In the $[Sb(SSO_3)_3]^{3-}$ trianion the thiosulfate ligands are primarily bound through the terminal sulfur atoms, the antimony-sulfur bond distances are longer than in $[SbS_4]^{3-}$, this is expected as in the thiosulfate anion the Sb-S is a single bond, whereas in the tetrathioantimonate anion the Sb-S bonds have multiple bond character. There also three long Sb-O interactions, the oxygens involved in these interactions are on the opposite face to the sulfurs completing a trigonal antiprismatic geometry.

In order to obtain a potential single source for the electrodeposition of Sb_2Se_3 thin films, the potassium salt of the analogous trianion, $K_3[SbSe_4]$, was also synthesised. This salt was obtained by the reaction of elemental Sb, Se and K in ethylenediamine. The resultant solid is a honey-yellow colour, consistent with literature reports.[39] The IR spectrum of the compound has a sharp peak at 253 cm^{-1}. There is no published IR data for the $[SbSe_4]^{3-}$

anion. To approximate the value, one might expect some assumptions can be made, using equation 1.3 from Chapter 1, if one assumes that the force constant for the sulfur and selenium analogues is the same then the ratio of the IR stretches of the sulfur and selenium analogues will be equal to the square root of the ratio of the reduced masses of the Sb-Se and Sb-S bonds. Using this approach, the T_2 IR peak should come at 286 cm^{-1}, which is reasonably close to the measured value. Treating bonds like harmonic springs and assuming the bond strength of Sb-S and Sb-Se are the same may not be very good assumptions and can explain the discrepancy observed.

7.3.2 Electrochemistry of $Na_3[SbS_4]\cdot 9H_2O$ in an aqueous electrolyte

The initial experiments to investigate the prospects of using the $[SbS_4]^{3-}$ anion for the electrodeposition of Sb_2S_3 were performed in an aqueous electrolyte using $Na_3[SbS_4]\cdot 9H_2O$ as the source of the anion. A glassy carbon button electrode was chosen as the working electrode, a platinum disc electrode was chosen as the counter electrode and the standard calomel electrode was chosen as the reference electrode. Trisodium citrate (100 mM) was chosen as the supporting electrolyte as it maintains the solution at a basic pH (the anion is stable in basic solution and unstable in acidic solution), the precursor concentration was chosen to be 2 mM. All electrolytes were deoxygenated by bubbling argon gas through the solution for 15 minutes. A blanket of argon was maintained above the electrolyte during the electrochemical experiments.

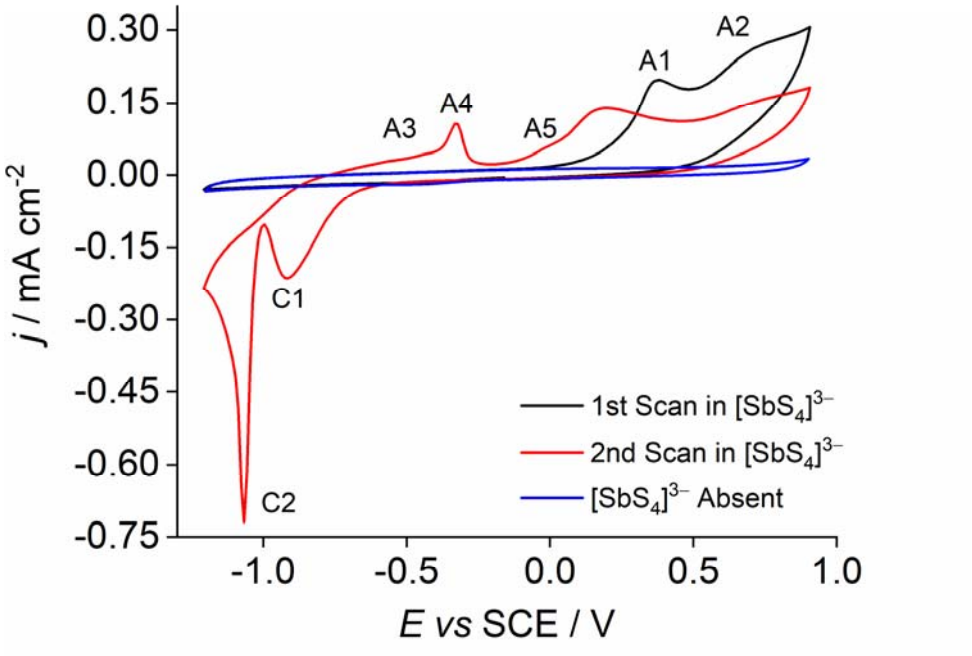

Figure 7.7 – CV on a button GC WE swept from -0.15 V vs SCE to -1.2 V vs SCE to 0.9 V vs SCE at 10 mV per s in 2 mM $Na_3[SbS_4]$ in 100 mM trisodium citrate. A background voltammogram where no $Na_3[SbS_4]$ was added to the electrolyte is shown in blue.

As shown by **Figure 7.7** there are two electroxidation processes which have peaks at +0.38 V and +0.73 V vs SCE, which are labelled A1 and A2. On the second scan there are two sharp reduction processes at -0.92 V and -1.05 V vs SCE, which are labelled with C1 and C2. As the scan sweeps to more positive potentials there are three more oxidation processes occurring at -0.77 to -0.4 V vs SCE (A3), -0.32 V vs SCE (A4) , and -0.1 to 0.05 V vs SCE (A5). The A1 process occurs at a lower potential in the second scan, possible due to change of the surface layer from glassy carbon to Sb_2S_3.

A1 and A2 correspond to the deposition of Sb_2S_3 and a by-product of either antimony hydroxide or antimony oxide. C1 corresponds to the electroreduction of the by-product to Sb(0) and C2 to the electroreduction of the anodically deposited Sb_2S_3 to Sb(0) as well as an aqueously soluble sulfur containing species. Process A3 is associated with the oxidation of the aqueous sulfur species (from process C2), both process A4 and A5 are related to the oxidation of Sb(0) on the surface.

The shape of the glassy carbon button electrode means some analysis techniques are difficult to perform on the film without specialised equipment and are impossible to anneal without destroying the electrode. In order to combat this, glassy carbon plate electrodes were used for further electrodeposition experiments. It can be seen from the CV in **Figure 7.8** that the peaks associated with the deposition of Sb_2S_3 are at ~1 V.

The plating process used involves firstly holding the electrode at a potential of +1 V for one minute, then stepping the potential to -0.55 V for ten seconds before sweeping to -1.05 V at a rate of 10 mVs^{-1}, this process is repeated 20 times to form a deposit of sufficient thickness for analysis.

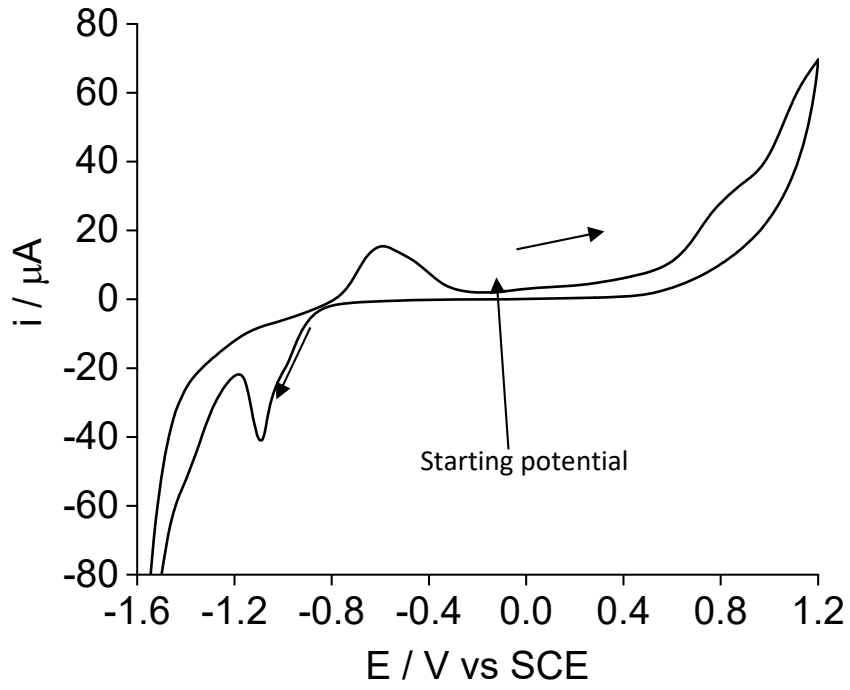

Figure 7.8 – Cyclic voltammogram obtained where the potential (E) on the GC WE is swept from -0.15 V vs SCE negative to -1.6 V then positive to 1.2 V at 10 mVs^{-1} in 2 mM $Na_3[SbS_4]$ in 100 mM trisodium citrate, 10 times.

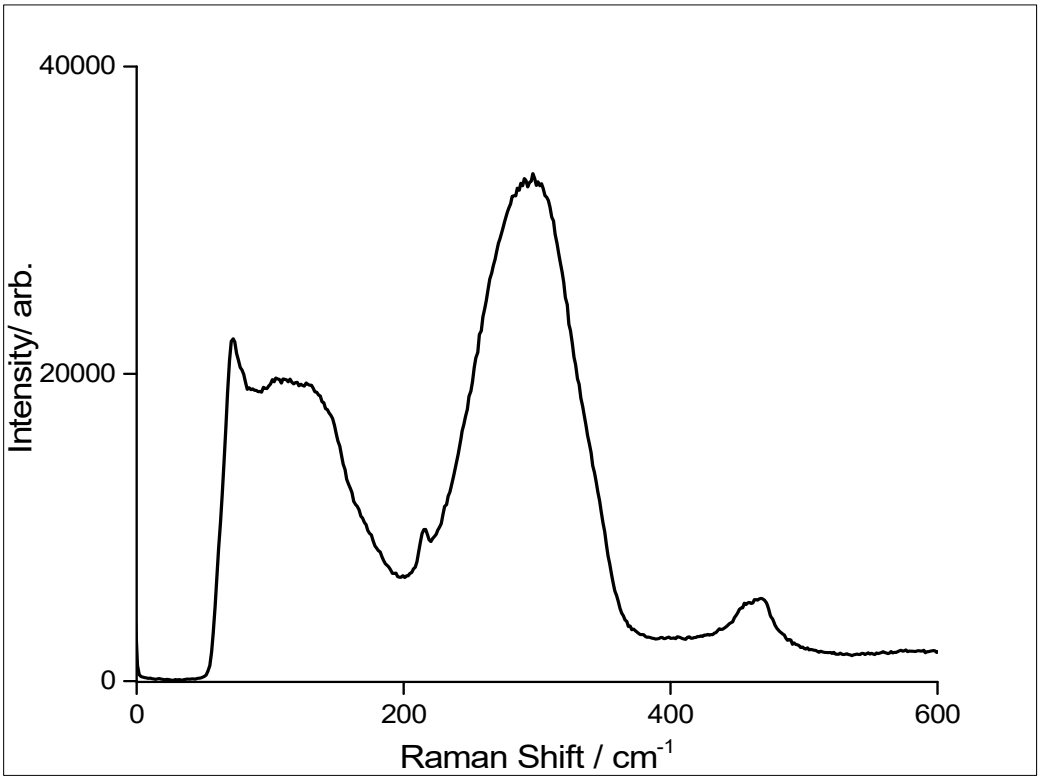

Figure 7.9 – Raman spectrum of the as-deposited film of Sb_2S_3.

The Raman spectrum of the as deposited film shows a peak at 290 cm^{-1}, which is consistent with the presence of amorphous Sb_2S_3 on the surface of the GC electrode (see **Figure 7.9**).[39] It is common for electrodeposited films to be amorphous as-deposited and to require annealing at elevated temperature to form a crystalline film. An SEM (scanning electron microscopy) image of the as-deposited film (see **Figure 7.10**) shows a continuous rough film. EDX spectroscopy was also performed on the film to better understand its elemental composition. The spectrum contains peaks associated with both Sb (Lα = 3.6 keV) and S (Kα = 2.3 keV) (see **Figure 7.11**), with an Sb:S ratio determined by EDX analysis to be 2:2.3-2.5 (EDX on a pellet of Sb_2S_3 power gives a ratio of 2:2.1-2.7), which further suggests that the deposited film is Sb_2S_3.

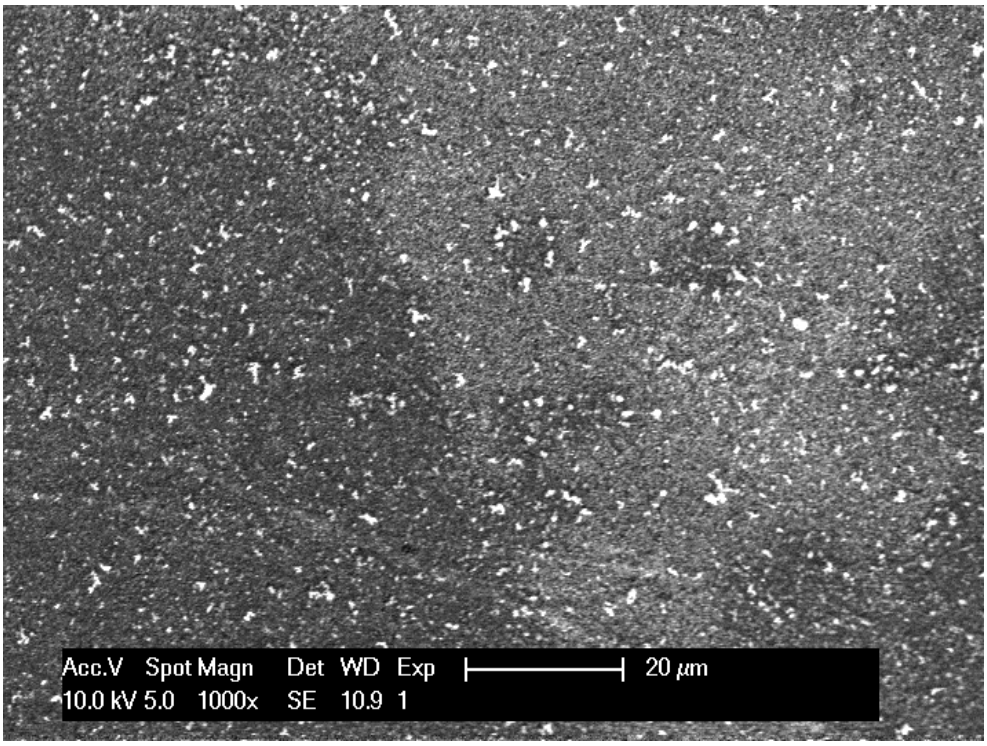

Figure 7.10 – SEM image of the as-deposited film

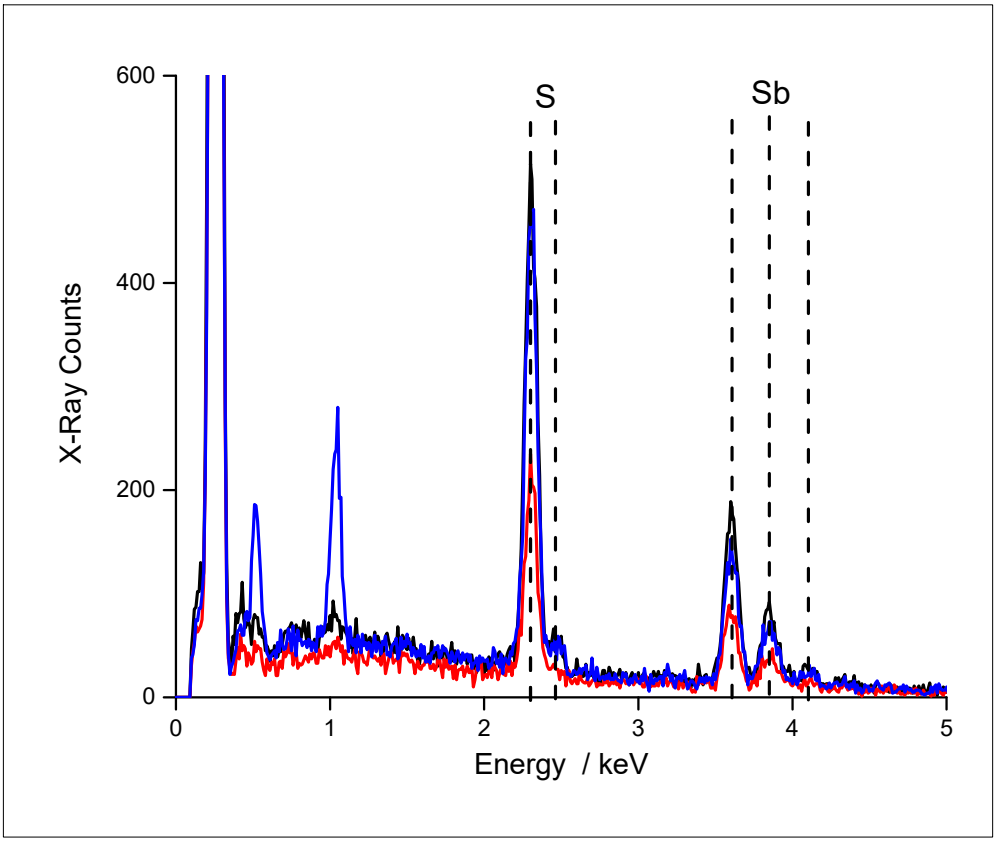

Figure 7.11 – EDX spectrum of the as deposited film with the peaks due to sulfur and antimony labelled, the blue, black and red lines represent different points on the film.

The data above suggest that the as-deposited films are amorphous. In an attempt to produce crystalline films, the tiles were annealed under an atmosphere of sulfur at 350˚C for one hour. Various annealing conditions have been used in the literature including with[41] and without[8] a sulfur atmosphere. Crystallisation of Sb_2S_3 begins at 250 ˚C, electrical conductivity improves as the annealing temperature increases, but at 400 ˚C it has been shown that cracks can develop,[42] these facts together lead to the choice of 350 ˚C as the annealing temperature. The film before annealing is a light brown colour, after annealing the film is a light grey colour.

Figure 7.12 shows the Raman spectrum of the annealed Sb_2S_3 film, which is consistent with the formation of crystalline Sb_2S_3. The Raman active vibrational modes are indicated on the diagram below and compare favourably with literature values, the peaks appear at 311 (B_{2g}), 281 (A_g^2), 239 (B_{3g}), and 196 cm^{-1} (A_g^1), peaks associated with B_{1g} and A_g^3 overlap with the peaks A_g^1 and B_{2g} respectively. [43] However, the annealed film is no longer continuous and appears as flakes on the electrode surface, suggesting some delamination during the annealing (**Figure 7.13**). However, EDX analysis on these flakes gives an Sb:S ratio of between 2:2.5-2.7, which strongly suggests that Sb_2S_3 is still present. Thin film XRD (X-ray diffraction) on the tile produces a diffraction pattern which is dominated by glassy carbon electrode, but peaks are seen at 15.7, 17.6, 25.0, and 35.6˚ (See **Figure 7.14**); which correspond to the planes (200), (120), (130), and (240) of Sb_2S_3.[44] These data together strongly suggest the presence of Sb_2S_3. The work to produce more continuous, better quality films is ongoing.

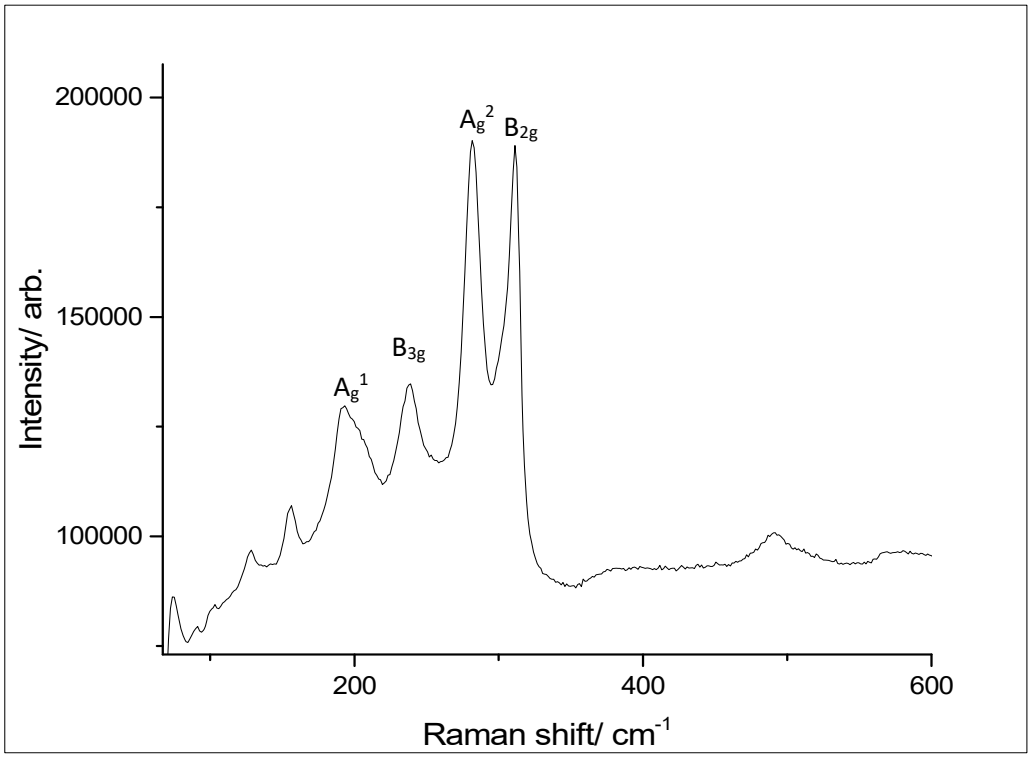

Figure 7.12 – Raman spectrum of the annealed film.

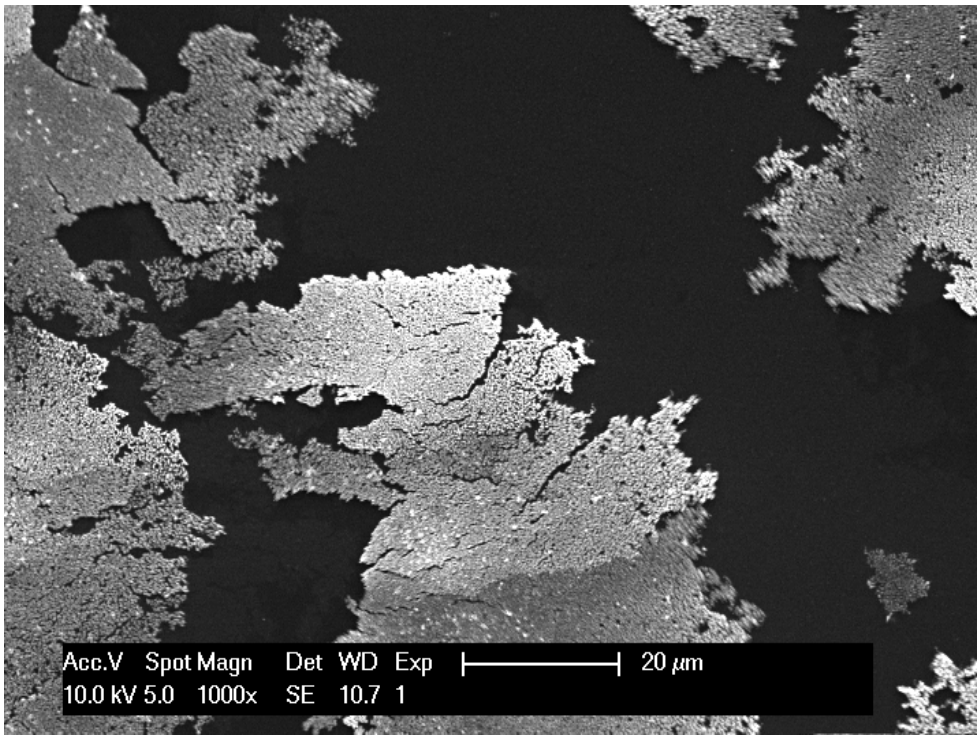

Figure 7.13 – SEM image of the crystalline Sb_2S_3 film after annealing with elemental sulfur at 350 ^oC for 1 h.

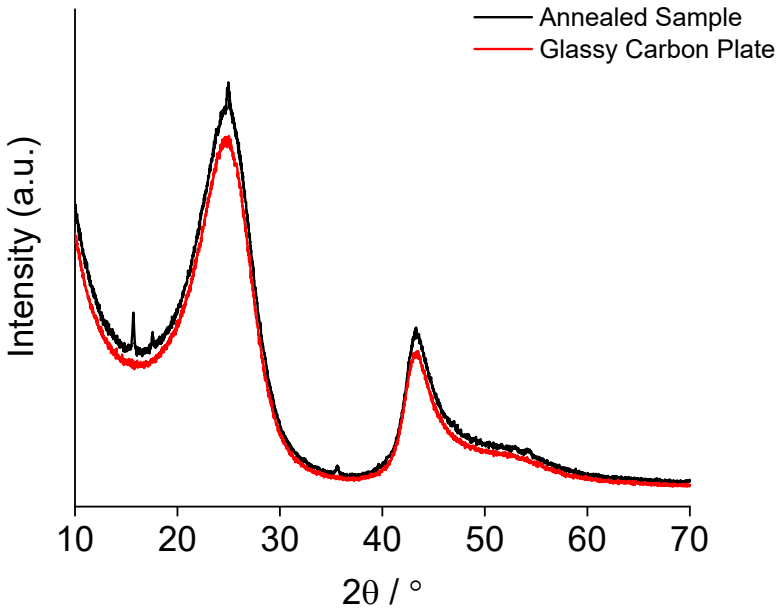

Figure 7.14 – XRD diffraction pattern of the annealed Sb_2S_3.

7.3.3 Electrochemistry of $[N^nBu_4]_3[SbS_4]$ in CH_2Cl_2

In order to try to target non-aqueous electrodeposition, CH_2Cl_2 was chosen as the solvent initially as it has previously been used to deposit a wide range of main group materials. The electrochemical solution contains $[N^nBu_4]_3[SbS_4]$ as a source of both antimony and sulfur, $[N^nBu_4]Cl$ as a supporting electrolyte and $[^nBu_3NH]Cl$ as a proton source in a 1:100:100 ratio. A GC button electrode was chosen as the working electrode (WE), Pt mesh as the counter electrode (CE) and a Ag/AgCl reference electrode. A proton source was found to be required for the deposition of MoS_2 using the analogous precursor $[NBu_4]_2[MoS_4]$; the role of the proton source is to remove sulfur anions from the solution and to prevent the deposition of sulfur on the electrode.

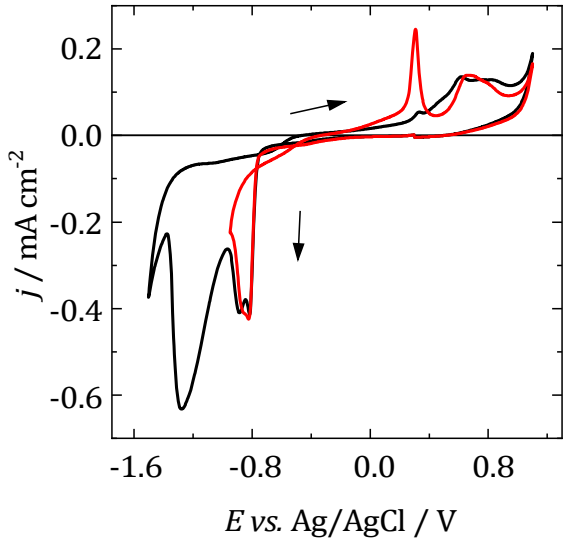

Figure 7.15 – CV of $[N^nBu_4]_3[SbS_4]$:$[^nBu_3NH]Cl$:$[N^nBu_4]Cl$ (1 mM: 100 mM: 100 mM), WE: *r* = 1.5 mm GC, CE: Pt mesh, RE: Ag/AgCl. v = 50 mV s^{-1}. Black: E_{rev} = -1.5 V, red: E_{rev} = -1.1 V

Using a glassy carbon (GC) electrode as the working electrode an electrochemical response was seen in the cyclic voltammogram (see **Figure 7.15**) indicative of redox process taking place in solution; a number of reduction peaks are seen in the region -0.8 V to -1.3 V. A possible stripping peak is seen if the potential is reversed after the first reduction peak, which could be indicative of stripping of a deposit. A similar stripping peak is seen if a platinum UME (ultra-micro electrode) is used instead. The voltammetry is reproducible over different batches of precursor and different experiments. An electrochemical deposition experiment was performed by holding the potential at E = -0.85 V. There was no visible film deposited so this was not pursued further.

Table 7.1 – Assigned electrochemical processes for the CV in Figure 7.7

Peak	**Potential vs SCE / V**	**Assignment**
A1	0.38	$[SbS_4]^{3-}$ oxidation to Sb_2S_3(s)
A2	0.73	$[SbS_4]^{3-}$ oxidation to by-product $Sb_2O_3/Sb(OH)_3$
C1	−0.92	Reduction of $Sb_2O_3/Sb(OH)_3$ to Sb(s)
C2	−1.05	Reduction of Sb_2S_3 to Sb(s) and soluble S species
A3	−0.77 to −0.40	Oxidation of soluble S species
A4	−0.32	Oxidation of Sb to soluble product
A5	−0.1 to 0.05	Oxidation of remaining Sb(s)

7.4 Conclusions

This chapter describes in the synthesis and characterisation of a series of tetrathioantimonate salts, including both alkali metal derivatives and the new $[NR_4]_3[SbS_4]$ family, with a view to investigating their prospects as single source precursors for the electrodeposition of Sb_2S_3 semiconductor thin films. Some of the latter have been shown to be soluble in aprotic solvents like CH_2Cl_2 and MeCN.

The sodium salt, $Na_3[SbS_4]\cdot 9H_2O$, was used to investigate the aqueous electrochemistry of the $[SbS_4]^{3-}$ anion on glassy carbon. It has been shown that amorphous films of Sb_2S_3 can be electrodeposited from this single source precursor. Annealing the thin film at 350˚C for 1 h in a sulfur atmosphere led to the formation of crystalline Sb_2S_3 as shown by SEM/EDX analysis and Raman spectroscopy. Further work is now on-going to optimise the electrodeposition conditions to further improve the film morphology and thickness and to allow improved X-ray diffraction data to be obtained to confirm unequivocally the presence of Sb_2S_3.

The electrochemistry of $[N^nBu_4]_3[SbS_4]$ has also been investigated in a non-aqueous CH_2Cl_2-based electrolyte. However, while the anion is electrochemically-active in CH_2Cl_2, no detectable deposit formed on the electrode, contrasting with recent work on the

growth of high quality MoS_2 thin films from CH_2Cl_2-based electrolytes.[45] Further work is required to explore the effect of alternative proton sources on this system.

7.5 X-ray crystallographic Data

Table 7.2 – X-ray crystallographic data[a]

Compound	$[N^nBu_4]_3[SbS_4]\cdot 9H_2O$	$[N^nBu_4]_3[Sb(SSO_3)_3]\cdot 2THF$
Formula	$SbS_4O_6N_3H_{120}C_{48}$	$SbS_6O_{11}N_3H_{124}C_{56}$
M	1085.529	1329.68
Crystal system	cubic	monoclinic
Space group (no.)	Pa-3 (205)	$P2_1$ (4)
a /Å	23.4668(1)	13.0864(2)
b /Å	23.4668(1)	16.3520(3)
c /Å	23.4668(1)	16.7313(3)
α /°	90	90
β /°	90	94.4970(10)
γ /°	90	90
U /Å^3	12922.95(10)	3569.29(11)
Z	8	2
μ(Mo-K_α) /mm^{-1}	0.596	0.614
F(000)	4736	1432
Total number reflns	253455	114441
R_{int}	0.058	0.035
Unique reflns	7617	24571
No. of params, restraints	224 0	719 1
GOF	1.244	1.042
R_1, wR_2 [I > 2σ(I)][b]	0.066, 0.163	0.042, 0.103
R_1, wR_2 (all data)	0.095, 0.215	0.047, 0.106

[a] Common items: T = 100 K; wavelength (Mo-K_α) = 0.71073 Å; θ(max) = 27.5°; [b] $R1 = \Sigma||F_o|-|F_c||/\Sigma|F_o|$; $wR_2=[\Sigma w(F_o^2-F_c^2)_2/\Sigma wF_o^4]^{1/2}$

7.6 Experimental

Refer to appendix A for sources of reagents, solvents, instrument specifications, and reference for NMR.

$[NMe_4]_3[SbS_4]$: A round bottom flask was charged with $[NMe_4]OH$ (4.83 g, 53.0 mmol), Sb_2S_3 (1.0 g, 3.00 mmol) and sulfur (0.56 g,18.0 mmol). To this 100 mL of distilled water was added and the mixture was refluxed for 2 h. The resulting solution was filtered and the solvent was removed *in vacuo* to afford a yellow solid, which was washed with water (1 x 20 ml), IPA (3 x 20 ml) and diethyl ether (3 x 20 ml), before the solid was dried *in vacuo*. Yield 2.51g (90%). Required for $C_{12}H_{36}N_3S_4Sb$ (472.40): C, 30.2; H, 7.7; N, 8.9. Found: C, 30.1; H, 7.8; N, 8.7%. IR (Nujol/cm^{-1}): ν = 385s (Sb-S). Raman (cm^{-1}): ν = 382 (Sb-S). ^{1}H NMR (D_2O, 298 K): δ = 3.16 (s, Me). ^{121}Sb NMR (D_2O, 298 K): δ = 1033.

$[NEt_4]_3[SbS_4]$: A round bottom flask was charged with Sb_2S_3 (1.00 g, 3.00 mmol) and sulfur (0.560 g ,18.0 mmol). To this 10 ml of water was added and to that 12.4g of $[NEt_4]OH$ is added in a 35% w/w solution. This mixture is stirred at reflux for 16 hr, the solution was filtered and the solvent was removed *in vacuo* to afford an yellow solid which was dissolved in 1:1 H_2O:THF and filtered the solvent was removed *in vacuo.* The resultant solid was washed with hexane (3 x 10 mL) and dried *in vacuo*. Yield 2.84g (75%). Required for $C_{24}H_{60}N_3S_4Sb$ (640.70): C, 45.0; H, 9.4; N, 6.6. Found: C, 44.6; H, 8.8; N, 6.4. IR (Nujol/cm^{-1}): ν = 386s (Sb-S). Raman (cm^{-1}): ν = 384, 357 (Sb-S). ^{1}H NMR (D_2O, 298 K): δ = 1.11 (tt, $^3J_{HH}$ = 7.30, J_{NH} = 2.00 Hz, [3H], -Me) 3.10 (d, $^3J_{HH}$ = 7.30, [2H], -CH_2) ^{121}Sb NMR (D_2O, 298 K): δ = 1035.

$[N^nPr_4]_3[SbS_4]$: A round bottom flask was charged with Sb_2S_3 (1.00 g, 3.00 mmol) of and sulfur (0.560g, 18.0 mmol). To this 10ml of water was added and then 29ml of a 1M solution of $[N^nPr_4]OH$ was added and the mixture was refluxed for 8 hr. The solution was then filtered and the filtrate was concentrated *in vacuo*. The oily solid was then extracted in CH_2Cl_2 (50ml) under anhydrous conditions, the solvent was then removed *in vacuo* yield an orange solid which was dried. Yield: 1.49g (31%), Required for $C_{36}H_{84}N_3S_4Sb$ (809.01): C, 53.4; H, 10.5; N, 5.2. Found: C, 53.1; H, 10.2; N, 5.2. Raman (cm^{-1}): 382 (Sb-S). ^{1}H NMR (D_2O, 298 K): δ = 0.79 (t, $^3J_{HH}$ =7.30 Hz, [12H], -Me), 1.52 (m, [8H], -CH_2), 3.00 (m, [8H], -CH_2) ^{121}Sb NMR (D_2O, 298 K): δ = 1035.

$[N^nBu_4][SbS_4]$: A round bottom flask was charged with Sb_2S_3 (0.500 g, 1.47 mmol) and sulfur (0.283 g, 8.84 mmol). To this 10 mL of distilled water was added to which $[^nBu_4N]OH$ (10.5g) was added as a 40% w/w solution causing the solution to turn red, the mixture was refluxed for 2 h leading to clear dark yellow solution which was filtered to remove unreacted starting material. The filtrate was concentrated to dryness and THF (100 mL) was added resulting in an orange/yellow solution

and a white precipitate, the solution was filtered to remove the precipitate, the filtrate was concentrated to ca. 5 mL and stored at -18 ˚C for three days, light yellow crystals formed which were collected by filtration and washed with hexane (3 x 10 mL) and dried *in vacuo* and stored at -18 ˚C. Yield: 1.62 g (56%) Required for $C_{48}H_{108}N_3S_4Sb$ (977.31): C, 59.0; H, 11.1; N, 4.3. Found: C, 58.8; H, 11.0; N, 4.2. IR (Nujol/cm^{-1}): ν = 385m (Sb-S). Raman (cm^{-1}): ν = 380, 347 (Sb-S). ^{1}H NMR (D_2O, 298 K): δ = 1.00 (t ,$^{3}J_{HH}$ = 7.3 [12H], -Me), 1.40 (m, [8H], -CH_2), 1.65 (m, [8H], -CH_2), 3.20, (m, [8H], -CH_2). ^{121}Sb NMR (D_2O, 298 K): δ = 1035.

$K_3[SbSe_4]$: A schlenk was charged with potassium (0.634 g, 16.2 mmol), to this dry ethylene diamine (20 ml) was added. The resultant mixture was heated to 80˚C and the potassium dissolved and the solution turned blue. Elemental selenium (1.71 g, 21.7 mmol) and antimony (0.660 g, 5.42 mmol) were added to the solution which turned brown. The mixture was refluxed for 24 h, the solution remained brown, on cooling the solution a yellow-brown solid precipitated out. The supernatant was filtered off and the resultant solid was washed with THF (3 x 20 mL) to yield a honey-yellow solid. Yield: 0.778 g (30 %). IR (Nujol/cm^{-1}): ν = 253s (Sb-Se).

$Na_3[SbS_4]\cdot 9H_2O$: Sb_2S_3 (7.50 g, 2.20 mmol) was added to a beaker and mixed with 60ml of 20% (w/w) NaOH in water. Sulphur (4.24 g, 13.0 mmol) was added to this solution, the mixture was boiled for 2 h while stirring until the solution goes from an orange-red colour to yellow. The volume of the resulting solution was reduced by half and allowed to cool to room temperature. After 16 h yellow crystals formed. The resultant crystals were collected and washed with isopropyl alcohol (3 x 20 ml) and diethyl ether (3 x 20ml) and then dried *in vacuo.* Yield 7.30 g (76%). IR (Nujol/cm^{-1}): ν = 390s (Sb-S). Raman (cm^{-1}): ν = 378, 363 (Sb-S). ^{121}Sb NMR (D_2O, 298 K): δ = 1033 (Sb-S).

$K_3[SbS_4]$: A round bottom flask was charged with of Sb_2S_3 (7.50 g, 2.20 mmol) and of sulfur (4.2g, 13.0 mmol). To this 60ml of 20% KOH solution was added and the mixture was boiled for 2 h, this solution was then filtered and the solvent volume was reduced by half, the solution was left to sit overnight, yellow crystals formed, which were washed by IPA (3 x 20ml) and Et_2O (3 x 20 ml) and dried *in vacuo*. Yield: 4.26g (26%). IR (Nujol/cm^{-1}): ν = 382m (Sb-S). Raman (cm^{-1}): 382, 370, 166 (Sb-S). ^{121}Sb NMR (D_2O, 298 K): δ = 1034.

$Rb_3[SbS_4]$: A round bottom flask was charged with Sb_2S_3 (2.00 g, 5.90 mmol) and sulphur (1.13 g, 3.5 mmol) of. To this 100ml of distilled water was added, to this 7.23 g of a 50 % w/w aqueous solution of RbOH was added. The solution was boiled stirred for 2 h. The resulting yellow solution was filtered and the solvent was removed *in vacuo* the resulting red solid is washed with IPA (3 x 20 ml) and dried *in vacuo*. Yield: 5.14g (87%). IR cm^{-1}: 385m (Sb-S). Raman (cm^{-1}): 387, 370, 181, 154 (Sb-S). ^{121}Sb NMR (D_2O, 298 K): δ = 1033.

$Cs_3[SbS_4]$: A round bottom flask was charged with (2.00 g, 5.90 mmol) of Sb_2S_3 and (1.13 g, 3.5 mmol) of sulphur. To this 100ml of distilled water was added and 17.8g of a 50% w/w solution of CsOH was added the resulting solution was boiled and stirred for 2 h. The resulting yellow solution was filtered and the solvent was removed *in vacuo*, the resulting gray solid was washed with IPA (3 x 20 ml) and dried *in vacuo*. Yield: 7.31g (96%). IR cm^{-1}: 392m (Sb-S). Raman (cm^{-1}): 395, 383, 368, 190, 165 (Sb-S). ^{121}Sb NMR (D_2O, 298 K): δ = 1033.

Electrochemical experiments

All aqueous electrochemical experiments were carried out in a three-electrode cell. The working electrodes (WE) used were either glassy carbon button electrodes that had been polished in a 1 µm alumina slurry before use or glassy carbon plates (HTW Hochtemperatur-Werkstoffe GmbH), with its geometric surface area constrained to approximately 9 mm^2. The counter electrode used was a platinum rod with a surface area far exceeding that of the WE. The reference electrode used was a saturated calomel electrode (SCE) stored in saturated KCl solution, and all potentials in this report shall be referenced against SCE. The background electrolyte used was always deoxygenated 100 mM sodium citrate tribasic dihydrate in ultrapure water (18.2MΩ cm, Pur1te).

Annealing

The samples were annealed in a quartz tube placed inside a tube furnace. Firstly, the sample was heated to 100 °C under a dynamic vacuum for 10 minutes to remove moisture from the system, the tube was then removed from the furnace, the furnace was then heated to 350 °C at which point the tube was reintroduced to the furnace for 1 hour under a sulfur rich atmosphere which was maintained by heating ~0.1 g of elemental sulfur with the samples in a static vacuum.

7.7 References

1 O. Simpson, G. B. B. M. Sutherland and D. E. Blackwell, Nature, 1948, 161, 281–281.

2 P. Guo, A. Sarangan and I. Agha, Appl. Sci., 2019, 9, 530.

3 M. Kumar, S. Rani, Y. Singh, K. S. Gour and V. N. Singh, RSC Adv., 2021, 11, 6477–6503.

4 P. N. Bartlett, D. Cook, C. H. de Groot, A. L. Hector, R. Huang, A. Jolleys, G. P. Kissling, W. Levason, S. J. Pearce and G. Reid, RSC Adv., 2013, 3, 15645–15654.

5 S. J. Reeves, Y. J. Noori, W. Zhang, G. Reid and P. N. Bartlett, Electrochim. Acta, 2020, 354, 136692.

6 I. Efthimiopoulos, C. Buchan and Y. Wang, Sci. Rep., 2016, 6, 24246.

7 A. Efstathiou and E. R. Levin, J. Opt. Soc. Am., 1968, 58, 373–377.

8 Y. Zeng, K. Sun, J. Huang, M. P. Nielsen, F. Ji, C. Sha, S. Yuan, X. Zhang, C. Yan, X. Liu, H. Deng, Y. Lai, J. Seidel, N. Ekins-Daukes, F. Liu, H. Song, M. Green and X. Hao, ACS Appl. Mater. Interfaces, 2020, 12, 22825–22834.

9 P. S. Pawar, R. Nandi, K. E. Neerugatti, J. Y. Cho and J. Heo, J. Alloys Compd., 2021, 162891.

10 S. Messina, M. T. S. Nair and P. K. Nair, Thin Solid Films, 2009, 517, 2503–2507.

11 R. G. Avilez Garcia, C. A. Meza Avendaño, M. Pal, F. Paraguay Delgado and N. R. Mathews, Mater. Sci. Semicond. Process., 2016, 44, 91–100.

12 R. Kondrotas, C. Chen and J. Tang, Joule, 2018, 2, 857–878.

13 X. Zhao, R. Tang, L. Zhang, C. Jiang, W. Lian, X. Wang, W. Han, C. Wu, H. Ju, T. Chen and C. Zhu, J. Phys. D. Appl. Phys., 2021, 54, 134001.

14 A. D. DeAngelis, K. C. Kemp, N. N. Gaillard and K. S. Kim, ACS Appl. Mater. Interfaces, 2016, 8, 8445–8451.

15 L. Fan and I. I. Suni, J. Electrochem. Soc., 2017, 164, D681–D686.

16 J.-H. Chen, S.-K. Chiu, J.-D. Luo, S.-Y. Huang, H.-A. Ting, M. Hofmann, Y.-P. Hsieh and C.-C. Ting, Sci. Rep., 2020, 10, 14873.

17 C. D. Lokhande, Mater. Chem. Phys., 1991, 27, 1–43.

18 O. Savadogo and K. C. Mandal, Sol. Energy Mater. Sol. Cells, 1992, 26, 117–136.

19 S. R. Gadakh and C. H. Bhosale, Mater. Chem. Phys., 2003, 78, 367–371.

20 J. Rodriguez-Castro, M. F. Mahon and K. C. Molloy, Chem. Vap. Depos., 2006, 12, 601–607.

21 J. R.- Castro, P. Dale, M. F. Mahon, K. C. Molloy and L. M. Peter, Chem. Mater., 2007, 19, 3219–3226.

22 G. Murtaza, M. Akhtar, M. Azad Malik, P. O'Brien and N. Revaprasadu, Mater. Sci. Semicond. Process., 2015, 40, 643–649.

23 N. S. Yesugade, C. D. Lokhande and C. H. Bhosale, Thin Solid Films, 1995, 263, 145–149.

24 R. G. Avilez Garcia, C. A. Meza Avendaño, M. Pal, F. Paraguay Delgado and N. R. Mathews, Mater. Sci. Semicond. Process., 2016, 44, 91–100.

25 R. G. A. García, A. Cerdán-Pasarán, E. A. R. Perez, M. Pal, M. M. Hernández and N. R. Mathews, J. Solid State Electrochem., 2020, 24, 185–194.

26 R. Huang, G. P. Kissling, R. Kashtiban, Y. J. Noori, K. Cicvarić, W. Zhang, A. L. Hector, R. Beanland, D. C. Smith, G. Reid, P. N. Bartlett and C. H. de Groot, Faraday Discuss., 2019, 213, 339–355.

27 I. Ciglenečki and G. R. Helz, Electroanalysis, 2003, 15, 145–150.

28 B. D. Falola, T. Wiltowski and I. I. Suni, J. Electrochem. Soc., 2016, 163, D568–D574.

29 E. A. Ponomarev, M. Neumann-Spallart, G. Hodes and C. Lévy-Clément, Thin Solid Films, 1996, 280, 86–89.

30 D. W. Redman, M. J. Rose and K. J. Stevenson, Langmuir, 2017, 33, 9354–9360.

31 N. M. Abdelazim, Y. J. Noori, S. Thomas, V. K. Greenacre, Y. Han, D. E. Smith, G. Piana, N. Zhelev, A. L. Hector, R. Beanland, G. Reid, P. N. Bartlett and C. H. Groot, Adv. Electron. Mater., 2021, 2100419.

32 D. Bélanger, G. Laperriére and B. Marsan, J. Electroanal. Chem., 1993, 347, 165–183.

33 G. Brauer, Handbook of preparative inorganic chemistry, Academic Press, New York, Vol 1. 2nd., 1963.

34 K. Nakamoto, Infrared and Raman Spectra of Inorganic and Coordination Compounds, John Wiley & Sons Ltd., New York, 1986.

35 J. Mason, Multinuclear NMR, Springer US, Boston, MA, 1987.

36 S. Thomas, D. E. Smith, V. K. Greenacre, Y. J. Noori, A. L. Hector, C. H. de Groot, G. Reid and P. N. Bartlett, J. Electrochem. Soc., 2020, 167, 106511.

37 M. Poisot, W. Bensch, S. Fuentes and G. Alonso, Thermochim. Acta, 2006, 444, 35–45.

38 H. V. Tartar and C. Z. Draves, J. Am. Chem. Soc., 1924, 46, 574–581.

39 J. S. Eensalu, A. Katerski, E. Kärber, I. Oja Acik, A. Mere and M. Krunks, Beilstein J. Nanotechnol., 2019, 10, 198–210.

40 C. Anderer, C. Näther and W. Bensch, Z. Naturforsch. B, 2016, 71, 395–401.

41 M. Y. Versavel and J. A. Haber, Thin Solid Films, 2007, 515, 7171–7176.

42 A. D. DeAngelis, K. C. Kemp, N. Gaillard and K. S. Kim, ACS Appl. Mater. Interfaces, 2016, 8, 8445–8451.

43 Y. A. Sorb, V. Rajaji, P. S. Malavi, U. Subbarao, P. Halappa, S. C. Peter, S. Karmakar and C. Narayana, J. Phys. Condens. Matter, 2016, 28, 015602.

44 L. Zhang, C. Wu, W. Liu, S. Yang, M. Wang, T. Chen and C. Zhu, J. Mater. Chem. A, 2018, 6, 21320–21326.

45 S. Thomas, V. K. Greenacre, D. E. Smith, Y. J. Noori, N. M. Abdelazim, A. L. Hector, C. H. de Groot, W. Levason, P. N. Bartlett and G. Reid, Chem. Commun., 2021, 57, 10194–10197.

Chapter 8 Summary and outlook

The anion $[SbS_4]^{3-}$ has been shown to act as a single source precursor for the electrodeposition of thin films of Sb_2S_3 from aqueous solution onto both button and plate glassy carbon electrodes. To develop this approach further, electrochemical experiments should be performed with the analogous anion $[SbSe_4]^{3-}$. As well as this, different electrode materials could be tested, with the ultimate aim of incorporating these films into devices.

The reactions of tin(IV) halide pnictine complexes with various halide abstractors was explored. The outcome of the reactions of tin chloride and bromide pnicitine complexes with halide abstraction agents was found to strongly depend on both the ligand type and abstraction agent used. The reactivity of tin(IV) and germanium(IV) fluoride phosphine complexes was investigated. It was shown that fluorides can be sequentially removed through the addition of TMSOTf as a fluoride abstractor. In some cases these complexes were shown to be unstable in solution and generated tin(II) and germanium(II) complexes (such as $[Ge(PMe_3)_3][OTf]_2$). For the bulkier P^iPr_3 ligand cationic complexes could be isolated.

After the serendipitous discovery of $[Ge(PMe_3)_3][OTf]_2$, a rational synthesis of this complex was developed and this chemistry was expanded to include a series monodentate and polydentate phosphine and arsine complexes. This provided the first examples of homoleptic phosphine and arsine Ge(II) dications. DFT calculations revealed that the pnictine ligand takes on a large portion of the positive charge and the germanium centre has a stereochemically active lone pair.

The first examples of silicon(IV) iodide complexes with phosphine ligands were prepared, including the first structurally authenticated complexes containing the 'SiI_4' unit. In the case of PMe_3 one of the iodides is displaced from the silicon centre to form the cationic complex $[SiI_3(PMe_3)_2][I]$. Related chloride and bromide complexes were synthesised by the reaction of the tetrahalide complex with $Na[BAr^F]$.

From a coordination chemistry perspective one way to build upon this work is to expand the range of ligand types, for example to chalcogenoethers, to compare their reactivity to the analogous phosphine complexes. Another route would be to explore the fluoride

abstraction chemistry of other main group fluoride phosphine complexes to establish differences and commonalities across the main group. Investigation of the Lewis acidic behaviour of the cationic group 14 complex described in this thesis towards catalysis or ring opening polymerisation of *rac*-lactide would be interesting.

For the Ge(II) work one direction it could be taken is exploring the reactivity of these complexes with small molecules, for example H_2O or NH_3, or even their use as ligands in their own right towards transition metal centres. Another option is to investigate if the weaker chalcogenoether ligands could stabilise a germanium(II) dication, to see where the limit is. The electrochemistry of these salts could be investigated to determine whether they could be used as alternatives to halometallate salts for the non-aqueous electrodeposition of germanium and related materials. A further interesting target would be the synthesis of neutral Si(II) phosphine complexes as well as dicationic derivatives, while neutral tetrahalide phosphine complexes cannot be reduced to Si(II), the cationic complexes synthesised in this work may be more reactive to reducing agents.

Appendix A General experimental considerations

Reactions were carried out under a dry dinitrogen atmosphere using standard Schlenk line and glove box techniques, other than the ones described in chapter 7, where in general the reactions were carried out under normal atmospheric conditions unless otherwise stated. Solvents were dried and degassed before use. Hexane and toluene and benzene were distilled over Na; CH_2Cl_2 and MeCN were distilled over CaH_2; Et_2O and THF were distilled over Na/benzophenone ketyl, all solvents were subsequently stored over 4Å molecule sieves. Purchased reagents were used as received, except for TMSOTf which was distilled prior to use. The ligands *o*-C6H_4(PMe_2)$_2$,[1] *o*-C_6H_4($AsMe_2$)$_2$,[2] $CH_3C(CH_2AsMe_2)_3$[2] and $SbEt_3$[3] were prepared according to the literature procedures, as well as $Na[BAr^F]_4$ (prepared by Kelsey Cairns) and $[SnF_4(MeCN)_2]$[5]. $SnCl_4$, $SnBr_4$, $AlCl_3$, $AlBr_3$, $CH_3(CH_2PPh_2)_3$, $P(CH_2CH_2PPh_2)_3$, [$GeCl_2$(dioxane)], [N^nBu_4][OH], [N^nPr_4][OH], [NEt_4][OH], [NMe_4][OH]·5H_2O, MOH (M = Na-Cs), Iodine, $SiCl_4$, $SiBr_4$, potassium, antimony, selenium, sulfur were obtained from Sigma-Aldrich, PMe_3, PEt_3, P^nPr_3, $AsEt_3$ were obtained from Strem. Tin(II) fluoride and SiI_4 were obtained from Alpha Aesar. GeF_4 was obtained from Fluorochem. $GeCl_4$ was obtained from Acros organics

Good laboratory practice was followed at all times, including the use of PPE and fumehoods and glove boxes for handling volatile or hazardous substances. Residues containing tin, antimony or selenium were treated as hazardous and were collected in a container for disposal. Organo-phosphorus or arsenic compounds are sometimes toxic and can be pyrophoric, so were handled only is small amounts and were treated with an aqueous sodium hypochlorite solution before disposal. Solvent residues were collected in chlorinated and non-chlorinated containers for disposal.

IR spectra were recorded as Nujol mulls between CsI plates using a Perkin Elmer Spectrum 100 spectrometer over the range of 200-4000 cm^{-1}. NMR spectra were recorded using a Bruker AVII400 or AVIIIHD400 spectrometers. ^1H and $^{13}C\{^1H\}$ NMR spectra were referenced to residual solvent resonances. $^{19}F\{^1H\}$ was referenced to external $CFCl_3$, $^{31}P\{^1H\}$ to aqueous 85% H_3PO_4, ^{27}Al to $[Al(H_2O)_6]^{3+}$, ^{29}Si to TMS (with tris(2,2,6,6-tetramethyl-3,5-heptanedionato)chromium(III) as a relaxation agent, ^{119}Sn to $SnMe_4$ [$Cr(acac)_3$] used as a relaxation agent, ^{121}Sb referenced to [$SbCl_6$][N^nBu_4]. Raman

spectra were collected by a Renishaw InVia Raman microscope with a 100mW He-Ne 785 nm Laser. Microanalytical measurements were performed by either Medac or London Metropolitan University.

Single crystal X-ray data were collected using a Rigaku AFC12 goniometer equipped with an enhanced sensitivity (HG) Saturn724+ detector mounted at the window of an FR-E+ SuperBright molybdenum (λ = 0.71073 Å) rotating anode generator with VHF or HF Varimax optics (70 or 100 µm focus), with the crystal held at 100 K (N2 cryostream). Structure refinements were performed with SHELX(T)-2018/2, SHELZ-2018/3 through Olex2,[6–8] with H atoms bonding to C atoms placed in calculated positions using default C-H distances. Where additional constraints or restraints were required details are provided in the cif file for each structure

X-ray diffraction (XRD) patterns were collected in grazing incidence mode (θ1 = 1°) or in-plane mode (θ1 = 0.5°, 2θχ scan with the detector scanning in the film plane) using a Rigaku SmartLab diffractometer (Cu-Kα, λ = 1.5418 Å) with parallel X-ray beam and a DTex Ultra 250 1D detector. Scanning electron microscopy (SEM) was performed on samples at an accelerating voltage of 10 or 15 kV using a Philips XL30 ESEM. Energy dispersive X-ray spectroscopy (EDX) spectra were obtained coupled to SEM, using a Thermo Scientific NORAN System 7 X-ray Microanalysis System.

A.1 References

1 E. P. Kyba, S. T. Liu and R. L. Harris, Organometallics, 1983, 2, 1877–1879.

2 R. D. Feltham, A. Kasenally and R. S. Nyholm, J. Organomet. Chem., 1967, 7, 285–288.

3 W. V. Taylor, U. H. Soto, V. M. Lynch and M. J. Rose, Inorg. Chem., 2016, 55, 3206–3208.

4 H. Kobayashi, T. Sonoda, H. Iwamoto and M. Yoshimura, Chem. Lett., 1981, 10, 579–580.

5 D. Tudela, J. A. Patron, D. Sherlock and R. R. Holmes, in Inorganic Syntheses, ed. A. H. Cowley, 31st edn., 1996, pp. 92–93.

6 G. M. Sheldrick, Acta Cryst. C, 2015, 71, 3–8.

7 G. M. Sheldrick, Acta Cryst. C, 2008, 64, 112–22.

8 O. V. Dolomanov, L. J. Bourhis, R. J. Gildea, H. J. A. K. and H. Puschmann, J. Appl. Crystallogr., 2009, 42, 339–41.

Appendix B Crystallographic information files

Cif files are located in the supplementary information. For structures that have been published the cifs correspond to the CCDC number, for those not published the file names correspond as follows:

[*o*-$C_6H_4(PMe_2)_2$][$AlCl_4$]$_2$	[diphos][AlCl4]2
[$SnCl_4(PEt_3)_2$]	[SnCl4(PEt3)2
[$SbEt_3Cl(OTf)$]	RK SnCl3OTf 3
[Sn{*o*-$C_6H_4(PMe_3)_2$}$(OTf)_2$]	SnF3(somephos)-OTf
[$SiI_3(PMe_3)_2$][I]·CH_2Cl_2	2021DPT_GR_RK_auto
[$SiCl_2(PMe_3)_2(OTf)_2$]	RK SiCl3(PMe3)2 OTf_auto
[$Ge(OPMe_3)_3$][GeI_3]$_2$	RK [GeI3(PMe3)2][I]_auto
[HP^nPr_3]$_2$[$Si(OTf)_6$]	RK [SiCl2(nPrP)2][OTF]2_auto
[$SiCl_3(PMe_3)_2$][BArF]	RK [Sicl3(PMe3)2][Barf]
[SiI_4{*o*-$C_6H_4(PMe_3)_2$}]	RKSi3odiphosI
[SiI_4{$Et_2P(CH_2)_2PEt_2$}]	twin1_hklf4
[$^nBu_4N$]$_3$[SbS_4]·$6H_2O$	rk TBA3sbs4
[$^nBu_4N$]$_3$[$Sb(SSO_3)_3$]·2THF	TBA3(Sb(SSO3)32THF
[$SbEt(SbEt_3)_2$][OTf]$_2$	[Ge(SbEt3)3][OTf]2 new
[Ge{$CH_3C(CH_2PPh_2)_3$}][OTf]$_2$	Ge(triphos)Otf -2